Cosmic ray interaction in molecular environment

Vo Hong Minh Phan

Université de Paris

Ecole Doctorale 560:
Sciences de la Terre et de l'Environnement et Physique de l'Univers

Cosmic Ray Interaction in Molecular Environment

Par:
Phan Vo Hong Minh

Dirigée par:
Stefano Gabici

Thèse de doctorat de Physique
au Laboratoire AstroParticule et Cosmologie (APC)

Présentée et soutenue publiquement le 4 septembre 2020
Devant un jury composé de :

Fabien Casse Laboratoire AstroParticule et Cosmologie, France	Président
Daniele Galli Istituto Nazionale di AstroFisica, Italy	Rapporteur
Alexei Ivlev Max-Planck-Institut für extraterrestrische Physik, Germany	Rapporteur
Cecilia Ceccarelli Université Grenoble Alpes, France	Examinatrice
Vincent Tatischeff Laboratoire Irène Joliot-Curie, France	Examinateur
Stefano Gabici Laboratoire AstroParticule et Cosmologie, France	Directeur de thèse

Acknowledgements

First, I would like to send the biggest thank to mom, dad, Tu, and Hon (my little Quyen) for your support which helps me a lot on the way to my dream to become a researcher.

For my LoL team, the association of funny good brothers (hoi anh em thien lanh vui tinh), the high school Physics team (hoi doi tuyen Ly nam ay), and my friends from the NPAC master, a big thank for your *hilarious* jokes that helped me to overcome stress and some other not-so-happy stuff in my life. Besides, group discussion with you guys is always great for me to enrich my knowledge not only in Physics but also in many other interesting fields of science.

I am also grateful to my physics teachers from high school thay Diem and co Lan Anh. It is thanks to them that I started to see the beauty of Physics.

Many thanks to anh Ninh who supervised my bachelor thesis projects. He has prepared me with all the necessary skills to actually survive the academic environment abroad.

I would like to thank also Denis Allard for his course in Astroparticle Physics at the NPAC master which has greatly motivated me to start working in this field. He was also in my thesis monitoring committee together with Vincent Tatischeff to help me in keeping track of the progress of my PhD.

It was also thanks to the support of Giovanni Morlino and Sarah Recchia that I managed to learn a lot about some of the basics of Cosmic Ray Astrophysics. Their help provided me with a better starting point for the PhD and I really really appreciate it. I would like to acknowledge also many other senior researchers including but not limited to (in alphabetical order) Alexei Ivlev, Cecilia Ceccarelli, Daniele Galli, Elena Amato, Jacco Vink, Marco Padovani, Philipp Mertsch, Regis Terrier, and Silvia Celli. It was with them that I managed to have many interesting discussions related to the work of my thesis.

I also wish express my sincere gratitude to my thesis supervisor, Stefano Gabici. At the end of my master in High Energy Physics, my knowledge on cosmic-ray transport is almost zero and he still gave me a chance. Working with him makes me realize that Cosmic Ray Astrophysics is even more interesting than I thought and it makes me feel more determined to pursue the career path of a researcher. More importantly, it is thanks to Stefano and all the Italian collaborators that I learnt a lot about sarcasm. Thanks again for all the great support!

Finally, I acknowledge the funding from the European Union's Horizon 2020 research and innovation programme under the Marie Skłodowska-Curie Grant agreement No. 665850.

Titre: **Interaction des Rayons Cosmiques en Environnement Moléculaire**

Résumé: De nombreuses évidences observationnelles parvenues de différentes expériences au début du 20e siècle ont révélé que la Terre est constamment bombardée par des rayons cosmiques, des particules de haute énergie d'origine extraterrestre. Étant donné que ces particules sont très énergétiques, on pense qu'elles pourraient pénétrer profondément dans les nuages moléculaires et ioniser les parties les plus denses de ces objets, où naissent de nouvelles étoiles. Cela signifie que les rayons cosmiques règlent le niveau d'ionisation qui contrôle non seulement la chimie des nuages moléculaires mais également le couplage entre le gaz et le champ magnétique qui soutient le nuage en contrastant la gravité pendant le processus de formation des étoiles. On remarque que les taux d'ionisation déduits des observations infrarouges et radio sont beaucoup plus importants que la valeur communément citée dans la littérature. Ce désaccord doit mener à une réévaluation du taux d'ionisation dans les nuages, d'un point de vue théorique. Cette tâche nécessite une meilleure compréhension du transport des rayons cosmiques dans les nuages et, plus important encore, la connaissance de la quantité de rayons cosmiques de basse énergie à différentes positions dans notre Galaxie. Le premier sujet a été étudié dans des documents pionniers des années 70 et 80, mais il pourrait y avoir de la place pour d'ultérieures améliorations. En ce qui concerne le deuxième, on a des connaissances récentes, du moins pour le milieu interstellaire local, grâce aux données des sondes Voyager. Il n'est cependant pas très clair si ces données pourraient être considérées comme des valeurs de référence pour la densité des rayons cosmiques de basse énergie dans l'ensemble de la Galaxie. L'objectif de ce travail est donc d'étudier la propagation des rayons cosmiques de basse énergie dans des environnements neutres et aussi de mieux interpréter les données d'observation du taux d'ionisation dans les nuages moléculaires isolés et ceux au voisinage des accélérateurs cosmiques, tels que les restes de supernova.

Mots clefs: rayons cosmiques, nuages moléculaires, taux d'ionisation, restes de supernova

Title: **Cosmic Ray Interaction in Molecular Environment**

Abstract: It has been revealed by observational evidences from various experiments at the beginning of the 20th century that the Earth is constantly bombarded by cosmic rays, high-energy particles of extraterrestrial origin. Since these particles are very energetic, it is believed that they could penetrate deep into molecular clouds and ionize the densest parts of these objects where new stars are born. This means that cosmic rays regulate the level of ionization that controls not only the chemistry of molecular clouds but also the coupling between the gas and the magnetic field which support the cloud against gravity during the process of star formation. Interestingly, the ionization rates inferred from infrared and radio observations are much larger than the commonly quoted value in the literature. This calls for a reassessment from a theoretical point of view of the ionization rate in clouds. This task requires a better understanding of the transport of cosmic rays into clouds and, more importantly, the knowledge of the amount of low energy cosmic rays at different positions in our Galaxy. The former has been investigated in some of the pioneering papers in the seventies and eighties but there might be room for some improvements. The latter is known not too long ago at least for the local interstellar medium thanks to the data from the Voyager probes. It is, however, not very clear whether or not these data could be considered as reference values for the density of low energy cosmic rays in the entire Galaxy. The aim of this work is, therefore, to study the propagation of low energy cosmic rays in neutral environments and also to better interpret the observational data of the ionization rate in both isolated molecular clouds and the ones in the vicinity of cosmic accelerators like supernova remnants.

Keywords: cosmic rays, molecular clouds, ionization rate, supernova remnants

Publication List

Part of this thesis has been first published in the following conference proceeding and journal articles:

- Phan, V. H. M., Morlino, G., Gabici, S. 2018, What causes the ionization rates observed in diffuse molecular clouds? The role of cosmic ray protons and electrons, *MNRAS*, 480, 5167
- Phan, V. H. M. 2018, Cosmic-ray ionization in diffuse molecular clouds, American Institute of Physics Conference Series, 020004
- Recchia, S., Phan, V. H. M., Biswas, S, Gabici, S. 2019, Can a cosmic ray carrot explain the ionization level in diffuse molecular clouds?, *MNRAS*, 485, 2276
- Phan, V. H. M., Gabici, S., Morlino, G., Terrier, R., Vink, J., et al. 2020, Constraining the cosmic ray spectrum in the vicinity of the supernova remnant W28: from sub-GeV to multi-TeV energies, *A&A*, 635, A40

Contents

Introduction

It has been more than a hundred years since we first realized that the Earth is under constant bombardment of cosmic rays, very energetic particles coming from outer space. The discovery of cosmic rays has been followed by many important findings in both Particle Physics and Astrophysics. From the astrophysical aspect, it is of great interest for us not only to better understand the origin of these particles but also to have better insight into their effects on the interstellar medium. In fact, cosmic rays are believed to play an essential role in determining the chemistry and the evolution of star-forming regions since they are the only ionizing agents capable of penetrating the interior of molecular clouds (Dalgarno, 2006). However, a comprehensive theoretical prediction for the ionization rate induced by low-energy cosmic rays in molecular clouds is still lacking and this seems to hinder the progress in the simulational and theoretical research in the field of Star Formation (Krumholz, 2014).

One of the main technique for the measurements of the ionization rate in clouds employs the data on the absorption line of the protonated molecule H_3^+ and it is not until quite recently that its destruction rate has been determined in a reliable way from laboratory experiments (McCall et al., 2003). This opens up the possibility to better infer the ionization rate in diffuse molecular clouds at various locations within our Galaxy with high enough precision. Other techniques which also make use of either the absorption or emission lines have provided us with data for the ionization rate for both diffuse and dense clouds (see e.g. Caselli et al., 1998; Vaupré et al., 2014). Interestingly, the ionization rates inferred from these data are much larger than the commonly quoted value of around 10^{-17} s^{-1} (the Spitzer value). This calls for a reassessment from a theoretical point of view of the ionization rate in clouds. This task requires a better understanding of the transport of cosmic rays into clouds and, more importantly, the knowledge of the amount of low-energy cosmic rays at different positions in our Galaxy. The former has been investigated in some of the pioneering papers by Skilling & Strong, 1976; Cesarsky & Volk, 1978 and Morfill (1982) but there might be room for some improvements. The latter is known not too long ago at least for the local interstellar medium thanks to the data from the Voyager probes (Cummings et al., 2016). It is, however, not very clear whether or not these data could be considered as reference values for the density of low-energy cosmic rays in the entire Galaxy.

The aim of this work is, therefore, to study the propagation of low-energy cosmic rays in neutral environments and also to better interpret the observational data of the ionization rate in both isolated molecular clouds and the ones in the vicinity of cosmic accelerators like supernova remnants. The thesis shall be organized as follows:

- Chapter 1 is dedicated to a brief introduction into the physics of cosmic rays. We shall begin with some fundamental knowledge which has been established with observational evidences. A systematic derivation of the cosmic ray transport equation from the commonly adopted framework known as Quasi-Linear Theory is then presented. Several important processes of energy losses are also provided to set the foundation for later discussions on the transport of cosmic rays.

- The role of molecular clouds as probes of cosmic rays is briefly discussed in Chapter 2. Several aspects of gamma-ray observations of supernova remnants and molecular clouds will be presented to better highlight their connection with high-energy cosmic rays. More importantly, we shall introduce a crucial physical quantity known as the ionization rate inside molecular clouds which could help us to better understand the population of low-energy cosmic rays.

- In Chapter 3, we test the hypothesis according to which cosmic rays are the main ionization agent for the interior of molecular clouds by limiting ourselves to the case of diffuse clouds and assuming that the average cosmic ray spectrum inside the Galaxy is equal to the one at the position of the Sun as measured by Voyager 1 and AMS-02. To calculate the cosmic ray spectrum inside the clouds, we solve the 1D transport equation for cosmic rays taking into account advection, diffusion, and energy losses. While outside the cloud particles diffuse, in its interior they are assumed to gyrate along magnetic field lines because ion-neutral friction is effective in damping all the magnetic turbulence. We show that ionization losses effectively reduce the cosmic-ray flux in the cloud interior for energies below ~ 100 MeV, especially for electrons, in such a way that the ionization rate decreases by roughly two orders of magnitude with respect to the case where losses are neglected. As a consequence, the predicted ionization rate is more than 10 times smaller than the one inferred from the detection of molecular lines. We discuss the implication of our finding in terms of spatial fluctuation of the Galactic cosmic ray spectra and possible additional sources of low-energy cosmic rays.

- Among several solutions proposed to explain the discrepancy between the ionization rate estimated with the cosmic ray spectrum measured by Voyager 1 and the observational data, we shall concentrate mainly on the *carrot* and the *stochastic fluctuation*. The carrot typically refers to an unknown low-energy cosmic-ray component first hypothesized by Reeves and collaborators in the seventies (Meneguzzi et al., 1971) and has recently been revised to explain the ionization rate observed in molecular clouds (Cummings et al., 2016). In the first part of Chapter 4, we shall investigate the energetic requirement of the carrot and show that the power needed to maintain such a low-energy component is comparable of even larger than that needed to explain the entire observed cosmic ray spectrum. Moreover, if the interstellar turbulent magnetic field has to sustain a *carrot*, through second-order Fermi acceleration, the required turbulence level would be definitely too large compared to the

one expected at the scale resonant with such low-energy particles. Such an argument basically rules out all the plausible sources of a cosmic ray *carrot*, thus making such hidden component unlikely to be an appealing and viable source of ionization in molecular clouds. Another potential solution to the problem of the ionization rate presented in Chapter 4 is the stochastic fluctuations which rely on the argument that the spectrum of cosmic rays might vary significantly from place to place and we could predict the most probable range of the cosmic-ray intensities using the distribution of the sources assumed to be supernova remnants for this work. It seems that the effect of stochasticity analyzed with the injection spectra and diffusion coefficients extrapolated from data at high energy could not boost the ionization rate by 1 or 2 orders of magnitude. This might imply that we should have either a different form of the diffusion coefficient for low-energy cosmic rays or other classes of sources for these particles like OB/Wolf-Rayet stars (Casse & Paul, 1982; Voelk & Forman, 1982; Binns et al., 2005) or even solar-type stars (Scherer et al., 2008).

- In the first part of Chapter 5 we test a posteriori the hyopthesis adopted in Chapter 4, i.e., that the spectrum of cosmic rays injected in the interstellar medium by supernova remnants is a pure power law in momentum. We found that the assumption is correct if the process of acceleration stops at the end of the Sedov-Taylor phase of the supernova remnant evolution and spectral breaks might appear if the release of cosmic rays occurs later. In the second part, we apply the result for the case of a supernova explosion taking place inside the Local Bubble and combine the cosmic-ray intensities from this local source with the ones transported from outside into the Local Bubble to fit the data from both Voyager 1 (Cummings et al., 2016) and AMS 02 (Aguilar et al., 2014; Aguilar et al., 2015). It seems that the local source scenario could explain the intensities of low-energy cosmic rays observed locally even if the amount of low-energy cosmic rays in the interstellar medium is higher as required by the data of the ionization rate in clouds. The quality of the fits, however, depends very strongly to the plasma density inside the Local Bubble and it seems to favour the value which is a few times higher than the commonly accepted one.

- It is also interesting to better understand low-energy cosmic rays in the vicinity of their sources and supernova remnants interacting with molecular clouds are ideal laboratories for such an analysis. The particular case of the supernova remnant W28 shall be discussed in depth Chapter 6. This remnant, over the years, has been observed in all energy domains from radio waves to very-high-energy gamma rays. The bright gamma-ray emission detected from molecular clouds located in its vicinity revealed the presence of accelerated GeV and TeV particles in the region. An enhanced ionization rate has also been measured by means of millimeter observations, but such observations alone cannot tell us whether the enhancement is due to low-energy (MeV) cosmic rays (either protons or electrons) or the X-ray photons emitted by the shocked gas. The

goal of this chapter is to determine the origin of the enhanced ionization rate and to infer from multiwavelength observations the spectrum of cosmic rays accelerated at the supernova remnant shock in an unprecedented range spanning from MeV to multi-TeV particle energies. To this end, we developed a model to describe the transport of X-ray photons into the molecular cloud, and we fitted the radio, millimeter, and gamma-ray data to derive the spectrum of the radiating particles. The contribution from X-ray photons to the enhanced ionization rate is negligible, and therefore the ionization must be due to cosmic rays. Even though we cannot exclude a contribution to the ionization rate coming from cosmic-ray electrons, we show that a scenario where cosmic-ray protons explain both the gamma-ray flux and the enhanced ionization rate provides the most natural fit to multiwavelength data. This strongly suggests that the intensity of cosmic-ray protons is enhanced in the region for particle energies in a very broad range covering almost six orders of magnitude: from $\lesssim 100$ MeV up to several tens of TeV.

- We summarize all the main results in the Conclusions and Outlooks. Several potential theoretical investigations in the field of low-energy cosmic rays shall also be outlined.

Chapter 1

Galactic Cosmic Rays

1.1 Introduction to Cosmic Ray Astrophysics

Cosmic rays (CRs) are very energetic particles made up mostly by protons, but there are also electrons and heavy nuclei. These particles were first discovered in 1912 when Victor Hess concluded, from the results of his balloon experiment, that the high level of the ionization rate in the upper atmosphere must be due to ionizing radiations of an extraterrestrial origin. Ever since this starting point of Cosmic Ray Astrophysics, the generation and propagation of these particles have been the subject of intensive research both observationally and theoretically. Despite the remarkable progress that has been made over more than a hundred years of study, these particles are still quite poorly understood and their origin remains one of the greatest challenge in Modern Astrophysics. This is because CRs, unlike photons or neutrinos, could not follow a rectilinear trajectory but rather they are expected to execute random-walk motion due to their interactions with both the Galactic and intergalactic magnetic field and, thus, it is difficult to backtrack the actual positions of their accelerators (Wentzel, 1974; Cesarsky, 1980; Strong et al., 2007).

Research in the field of Cosmic Ray Astrophysics is actually of fundamental importance for many reasons. Since CR interactions with the surrounding medium could produce secondaries like photons and neutrinos observable on Earth, a better understanding of CRs is surely required for an improved insight into the extreme conditions of their sources such as supernova explosions. More importantly, the energy density of CRs is comparable to the ones of the Galactic magnetic field and the thermal gas in the Galactic disk. It is for this reason that they are believed to play an essential role in determining the dynamics of the interstellar medium (ISM) of our Galaxy (see e.g. Parker, 1969). Last but not least, CRs are the only ionizing agent capable of penetrating deep into the densest parts of molecular clouds (MCs) where new stars are born. This means that these energetic particles regulate the level of ionization that controls not only the chemistry of MCs but also the coupling between the gas and the magnetic field which support the cloud against gravity during the process of star formation (Mestel & Spitzer, 1956).

The key quantity for the direct observations of CRs on Earth is the intensity (typically denoted as $j(E)$) which counts the number of CR particles of a particular species with kinetic energy E detected by both ground-based and satellite telescopes per unit of energy, per unit of area, per unit of time, and per unit of solid angle. We have summarized some of the most recent measurements of the intensities in Fig.

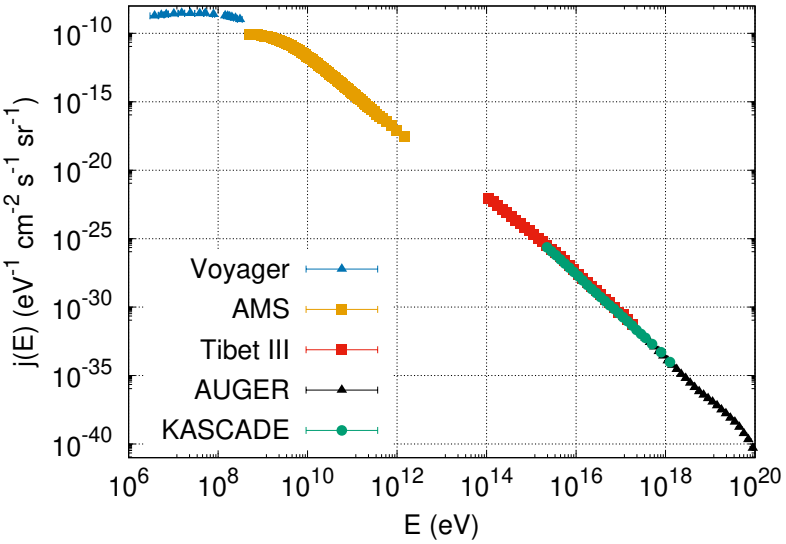

FIGURE 1.1: The intensities of CRs observed on Earth from various collaborations. Data points at high energy are the cosmic-ray intensity of all species from Amenomori et al. (2008) (Tibet III; red squares), Apel et al. (2013) (KASCADE; green filled circles), and Fenu & Pierre Auger Collaboration (2017) (AUGER; black trangles). Data at low energy are the cosmic-ray intensity of protons from Cummings et al. (2016) (Voyager 1; blue triangles) and Aguilar et al. (2015) (AMS 02; yellow squares).

1.1 which includes the data for CRs of energy from a few MeVs to a few hundreds EeV (10^{20} eV). As we can see, the CR intensities are actually quite featureless since they could be described simply by using a few power laws in energy, $j(E) \sim E^{-\delta}$. In particular, we have $\delta \simeq 2.7$ for quite broad energy range from about 10 GeV to roughly 3 PeV. The slope δ suddenly steepens to the value $\delta \simeq 3$ above 3 PeV before flattening back again to $\delta \simeq 2.6$ above 3 EeV. The two energy points where there are transitions in the slope of the CR intensities are typically referred to as the *knee* ($\simeq 3$ PeV) and the *ankle* ($\simeq 3$ EeV). Around the knee, there are observational evidences for a change of the chemical composition of CRs which promotes the idea that this energy actually marks the maximum achievable energy for protons accelerated by the Galactic sources and the slope above the knee is created by the successive cut-offs[1] in the spectrum of heavier CR nuclei (Hörandel, 2008). It is then quite natural to characterize the ankle as the transition from Galactic to extragalactic CRs which is also supported from the fact that these particles of energy above 3 EeV are hard to be confined by the Galactic magnetic field since their gyroradii (with typical value of the galactic magnetic field) are of the same order or even larger than the thickness of the Galactic disk. So far, these are simply the possible interpretations of the CR intensities above 10 GeV and more works are needed for a more conclusive picture.

Cosmic rays of energy below a few GeVs are also of great interest for astrophysicists. However, the progress on the study of these particles was tremendously

[1]Notice that theories of CR acceleration generally predicts that the maximum achievable energy of CRs of species a is Z_a times to that of protons meaning $E_a^{\max} = Z_a E_p^{\max}$ where Z_a is the corresponding atomic number of species a.

hindered in the past mostly because the observations of CRs of energy below approximately 30 GeV are, in general, obscured due to the interactions of these particles with the solar wind. In particular, the intensities of Galactic CRs at low energy would suffer significant spatial and temporal modifications at different positions inside the heliosphere (this phenomenon is commonly referred to as the solar modulation of CRs, see e.g. Potgieter, 2013). It is not until quite recently that the community of Cosmic Ray Astrophysics started to devote more attention to the low-energy component of Galactic CRs thanks to the availability of new data over the past 20 years which, in fact, has drastically changed the pictures and increased a lot the information we have about these low-energy particles. Remarkably, since the two space probes known as Voyager 1 and 2 have recently entered the region at a distance more than 120 AU from the Sun, they are now observing, for the first time, the intensities of low-energy CRs beyond the heliopause (see the Voyager data in Fig. 1.1). Although it is still debated whether or not these CRs are really from the local ISM, these direct observations should provide us with a good starting point for a more insightful study of low-energy CRs (Cummings et al., 2016; Stone et al., 2019).

Having established some of the basics of Cosmic Ray Astrophysics from direct measurements of the CR intensities, we shall now proceed to further discuss some of the crucial observational constraints for these particles with a concentration on the energy range below the knee. We shall first provide some more data on the chemical composition of CRs and illustrate how they could teach us an interesting lesson about the propagation and confinement of CRs within the Galactic disk. Once the residence time of CRs in the Galactic disk is known, we could proceed to make some educated guesses about the possible sources of these particles

1.1.1 Cosmic-Ray Propagation in the Galaxy

Since the nature of CR transport could be revealed by studying their chemical composition, we shall start our discussion with the data on the abundances of CRs observed on Earth. Let's first limit ourselves to CRs in the GeV energy range as these particles carry the bulk of the total energy in CRs (as could be computed from the intensities) and also the chemical composition of CRs in this energy range is well determined from observations. From direct measurements, we know that only about 1% of the CRs observed on Earth are electrons and the rest are atomic nuclei of which 89% are protons, 10% are Helium, and roughly 1% are heavier nuclei. The relative abundances of CRs and of elements in the solar system are shown in Fig. 1.2. It is quite straightforward to see that nuclei with even Z (where Z is the corresponding atomic number) are, in general, more abundant than the one with odd Z for both CRs and matters of the solar system. This could be understood as a manifestation of the odd-even effect which suggests that nuclei with even Z are usually more tightly bound and, thus, more stable.

Another striking feature, as we can see in Fig. 1.2, is the overabundance in CRs of the two groups of elements Li, Be, B and Sc, Ti, V, Cr, Mn whose relative abundances are many orders of magnitude higher than the ones of the solar system.

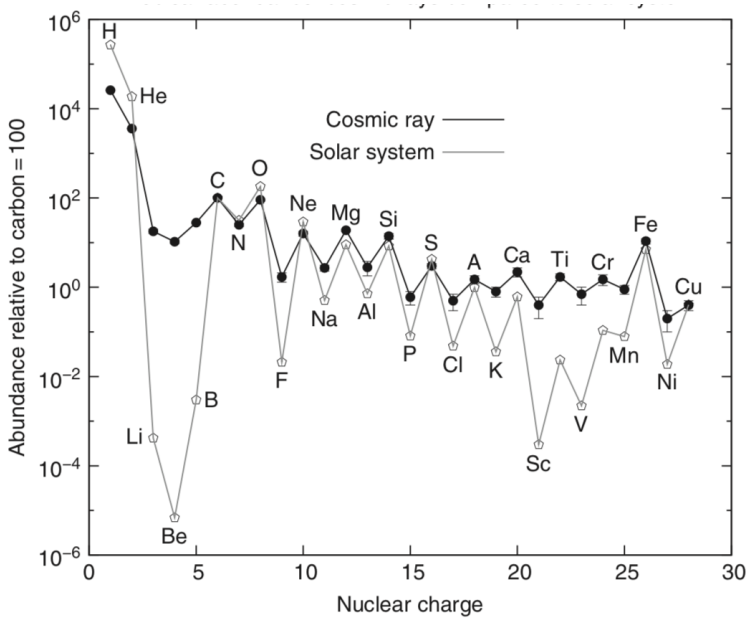

FIGURE 1.2: The chemical abundances of CRs (filled circles) in comparison with the solar system abundances (open cricles), all relative to carbon=100 (adopted from Gaisser, 1990).

Since these elements could not be efficiently produced during the process of stellar nucleosynthesis, they do not exist in large amount in the solar system. Nevertheless, the abundances of CR nuclei from the two groups of elements presented above could be explained if these particles are not accelerated at the CR sources but rather they are *secondary* products created from the *spallative reactions* between *primary* CR nuclei and the gas of the ISM. In this scenario, the rate of change for the intensity of any purely secondary CR species $j_s(E)$ should be governed by the rate of production from the intensity of primary CRs $j_p(E)$ and the rate of escape due to CR transport and, thus, we should have:

$$\frac{\mathrm{d}j_s(E)}{\mathrm{d}t} = j_p(E) n_{ISM} \sigma_s c - \frac{j_s(E)}{\tau_{res}}, \tag{1.1}$$

where σ_s is the relevant spallative cross-section, c is the speed of light (assuming CR particles are relativistic), and τ_{res} is the residence of secondary CRs in the Galactic disk. If the intensity of secondary CRs is in steady state, we could relate the residence time to the ratio between intensities of secondary and primary CRs as:

$$\tau_{res} = \frac{j_s(E)}{j_p(E) n_{ISM} \sigma_s c}. \tag{1.2}$$

Since σ_s is known with high precision from accelerator experiments for Particle Physics, $j_s(E)/j_p(E)$ could be directly observed on Earth, and n_{ISM} is expected to be about one proton per cubic centimeter in the Galactic disk, we could deduce, for example from the B/C ratio, $\tau_{res}(E = 1 \text{ GeV}) \simeq 3$ Myr. It is should be stressed

that the propagation time deduced in this way is much longer then the time for a CR of energy 1 GeV to cross the size of the Galaxy if it simply moves on a straight line. This simple argument provided by the data of the chemical composition of CRs has, therefore, allowed us to conclude that *the transport of CRs in the Galaxy is diffusive*.

The diffusion of CRs in the Galaxy is believed to be due to the interactions of these particles with the random fluctuations of the Galactic magnetic field. From a theoretical point of view, these random components of the field (typically referred to as the *magnetic turbulence*) could be treated as the superposition of plasma waves each with their own random phases and the diffusive motion of CRs emerges naturally from the frequent interactions of CRs with these waves. We shall elaborate further on this point in Section 1.2 which is dedicated for the formulation of the framework commonly used in modeling CR transport known as *Quasi-Linear Theory* (QLT). For now, it is sufficient to note that the diffusion coefficient from QLT is typically predicted to be of the following form $D = D_0\beta(R/R_0)^\alpha$ where D_0 is a normalization factor, β is the ratio between the particle's speed and the speed of light, and R is the particle rigidity[2]. Given the current data on the B/C ratio, the best fit for the diffusion coefficient gives $D_0 \simeq 1.1 \times 10^{28}$ cm^2/s, $R_0 = 1$ GV, and $\alpha = 0.63$ for $R < R_b \simeq 300$ GV. For $R > R_b$, the slope of the diffusion coefficient changes to $\alpha \simeq 0.45$ (Génolini et al., 2017) and the origin of this transition is still debated (see e.g. Gabici et al., 2019, and references therein). As a remark, we note that this break could be explained by employing different mechanisms responsible for the generation of magnetic turbulence. In particular, the turbulence could be excited by the motion of CRs themselves via the streaming instability in the low-energy range ($R < R_b$) and, for high-energy CRs ($R > R_b$), it is resulted from the cascade of the turbulence injected at large spatial scale, for example due to supernova bubbles (Blasi et al., 2012).

1.1.2 Possible Sources of Galactic Cosmic Rays

One of the best strategies to select the potential sources of Galactic CRs is to start with some estimates on the energetics. From the intensities of CRs observed on Earth, we know that the energy density of CRs is about $\rho_{CR} = 1$ eV/cm^3 and, as mentioned above, most of this energy is carried by CR protons and helium nuclei with kinetic energy of a few GeVs. Since gamma ray surveys of MCs seem to indicate that, above a few GeVs, the CR spectrum is quite uniform in our Galaxy (Yang et al., 2014), we shall take $\rho_{CR} = 1$ eV/cm^3 as the representative value over the whole Galactic disk. We could now estimate the power required to keep this energy density in the Galactic disk by using the residence time $\tau_{res}(E = 1\text{ GeV})$ evaluated in the previous subsection:

$$P_{CR} = \frac{\rho_{CR} V_{disk}}{\tau_{res}(E = 1\text{ GeV})} \simeq 3 \times 10^{48}\text{ erg/yr} \tag{1.3}$$

[2]The rigidity of a particle is $R = pc/(Ze)$, where p is the particle momentum, c is the speed of light, Z is the atomic number of the particle, and e is the elementary charge.

where we have taken the radius of the disk to be 15 kpc and the height, as indicated above, is about 300 pc. There are only a few classes of objects in the Galaxy that could accommodate such power and supernova explosions are one of them as first suggested by Baade & Zwicky (1934). Since the rate of supernova explosions is about three per century and the mechanical energy released in these explosions is roughly 10^{51} erg, the power injected into the ISM for these sources is about 3×10^{49} erg/yr which means that an efficiency of energy conversion of only 10% would be sufficient for the power requirement of CRs.

It is believed that the conversion of the supernovae kinetic energy into CR energy proceeds via a mechanism called *diffusive shock acceleration* (also known as *first order Fermi acceleration*). The process of acceleration takes place thanks to the shock created by the expanding supernova shell commonly referred to as the *supernovae remnant* (SNR). In this case, it is also the magnetic turbulence that scatters CRs back and forth around the shock and, for each passage, particles gain an amount of energy roughly proportional to u/v where u and v are respectively the speed of the shock and the particle (Axford et al., 1977; Krymskii, 1977; Bell, 1978; Blandford & Ostriker, 1978). It can be proven that, in the case where no feedback of CRs either on the shock structure or on the magnetic field of the supernovae is considered, the intensity of accelerated particles around the shock would be $j_{acc}(E) \sim E^{-\nu}$ with $\nu = 2$ for strong shock ($u \gg c_s$ where c_s is the sound speed in the surrounding ISM). When nonlinear effects are included, we could expect a steepening in the intensity of accelerated particles which should give the slope $\nu = 2.1 - 2.4$ (see e.g. Gabici et al., 2019, and references therein). Also, it is important to note that the intensity of accelerated CRs around the shock and the intensity of CRs injected into the ISM do not necessarily have the same slope. Theoretical investigations, however, indicate that the shape of the intensity remains unchanged when CRs are released from the acceleration region.

Since the combination of the injection intensity from the theory of shock acceleration and the diffusion coefficient constrained from observational data could satisfactorily reproduce the shape of the intensities observed on Earth, the picture in which SNRs are the principal sources of CRs are commonly accepted as the standard paradigm in Cosmic Ray Astrophysics. Indeed, there are still many challenges remained before some conclusive arguments could be made. The interested readers are referred to the recent review by Gabici et al. (2019) for a more thorough discussion.

1.2 Quasi-Linear Theory for Cosmic-Ray Transport

We shall continue our story by the formal derivation of the CR transport equation in the framework of QLT commonly used in modeling both the propagation and acceleration of CRs. The procedure introduced here was first proposed around 50 years ago with the pioneering works by Jokipii (1966), Kennel & Engelmann (1966), and Lerche (1968), and Kulsrud & Pearce (1969). In this thesis, we provide only the formal derivation in a simplified setup suitable for later discussions. The interested readers are referred to standard textbooks such as in Berezinskii et al. (1990) or

Schlickeiser (2002) for a more general picture of QLT. Conceptually speaking, QLT relies on a perturbative approach which means that it should strictly be applicable only in the case where the strength of turbulence is much smaller than that of the mean field and this is not always the case for astrophysical systems. However, it has been argued that this is not the only problem of QLT and, in fact, it suffers from a few more problems which concern the transport of CRs with pitch angle close to 90° and also the diffusion perpendicular to the mean field (Shalchi, 2009). Although there exists many peculiarities that seems to make its validity questionable, it is still the most widely accepted framework for studying the transport of CRs so far.

In this section, we shall first present the concept of the distribution function of CRs together with all the fundamental equations upon which the equation of CR transport is built. We then go though a few layers of approximations to obtain different forms of the transport equation. At the end of this chapter, we will arrive at the advection-diffusion equation which shall be the basis of the analysis of CR transport into MCs in Chapter 3 and also the study of Galactic CR spectra in Chapter 4.

1.2.1 The Quasi-Linear Approximation

Let's consider a system consisting of CRs from various species (protons, electrons, Helium, and so on) and a background plasma which represents the ISM. For simplicity, we could assume that the background plasma is at rest (no large-scale motion) and also it is made up by only protons and electrons. This means that the state of the background plasma is determined and we are only interested in the evolution of the CR population.

Since we seek for a statistical description of a large number of CR particles, we shall first define a probability distribution function $f_a(\mathbf{x}, \mathbf{p}, t)$ for particles of species a at the position $\mathbf{x}$ with momentum $\mathbf{p}$ at time t, also referred to as the phase space density. This function should be defined such that the quantity $f_a(\mathbf{x}, \mathbf{p}, t)\,\mathrm{d}^3\mathbf{x}\,\mathrm{d}^3\mathbf{p}$ gives the number of particles of species a within the infinitesimal phase space volume $\mathrm{d}^3\mathbf{x}\,\mathrm{d}^3\mathbf{p}$ at time t. For a collisionless plasma which is quite common in the context of Cosmic Ray Astrophysics, the distribution function should follow the Vlasov equation:

$$\frac{\partial f_a}{\partial t} + \mathbf{v}\cdot\frac{\partial f_a}{\partial \mathbf{x}} + q_a\left[\mathbf{E}(\mathbf{x},t) + \frac{\mathbf{v}\times\mathbf{B}(\mathbf{x},t)}{c}\right]\cdot\frac{\partial f_a}{\partial \mathbf{p}} = S(\mathbf{r},\mathbf{p},t), \tag{1.4}$$

where q_a is the charge of a particle of species a, $\mathbf{v}$ is the corresponding velocity of a particle of species a with momentum $\mathbf{p}$, $\mathbf{E}$ and $\mathbf{B}$ are respectively the average electric and magnetic field, and $S(\mathbf{x}, \mathbf{p}, t)$ represents all the additional sources and sinks of CR particles. Let's first concentrate on the case where there are no external sources or sinks meaning setting the RHS of Eq. 1.4 to zero. The electromagnetic

field in Eq. 1.4 could be described using the Maxwell's equations:

$$\nabla \times \mathbf{B} = \frac{1}{c}\frac{\partial \mathbf{E}}{\partial t} + \frac{4\pi}{c}\sum_a q_a \int \mathrm{d}^3\mathbf{p} f_a(\mathbf{x},\mathbf{p},t)\mathbf{v}, \tag{1.5}$$

$$\nabla \cdot \mathbf{B} = 0, \tag{1.6}$$

$$\nabla \times \mathbf{E} = -\frac{1}{c}\frac{\partial \mathbf{B}}{\partial t}, \tag{1.7}$$

$$\nabla \cdot \mathbf{E} = 4\pi \sum_a q_a \int \mathrm{d}^3\mathbf{p} f_a(\mathbf{x},\mathbf{p},t). \tag{1.8}$$

Solving together the Vlasov equation and the Maxwell's equations is quite a daunting task. To proceed, we shall assume that the distribution function and the electromagnetic fields are composed of a zeroth-order component which varies slowly in time and a first-order component that evolves more rapidly (sometimes referred to as the *quasi-linear approximation*):

$$f_a(\mathbf{x},\mathbf{p},t) = f_a^{(0)}(\mathbf{x},\mathbf{p},t) + f_a^{(1)}(\mathbf{x},\mathbf{p},t), \tag{1.9}$$

$$\mathbf{E}(\mathbf{x},t) = \mathbf{E}_0(\mathbf{x},t) + \mathbf{E}_1(\mathbf{x},t), \tag{1.10}$$

$$\mathbf{B}(\mathbf{x},t) = \mathbf{B}_0(\mathbf{x},t) + \mathbf{B}_1(\mathbf{x},t). \tag{1.11}$$

The fields $\mathbf{E}_1$ and $\mathbf{B}_1$ are sometimes referred to as the turbulent field and, indeed, different *initial conditions* of these fields would lead to different values of the $f_a^{(1)}(\mathbf{x},\mathbf{p},t)$. However, we are, in general, not interested in the small variation of the distribution function and also the initial conditions for the turbulent fields could not be specified in real physical problems. It is, therefore, more reasonable to consider an ensemble of realizations of the turbulent fields, each of them with their own initial conditions, and study $f_a^{(0)}$ by requiring that all the fluctuating first-order part should vanish over the ensemble average meaning $\langle f_a^{(1)}\rangle = 0$, $\langle \mathbf{E}_1\rangle = \mathbf{0}$, and $\langle \mathbf{B}_1\rangle = \mathbf{0}$. For our purposes, it is sufficient to focus on the system where $\mathbf{E}_0 = \mathbf{0}$ (which should be justified by the high conductivity in astrophysical plasmas) and $\mathbf{B}_0$ is uniform in space and time. Inserting the above expansion into the Vlasov equation and taking the ensemble average to obtain separate equations for zeroth-order and first-order quantities, we shall have:

$$\frac{\partial f_a^{(0)}}{\partial t} + \mathbf{v}\cdot\frac{\partial f_a^{(0)}}{\partial \mathbf{x}} + q_a\frac{\mathbf{v}\times\mathbf{B}_0}{c}\cdot\frac{\partial f_a^{(0)}}{\partial \mathbf{p}} = -\left\langle q_a\left(\mathbf{E}_1 + \frac{\mathbf{v}\times\mathbf{B}_1}{c}\right)\cdot\frac{\partial f_a^{(1)}}{\partial \mathbf{p}}\right\rangle, \tag{1.12}$$

$$\frac{\partial f_a^{(1)}}{\partial t} + \mathbf{v}\cdot\frac{\partial f_a^{(1)}}{\partial \mathbf{x}} + q_a\frac{\mathbf{v}\times\mathbf{B}_0}{c}\cdot\frac{\partial f_a^{(1)}}{\partial \mathbf{p}} = -q_a\left(\mathbf{E}_1 + \frac{\mathbf{v}\times\mathbf{B}_1}{c}\right)\cdot\frac{\partial f_a^{(0)}}{\partial \mathbf{p}}. \tag{1.13}$$

It is interesting to note that the rate of change in time of $f_a^{(0)}$ is actually a second-order quantity as we could see from the RHS of Eq. 1.12 which is consistent with the assumption of the perturbative approach. The quasi-linear approximation also

allows us to obtain the linearized form of Maxwell's equations:

$$\nabla \times \mathbf{B}_1 = \frac{1}{c}\frac{\partial \mathbf{E}_1}{\partial t} + \frac{4\pi}{c}\sum_a q_a \int \mathrm{d}^3\mathbf{p} f_a^{(1)}(\mathbf{x},\mathbf{p},t)\mathbf{v}, \tag{1.14}$$

$$\nabla \cdot \mathbf{B}_1 = 0, \tag{1.15}$$

$$\nabla \times \mathbf{E}_1 = -\frac{1}{c}\frac{\partial \mathbf{B}_1}{\partial t}, \tag{1.16}$$

$$\nabla \cdot \mathbf{E}_1 = 4\pi \sum_a q_a \int \mathrm{d}^3\mathbf{p} f_a^{(1)}(\mathbf{x},\mathbf{p},t). \tag{1.17}$$

We shall now continue by finding the formal solution of $f_a^{(1)}$ in terms of $f_a^{(0)}$, $\mathbf{E}_1$, and $\mathbf{B}_1$ and inserting it into Eq. 1.12 to arrive at the closed differential equation for $f_a^{(0)}$. Let's now perform the Laplace-Fourier expansion for all the first-order quantities:

$$f_a^{(1)}(\mathbf{x},\mathbf{p},t) = \int \mathrm{d}\omega \int_{-\infty}^{\infty} \mathrm{d}^3\mathbf{k} e^{i(\mathbf{k}\cdot\mathbf{x}-\omega t)} \delta f_a(\mathbf{k},\mathbf{p},\omega), \tag{1.18}$$

$$\mathbf{E}_1(\mathbf{x},t) = \int \mathrm{d}\omega \int_{-\infty}^{\infty} \mathrm{d}^3\mathbf{k} e^{i(\mathbf{k}\cdot\mathbf{x}-\omega t)} \delta \mathbf{E}(\mathbf{k},\omega), \tag{1.19}$$

$$\mathbf{B}_1(\mathbf{x},t) = \int \mathrm{d}\omega \int_{-\infty}^{\infty} \mathrm{d}^3\mathbf{k} e^{i(\mathbf{k}\cdot\mathbf{x}-\omega t)} \delta \mathbf{B}(\mathbf{k},\omega). \tag{1.20}$$

We should note that ω is, in general, a complex number $\omega = \omega_r + i\Gamma$ and the integration has to be from $-\infty + iC$ to $\infty + iC$ with C is a constant chosen sufficiently positive that the Laplace integral converges (see e.g. Schlickeiser, 2002). In a sense, these expansions represents the fact that the fluctuations of the electromagnetic fields could be decomposed into waves of different frequency ω and wave vector $\mathbf{k}$. Inserting these Fourier-Laplace transform into Eq. 1.13 and Eq. 1.16, we shall have:

$$ic\mathbf{k} \times \delta\mathbf{E} = i\omega\delta\mathbf{B}, \tag{1.21}$$

$$i\left(\omega + \mathbf{v}\cdot\mathbf{k}\right)\delta f_a + q_a \frac{\mathbf{v}\times\mathbf{B}_0}{c}\cdot\frac{\partial \delta f_a}{\partial \mathbf{p}} = -q_a\left(\delta\mathbf{E} + \frac{\mathbf{v}\times\delta\mathbf{B}}{c}\right)\cdot\frac{\partial f_a^{(0)}}{\partial \mathbf{p}}. \tag{1.22}$$

It should be noted that we have neglected all the terms that contain the initial conditions of the electromagnetic fields since they would vanish once inserted into the ensemble average on the RHS of Eq. 1.12. At this point, it should be more convenient to choose the coordinate system such that $\mathbf{B}_0$ is in the z-direction. We shall introduce also the components of the momentum vector $\mathbf{p}$ and the wave vector $\mathbf{k}$ in this system as follows:

$$p_x = p_\perp \cos\phi, \qquad p_y = p_\perp \sin\phi, \qquad p_z = p_\parallel, \tag{1.23}$$

$$k_x = k_\perp \cos\psi, \qquad k_y = k_\perp \sin\psi, \qquad k_z = k_\parallel. \tag{1.24}$$

With this choice, we may simplify the operator in the second term of Eq. 1.22 into:

$$q_a \frac{\mathbf{v}\times\mathbf{B}_0}{c}\cdot\frac{\partial}{\partial \mathbf{p}} = -\Omega_a \frac{\partial}{\partial \phi}, \tag{1.25}$$

where $\Omega_a = q_a B_0/(\gamma m_a c)$ which is the relativistic gyrofrequency of a particle of species a. Combining Eq. 1.21, Eq. 1.22, and Eq. 1.25, we shall arrive at the following equation for $\delta f_a(\mathbf{k}, \mathbf{p}, \omega)$:

$$\frac{\partial \delta f_a}{\partial \phi} - \frac{i\left(\omega + \mathbf{v}\cdot\mathbf{k}\right)}{\Omega_a}\delta f_a = \frac{q_a}{\Omega_a}\left[\delta\mathbf{E} + \frac{\mathbf{v}\times\left(\mathbf{k}\times\delta\mathbf{E}\right)}{\omega}\right]\cdot\frac{\partial f_a^{(0)}}{\partial \mathbf{p}}, \tag{1.26}$$

which could easily be solved to give:

$$\delta f_a(\mathbf{k}, \mathbf{p}, \omega) = \frac{q_a}{\Omega_a}\int_{\infty \mathrm{sign}(\Gamma)}^{\phi} \mathrm{d}\phi' \left[\delta\mathbf{E} + \frac{\mathbf{v}'\times\left(\mathbf{k}\times\delta\mathbf{E}\right)}{\omega}\right]\cdot\frac{\partial f_a^{(0)}}{\partial \mathbf{p}'} \exp\left\{\frac{i\left(k_\parallel v_\parallel - \omega\right)\left(\phi - \phi'\right) + i k_\perp v_\perp\left[\sin\left(\phi - \psi\right) - \sin\left(\phi' - \psi\right)\right]}{\Omega_a}\right\}, \tag{1.27}$$

where $\mathbf{v}' = (v_\perp \cos\phi', v_\perp \sin\phi', v_\parallel)$ and $\mathbf{p}' = (p_\perp \cos\phi', p_\perp \sin\phi', p_\parallel)$. We note that the lower limit of the integral has been chosen to be $\phi \to \infty\mathrm{sign}(\Gamma)$ since, in this limit, $\delta f(\mathbf{k}, \mathbf{p}, \omega)$ tends to zero. We refer the interested readers to Chapter 8 and Appendix B of the monograph by Schlickeiser (2002) for a more detailed discussion on this choice. It should be noted, however, that this quantity would not appear in our final equation for $f_a^{(0)}$. It would be more convenient to decompose the fields into components of different polarizations and we shall adopt the following notation:

$$\delta E_L = \delta E_x + i\delta E_y, \tag{1.28}$$

$$\delta E_R = \delta E_x - i\delta E_y, \tag{1.29}$$

where L and R stand for the left- and right-handed polarizations respectively. We now could rewrite the electric field as $\delta\mathbf{E} = \left(\left(\delta E_R + \delta E_L\right)/2, i\left(\delta E_R - \delta E_L\right)/2, \delta E_\parallel\right)$. In order to proceed and perform the integration over ϕ', we shall assume that $f_a^{(0)}(\mathbf{x}, \mathbf{p}, t) = f_a^{(0)}(\mathbf{x}, p_\perp, p_\parallel, t)$ meaning the zeroth-order component of the distribution function is independent of ϕ (a reasonable approximation in the limit of weak turbulent electromagnetic field, see Kulsrud & Pearce, 1969 and references therein for more details). The integration over ϕ' could now be carried on by making use of the following Bessel-function identities:

$$\exp\left[i\frac{k_\perp v_\perp}{\Omega_a}\sin(\phi - \psi)\right] = \sum_{m=-\infty}^{\infty} J_m\left(\frac{k_\perp v_\perp}{\Omega_a}\right) e^{im(\phi-\psi)}, \tag{1.30}$$

$$\exp\left[-i\frac{k_\perp v_\perp}{\Omega_a}\sin(\phi' - \psi)\right] = \sum_{n=-\infty}^{\infty} J_n\left(\frac{k_\perp v_\perp}{\Omega_a}\right) e^{-in(\phi'-\psi)}. \tag{1.31}$$

We shall from now on abbreviate $J_m(k_\perp v_\perp/\Omega_a)$ simply as J_m. The resulting expression for $\delta f(\mathbf{k},\mathbf{p},\omega)$ is then:

$$\delta f(\mathbf{k},\mathbf{p},\omega) = -iq_a\Omega_a \sum_{m,n=-\infty}^{\infty} \frac{J_m e^{i(m-n)(\phi-\psi)}}{\omega - k_\parallel v_\parallel - n\Omega_a} \left(\delta E_\perp \mathcal{P}_{a,\perp} + \delta E_\parallel J_n \mathcal{P}_{a,\parallel}\right) f_a^{(0)}, \quad (1.32)$$

where

$$\delta E_\perp = \frac{1}{2}\left(\delta E_R e^{i\psi} J_{n+1} + \delta E_L e^{-i\psi} J_{n-1}\right), \quad (1.33)$$

$$\mathcal{P}_{a,\perp} = \left(1 - \frac{k_\parallel v_\parallel}{\omega}\right)\frac{\partial}{\partial p_\perp} + \frac{k_\parallel v_\perp}{\omega}\frac{\partial}{\partial p_\parallel}, \quad (1.34)$$

$$\mathcal{P}_{a,\parallel} = \frac{v_\parallel}{v_\perp}\frac{n\Omega_a}{\omega}\frac{\partial}{\partial p_\perp} + \left(1 - \frac{n\Omega_a}{\omega}\right)\frac{\partial}{\partial p_\parallel}. \quad (1.35)$$

Inserting Eq. 1.32 into the RHS of Eq. 1.12 and perform the Laplace-Fourier transform for $\mathbf{E}_1$ and $\mathbf{B}_1$ (notice also Eq. 1.25), we shall have:

$$\begin{aligned}
&\frac{\partial f_a^{(0)}}{\partial t} + \mathbf{v}\cdot\frac{\partial f_a^{(0)}}{\partial \mathbf{x}} \\
&\quad = iq_a^2 \left\langle \int \mathrm{d}\varepsilon\, \mathrm{d}^3\mathbf{q} e^{-i(\mathbf{q}\cdot\mathbf{x}-\varepsilon t)} \left[\delta\mathbf{E}^*(\mathbf{q},\varepsilon) + \frac{\mathbf{v}\times(\mathbf{q}\times\delta\mathbf{E}(\mathbf{q},\varepsilon))}{\varepsilon}\right]\cdot\frac{\partial}{\partial\mathbf{p}} \right. \\
&\quad \left. \int \mathrm{d}\omega\, \mathrm{d}^3\mathbf{k} e^{i(\mathbf{k}\cdot\mathbf{x}-\omega t)} \sum_{m,n=-\infty}^{\infty} \frac{J_m e^{i(m-n)(\phi-\psi)}}{\omega - k_\parallel v_\parallel - n\Omega_a}\left(\delta E_\perp \mathcal{P}_{a,\perp} + \delta E_\parallel J_n \mathcal{P}_{a,\parallel}\right) f_a^{(0)} \right\rangle .
\end{aligned} \quad (1.36)$$

At this point, if we write down the explicit form of all the operators on the RHS of the above equation, we will encounter quantities of type $\langle \delta E_i^*(\mathbf{q},\varepsilon)\delta E_j(\mathbf{k},\omega)\rangle$ $(i,j = x,y,z)$ which are components of the so-called correlation tensor $\langle \delta\mathbf{E}^*(\mathbf{q},\varepsilon)\delta\mathbf{E}(\mathbf{k},\omega)\rangle$. In principle, the analysis of this tensor requires a proper discussion on the plasma waves which is not particularly relevant within the scope of this thesis. Therefore, we shall simply adopt the results that have been provided in the past literature to further simplify Eq. 1.36. The interested readers are referred to Chapter 8 of the monograph by Schlickeiser, 2002 and references therein for more details (see also Kulsrud & Pearce, 1969).

For now, we might proceed by noticing that the correlation tensor is typically of the following form:

$$\langle \delta\mathbf{E}^*(\mathbf{q},\varepsilon)\delta\mathbf{E}(\mathbf{k},\omega)\rangle \sim \delta(\mathbf{q}-\mathbf{k})\delta(\varepsilon-\omega), \quad (1.37)$$

which should allow us to simplify the integration over $\mathbf{q}$ and ε together with the exponential factor $\exp\left[i(\mathbf{k}-\mathbf{q})\cdot\mathbf{x} - i(\omega-\varepsilon)t\right]$

Notice that although we have assumed $f_a^{(0)}$ is independent of ϕ, $f_a^{(1)}$ still depends on ϕ (as could be seen from the factor $e^{i(m-n)(\phi-\psi)}$ in the expression for $\delta f(\mathbf{k},\mathbf{p},\omega)$). This means that we should keep all the terms that contain the partial derivative

in ϕ while applying the operator $\partial/\partial\mathbf{p}$ to $f_a^{(1)}$ in the above equation. Since $f_a^{(0)}$ is independent of ϕ, we might take the average of Eq. 1.36 over the angle ϕ and simplify it into:

$$\frac{\partial f_a^{(0)}}{\partial t} + v_\parallel \frac{\partial f_a^{(0)}}{\partial z} = iq_a^2 \int \mathrm{d}\omega\, \mathrm{d}^3\mathbf{k} \frac{1}{2\pi} \int_0^{2\pi} \mathrm{d}\phi \left\langle \left[\delta\mathbf{E}^*(\mathbf{k},\omega) + \frac{\mathbf{v}\times(\mathbf{k}\times\delta\mathbf{E}^*(\mathbf{k},\omega))}{\omega^*} \right] \cdot \frac{\partial}{\partial\mathbf{p}} \sum_{m,n=-\infty}^{\infty} \frac{J_m e^{i(m-n)(\phi-\psi)}}{\omega - k_\parallel v_\parallel - n\Omega_a} \left(\delta E_\perp \mathcal{P}_{a,\perp} + \delta E_\parallel J_n \mathcal{P}_{a,\parallel}\right) f_a^{(0)} \right\rangle . \tag{1.38}$$

For simplicity, we shall neglect the imaginary part of ω meaning to assume that $\Gamma \ll \omega_r$ and approximate the Breit-Wigner type resonance function with the δ-function representation (this approximation is sometimes referred to as the *resonant diffusion limit*):

$$\frac{1}{\omega - k_\parallel v_\parallel - n\Omega_a} = -i\pi\delta\left(\omega_r - k_\parallel v_\parallel - n\Omega_a\right) \tag{1.39}$$

At this point, it is straightforward to perform the integration over ϕ and take the sum over m which leaves us with the gyrophase-averaged equation for $f_a^{(0)}(\mathbf{x}, p_\perp, p_\parallel, t)$ in the resonant diffusion limit:

$$\frac{\partial f_a^{(0)}}{\partial t} + v_\parallel \frac{\partial f_a^{(0)}}{\partial z} = \pi q_a^2 \int_{-\infty}^{\infty} \mathrm{d}\omega_r \int_{-\infty}^{\infty} \mathrm{d}^3\mathbf{k} \sum_{n=-\infty}^{\infty} \left\langle \left\{ \left[\mathcal{P}_{a,\perp} + \frac{1}{p_\perp}\left(1 - \frac{k_\parallel v_\parallel}{\omega_r}\right) \right] \delta E_\perp^* + \mathcal{P}_{a,\parallel} \delta E_\parallel^* J_n \right\} \delta\left(\omega_r - k_\parallel v_\parallel - n\Omega_a\right) \left(\delta E_\perp \mathcal{P}_{a,\perp} + \delta E_\parallel J_n \mathcal{P}_{a,\parallel}\right) f_a^{(0)} \right\rangle \tag{1.40}$$

The above equation has been first introduced by Lerche, 1968 for a system of relativistic plasma (see also Kennel & Engelmann, 1966, for a similar approach in the non-relativistic case). Since the whole procedure has started with the quasilinear approximation, this framework is commonly referred to as *Quasi-Linear Theory*.

1.2.2 Pitch Angle Diffusion

Further simplification at this stage requires some more assumptions on the correlation tensor. In principal, this tensor should have the contribution from all the *modes* of plasma waves since the turbulent electric field could be treated as the superposition of waves of different plasma wave modes. Each of these modes is represented

by their respective dispersion relation $\omega_\alpha(\mathbf{k})$ (see Chapter 8 of Schlickeiser, 2002, for a discussion on kinetic theory of plasma waves).

In astrophysical environments such as in the ISM or SNRs, we shall focus essentially on the Alfvén wave modes propagating parallel and antiparallel to the ordered magnetic field (from now on referred to as forward and backward waves) since these waves have the shortest growth times (Schlickeiser, 1989). The dispersion relations of these modes are:

$$\omega_\pm = \pm |k_\parallel| v_A, \tag{1.41}$$

where the sign '+' and '−' are for the forward and backward waves respectively and, in the fully ionized background plasma made up mostly by protons and electrons, we shall have the Alfvén speed as:

$$v_A = \frac{B_0}{\sqrt{4\pi n_i m_p}}, \tag{1.42}$$

with n_i is the number density of protons in the plasma and m_p is the mass of proton. By restricting ourselves to the parallel propagating Alfvén modes and noticing that $k_\perp = 0$ and $\delta E_\parallel = 0$, Eq. 1.40 could be re-written in a more elegant form:

$$\begin{aligned}
&\frac{\partial f_a^{(0)}}{\partial t} + v\mu \frac{\partial f_a^{(0)}}{\partial z} \\
&\quad = \frac{\pi^2 q_a^2 v_A^2}{p^2 c^2} \sum_\alpha \int_{-\infty}^{\infty} \mathrm{d}\omega_r \int_{-\infty}^{\infty} \mathrm{d}k_\parallel \delta(\omega_r - \omega_\alpha(\mathbf{k})) \left[\frac{\partial}{\partial p} p + \frac{\partial}{\partial \mu} \left(\frac{k_\parallel v}{\omega_r} - \mu \right) \right] \\
&\qquad \left\{ \left(1-\mu^2\right) \left[I_R^\alpha(k_\parallel) \delta\left(\omega_r - k_\parallel v_\parallel + \Omega_a\right) + I_L^\alpha(k_\parallel) \delta\left(\omega_r - k_\parallel v_\parallel - \Omega_a\right) \right] \right\} \\
&\qquad\qquad \left[\frac{\partial}{\partial p} + \frac{1}{p} \left(\frac{k_\parallel v}{\omega_r} - \mu \right) \frac{\partial}{\partial \mu} \right] f_a^{(0)}
\end{aligned} \tag{1.43}$$

where $p = \sqrt{p_\perp^2 + p_\parallel^2}$, $\mu = p_\parallel / p$, and v is the speed of a particle of species a with momentum p. It should be noted that the sum over α arises from both the forward and backward Alfvén wave modes. Also, we have introduced $I_{R,L}^\alpha(k_\parallel)$ which is the power spectrum of the forward ($\alpha = +$) and backward ($\alpha = -$) waves with right-hand or left-hand polarization:

$$\begin{aligned}
&\int_{-\infty}^{\infty} \mathrm{d}k_\parallel I_{R,L}^\alpha(k_\parallel) \int_{-\infty}^{\infty} \mathrm{d}\omega_r \delta(\omega_r - \omega_\alpha(\mathbf{k})) \\
&\qquad = \frac{c^2}{v_A^2} \int_{-\infty}^{\infty} \mathrm{d}\omega_r \int_{-\infty}^{\infty} \mathrm{d}^3\mathbf{k} \frac{\langle \delta E_{R,L}^*(\mathbf{k}, \omega_r) \delta E_{R,L}(\mathbf{k}, \omega_r) \rangle}{4\pi},
\end{aligned} \tag{1.44}$$

where $I_{R,L}^\alpha(k_\parallel)\, \mathrm{d}k_\parallel$ represents the energy density in the waves of wave vector $k_\parallel$ with right-hand or left-hand polarization.

We could now perform the integration over ω_r and $k_\parallel$ and express explicitly the contribution from the two wave modes in Eq. 1.43:

$$\frac{\partial f_a^{(0)}}{\partial t} + v\mu\frac{\partial f_a^{(0)}}{\partial z} = \frac{v_A^2}{p^2}\left[\frac{\partial}{\partial p}p + \frac{v}{v_A}\frac{\partial}{\partial \mu}\right]\left[\frac{p^3}{v^2}\nu_+\frac{(1-\mu^2)}{2}\right]\left[\frac{\partial}{\partial p} + \frac{1}{p}\frac{v}{v_A}\frac{\partial}{\partial \mu}\right] f_a^{(0)} + \frac{v_A^2}{p^2}\left[\frac{\partial}{\partial p}p - \frac{v}{v_A}\frac{\partial}{\partial \mu}\right]\left[\frac{p^3}{v^2}\nu_-\frac{(1-\mu^2)}{2}\right]\left[\frac{\partial}{\partial p} - \frac{1}{p}\frac{v}{v_A}\frac{\partial}{\partial \mu}\right] f_a^{(0)} \tag{1.45}$$

where we have, for simplicity, approximated $(v/v_A \pm \mu) \simeq v/v_A$ due to the fact that $v \gg v_A$ for CRs and we also introduce the quantity $\nu^\pm$ which is typically referred to as the *pitch angle scattering rate*:

$$\nu_\pm = \frac{2\pi^2}{|v\mu \mp v_A|}\left(\frac{\Omega_a}{B_0}\right)^2\left[I_R^\pm\left(k_\parallel = \frac{\Omega_a}{v\mu \mp v_A}\right) + I_L^\pm\left(k_\parallel = -\frac{\Omega_a}{v\mu \mp v_A}\right)\right] \tag{1.46}$$

As a remark, we note that $I_{R,L}^+(k_\parallel) = 0$ for $k_\parallel < 0$ and $I_{R,L}^-(k_\parallel) = 0$ for $k_\parallel > 0$. This means that, if we neglect v_A in the denominator of the resonant value of $k_\parallel$, we could clearly see that the scattering rate for a proton moving forward with $\mu > 0$ (backward with $\mu < 0$) only comes from forward right-hand or backward left-hand (backward right-hand or forward left-hand) waves.

We note also that Eq. 1.46 is of a Fokker-Planck type and it contains various diffusion terms including the pitch angle diffusion which, as we shall see later, is of critical importance to obtain the final form of the transport equation.

1.2.3 The Cosmic-Ray Transport Equation

To proceed to the final form of the transport equation, we should note that the CR distribution function is typically observed (at least locally) to be independent (or weakly dependent) of μ. This is due to the fact that the scattering rates $\nu^\pm$ are typically large enough that the process of pitch angle diffusion seen in Eq. 1.46 would isotropize all the CR particles. From this argument, we might now expand $f_a^{(0)}$ in the following way:

$$f_a^{(0)}(\mathbf{x}, p, \mu, t) = \bar{f}_a^{(0)}(\mathbf{x}, p, t) + g_a(\mathbf{x}, p, \mu, t) \tag{1.47}$$

where $g_a(\mathbf{x}, p, \mu, t)/\bar{f}_a^{(0)}(\mathbf{x}, p, t)$ should be a small quantity of order v_A/v. Inserting the above expansion into Eq. 1.46 and taking the average over μ, we shall have:

$$\begin{aligned}\frac{\partial \bar{f}_a^{(0)}}{\partial t} + v\frac{\partial}{\partial z}\langle \mu g_a\rangle_\mu = \frac{v_A^2}{p^2}\frac{\partial}{\partial p}\left[\frac{p^4}{v^2}\left\langle (\nu_+ + \nu_-)\frac{1-\mu^2}{2}\right\rangle_\mu \frac{\partial \bar{f}_a^{(0)}}{\partial p}\right] \\ + \frac{v_A^2}{p^2}\frac{\partial}{\partial p}\left[\frac{p^4}{v^2}\left\langle (\nu_+ + \nu_-)\frac{1-\mu^2}{2}\frac{\partial g_a}{\partial p}\right\rangle_\mu\right] \\ + \frac{v_A}{p^2}\frac{\partial}{\partial p}\left[\frac{p^3}{v}\left\langle (\nu_+ - \nu_-)\frac{1-\mu^2}{2}\frac{\partial g_a}{\partial \mu}\right\rangle_\mu\right].\end{aligned} \tag{1.48}$$

where the operator $\langle \quad \rangle_\mu$ represents

$$\langle \quad \rangle_\mu = \frac{1}{2}\int_{-1}^{1} \mathrm{d}\mu. \tag{1.49}$$

To proceed further, it is conventional to subtract Eq. 1.46 from Eq. 1.48 and examine the order of magnitude of each term in the remaining equation. We note that

$$\frac{\partial \bar{f}_a^{(0)}}{\partial t} \sim v\frac{\partial \bar{f}_a^{(0)}}{\partial z} \sim \mathcal{O}\left(\frac{\bar{f}_a^{(0)}}{T}\right), \tag{1.50}$$

where T is the time scale over which $\bar{f}_a^{(0)}$ varies significantly. Since pitch angle scattering is very effective, we expect $\nu_+ \sim \nu_- \sim 1/(\sigma T)$ with $\sigma \ll 1$. If we keep only terms that are of order $\mathcal{O}\left(\bar{f}_a^{(0)}/T\right)$ and $\mathcal{O}\left(v_A \bar{f}_a^{(0)}/\left(v\sigma T\right)\right)$, we shall obtain

$$v\mu\frac{\partial \bar{f}_a^{(0)}}{\partial z} = \frac{v_A}{p^2}\frac{\partial}{\partial \mu}\left[\frac{p^3}{v}\left(\nu_+ - \nu_-\right)\frac{1-\mu^2}{2}\frac{\partial \bar{f}_a^{(0)}}{\partial p}\right] + \frac{\partial}{\partial \mu}\left[\left(\nu_+ + \nu_-\right)\frac{1-\mu^2}{2}\frac{\partial g_a}{\partial \mu}\right]. \tag{1.51}$$

We could now integrate over the pitch angle from $\mu = -1$ to some arbitrary value μ and rearrange the terms to get

$$\frac{\partial g_a}{\partial \mu} = -\frac{v}{\nu_+ + \nu_-}\frac{\partial \bar{f}_a^{(0)}}{\partial z} - \frac{v_A}{v}p\frac{\nu_+ - \nu_-}{\nu_+ + \nu_-}\frac{\partial \bar{f}_a^{(0)}}{\partial p}. \tag{1.52}$$

We shall now insert the above equation into Eq. 1.46 and note that we should keep only terms of order $\mathcal{O}\left(\bar{f}_a^{(0)}/T\right)$, $\mathcal{O}\left(v_A \bar{f}_a^{(0)}/\left(vT\right)\right)$, and $\mathcal{O}\left(v_A^2 \bar{f}_a^{(0)}/\left(v^2\sigma T\right)\right)$.

Equation 1.48 then becomes:

$$\frac{\partial \bar{f}_a^{(0)}}{\partial t} + \frac{1}{3p^2}\frac{\partial}{\partial p}\left[p^3 v_A \left\langle \frac{3\left(1-\mu^2\right)\left(\nu_+ - \nu_-\right)}{2\left(\nu_+ + \nu_-\right)} \right\rangle_\mu\right] \frac{\partial \bar{f}_a^{(0)}}{\partial z} - \frac{\partial}{\partial z}\left[v^2 \left\langle \frac{1-\mu^2}{2\left(\nu_+ + \nu_-\right)} \right\rangle_\mu \frac{\partial \bar{f}_a^{(0)}}{\partial z}\right] - \frac{p}{3}\frac{\partial}{\partial z}\left[v_A \left\langle \frac{3\left(1-\mu^2\right)\left(\nu_+ - \nu_-\right)}{2\left(\nu_+ + \nu_-\right)} \right\rangle_\mu\right] \frac{\partial \bar{f}_a^{(0)}}{\partial p} - \frac{1}{p^2}\frac{\partial}{\partial p}\left[p^4 \frac{v_A^2}{v^2} \left\langle \frac{2\left(1-\mu^2\right)\nu_+\nu_-}{\nu_+ + \nu_-} \right\rangle_\mu \frac{\partial \bar{f}_a^{(0)}}{\partial p}\right] = 0. \tag{1.53}$$

We shall, from now on, replace the notation $\bar{f}_a^{(0)} = \bar{f}_a^{(0)}(\mathbf{x}, p, t)$ with $f = f(\mathbf{x}, p, t)$ for brevity and please note that the species of the relevant particles shall be specified when needed. The final form of the one-dimensional equation used for the study of CR transport into MCs (see Chapter 3) is achieved by adding a term that describes the change of the distribution function due to energy losses of CRs as they propagate in the ISM:

$$\frac{\partial f}{\partial t} + \frac{1}{3p^2}\frac{\partial}{\partial p}\left(p^3 u\right)\frac{\partial f}{\partial z} - \frac{\partial}{\partial z}\left(D\frac{\partial f}{\partial z}\right) - \frac{p}{3}\frac{\partial u}{\partial z}\frac{\partial f}{\partial p} - \frac{1}{p^2}\frac{\partial}{\partial p}\left(p^2 D_{pp}\frac{\partial f}{\partial p}\right) + \frac{1}{p^2}\frac{\partial}{\partial p}\left(\dot{p}p^2 f\right) = 0, \tag{1.54}$$

where $\dot{p}$ is the rate of momentum loss which we shall discuss in depth in the next section and we have introduced also the advection velocity u, the spatial diffusion coefficient D, and the diffusion coefficient in momentum space D_{pp}:

$$u = v_A \left\langle \frac{3\left(1-\mu^2\right)\left(\nu_+ - \nu_-\right)}{2\left(\nu_+ + \nu_-\right)} \right\rangle_\mu, \tag{1.55}$$

$$D = v^2 \left\langle \frac{\left(1-\mu^2\right)}{2\left(\nu_+ + \nu_-\right)} \right\rangle_\mu, \tag{1.56}$$

$$D_{pp} = p^2 \frac{v_A^2}{v^2} \left\langle \frac{2\left(1-\mu^2\right)\nu_+\nu_-}{\nu_+ + \nu_-} \right\rangle_\mu. \tag{1.57}$$

In the following, we shall briefly discuss all the quantities that have emerged from the transport equation and also the physical interpretation of each term that they involve.

Equation 1.55 represents the advection velocity of particles for a background plasma at rest. It is a weighted mean between v_A and $-v_A$, the weight given by the relative importance of forward and backward moving waves. As a remark, we note that, in the case where the background plasma also moves with some velocity

v_0 along the magnetic field, it could be proven that the advection velocity becomes:

$$u = v_0 + v_A \left\langle \frac{3\left(1-\mu^2\right)\left(\nu_+ - \nu_-\right)}{2\left(\nu_+ + \nu_-\right)} \right\rangle_\mu . \tag{1.58}$$

We refer the interested readers to Skilling, 1975 for a more detailed discussion in the case of a background plasma with large-scale motion. It is also straightforward to see that if one of the wave modes (either forward or backward) dominates over the other meaning ν_+ or ν_- tends to zero, then $u = v_0 \pm v_A$ ('+' or '−' depending on the direction of the dominant wave mode). In the other, limiting case where $\nu_+ = \nu_-$, the advection becomes that of the background plasma, i.e. $u = v_0$.

Let's now turn our attention to one of the most important feature of the transport equation which is the emergence of the spatial diffusion coefficient. Using the quasi-linear approximation, we have successfully built up a theoretical framework capable of describing the diffusive motion of CRs which is expected from observational constraints as previously discussed in Section 1.1. In this framework, the resonant plasma waves act as the *scatterering centers* which prevent CRs from propagating ballistically. This means that if the waves are provided with more energy, CRs may interact more frequently and, as a result, have a shorter mean free path or, equivalently, smaller diffusion coefficient. It is for this reason that the diffusion coefficient is inversely proportional to the scattering rate or, more precisely, the power spectrum of the resonant plasma waves.

Another interesting feature of the transport equation is that it also leads to the diffusion in momentum space. This is an interesting mechanism for energy gain of CRs in a stochastic way that was first pointed out in the seminal paper by Fermi, 1949 and it is often referred to as the second order Fermi acceleration (the first order acceleration mechanism is also incorporated in the transport equation and shall be discussed below). In the original version by Fermi, CRs gain energy by scattering of moving magnetic fields in the ISM and, in the framework of Quasi-Linear Theory, this is realized by the resonant interaction of CRs with forward and backward plasma waves. Since this stochastic acceleration mechanism requires the existence of waves in both directions, we could see that the diffusion coefficient in momentum space would disappear if one of the two wave modes is suppressed, i.e. $\nu_+ = 0$ or $\nu_- = 0$.

Having discussed all the relevant physical quantities associated with the transport equation, we could now proceed to give a brief summary on the meaning of all the terms in Eq. 1.54:

- The second term on the LHS is referred to as the advection term and it describes the transport of CRs due to a bulk motion of the background plasma and the Alfveén waves.

- The third term on the LHS describes the diffusive motion of CRs along the magnetic field line which, as discussed above, originates from the frequent interactions between CRs and plasma waves.

- The fourth term on the LHS, which has the factor $\partial u/\partial z$, characterizes the adiabatic energy loss or gain of CRs due to the expansion or compression of

the background plasma. For example, in the case of supernova explosions as discussed in Section 1.1, the abrupt change of the velocity profile around the shock leads to the erergy gain of CRs and solving the transport equation for this system results in a distribution function that is a power law in momentum. In fact, the inclusion of this term and the spatial diffusion term gives rise to the first order Fermi acceleration mechanism (see e.g. Blasi, 2013, for a more detailed discussion).

- The fifth term on the LHS depicts the second order Fermi acceleration process (or the diffusion in momentum space) which is the stochastic energy gain of CRs due to the scattering of these particles by plasma waves.

- The sixth term takes into account all the relevant processes of energy loss of CRs as these particles propagate in the ISM. The main processes for CR protons are ionization and Coulomb collisions at low energy and proton-proton interaction at high energy. Cosmic ray electrons also suffer from energy loss by ionization and Coulomb collisions at low energy and, at high energy, they lose energy mostly due to interactions with the electromagnetic field in the ISM via bremsstrahlung radiation, synchrotron radiation, and inverse Compton scattering. All of these energy loss mechanisms shall be discussed in more detail in the next section.

Finally, we note that the observations of CRs typically involve the determination of the intensity as a function of kinetic energy as mentioned in Section 1.1. It would be, therefore, more convenient to establish the connection between the distribution function and the intensity of CRs. From dimensional analysis, we could see that the intensity of CRs should be:

$$j(\mathbf{x}, E, t) = p^2 f(\mathbf{x}, p, t) \tag{1.59}$$

It would be convenient to introduce also $f(\mathbf{x}, E, t)$ which we shall refer to as the spectrum of CRs:

$$f(\mathbf{x}, E, t) = \frac{4\pi p^2 f(\mathbf{x}, p, t)}{v} = \frac{4\pi j(\mathbf{x}, E, t)}{v}. \tag{1.60}$$

Notice that the above definition has been chosen such that the normalizations of the spectrum and the distribution function both satisfy:

$$\int_{E_{min}}^{E_{max}} f(\mathbf{x}, E, t)\, \mathrm{d}E = \int_{p_{min}}^{p_{max}} 4\pi p^2 f(\mathbf{x}, p, t)\, \mathrm{d}p = n_{CR}, \tag{1.61}$$

where n_{CR} is the number density of CRs with kinetic energy in the range from E_{min} to E_{max}.

1.3 Mechanisms for Energy Loss of Cosmic Rays

Covering all the energy loss mechanisms in the range of the observed cosmic ray spectrum from a few MeVs to a few hundred EeVs is quite a daunting task and, thus, we may instead list (without any rigorous derivation) the energy loss rate of processes that are relevant to the context of this thesis which are: i) Coulomb and ionization interactions of both CR protons and electrons, ii) bremsstrahlung, synchrotron radiation, and inverse Compton scattering for CR electrons, and iii) proton-proton interactions. The interested readers are referred to the monography by Schlickeiser (2002) for a more extended discussion. We note also that here we give only formulae for the rate of energy loss and not the rate of momentum loss introduced for the transport equation, however, switching between the two is quite straightforward since:

$$\dot{p} = \frac{\dot{E}}{v}. \tag{1.62}$$

Also, for ease of later discussion, let's denote $n_{\rm H}$ as the total number density of hydrogen atoms (both in molecular and atomic forms) and n_e as the number density of free electrons.

1.3.1 Interactions of Cosmic-Ray Protons

Coulomb and Ionization Interactions

For CR protons of kinetic energy below a few hundreds MeV, the dominant mechanisms for energy loss are either ionization or Coulomb interactions depending on whether the ISM is neutral or ionized (Schlickeiser, 2002).

In ionized matter, the energy loss rate of CR protons due to Coulomb interactions is given by the following phenomenological formula (Schlickeiser, 2002):

$$\dot{E}_{Coulomb} = 3.1 \times 10^{-7} \left(\frac{n_e}{1\ \mathrm{cm}^{-3}}\right) \frac{\beta^2}{x_m^3 + \beta^3}\ \mathrm{eV/s}, \tag{1.63}$$

where β is the ratio between the speed of the particle and the speed of light, $x_m = 0.0286\sqrt{T_e/(2 \times 10^6\ \mathrm{K})}$, and T_e is the temperature of the electrons in the plasma.

In neutral matter, the energy loss rate of CR protons due to ionization interactions could be deduced from the Bethe-Bloch formula (see e.g. Longair, 2011):

$$\dot{E}_{ion}(v > v_0) = \frac{3}{2} c\sigma_T \frac{m_e c^2}{\beta} \sum_s n_s Z_s \left[\ln\left(\frac{2m_e c^2}{\bar{I}_s}\right) + 2\ln(\gamma\beta) - \beta^2\right], \tag{1.64}$$

where c is the speed of light, σ_T is the Thompson cross-section, m_e is the electron mass, n_s, Z_s and I_s are respectively the number density, the atomic number, and the ionization potential of the species s of the ISM, and γ is the Lorentz factor of the CR particle. Since the abundances of heavier elements are increasingly small, we shall mostly consider the contribution of the ionization interaction of CR protons with

hydrogen and helium of the ISM (Schlickeiser, 2002) whose ionization potentials are respectively $\bar{I}(\mathrm{H}) \simeq 19$ eV and $\bar{I}(\mathrm{He}) \simeq 44$ eV[3]. It should be noticed, however, that the formula above is applicable only for particles of speed higher than a characteristic speed v_0. We shall have, in the case of a medium made up only by hydrogen atoms, $v_0 = e^2/\hbar \simeq 2.19 \times 10^8$ cm/s which is the orbital speed of electrons. For slow protons with $v < v_0$, there exists also a phenomenological formula for the ionization loss rate first presented by Ginzburg & Syrovatskii (1964):

$$\dot{E}_{ion}(v < v_0) = 2.34 \times 10^{-23} \left(\frac{v}{1 \text{ cm/s}}\right)^2 \sum_s \left(\frac{n_s}{1 \text{ cm}^{-3}}\right) (1 + Z_s) \text{ eV/s}, \quad (1.65)$$

where Z_s is the atomic number of the species s of the ISM. For numerical application, it might be more convenient to introduce also the phenomenological formula for the ionization loss rate of CR protons using the asymptotic behaviours above and below the characteristic velocity v_0:

$$\dot{E}_{ion} \simeq 2.70 \times 10^{-7} \left(\frac{n_{\mathrm{H}}}{1 \text{ cm}^{-3}}\right) \frac{\beta^2}{9.15 \times 10^{-6} + \beta^{2.65}} \text{ eV/s}, \quad (1.66)$$

where all the heavy elements have been taken into account by assuming solar abundances. It should be noticed also that, for the ISM of solar abundances, $n_{\mathrm{He}} \simeq 0.1 n_{\mathrm{H}}$ and, thus, the contribution of helium to the ionization loss becomes negligible in the energy range where $\beta > v_0/c$. This means that the above formula could also be adopted for the gas made up only by hydrogen in this energy range and the error induced for the extrapolation to lower energy ($\beta < v_0/c$) is less than a factor of two.

Proton-Proton Interactions

Cosmic-ray protons of kinetic energy $E \gtrsim E_{th} \simeq 280$ MeV could also lose energy due to the production of both charged and neutral pions in their inelastic collisions with the matter of the ISM. We generally refer to this mechanism of energy loss as proton-proton interaction (see e.g. Kafexhiu et al., 2014, and references therein for more discussions about the underlying channels hadronic interactions). The energy loss rate for this channel is:

$$\dot{E}_{pp} = 1.31 \times 10^{-7} \left(\frac{n_{\mathrm{H}}}{1 \text{ cm}^{-3}}\right) \gamma^{1.28} H(\gamma - 1.28) \text{ eV/s}, \quad (1.67)$$

where γ is the Lorentz factor of the particle. It should be noted that we have implicitly assumed the solar abundances for the ISM.

Notice that neutral pions decay instantaneously into gamma rays[4]. Since the

[3] It might not be very precise to refer to $\bar{I}_s$ as the ionization potential since it takes into account also the excitation of electrons of molecules in the neutral gas. The values of $\bar{I}_s$ are commonly obtained from the fit with experimental data (see e.g. Chapter 5 of the monograph by Longair, 2011).

[4] We note that proton-proton interaction could also lead to the production of charged pions. These pions could, in turn, decay into electrons, positrons, and neutrinos which are also of critical importance for observations.

spectrum of π_0 gamma rays of energy $E_\gamma \gg m_{\pi^0}c^2/2$ follows quite closely the one of CR protons and also these particles could propagate without suffering the frequent collisions with the turbulent fields in the ISM, they can be used as a powerful tool to probe CRs at energy above 280 MeV. A brief discussion on the use of gamma rays to gain more insight to CR sources like SNR will be provided in the next chapter and, in Chapter 6, we shall demonstrate how a combined study of physical observables like the ionization rate (see Chapter 2 for a brief overview of this quantity) and the spectrum of gamma rays could provide a constraint for the CR spectrum from low to high energy.

1.3.2 Interactions of Cosmic-Ray Electrons

Coulomb and Ionization Interactions

The energy loss rate of electrons and positrons is dominated by ionization interactions in a neutral gas and by Coulomb interactions in a fully ionized plasma for kinetic energy below a few hundreds MeV.

In neutral matter, the loss rate due to ionization interactions is (Longair, 2011):

$$\dot{E}_{ion} = \frac{3}{4}c\sigma_T\frac{m_ec^2}{\beta}\sum_s n_sZ_s\left\{\ln\left[\frac{\gamma^3\beta^4m_c^2c^4}{2\left(1+\gamma\right)\bar{I}_s^2}\right] - \left(\frac{2}{\gamma}-\frac{1}{\gamma^2}\right)\ln 2 + \frac{1}{\gamma^2} + \frac{1}{8}\left(1-\frac{1}{\gamma}\right)^2\right\}, \tag{1.68}$$

where c is the speed of light, σ_T is the Thompson cross-section, m_e is the electron mass, β is the ratio between the speed of the CR particle and the speed of light, n_s, Z_s, and $\bar{I}_s$ are respectively the number density, the atomic number, and the ionization potential of the species s of the ISM, and γ is the Lorentz factor of the CR particle. For the ISM with solar abundances, we shall have:

$$\dot{E}_{ion} = \frac{7.65\times10^{-9}}{\beta}\left(\frac{n_{\rm H}}{1\ {\rm cm}^{-3}}\right)\left[23.31+1.2\ln\left(\frac{\gamma^3\beta^4}{1+\gamma}\right)\right]\ {\rm eV/s}. \tag{1.69}$$

In ionized matter, the energy loss rate due to Coulomb interactions is (Dermer & Menon, 2009):

$$\dot{E}_{Coulomb} = \frac{3}{2}c\sigma_T\frac{m_ec^2}{\beta}n_e\ln\left(\frac{\sqrt{\gamma}m_ec^2}{\hbar\omega_p}\right) \tag{1.70}$$

where $\hbar$ is the reduced Planck constant and ω_p is the electron plasma frequency computed as:

$$\omega_p = \sqrt{\frac{4\pi n_ee^2}{m_e}} \simeq 5.64\times10^4\sqrt{\frac{n_e}{1\ {\rm cm}^{-3}}}\ {\rm rad/s}. \tag{1.71}$$

We note also that the above formula is, strictly speaking, applicable only for CR electrons of energy $E > m_e c^2$ propagating in a cold plasma (Dermer & Menon, 2009). However, the error induced by extrapolating this formula down to energy $E < m_e c^2$ is rather negligible and also we are only interested in CR electrons of energy above 1 keV which means $E \ll k_B T_e$ even for the hot ISM. Thus, Eq. 1.70 could be adopted to describe the energy loss rate for Coulomb interaction of CR electrons within the energy range of interest. It would also be more convenient to obtain a phenomenological formula for the loss rate:

$$\dot{E}_{Coulomb} \simeq \frac{7.65 \times 10^{-9}}{\beta} \left(\frac{n_e}{1\ \mathrm{cm}^{-3}}\right) \left[74.32 + \ln\left(\frac{\gamma}{n_e/1\ \mathrm{cm}^{-3}}\right)\right]\ \mathrm{eV/s}. \tag{1.72}$$

It should be noticed that, for both of Coulomb and ionization interaction, the loss rates depend very weakly on energy.

Radiative Energy Loss of Cosmic-Ray Electrons

Cosmic-ray electrons and positrons of energy above a few hundreds MeV lose energy more efficiently due to the inverse Compton scattering and also due to the emission of bremsstrahlung and synchrotron radiation (Schlickeiser, 2002).

The energy loss rate of CR electrons due to bremsstrahlung radiation in a neutral gas is (Schlickeiser, 2002):

$$\dot{E}_{brem} = \frac{3\alpha c \sigma_T}{8\pi} m_e c^2 \gamma \sum_s n_s \phi_s, \tag{1.73}$$

where $\alpha \simeq 1/137$ is the fine-structure constant, σ_T is the Thompson cross section, n_s and ϕ_s are respectively the number density and the scattering function of the species s of the ISM. As discussed above, we shall consider only the loss rate due to interactions with hydrogen and helium whose scattering functions, in the case of a neutral environment (corresponding to the strong shielding limit), take the values $\phi_{\mathrm{H}} \simeq \phi_{\mathrm{He}}/3 \simeq 45$ (Schlickeiser, 2002).

In a fully ionized medium, the energy loss rate due to bremsstrahlung radiation of CR electrons is (Schlickeiser, 2002):

$$\dot{E}_{brem} = \frac{3\alpha c \sigma_T}{2\pi} m_e c^2 \gamma \sum_s n_s Z_s (Z_s + 1) \left[\ln \gamma + \ln 2 - \frac{1}{3}\right], \tag{1.74}$$

where Z_s is the atomic number of the species s. It should be noticed also that, for a fully ionized medium, $\sum_s n_s Z_s = n_e$ and, thus, we could approximate $\sum_s n_s Z_s (Z_s + 1) \simeq 2 n_e$ by assuming the solar abundances of the ISM. This allow us to write down a more practical form of the formula for the energy loss rate due to bremsstrahlung radiation for both ionized and neutral media:

$$\dot{E}_{brem} = 5.2 \times 10^{-10} \left(\frac{n_{\mathrm{H}}}{1\ \mathrm{cm}^{-3}}\right) \gamma \left[1 + 0.137 x \left(\ln \gamma + 0.36\right)\right]\ \mathrm{eV/s}, \tag{1.75}$$

where $x = n_e/n_{\rm H}$ is the ionization fraction of the medium. It is essential to stress again that the above formula has been obtained under the assumption of solar abundances for the ISM.

The energy loss rate due to synchrotron radiation and inverse Compton scattering could be described as:

$$\dot{E}_{syn+IC} = 9.90 \times 10^{-16} \gamma^2 \left[\left(\frac{B}{1\ \mu\mathrm{G}} \right)^2 + 26.84 \left(\frac{w}{1\ \mathrm{eV\ cm^{-3}}} \right) \right]\ \mathrm{eV/s} \tag{1.76}$$

where B is the magnitude of the magnetic field and w is the energy density of the interstellar radiation field at the position of interest.

1.3.3 Energy Loss Function and Energy Loss Time

For ease of later discussion, we shall follow Padovani et al. (2009) and introduce the energy loss function:

$$L(E) = -\frac{2}{n_{\rm H}} \frac{\mathrm{d}E}{\mathrm{d}l}, \tag{1.77}$$

where $n_{\rm H} = n(\mathrm{H}) + 2n(\mathrm{H_2})$ is the number density of hydrogen atoms as denoted in the previous section, l is the path length and $\mathrm{d}E/\,\mathrm{d}l$ is the average energy loss per unit of travelling distance. Notice that the factor 1/2 appear since we define this function here with the number density of hydrogen atoms instead of the number density of hydrogen molecules. The two definitions are the same for the case of clouds made up mainly by molecular hydrogen. It is quite straightforward to relate the energy loss rate and the energy loss function:

$$\dot{E} = \frac{1}{2} n_{\rm H} v L(E). \tag{1.78}$$

As a remark, we note that the loss function does not vary with the density of MCs. This is due to the fact that $L(E) \sim \dot{E}/n_{\rm H}$ (from Eq. 1.78) and also the loss rate in a neutral medium is typically proportional to $n_{\rm H}$. In fact, the only two important loss mechanism that do not hold follow this behaviour are synchrotron radiation and inverse Compton scattering for CR electrons. For this thesis, we will, however, place our concentration on CRs of energy from about 1 keV to 10 GeV as they are most relevant for ionization processes and since synchrotron radiation and inverse Compton could never be dominant mechanisms of energy loss below 10 GeV for typical values of the magnetic field and energy density of photon fields in the ISM ($B \lesssim 3\ \mu$G and $w \lesssim 1$ eV/cm^3), it is still reasonable to assume that $L(E)$ is, in general, independent of $n_{\rm H}$.

For the case of clouds made up by mainly molecular hydrogen, the energy loss functions have been collected and fitted with experimental values by Padovani et al. (2009). The corresponding energy loss rates for both CR protons and electrons with energy ranging from 1 keV to 10 GeV determined from the fit (using Eq. 1.78) are

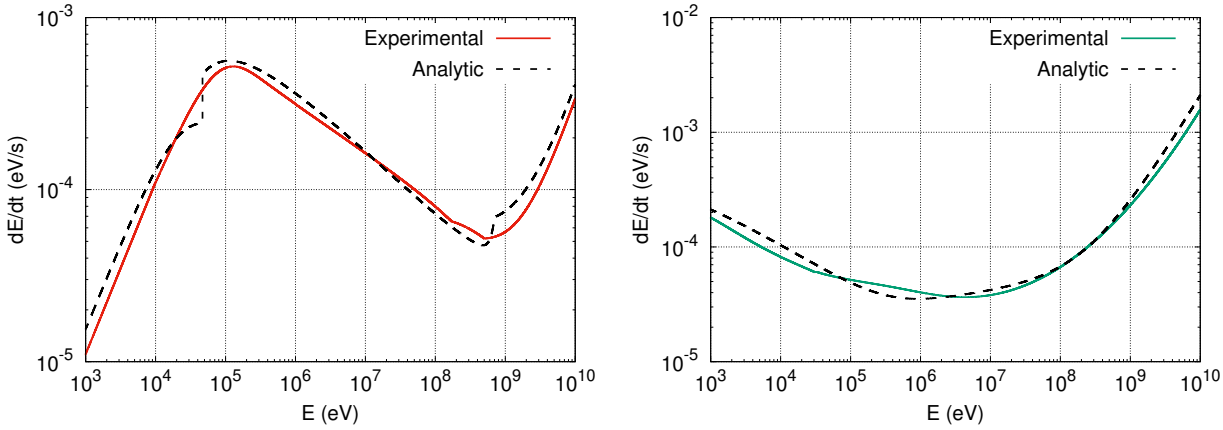

FIGURE 1.3: Illustration of the energy loss rate in the case where $n(H_2) = 100$ cm^{-3} for both CR protons (left panel) and electrons (right panel). The analytic version of the energy loss rates are divided by a factor of approximately 1.4 to take into account only molecular hydrogen and not other heavy elements of the ISM.

shown in Fig. 1.3 together with the analytic ones for the molecular hydrogen density $n(H_2) = 100$ cm^{-3}.

Notice that the experimental data has been obtained for the gas made up by only molecular hydrogen while the analytic formulae are derived for the ISM of solar abundances with several underlying approximations on the scaling of atomic models for the ionization and Coulomb interactions (see e.g. Schlickeiser, 2002, and references therein for the formal derivation). It might be due to this difference in the elemental compositions considered for the two cases that the analytic loss rates deviate from the experimental ones, especially at low energy, as could be seen in Fig. 1.3. We have checked that the analytic formula reproduces very well the experimental data of both CR protons and electrons in the case of the ISM made up by hydrogen molecules within the energy range most relevant for later discussion of the ionization rate. Since the experimental form of the loss rate would a provide a more precise description of the transport inside MCs, especially for the case of MCs made up mainly by H_2, we shall adopt this form for the analysis in Chapter 3. The more simple analytic version of the loss rates will be dedicated for the more complicated modeling in Chapter 4 where the loss rates in various phases of the ISM with both neutral and ionized gas are required.

Let's now define also the energy loss time which provides a rough estimate for the time of propagation after which CRs would lose a significant amount of energy:

$$\tau_l = -\frac{p}{\dot{p}} = -\frac{pv}{\dot{E}} \tag{1.79}$$

It should be noted that this quantity could also be defined as $\tau_l = -E/\dot{E}$ which seems to be more appropriate as the energy loss time. The two definitions are, however, equivalent for relativistic particles and they are different only by a factor of two in the non-relativistic regime. We have compared also the experimental and analytic forms of the energy loss time in an MC of $n(H_2) = 100$ cm^{-3} in Fig. 1.4.

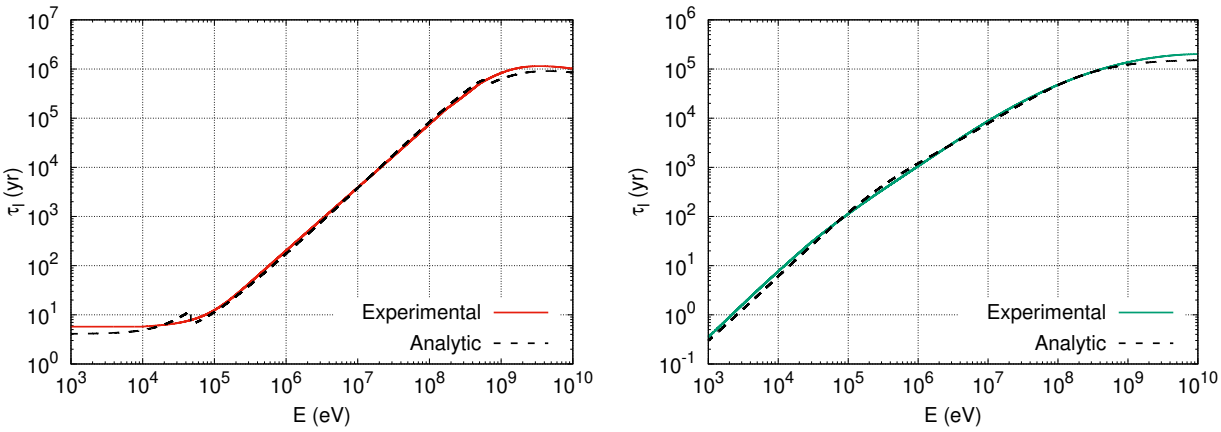

FIGURE 1.4: Illustration of the loss time in a cloud of H_2 density $n_H = 100$ cm^{-3} for both CR protons (left panel) and electrons (right panel). The analytic version of the energy loss rates are multiplied by a factor of approximately 1.4 to take into account only molecular hydrogen and not other heavy elements of the ISM.

Chapter 2

Molecular Clouds as Cosmic-Ray Barometers

With the term *clouds* astronomers refer to the cold neutral phase of the ISM (Snow & McCall, 2006). These objects are, simply put, accumulations of neutral atomic or molecular gas of density ranging from 10 cm^{-3} to more than 10^4 cm^{-3}. Since they are very rich in chemical phenomena, there exist many formal classifications for clouds which employ, for example, the fractional abundances of H_2, C^+, and CO to better highlight the chemical properties of these objects (see e.g. Snow & McCall, 2006, for a review). For the purpose of this thesis, it might be, however, sufficient to characterize clouds using simply the *column density* of hydrogen atoms which is defined as $N_{\rm H} \simeq n_{\rm H} L$ where $n_{\rm H}$, as introduced in Section 1.3, is the total number density of hydrogen atoms and L is the characteristic size of the cloud. We shall focus essentially on diffuse MCs ($N_{\rm H} \simeq 10^{21} - 10^{22}$ cm^{-2}) and dense MCs ($N_{\rm H} > 10^{22}$ cm^{-2}).

Molecular clouds have always played an essential role in the context of Cosmic Ray Astrophysics since they could serve as targets in various types of interactions with CRs. At high energy, the interaction of hadronic CRs with the nuclei of MCs could result in the production of gamma rays detectable on Earth. The studies of these gamma-ray data from isolated giant MCs or complexes of clouds in the Galaxy could, in turn, provide more information on the possible fluctuations of the CR distribution on the Galactic scale. More importantly, since gamma-ray data from SNRs are, most of the time, hard to interpret due to the absence of concrete evidences for distinguishing a hadronic orgin from a leptonic one[1], the observations of enhanced gamma-ray fluxes from dense MCs located in the vicinity of SNRs might help us to better understand the capability of these remnants as CR sources. Furthermore, cosmic rays with energy below a few GeV are believed to regulate the abundances of many chemical species (such as H_3^+, CO, HCO^+ or DCO^+) which are also observable on Earth via their emission or absorption lines in the infrared or millimeter domains. This means that the combination of these radiative signatures from MCs could provide a unique way to probe Galactic CRs from low to high energy.

We shall begin this chapter with a brief discussion on the connection between high energy CRs and gamma-ray observations of MCs. For completeness, some basics of

[1]Notice that electrons and positrons accelerated from SNRs could also produce gamma rays due to mechanism such as bremsstrahlung radiation and inverse Compton scattering.

gamma rays from SNRs will also be incorporated to better highlight the paramount importance of complementary gamma-ray observations for the surroundings of MCs. These are some of the most crucial elements to set the stage for Chapter 6 where we illustrate an example of how observational data from an MC is used to constrain both the low and high energy parts of the CR spectra in the vicinity of the SNR W28. The rest of this chapter will focus mostly on the link between low-energy CRs and the chemistry of MCs from which an important quantity known as the ionization rate could be obtained both theoretically and observationally. The CR induced ionization rate together with the transport equation derived in the previous chapter will lay the foundation for all the subsequent discussions on low-energy CRs presented in Chapter 3 and Chapter 4.

2.1 Probing High Energy Cosmic Rays with Gamma Rays

2.1.1 Gamma-Ray Astronomy for Supernovae Remnants

As briefly mentioned in the previous chapter, the hadronic interactions between CRs of kinetic energy $E \gtrsim E_{th} \simeq 280$ MeV and matters of the ISM could lead to the production of neutral pions which, eventually, decay into gamma rays that could be observed on Earth. For the proton-proton interaction, we shall have:

$$p + p \rightarrow p + p + \pi^0 \tag{2.1}$$

$$\pi^0 \rightarrow \gamma + \gamma \tag{2.2}$$

For simplicity, we shall restrict ourselves on the case of π^0 gamma rays from the proton-proton interaction and the contribution from the heavy nuclei will be taken into account using the so-called nuclear enhancement factor (see e.g. Kafexhiu et al., 2014, for a more detailed discussion). The resulting gamma rays from this type of interaction carry roughly 10% of the energy of the incoming CR protons[2]. This mechanism for the production of gamma rays was employed in the pioneering works by Drury et al. (1994) (see also Naito & Takahara, 1994) to propose that the gamma-ray observations of SNRs could help to test the standard paradigm for the origin of Galactic CRs. Let's consider, for example, an SNR with the volume integrated spectrum of accelerated CRs to be $N(E) \sim f(E)V_{SNR} \sim E^{-2}$. The gamma-ray flux could then be estimated as follows (see e.g. Gabici, 2013, for a more detailed discussion):

$$E_\gamma^2 F_\gamma(E_\gamma) \simeq 10^{-11} \left(\frac{W_{CR}^{tot}}{10^{50}\ \mathrm{erg}}\right) \left(\frac{n_\mathrm{H}}{1\ \mathrm{cm}^{-3}}\right) \left(\frac{d}{1\ \mathrm{kpc}}\right)^{-2} \mathrm{erg\ cm^{-2}\ s^{-1}} \tag{2.3}$$

where W_{CR}^{tot} is the total energy channeled into CRs from the supernovae explosion, n_H is the total density of hydrogen atoms in the ambient medium surrounding the

[2]Notice that this is only a rough estimate in the limit where $E \gg E_{th}$.

SNR, and d is the distance of the SNR from Earth. It should be noted that, in the derivation of the gamma-ray flux in the above equation, we have implicitly assumed that the gas in the shocked region of the SNR is compressed with the density increased by a factor of four. Interestingly, the flux predicted from the above equation is within the sensitivity range of current gamma-ray instruments, especially in the TeV energy range, and several Cherenkov telescopes such as HESS, MAGIC, or VERITAS have actually reported the detection of many isolated SNRs[3] (see e.g. Aharonian et al., 2008; Hinton & Hofmann, 2009, for reviews).

It is, however, not clear whether or not we could infer the presence of CR protons accelerated in SNRs from these gamma-ray data. This is because SNRs are also sources of CR electrons[4] which could, indeed, generate gamma rays via bremsstrahlung radiation or inverse Compton scattering. Since the interpretations of gamma rays from SNRs using either a hadronic scenario or a leptonic one are often obscured by these competing mechanisms, the analyses of the underlying CR populations responsible for these high energy radiations remain quite challenging and the detection of gamma rays from SNRs could not provide an official confirmation for the standard hypothesis according to which SNRs are the principal sources of Galactic CRs.

The ambiguity in the nature of gamma rays from SNRs has provoked many intense discussions in the field of Gamma Ray Astronomy. There are two main arguments that are typically involved in resolving this problem. The first one concerns the complementary study of the magnetic field from X-ray synchrotron data. A leptonic origin of the gamma rays would require a value of the magnetic field smaller than or comparable to 10 μG since, in this case, a large amount of electrons would be needed to explain both the X-ray and gamma-ray emissions. However, the X-ray observations of narrow synchrotron filaments located at the position of the shock (Bamba et al., 2003; Vink & Laming, 2003; Völk et al., 2005) or very fast temporal variations of the synchrotron emissions from small knots within the SNR (Uchiyama et al., 2007; Uchiyama & Aharonian, 2008) seems to suggest the existence of very strong magnetic field with values in the range from 100 μG to 1 mG in several SNRs. Such a strong magnetic field might not require too many CR electrons to explain the sychrotron X-ray emission and, as a result, the predicted gamma-ray due to inverse Compton scattering would become negligible. On the contrary, we should notice that, most of these measurements allow the determination of the field only within small regions which constitute only a fraction of the SNR shells and, therefore, they simply indicate the local values of the field rather than the average ones for the entire SNR. This means that we might also expect the global magnetic field of SNRs to be significantly less than the one inferred from the observations of the knots and filaments and, thus, the leptonic scenario for gamma-ray emissions from SNRs could not be completely ruled out. The other argument typically employed for distinguishing the hadronic or leptonic nature of gamma rays from SNRs relies on the slope of the gamma-ray spectrum. If the spectrum of both hadronic and

[3]SNRs are referred to as isolated in a sense that they are not associated to any nearby MC.

[4]The concrete evidence for this claim comes from the detection of X-ray synchrotron from many SNRs.

leptonic CRs accelerated at SNR shocks in the relativistic regime follows the power law $N(E) \sim p^{-\alpha} \sim E^{-\alpha}$ with $\alpha \simeq 2.1-2.4$ as briefly mentioned in Chapter 1, it can be shown that the expected gamma-ray spectrum is also a power law $F(E_\gamma) \sim E_\gamma^{-\delta}$ where $\delta \simeq 2.1 - 2.4$ for hadronic gamma rays and $\delta \simeq 1.55 - 1.7$ for leptonic ones. This means that the slope in the hadronic scenario is often steeper than $\delta = 2$ and, conversely, it is softer than $\delta = 2$ for gamma rays of the leptonic origin and, thus, we could take advantage of this difference to discriminate the two cases. It is quite straightforward to see that the realization of this method requires the gamma-ray data in a broad energy range from GeV to TeV. The two most famous examples for this type of reasoning are the cases of the SNRs RX J1713.7-3946 and Tycho which are revealed with help of the complementary observations of the *Fermi*-LAT telescope in the GeV energy range to have the slope $\delta \simeq 1.5$ and $\delta \simeq 2.3$ respectively (see e.g. Gabici, 2013, and references therein). Thus, gamma rays from RX J1713.7-3946 are often interpreted with a leptonic origin (Abdo et al., 2011) while the ones from Tycho are believed to be hadronic gamma rays (Giordano et al., 2012; Morlino & Caprioli, 2012). Nevertheless, we note that there exist other ways of reasoning to explain gamma-ray data from RX J1713.7-3946 with the hadronic origin (Fukui et al., 2012; Inoue et al., 2012; Gabici & Aharonian, 2014) and from Tycho with leptonic origin (Atoyan & Dermer, 2012) which means that the identification of the underlying mechanism for emission is still quite ambiguous even for some of the most investigated sources.

2.1.2 High Energy Cosmic Rays and Molecular Clouds

It is clear from the discussion above that the constraints for the spectrum of hadronic CRs are, in general, difficult to obtain simply with the gamma-ray observations of SNRs. The story is, however, completely different for the case of gamma-ray observations of MCs thanks to the particularly high mass of gas of these objects, which makes the hadronic origin of the gamma-ray emission more likely. The detection of these MCs with current gamma-ray instruments could, therefore, be used to estimate the intensity of CR protons and nuclei in the energy range above a few GeVs. This is essentially the reason why MCs, especially the ones located in the vicinity of SNRs, are of great interest to Cosmic Ray Astrophysics. In the following, we shall better illustrate how gamma-ray data from MCs could provide us with better insight into Galactic CR hadrons with some very interesting ideas that have been pushed forward in the past literature.

Let's consider an MC located in the region where the proton CR spectrum has the same slope as the one observed on Earth, $f(E) \sim E^{-2.7}$. The integral gamma-ray flux for this MC reads (see e.g. Gabici, 2013):

$$F(E_\gamma) \simeq 2 \times 10^{-13} \varepsilon \left(\frac{M}{10^5\ M_\odot}\right) \left(\frac{d}{1\ \mathrm{kpc}}\right)^{-2} \left(\frac{E_\gamma}{1\ \mathrm{TeV}}\right)^{-1.7}\ \mathrm{cm}^{-2}\ \mathrm{s}^{-1}, \qquad (2.4)$$

where M is the mass of the MC, $M_\odot$ is the solar mass, and d is distance from Earth. Notice that the contribution of the gamma rays produced from the interaction CR nuclei heavier than proton with matters inside the MC is already taken into account

by the nuclear enhancement factor (Kafexhiu et al., 2014). Also, the factor ε is introduced to incorporate any possible fluctuation in the density of CRs at the position of the cloud[5]. We should also note that, in the case where the CR spectrum follows a power law with index different from 2.7, we expect ε to vary also with the energy of gamma rays. If MCs with masses and distances known from other measurements are detected in gamma rays, the value of ε could be obtained and, thus, it allows us to determine the spectrum of CR hadrons at the position of the cloud.

Such a measurement has been performed, for example, with the HESS telescope for an MC complex located in the inner Galaxy (also known as *Galactic Center ridge*). The spatial extension of the gamma-ray emission is roughly 1° around the galactic center and it coincides with the region of dense gas which could also be traced with the emission line of CS (Aharonian et al., 2006). Interestingly, the analyses of these gamma-ray data suggest that not only the value of the CR intensity in the Galactic Center ridge at 10 TeV is about three to ten times higher than the one observed on Earth but also the slope (approximately 2.3) is much harder than the typical value of 2.7 observed locally. These properties could be inferred as evidences for the presence of CR sources in the Galactic Centre that have been active in the last 10000 years (Aharonian et al., 2006; HESS Collaboration et al., 2016).

Another interesting example is the constraint of the proton CR spectrum on the Galactic scale using gamma-ray data from giant MCs or cloud complexes in the GeV energy range obtained by the *Fermi*-LAT telescope (Casanova et al., 2010; Yang et al., 2014; Aharonian et al., 2018). The analyses of these data seems to indicate a quite homogeneous distribution of CRs in the GeV energy range within our Galaxy meaning the value of ε from Eq. 2.4 fluctuates within only a factor of a few on large spatial scale. In particular, several works by the Fermi collaborations on the gamma-ray emissions from regions of dense gas in the second and the third Galactic quadrant suggests that the variation of the CR intensity with the galactocentric distance is even weaker than expected from typical models for the propagation of Galactic CRs (Abdo et al., 2010b; Ackermann et al., 2011). More recent works by Yang et al. (2014) and Aharonian et al. (2018) concentrated more on gamma rays from giant MCs have arrived at the almost same conclusion[6] and, more importantly, the inferred spectral indices of CRs at the positions of these clouds also varies slightly around the common value of 2.7 reported from direct observations.

These examples clearly illustrate the use of MCs as *CR barometers* meaning the analyses of gamma-ray data from these objects could be help to pinpoint regions of CR over- or under-density. In this sense, MCs located near SNRs would be even more stimulating to be targeted for gamma-ray observations since their detection in gamma rays might provide an evidence for the presence of CR hadrons injected into these clouds after being accelerated from the SNR shocks. An interesting example

[5]It should be noted that $\varepsilon = 1$ would indicate an intensity of CRs that is exactly the same as the one detected on Earth.

[6]In the recent paper by Aharonian et al. (2018), some variations have been spotted for the region with galactocentric distances between 4 to 6 kpc. However, it is argued that the enhancement of the CR intensities is more likely due to the existence of active accelerators in this region.

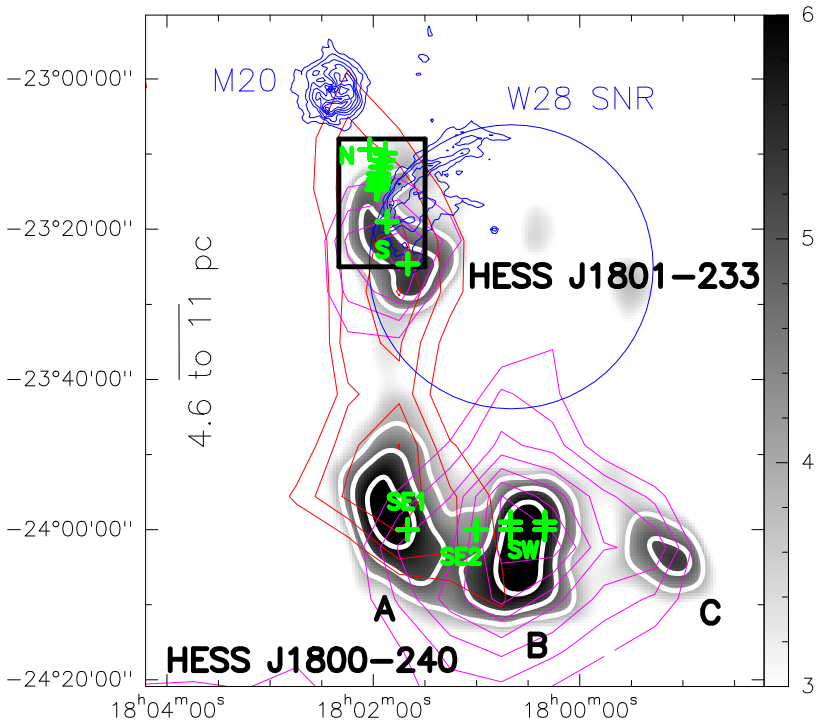

FIGURE 2.1: The W28 complex adopted from Vaupré et al. (2014). The grey scale (in σ) illustrates the regions of TeV emission as seen by HESS with the $4-6\sigma$ significance of the gamma-ray excess represented by the white contours (Aharonian et al., 2008). The red and magenta contours depict the CO(1-0) emission integrated over 15−25 km/s and 5−15 km/s respectively (Dame et al., 2001). The positions observed by the IRAM 30m telescope are also shown with the green crosses (Vaupré et al., 2014). The 20 cm free-free emission in the M20 region is also illustrated with the blue contours (Yusef-Zadeh et al., 2000). The approximate radio boundary of the SNR W28 is also shown as the blue circle (Brogan et al., 2006).

is the complex of clouds in the vicinity of the SNR W28. As we can see in Fig. 2.1, there are several regions of high-density gas as traced by the CO emission line which are also observed with gamma-ray telescopes in the energy range from GeV to TeV. The value of $\varepsilon \simeq 10-30$ inferred from gamma-ray data suggests that the CRs responsible for these emissions are particles escaped from the SNR. A more in-depth discussion for the CR spectrum in the vicinity of SNR W28 will be postponed until Chapter 6 where the analysis for low-energy CRs will also be included. As a remark, we note that gamma rays in the GeV energy range have been detected only from the north-eastern MC (HESS J1801-233) and not from the southern cloud complex (HESS J1800-240) which seems to indicate that the escape and diffusive propagation of these particles are energy dependent. This means that these gamma-ray observations could also help us to better understand the transport of CRs in the vicinity of their sources where there might be a supression of the diffusion coefficient due to, for instance, non-linear effects like streaming instability (Gabici et al., 2010; Nava & Gabici, 2013; Nava et al., 2016).

Since the pion production due to proton-proton interactions has the kinetic

threshold at the proton kinetic energy $E = E_{th} \simeq 280$ MeV, gamma-ray observations of MCs with current instruments provide constraints only for CRs with energy above a few GeVs. Nevertheless, probing CRs with MCs remains feasible at low energy thanks to the physical quantity known as the ionization rate which reflects in a quantitative way the impact of CRs on the chemistry in molecular environments. In the following, we shall briefly present how this quantity could be measured from observational data in the millimeter and infrared domains. All the necessary tools to predict its value from a theoretical point of view will also be introduced for later discussion.

2.2 Cosmic-Ray Induced Ionization Rate from Observations

As briefly mentioned in Chapter 1, CRs are crucial for the cloud chemistry since they are the only agent capable of ionizing molecules in the interior of MCs. In particular, low-energy CRs regulate the H_2 ionization rate (denoted as $\zeta(H_2)$) which represents the number of H_2 ionizations per unit of time and per H_2 molecules of the interacting medium. The ionization rate, to a good approximation, determines directly the formation rate of the ion H_3^+ which is, in fact, the most fundamental initiator for most ion-neutral chemical reactions in the ISM. Since many of the chemical species produced from these reactions and also H_3^+ itself have spectroscopic features either in absorption or emission observable by infrared and radio telescopes, we could now measure the CR induced ionization rate and, thus, it has opened up the possibilities to gain more insight into the low-energy CR spectrum in our Galaxy by comparing the observed and modelled values of $\zeta(H_2)$ for MCs at various positions.

Before the indirect measurements of this quantity became possible, the ionization rate could only be obtained from theoretical estimates using the CR spectra observed on Earth. The main problem of this approach was that the CR spectra were also unknown in the energy range most relevant for ionization due to the effect of solar modulation as briefly mentioned in Chapter 1. In the end, most of the pioneering theoretical investigations were done by simply extrapolating to low energies the spectra of CRs observed at high energies. The most well-known result of this type is perhaps that of Spitzer & Tomasko (1968). The predicted value of the CR ionization rate is approximately 10^{-17} s^{-1} which is now known as the *Spitzer value*. However, recent data on the CR spectra beyond the heliospheric boundary from both Voyager 1 and 2 seem to indicate that there exists a spectral break in the intensities of CRs at energy around a few hundreds MeV. More importantly, observational data seems to point towards a much higher value for the ionization rate for diffuse MCs. The validity of the Spitzer value has, therefore, become questionable. The reassessment of the ionization rate given our current understanding of the CR spectra at low energy will be discussed further in Chapter 3. For now, we shall continue with an overview on two of the most popular techniques to determine $\zeta(H_2)$ from an observational point of view.

In general, the ionization of H_2 in MCs by low-energy CRs is due to the following three most important channels (see Padovani et al., 2009, and references therein):

$$p_{CR} + H_2 \longrightarrow p_{CR} + H_2^+ + e, \tag{2.5}$$
$$p_{CR} + H_2 \longrightarrow H + H_2^+, \tag{2.6}$$
$$e_{CR} + H_2 \longrightarrow e_{CR} + H_2^+ + e, \tag{2.7}$$

which are respectively referred to as ionization of H_2 by proton impact, ionization by electron capture, and ionization of H_2 by electron impact. The ion H_3^+ is then formed in the reaction (see e.g. Oka, 2006):

$$H_2^+ + H_2 \longrightarrow H_3^+ + H. \tag{2.8}$$

Since the reaction rate of the above reaction is much faster than the H_2 ionization rate, it is typically assumed that the rate of H_3^+ production per unit of volume is $\zeta(H_2)n(H_2)$. In diffuse MCs, the destruction of H_3^+ is mostly due to the dissociative recombination with electrons[7] which occur at the rate per unit of volume of $k_e n(H_3^+)n_e$. Thus, the rate of change of $n(H_3^+)$ could be estimated from the following equation:

$$\frac{\mathrm{d}n(H_3^+)}{\mathrm{d}t} = \zeta(H_2)n(H_2) - k_e n(H_3^+)n_e. \tag{2.9}$$

In a steady state, we should expect the production and destruction rates to be balanced and, thus, the ionization rate could be calculated as:

$$\zeta(H_2) = \frac{2}{f_{H_2}} k_e x_e \frac{N(H_3^+)}{L}, \tag{2.10}$$

where $f_{H_2} = 2n(H_2)/n_H$ is the fraction of hydrogen atoms in molecular form, $k_e \simeq 2.6 \times 10^{-7}$ cm^3/s at temperature $T = 27$ K typical for MCs is the rate coefficient for the recombination reaction (McCall et al., 2003), $x_e = n_e/n_H$ is the electron fraction, L is the depth of the cloud, and $N(H_3^+) = n(H_3^+)L$ is the column density of H_3^+ in the cloud. The reference value for the electron fraction in diffuse clouds is roughly $x_e \simeq 1.5 \times 10^{-4}$ (Indriolo & McCall, 2012) and, thus, the ionization rate is (Oka, 2006):

$$\zeta(H_2) \simeq \frac{2.6 \times 10^{-15}}{f_{H_2}} \left[\frac{N(H_3^+)}{10^{14}\ \mathrm{cm}^{-2}}\right] \left(\frac{L}{1\ \mathrm{pc}}\right)^{-1}\ \mathrm{s}^{-1}. \tag{2.11}$$

This means that if we could estimate the column density of H_3^+ and the size of the cloud (assuming that the three dimensions are roughly the same), the ionization rate could then be evaluated using Eq. 2.11.

For diffuse clouds, the column density of H_3^+ is typically determined by studying the absorption lines of H_3^+ in the infrared domain. Since this technique relies on

[7] In diffuse MCs, these electrons are released by the photo-ionization of C into C^+.

the detection of H_3^+ in absorption, it could only be realized in the case where there is a infrared-bright star behind (or embedded within) the MC. A recent survey of H_3^+ towards isolated diffuse MCs has been performed by Indriolo & McCall (2012) where H_3^+ has been detected for 21 out of 50 lines of sight examined. It is found that the mean value of CR ionization rate is around $\zeta(H_2) \sim 3.5 \times 10^{-16}$ s^{-1} which is more than an order of magnitude larger than the Spitzer value. As we shall see later in Chapter 3, this is, in fact, a quite problematic issue for the study of low-energy CRs since such a high level of ionization would require much more low enery CRs than what has been observed in the local ISM. More importantly, the data for only diffuse clouds do not seem to highlight a clear dependence of the ionization rate on the column density of the clouds.

Let's now turn our attention to the case of dense MCs. For these clouds, H_3^+ are destroyed more efficiently from the following reaction with CO:

$$H_3^+ + CO \longrightarrow HCO^+ + H_2. \tag{2.12}$$

If we also take into account the rate of destruction of H_3^+ due to the dissociative recombination, the rate of change for $n(H_3^+)$ is then:

$$\frac{dn(H_3^+)}{dt} = \zeta(H_2)n(H_2) - k_{CO}n(H_3^+)n(CO) - k_e n(H_3^+)n_e. \tag{2.13}$$

We could then follow the same procedure as in the case of diffuse clouds which is to consider the steady state and balance the rate of production and destruction to obtain an expression for the ionization in terms of the column density of H_3^+ similar to Eq. 2.11. Under typical conditions for MCs, we should obtain:

$$\zeta(H_2) \simeq 2 \times 10^{-17} \left[\frac{N(H_3^+)}{10^{14}\ \text{cm}^{-2}}\right] \left(\frac{L}{\text{pc}}\right)^{-1}\ \text{s}^{-1}. \tag{2.14}$$

Although there are cases of dense MCs where this technique has been adopted and the resulting ionization rates are estimated to be of order of the Spitzer value (Geballe & Oka, 1996; McCall et al., 1999), the detection of H_3^+ for clouds with large column density is, in general, more difficult. This is because the spectroscopic features of the background sources might be completely obscured by the cloud itself. It is for this reason that an alternative approach is required for dense MCs. We shall now present the method proposed by Caselli et al. (1998) which relies on the millimeter emission lines of the molecular ions HCO^+ and DCO^+.

Let's first discuss the chemistry at work for HCO^+ and DCO^+. We note that the production of DCO^+ is mostly due to the following chain of reaction:

$$H_3^+ + HD \longrightarrow H_2D^+ + H_2, \tag{2.15}$$
$$H_2D^+ + CO \longrightarrow DCO^+ + H_2. \tag{2.16}$$

Now, if we take into account the destruction of H_2D^+, DCO^+ and HCO^+ due to the process of dissociative recombination with electrons, the equations describing the

rates of change of $n(H_2D^+)$, $n(DCO^+)$, and $n(HCO^+)$ read:

$$\frac{dn(H_2D^+)}{dt} = k_D n(H_3^+) n(HD) - k'_{CO} n(H_2D^+) n(CO) - k'_e n(H_2D^+) n_e \quad (2.17)$$

$$\frac{dn(HCO^+)}{dt} = k_{CO} n(H_3^+) n(CO) - \beta_e n(HCO^+) n_e \quad (2.18)$$

$$\frac{dn(DCO^+)}{dt} = k'_{CO} n(H_2D^+) n(CO) - \beta_e n(DCO^+) n_e \quad (2.19)$$

where we have assumed that the rate coefficients for the recombination with electrons of HCO^+ and DCO^+ (denoted as β_e) are the same (Lee et al., 1996) and also $k'_{CO} \simeq k_{CO}/3$ since H_2D^+, when interacts with CO, could also form HCO^+ at a rate two times larger than that for DCO^+ production (Caselli, 2002). In steady state, the combination of Eq. 2.13 and the three equations above give:

$$R_H \equiv \frac{n(HCO^+)}{n(CO)} = \frac{k_{CO}\zeta(H_2) n(H_2)}{\beta_e n_e \left[k_{CO} n(CO) + k_e n_e\right]}, \quad (2.20)$$

$$R_D \equiv \frac{n(DCO^+)}{n(HCO^+)} = \frac{k_D n(HD)}{3\left[k_{CO} n(CO) + k'_e n_e\right]}. \quad (2.21)$$

Notice that the gas is typically assumed to be fully molecular for dense clouds meaning $n(H) = 0$ and, thus, $n_H = 2n(H_2)$. Taking the values for the fractional abundance of CO to be $x(CO) = n(CO)/2n(H_2) \simeq 9.5 \times 10^{-5}$, the abundance of deuterium relative hydrogen to be $n(HD)/n(H_2) \simeq 1.5 \times 10^{-5}$, and the numerical values for the rate coefficients to be $k_D \simeq 1.7 \times 10^{-9}$ cm^{-3}/s, $k_{CO} \simeq 6.6 \times 10^{-10}(T/300\ \mathrm{K})^{-0.5}$ cm^{-3}/s, and $k'_e \simeq 6.0 \times 10^{-8}(T/300\ \mathrm{K})^{-0.5}$ cm^{-3}/s (see e.g. Caselli, 2002; Ceccarelli & Dominik, 2005), we could transform Eq. 2.21 and Eq. 2.20 into the equations for the ionization fraction and the ionization rate for a typical dense MC at temperature $T = 10$ K:

$$x_e \simeq 10^{-7}\left(\frac{0.13}{R_D} - \frac{10}{f_D}\right) \quad (2.22)$$

$$\frac{\zeta(H_2)}{n_H} \simeq R_H x_e \left(0.001 x_e + \frac{9.7 \times 10^{-10}}{f_D}\right) \quad (2.23)$$

where f_D is the fraction of CO in gaseous form. Once the values of R_H and R_D are determined from the spectroscopic analyses, these two equations[8] provide a straightforward way to estimate the ratio $\zeta(H_2)/n_H$ and the ionization rate is then retrieved with some further chemical modelings.

Although the chemistry inside MCs has been greatly simplified in the models discussed above, they still help emphasize crucial ideas behind the indirect measurements of the ionization rate using the infrared and millimeter spectroscopic features of these objects. Indeed, we have placed our attention on some of the well studied

[8]Notice that this simple chemical model would not work for the case $R_D > 0.013 f_D$ since it would result in a negative value for x_e.

ions like H_3^+, DCO^+ and HCO^+, but it should be stressed that other chemical species such as H_2^+ , OH^+, H_2O^+, H_3O^+ and so on have been proposed and even used to infer the value of the ionization rate (see Becker et al., 2011; Indriolo et al., 2015, and references therein).

2.3 Theoretical Estimate of the Ionization Rate

Having established some of the key features of the ionization rate in observations, we shall proceed to introduce the framework for the evaluation of the ionization rate given an arbitrary spectrum of CRs. Following Padovani et al. (2009) we define the ionization rate of H_2 due to CR protons and electrons as:

$$\zeta_p(H_2) = \int_I^{E_{\max}} f_p(E)\, v \left[1 + \phi_p(E)\right] \sigma^p_{\rm ion}(E)\, \mathrm{d}E + \int_0^{E_{\max}} f_p(E)\, v\, \sigma_{\rm ec}(E)\, \mathrm{d}E \tag{2.24}$$

$$\zeta_e(H_2) = \int_I^{E_{\max}} f_e(E)\, v_e \left[1 + \phi_e(E)\right] \sigma^e_{\rm ion}(E)\, \mathrm{d}E \tag{2.25}$$

where $f_p(E)$ and $f_e(E)$ are respectively the spectra of CR protons and electrons spatially averaged over the whole MC, $\sigma^p_{\rm ion}$, $\sigma_{\rm ec}$, and $\sigma^e_{\rm ion}$ are the proton ionization cross section, the electron capture cross section, and the electron ionization cross section, respectively. The functions $\phi_p(E)$ and $\phi_e(E)$ represents the average secondary ionization per primary ionization due to CR protons and electrons respectively as in Krause et al., 2015. The ionization potential of H_2 is taken to be $I \simeq 15.426$ eV. It should be noted that the contribution of CR nuclei heavier than proton should also be incorporated using an effective enhancement factor $\eta \simeq 1.5$ (see Padovani et al., 2009, for the formal derivation) and, thus, the CR induced ionization rate reads:

$$\zeta(H_2) = \eta\zeta_p(H_2) + \zeta_e(H_2). \tag{2.26}$$

In the following, we shall present in more details all the empirical models of the cross sections used in the calculation of the ionization rate. Also, the formal derivation for the form of $\phi_p(E)$ and $\phi_e(E)$ will be discussed in more details. For the rest of this section, we will denote the kinetic energy of primary CRs (either protons or electrons) and secondary electrons to be E and W respectively.

2.3.1 Cross Section for Cosmic Ray Ionization of H_2

Ionization by Proton Impact

Let's first introduce the following quantities that appear in the differential cross section:

$$T = \frac{E}{\lambda}, \qquad w = \frac{W}{I}, \qquad v_m = \sqrt{\frac{m_p c^2}{2\lambda I}}\beta, \qquad w_c = \frac{4E - 2\sqrt{IT} + (R/4)}{I}, \tag{2.27}$$

where λ is the ratio between the proton mass and the electron mass $\lambda = m_p/m_e$, $R \simeq 13.6$ eV is the binding energy of the electron in the hydrogen atom, and β is the ratio between the speed of the particle and the speed of light. Here, the differential cross section for proton ionization is the one developed from an empirical model by Rudd (1988) (see Krause et al., 2015, for the relativistic correction):

$$\frac{\mathrm{d}\sigma^p_{\mathrm{ion}}}{\mathrm{d}w} = 4\pi a_0^2 N \left(\frac{R}{I}\right)^2 \frac{\Big[F_1(v_m) + F_2(v_m)w\Big]}{\Big\{1 + \exp\left[\alpha'(w - w_c)/v_m\right]\Big\}\,(1+w)^3}. \tag{2.28}$$

where a_0 is the Bohr radius, N is the orbital electron occupation number ($N = 2$ for H_2), and the functions $F_1(v_m)$ and $F_2(v_m)$ are as follows:

$$F_1(v_m) = \frac{A_1 \ln\left(1 + v_m^2\right)}{v_m^2 + \dfrac{B_1}{v_m^2}} + \frac{C_1 v_m^{D_1}}{1 + E_1 v_m^{D_1+4}}, \tag{2.29}$$

$$F_2(v_m) = \frac{\left(\dfrac{A_2}{v_m^2} + \dfrac{B_2}{v_m^4}\right) C_2 v_m^{D_2}}{\dfrac{A_2}{v_m^2} + \dfrac{B_2}{v_m^4} + C_2 v_m^{D_2}}. \tag{2.30}$$

Here, the fit parameters are $A_1 = 0.8$, $B_1 = 2.9$, $C_1 = 0.86$, $D_1 = 1.48$, $E_1 = 7.0$, $A_2 = 1.06$, $B_2 = 4.2$, $C_2 = 1.39$, and $D_2 = 0.48$.

The cross section for this process of ionization could be obtain by integrating numerically the differential cross section with respect to w in the range from $w = 0$ to $w_{\max} = Q_{\max}/I$ with $Q_{\max}$ is the maximum possible energy transferred to be estimated from a binary collision between a proton and a stationary electron. For an imcoming proton with Lorentz factor γ, we shall have:

$$Q_{\max} = \frac{2m_e c^2 \beta^2 \gamma^2 \lambda^2}{1 + 2\gamma\lambda + \lambda^2}, \tag{2.31}$$

Ionization by Electron Impact

Using again the dimensionless notations $t = E/I$ and $w = W/I$, we have the differential cross section of this reaction obtained from the relativistic binary-encounter-dipole model as follows (Kim et al., 2000):

$$\begin{aligned}\frac{\mathrm{d}\sigma^e_{\mathrm{ion}}}{\mathrm{d}w} = \frac{2\pi a_0^2 \alpha^4 N}{(\beta_t^2+\beta_u^2+\beta_b^2)b'}\Bigg\{&\frac{N_i/N-2}{t+1}\left(\frac{1}{w+1}+\frac{1}{t-w}\right)\frac{1+2t'}{(1+t'/2)^2}\\&+[2-(N_i/N)]\left[\frac{1}{(w+1)^2}+\frac{1}{(t-w)^2}+\frac{b'^2}{(1+t'/2)^2}\right]\\&+\frac{1}{N(w+1)}\frac{df}{dw}\left[\ln\left(\frac{\beta_t^2}{1-\beta_t^2}\right)-\beta_t^2-\ln(2b')\right]\Bigg\},\end{aligned} \tag{2.32}$$

where α is the fine-structure constant, and N is the orbital electron occupation number. With v_t, v_b, and v_u as the speed of electrons with correspondingly kinetic energy E, I, and U ($U = 39.603$ eV is the average orbital kinetic energy of electrons), we have:

$$\beta_t = v_t/c, \quad \beta_t^2 = 1-\frac{1}{(1+t')^2}, \quad t' = E/m_e c^2, \tag{2.33}$$

$$\beta_b = v_b/c, \quad \beta_b^2 = 1-\frac{1}{(1+b')^2}, \quad b' = I/m_e c^2, \tag{2.34}$$

$$\beta_u = v_u/c, \quad \beta_u^2 = 1-\frac{1}{(1+u')^2}, \quad u' = U/m_e c^2. \tag{2.35}$$

The function df/dw is called the differential dipole oscillator strength which is approximated as a power law series as follows:

$$\frac{df}{dw} = \frac{C_0}{(1+w)^3}+\frac{D_0}{(1+w)^4}+\frac{E_0}{(1+w)^5}+\frac{F_0}{(1+w)^6}, \tag{2.36}$$

For the case of H_2, the fit parameters are: $C_0 = 1.1262$, $D_0 = 6.382$, $E_0 = -7.8055$, and $F_0 = 2.144$. Finally, N_i is given by:

$$N_i = \int_0^\infty \frac{df}{dw}dw = \frac{C_0}{2}+\frac{D_0}{3}+\frac{E_0}{4}+\frac{F_0}{5}. \tag{2.37}$$

The total ionization cross section could be obtained by integrating Eq. 2.32 over w from $w = 0$ to $w = (t-1)/2$:

$$\begin{aligned}\sigma^e_{\mathrm{ion}} = \frac{2\pi a_0^2 \alpha^4 N}{(\beta_t^2+\beta_u^2+\beta_b^2)b'}\Bigg\{&D(t)\left[\ln\left(\frac{\beta_t^2}{1-\beta_t^2}\right)-\beta_t^2-\ln(2b')\right]\\&+\left(2-\frac{N_i}{N}\right)\left[1-\frac{1}{t}-\frac{\ln t}{t+1}\frac{1+2t'}{(1+t'/2)}\right]\Bigg\},\end{aligned} \tag{2.38}$$

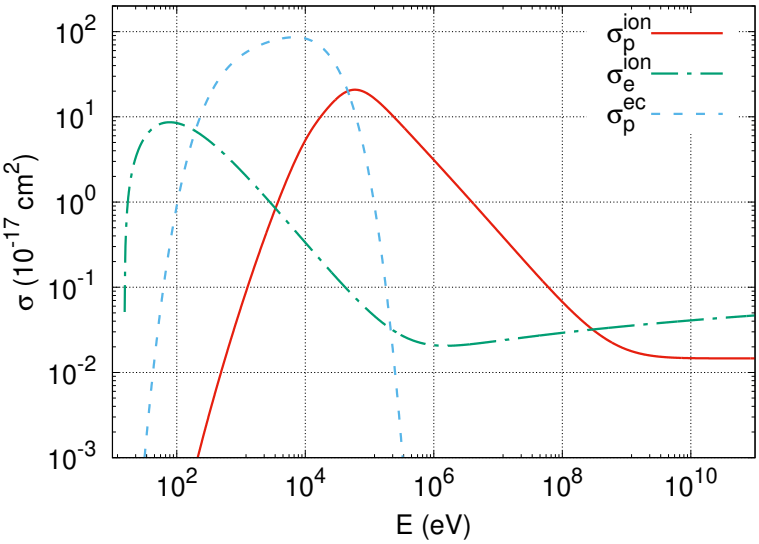

FIGURE 2.2: Cross sections of the three most important channels of ionization. The solid red curve shows the ionization cross section by proton impact. The dot-dash green curve depicts the ionization cross section by electron impact. The dashed blue curve corresponds to the electron capture cross section.

where the function $D(t)$ is defined as:

$$\begin{aligned} D(t) &= \frac{1}{N}\int_0^{(t-1)/2}\left(\frac{1}{1+w}\right)\frac{df}{dw}dw \\ &= -\frac{1}{N}\left\{\frac{C_0}{3}\left[\left(\frac{2}{t+1}\right)^3-1\right]+\frac{D_0}{4}\left[\left(\frac{2}{t+1}\right)^4-1\right]\right. \\ &\qquad \left.+\frac{E_0}{5}\left[\left(\frac{2}{t+1}\right)^5-1\right]+\frac{F_0}{6}\left[\left(\frac{2}{t+1}\right)^6-1\right]\right\}. \end{aligned} \tag{2.39}$$

Ionization by Electron Capture

For the electron capture cross section, we also use a fit provided in Padovani et al., 2009 as follows:

$$\sigma_p^{\rm ec}(E) = 10^{d_0+d_1\log(E)+d_2\log^2(E)+d_3\log^3(E)+d_4\log^4(E)} \tag{2.40}$$

where the cross section is in cm^2, E is in eV, and the fit parameters are $d_0 = -52.793928$, $d_1 = 41.219156$, $d_2 = -17.304947$, $d_3 = 3.292795$, and $d_4 = -0.238372$. In figure 2.2, the cross sections of the three processes presented above are shown to give a better view of the relative contribution of each process to the ionization rate.

2.3.2 Secondary Ionization

The final ingredient for the evaluation of the ionization rate is the contribution of secondary ionization. After being stripped from its molecules, the secondary electrons could sometimes produce further ionization if they are energetic enough. Since the energy of secondary electrons vary with the kinetic energy of the primary (incident) particle E, the average number secondary ionizations per primary ionizations should be a function of the form $\phi = \phi(E)$.

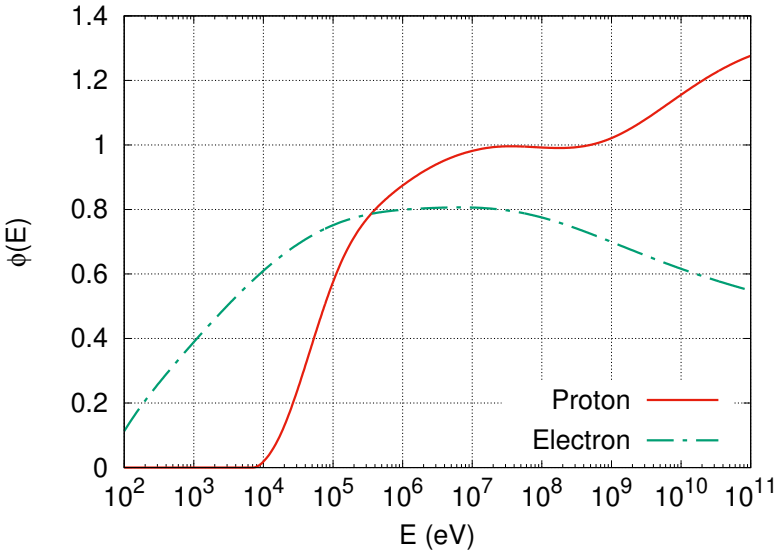

FIGURE 2.3: Average number of secondary ionizations per primary ionization. The solid red and dot-dash green curves show the number of secondary ionizations for protons and electrons respectively.

Let's denote $j_i(E)$ to be the intensity of primary CRs ($i = p$ and $i = e$ for the case of primary protons and electrons respectively) and, thus, the number of primary ionizations per unit of time induced by particles with kinetic energy E should be:

$$N_i(E) = j_i(E)\sigma^i_{\text{ion}}(E)\,\mathrm{d}E, \tag{2.41}$$

where $\sigma^i_{\text{ion}}(E)$ is the ionization cross section for primary particles. The intensity of secondary electrons with kinetic energy W that are generated from primary particles with kinetic energy E reads:

$$j_s(E, W) = n(\mathrm{H}_2)j_i(E)\,\mathrm{d}E\frac{\mathrm{d}\sigma^i_{\text{ion}}}{\mathrm{d}W}\,\mathrm{d}W v_s\left(-\frac{W}{\dot{W}}\right), \tag{2.42}$$

where $\mathrm{d}\sigma^i_{ion}/\,\mathrm{d}W$ is the differential ionization cross section of primary particles, v_s is the speed of secondary electrons, and the factor $-W/\dot{W}$ represents the residence time of secondary electrons which we have approximated to be roughly the energy loss time of these electrons. In the case where the cloud is fully molecular, $n_{\mathrm{H}} = 2n(\mathrm{H}_2)$,

we should have:

$$j_s(E, W) = j_p(E)\,\mathrm{d}E \frac{\mathrm{d}\sigma^i_{\mathrm{ion}}}{\mathrm{d}W}\,\mathrm{d}W \frac{W}{L_e(W)}. \tag{2.43}$$

The total number of secondary ionization per unit of time induced by primary particles with kinetic energy E could be estimated as:

$$N_s(E) = \int_I^{Q^i_{\max}} j_s(E, W)\sigma^e_{\mathrm{ion}}(W)\,\mathrm{d}W, \tag{2.44}$$

where $Q_{\max}$ is the maximum possible energy transferred in the binary collision between the primary particle and the secondary electron assumed to be initially at rest. If the primary particle is a proton, the form of $Q^p_{\max}$ is given in Eq. 2.31. For the case of electrons, we shall have $Q^e_{\max} = (E - I)/2$. From Eq. 2.41 and Eq. 2.44, we shall have the average secondary ionization per primary ionization to be:

$$\phi_i(E) = \frac{N_s(E)}{N_i(E)} = \frac{1}{\sigma^i_{\mathrm{ion}}(E)} \int_I^{Q_{\max}} \frac{W}{L_e(W)} \sigma^e_{\mathrm{ion}}(W) \frac{\mathrm{d}\sigma^i_{\mathrm{ion}}}{\mathrm{d}W}\,\mathrm{d}W. \tag{2.45}$$

The corresponding secondary ionization for both protons and electrons are shown in Figure 2.3. We could see that for both species the contribution is non-negligible starting from $E \simeq 10$ keV. As we shall see later in Chapter 3, the energy range that is most relavant for ionization is around a few hundreds MeV and, thus, the contribution of secondary ionizations to the CR induced ionization rate should be roughly same as the one for primary ionizations.

Chapter 3

Cosmic-Ray Ionization in Diffuse Molecular Clouds

As mentioned in Chapter 1, since MCs shield quite effectively both UV photons and X-rays (McKee, 1989; Krolik & Kallman, 1983; Silk & Norman, 1983), CRs seem to be the only agents capable of ionizing their interior. It is for this reason that CRs are believed to play an essential role in determining the chemistry (Dalgarno, 2006) and the evolution of these star-forming regions (e.g., Wurster et al., 2018). Recent observations (Caselli et al. 1998; Indriolo & McCall 2012, see also Padovani & Galli 2013; Padovani et al. 2020 for reviews) have suggested that the CR induced ionization rate decreases for increasing column density of MCs and it varies from around $\approx 10^{-16}$ s^{-1} for diffuse MCs down to $\approx 10^{-17}$ s^{-1} for dense ones.

The ionization rates measured in MCs are tentatively interpreted as the result of the penetration of ambient CRs into clouds (Padovani et al., 2009). Thus, in order to model this process and test this hypothesis one needs to know: *i)* the typical spectrum of low-energy CRs in the Galaxy, and *ii)* the details of the transport process of CRs into MCs. Remarkably, the spectra of both proton and electron CRs in the local ISM at least down to particle energy of a few MeVs are now known with some confidence, thanks to the recent data collected by the Voyager probe at large distances from the Sun (Stone et al., 2013; Cummings et al., 2016; Stone et al., 2019). Whether or not such spectra are the representative of the average Galactic spectra, especially for MeV CRs, is still not clear (this is an old standing issue, see e.g. Cesarsky 1975 and the discussion in Chapter 4). However, the analysis of gamma rays from MCs (e.g., Yang et al., 2014) seems to indicate that at least the spectrum of CR protons of energy above a few GeV is quite homogeneous in our Galaxy.

Several theoretical estimates of the CR induced ionization rate in MCs have been performed over the years. The first attempts were done by simply extrapolating to low energies the spectra of CRs observed at high energies, without taking into account the effect of CR propagation into clouds (e.g., Hayakawa et al., 1961; Spitzer & Tomasko, 1968; Nath & Biermann, 1994; Webber, 1998). Such estimates, as noted in the previous chapter, provide a reference value of the CR ionization rate is known as the *Spitzer value* which is an order of magnitude below the observed data for diffuse clouds, and roughly similar to the value found in dense ones.

Later works included also a treatment of the transport of CRs into MCs and considered the role of energy losses (mainly ionization) suffered by CRs in dense

and neutral environments. A natural starting point is to consider the scenario that maximizes the penetration of CRs into clouds. This was done, most notably, by Padovani et al. (2009), who assumed that CRs penetrate MCs by moving along straight lines. A more realistic description, however, should take into account the fact that the process of CR penetration into MC is highly nonlinear in nature. This is because CRs themselves, as they stream into the cloud, generate magnetic turbulence through streaming instability (Wentzel, 1974). The enhanced magnetic turbulence would, in turn, induce an increase in the CR scattering rate onto MHD waves, which regulates their flux into clouds. The exclusion mechanism of CRs from MCs due to this type of self-generated turbulence was first studied in the pioneering works of Skilling & Strong (1976), Cesarsky & Volk (1978), and Morfill (1982), while recent studies in this direction include the works by Everett & Zweibel (2011), Morlino & Gabici (2015), Schlickeiser et al. (2016), and Ivlev et al. (2018). Some of these models, e.g. Phan et al. (2018) and Silsbee & Ivlev (2019), which include a more thorough treatment of the effect of CR penetration into clouds have even proceeded to confront their predictions for the ionization rate with the available observational data.

The main goal of this chapter is to present the model of CR transport from the ISM into MCs as formulated in Morlino & Gabici (2015) and Phan et al. (2018) and also to provide the corresponding ionization rate from this model in the case where the CR spectrum in the ISM is the one observed by Voyager 1. We anticipate here the main results obtained in the following: the intensity of CRs in the local ISM as revealed by Voyager measurements is too weak to explain the level of ionization rate observed in clouds. Possible solutions to this problem include the presence of another source of ionization or a non-uniform intensity of low-energy CRs throughout the Galaxy.

The chapter is organized as follows: in Section 3.1 we describe a model for the penetration of CRs into clouds. The model is then used to derive the spectra of CR protons and electrons inside MCs (Section 3.2) and to predict the CR ionization rate, which is then compared to available data (Section 3.3). We discuss our results and conclude in Section 3.4.

3.1 A Model for Cosmic-Ray Penetration in Diffuse Clouds

The penetration of CRs into diffuse clouds can be described by means of a one-dimensional transport model, where CRs are assumed to propagate only along magnetic field lines. This is a good description of CR transport provided that: *i)* the propagation of particles *across* magnetic field lines can be neglected, and *ii)* the spatial scales relevant to the problem are smaller than, or at most comparable to the magnetic field coherence length in the ISM (here we assume $\approx 50 - 100$ pc). Both conditions are believed to be often satisfied and thus this setup was commonly adopted in the past literature to describe the penetration of CRs into MCs (e.g.

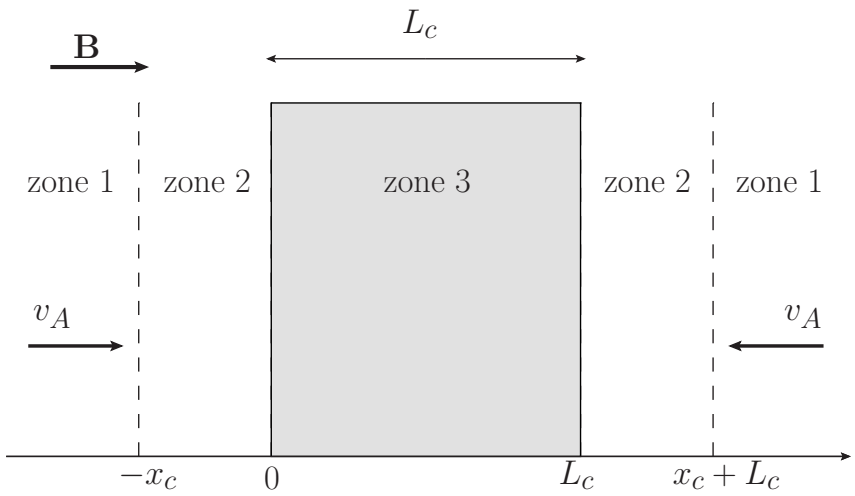

FIGURE 3.1: Setup of the problem. A cloud of size L_c is embedded in an homogeneous magnetic field of strength B directed along the $x-$axis. The direction of the Alfvén speed is also shown. See text for the definition of zone 1, 2, and 3, and of the diffusion scale x_c.

Skilling & Strong, 1976; Cesarsky & Volk, 1978; Morfill, 1982; Everett & Zweibel, 2011; Morlino & Gabici, 2015; Schlickeiser et al., 2016; Ivlev et al., 2018).

In the following, we describe an improved version of the model developed by Morlino & Gabici (2015), who considered a diffuse cloud of size L_c and uniform molecular hydrogen density $n(H_2)$ embedded in a spatially homogeneous magnetic field of strength B directed along the $x-$axis (see Fig. 3.1).

A spatially uniform field in Zones 1 to 3 (see Fig. 3.1) is appropriate to describe diffuse clouds, but not dense ones (see the observational results reported in e.g. Crutcher et al., 2010) that, for this reason, are not considered in this chapter. Note that, for simplicity, the transition from the low density and ionized ISM gas (of density n_i) to the dense and neutral cloud environment (of density $n(H_2) \gg n_i$) is taken to be sharp and located at $x = 0$ and $x = L_c$. Morlino & Gabici (2015) limited themselves to consider the transport of CR protons only, while here we extend the analysis to include also CR electrons. Moreover, as discussed in the remainder of this Section, we improve the description of the transport of CRs inside the cloud.

In the pioneering papers by Skilling & Strong (1976), Cesarsky & Volk (1978) and Morfill (1982) it was suggested that MCs may act as sinks for low-energy CRs. This is because low-energy CR particles lose very effectively their energy due to severe ionization losses in the dense gas of the cloud. In steady state, the rate at which CR particles are removed from the cloud due to energy losses has to be balanced by an incoming flux of CR particles entering the cloud (Skilling & Strong, 1976; Morlino & Gabici, 2015). The penetration of CR particles into the cloud is accompanied by the excitation of Alfvén waves due to streaming instability (Wentzel, 1974). Such instability mainly excites waves propagating in the direction of the streaming of CRs. Therefore, a converging flow of Alfvén waves is generated outside of the cloud (see Fig. 3.1). Once inside the cloud, Alfvén waves are believed to be damped very quickly due to ion-neutral friction (Zweibel & Shull, 1982). It should be noticed that the

effectiveness of streaming instability is ultimately connected to the spatial gradient of the density of CRs and, thus, there might exist also an alternative scenario in dense MCs where the drop of CR density deep inside the cloud makes it possible for streaming instability to sustain Alfvén waves (Ivlev et al., 2018). However, we shall later see that CRs, at least within the energy range relevant for ionization, are uniformly distributed within diffuse MCs and we could, therefore, safely assume that there is no Alfvén wave inside the clouds of interest. Following Morlino & Gabici (2015), we shall consider three regions (see Fig. 3.1):

1. *Zone 1*, located far away from the MC ($x < -x_c$ and $x > x_c + L_c$), where the CR intensity is virtually unaffected by the presence of the cloud. As a consequence, in this zone the CR particle distribution function $f(x, p)$ (p is the particle momentum) is roughly constant in space and equal to the *sea* of Galactic CRs $f_0(p)$. The quantity x_c will be defined later.

2. *Zone 2*, located immediately outside of the cloud ($-x_c < x < 0$ and $L_c < x < L_c + x_c$). In this zone the CR particle distribution function is significantly affected by the presence of the cloud and is significantly different (i.e. smaller) than $f_0(p)$.

3. *Zone 3*, which represents the cloud ($0 < x < L_c$), and where particles suffer energy losses (mainly due to ionization).

The setup of the problem discussed above is intendedly simplified. A more realistic description of a cloud should include, between Zone 2 and 3, an envelope of atomic hydrogen characterized by a quite small column density of the order of few times 10^{20} cm^{-2} (see e.g. Snow & McCall 2006 for a review of cloud properties). Moreover, a smooth transition between the fully ionized and diffuse ISM and the dense and neutral MC should also be considered. In practice, the setup described in Fig. 3.1 can still be considered an appropriate description if the edge of the cloud ($x = 0$ and $x = L_c$) is defined as the position at which the ionization fraction of the gas is small enough to allow for a very effective damping of Alfvén waves due to ion-neutral friction.

Here, we follow Morlino & Gabici (2015) and Phan et al. (2018) to assume that the transport of CRs is diffusive (regulated by the scattering of CRs off Alfvén waves) outside of the cloud (Zones 1 and 2), while it is ballistic inside the cloud (Zone 3), where Alfvén waves are virtually absent (see Ivlev et al. 2018 for a discussion on wave transport in clouds). These authors argued that the propagation of CRs in all three zones could be described by the transport equation as introduced in Chapter 1 (see Eq. 1.54):

$$\frac{\partial f}{\partial t} = \frac{\partial}{\partial x}\left[D(x,p)\frac{\partial f}{\partial x}\right] - v_A\frac{\partial f}{\partial x} - \frac{1}{p^2}\frac{\partial}{\partial p}\left[\dot{p}(x,p)p^2 f\right], \tag{3.1}$$

where $f = f(t, x, p)$ is the isotropic part of the CR particle distribution function, which depends on time t, position x, and particle momentum p, $D(x, p)$ is the CR diffusion coefficient, $\dot{p}(x, p)$ is the rate of momentum loss of CRs which is non-zero

only inside the cloud (since energy loss is mainly due to interaction between CRs and gas), and $v_A = B/\sqrt{4\pi\rho_i}$ is the Alfvén speed (ρ_i is the mass density of the ionized gas). Since we assume here that the density of the ionized gas in all three zones is spatially homogeneous, the Alfvén speed v_A is a constant.

As explained above, the waves propagate in opposite directions on the two sides of the cloud. This means that Eq. 3.1 is, strictly speaking, applicable only in the range $x < 0$ since the advection term would change the sign for waves propagating in the negative direction of the x-axis. Indeed, this complication could be overcome by solving the problem in the range $x < L_c/2$ only and adopting the symmetric condition introduced in Morlino & Gabici (2015) which gives $f(x,p) = f(L_c - x, p)$.

It should be noticed that using the diffusion approach in Zone 3 is not formally correct since the motion of CRs in this zone is not diffusive since we have assumed that there is no Alfvén wave inside the cloud as mentioned above. However, the ballistic motion of CRs could be mimicked by imposing a very large diffusion coefficient in Zone 3. More quantitatively, the assumption to be made is: $D(x,p) = D_c \gg L_c^2/\tau_l$ for $0 < x < L_c$, where D_c is the diffusion coefficient inside the cloud. This approximation should justify the applicability of Eq. 3.1 for our problem of diffuse clouds. Also, we search here for steady-state solutions and thus we set $\partial f/\partial t = 0$ which allows us to re-write the transport equation as:

$$\frac{\partial}{\partial x}\left\{D(x,p)\frac{\partial f}{\partial x}\exp\left[-\int_{-\infty}^{x}\frac{v_A\,\mathrm{d}x'}{D(x',p)}\right]\right\} = \frac{1}{p^2}\frac{\partial}{\partial p}\left[\dot{p}(x,p)p^2 f\right]\exp\left[-\int_{-\infty}^{x}\frac{v_A\,\mathrm{d}x'}{D(x',p)}\right] \tag{3.2}$$

Equation 3.2 could be integrated within the range from an arbitrary value of x (with $x \leq 0$) to $x = L_c/2$ which, after some simple manipulations, gives:

$$D_0\frac{\partial f}{\partial x} = \frac{1}{p^2}e^{\frac{x}{x_c}}\int_0^{L_c/2}\frac{\partial}{\partial p}\left[\dot{p}(x',p)p^2 f_c(x',p)\right]\mathrm{d}x', \tag{3.3}$$

where D_0 is the CR diffusion coefficient in Zone 1 and 2, $x_c = D_0/v_A$ is a characteristic length that defines the extension of Zone 2 in Fig. 3.1, and $f_c(x,p)$ is the distribution function of CRs inside the cloud. It should be noted that in deriving Eq. 3.3 we have employed a consequence of the above-mentioned symmetric condition which is $\partial f(x,p)/\partial x|_{x=L_c/2} = 0$. More importantly, we have also implicitly assumed that $\dot{p} \simeq 0$ in Zones 1 and 2. This is a valid assumption for both protons and electrons, because the energy loss time outside the cloud is much longer than the characteristic dynamical time of the problem, which can be defined as $\sim D_0/v_A^2$ (Morlino & Gabici, 2015). We shall now perform another integration from $x \to -\infty$ to an arbitrary value of x in the range $x \leq 0$ to retrieve an integral equation for the distribution function of CRs outside the cloud (Phan et al., 2018):

$$f(x,p) = f_0(p) - \frac{1}{v_A p^2}e^{\frac{x}{x_c}}\int_0^{L_c/2}\frac{\partial}{\partial p}\left[\dot{p}(p)p^2 f_c(x',p)\right]\mathrm{d}x'\,. \tag{3.4}$$

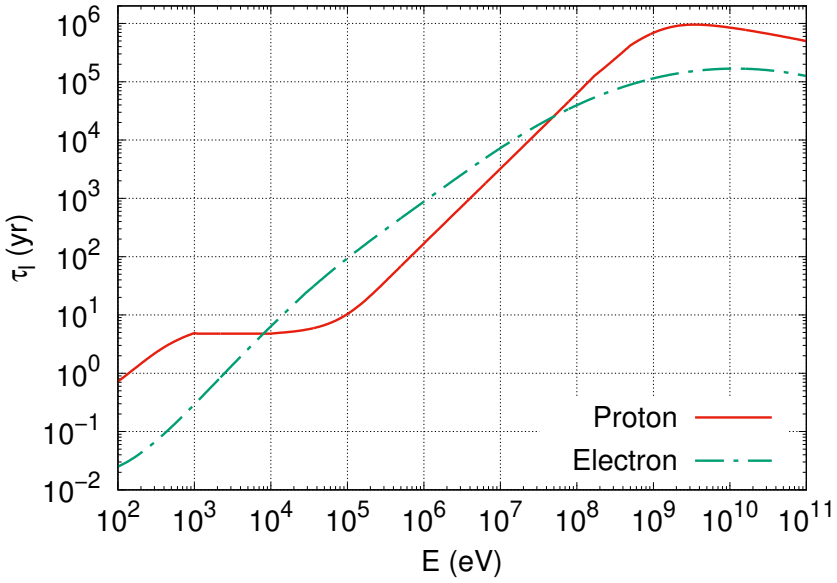

FIGURE 3.2: Energy loss time for CR protons and electrons in a cloud of density $n(H_2) = 100$ cm^{-3}. The loss times are obtained with the energy loss function $L(E)$ from Padovani et al. (2009).

Equation 3.4 provides a quantitative way to connect the distribution of CRs in Zone 1 and 2 with the one in Zone 3.

To find the distribution of CRs inside the cloud, it is convenient to consider separately CRs of high and low energy, with E_* being the energy defining the transition between the two domains (see Ivlev et al. 2018 for a similar approach). Following Morlino & Gabici (2015), E_* is defined in such a way that particles with energy $E > E_*$ can cross ballistically the cloud without losing a significant fraction of their energy. If τ_l is the energy loss time of CRs inside the cloud (see Fig. 3.2), then the energy E_* is obtained by equating τ_l with the CR ballistic crossing time $\tau_c \simeq L_c/\bar{v}(E_*)$, where $\bar{v}$ is the CR particle velocity averaged over pitch angle (the angle between the particle velocity and the direction of the magnetic field). Obviously, for $E > E_*$ the spatial distribution of CRs inside the cloud is, to a very good approximation, constant. It is important to stress that energy losses play an important role also for particle energies $E > E_*$ (no energy losses in a single cloud crossing), because such CRs are confined in the vicinity of the MC by the converging flow of Alfvén waves, and can thus cross and recross the cloud a very large number of times (for a more detailed discussion of this issue the reader is referred to Morlino & Gabici 2015).

3.1.1 Spectra at High Energy

Morlino & Gabici (2015) argued that, for $E > E_*$, the distribution function of CRs inside the cloud is spatially uniform which means that $f_c(x, p) \simeq f_c(p) = f(x = 0, p)$.

This reduces Eq.(3.4) to:

$$f_c(p) = f_0(p) - \frac{L_c}{2v_A p^2}\frac{\partial}{\partial p}\left[\dot{p}(p)p^2 f_c(p)\right] \ . \tag{3.5}$$

From Eq. 3.5 a semi-analytical expression for $f_c(p)$ can be easily derived, and it reads (Phan et al., 2018):

$$f_c(p) = \frac{2v_A\tau_l(p)}{L_c p^3}\int_p^{p^{\rm max}} q^2 f_0(q)\exp\left[-\frac{2v_A}{L_c}\int_p^q \frac{\tau_l(k)}{k}\,{\rm d}k\right]{\rm d}q, \tag{3.6}$$

where we have introduced the loss time inside the cloud $\tau_l(p) = -p/\dot{p}$. Notice that $\dot{p} = -n({\rm H}_2)L(E)$ with $L(E)$ is the energy loss function introduced in Chapter 1. In the following, we shall restrict ourselves to the case where MCs are made up mainly by molecular hydrogen and adopt the loss function of H_2 from Padovani et al. (2009). The corresponding energy loss time is also reported in Fig. 3.2 for both CR protons and electrons.

As said above, Eq. 3.6 provides a general solution for spectrum of CRs with energy $E > E_*$, or equivalently, of momentum larger than $p > p_*$. The numerical values for the critical energy E_* and momentum p_* can be found from the expression $\tau_l(p_*) \simeq 2L_c/v(p_*)$ where $v(p^*)$ is the speed of a particle of momentum p_* (here we set $\bar{v} \simeq v/2$). For a cloud of size $L_c = 10$ pc and $n({\rm H}_2) = 100$ cm^{-3} (or equivalently of column density $N({\rm H}_2) = n({\rm H}_2)L_c = 3.1\times10^{20}$ cm^{-2}), we find $p_{*,p} \simeq 75$ MeV/c and $p_{*,e} \simeq 0.34$ MeV/c corresponding to a kinetic energy of $E_{*,p} \simeq 3.0$ MeV and $E_{*,e} \simeq 0.10$ MeV for protons and electrons, respectively.

3.1.2 Spectra at Low Energy

Particles lose a significant fraction of their energy E in a cloud crossing time τ_c if $E < E_*$. In this case, the approach described in the previous Section still provides a good description of CR transport outside of the cloud (Zones 1 and 2 in Fig. 3.1), but might fail inside the cloud (Zone 3). The reason is that at such low energies the spatial distribution of cosmic rays in Zone 3 is not necessarily constant. Thus, in order to describe the transport of CRs inside the cloud, we will adopt the continuously slowing down approximation as done in Padovani et al., 2009. This consists in connecting the momentum p of a particle located at a position x inside the cloud to the momentum the particle had when it entered the cloud. We will denote this momentum as p_{01} or p_{02} for particles that entered the cloud from the left and right edge of the cloud, respectively. Thanks to the symmetry of the problem (the flux of CRs impinging onto the left and right side of the cloud is identical) we can write:

$$f_c(x,p)\,{\rm d}^3p = \frac{1}{2}\left[f_b(p_{01})\,{\rm d}^3p_{01} + f_b(p_{02})\,{\rm d}^3p_{02}\right]. \tag{3.7}$$

where $f_b(p)$ is the CR particle distribution function at the cloud border, which is assumed to be quite close to an isotropic distribution. Equation 3.7 can be reduced

to:

$$f_c(x,p) = \frac{1}{2}\left[f_b(p_{01})\frac{p_{01}^2\dot{p}(p_{01})}{p^2\dot{p}(p)} + f_b(p_{02})\frac{p_{02}^2\dot{p}(p_{02})}{p^2\dot{p}(p)}\right], \tag{3.8}$$

which can be further simplified by noting that $p_{01} = p_0(x,p)$ and $p_{02} = p_0(L_c - x, p)$.

The function $p_0(x,p)$ can be determined by solving the equation:

$$x = \bar{\mu}\int_{p_0}^{p}\frac{v}{\dot{p}(q)}\,\mathrm{d}q \approx \frac{1}{2}\int_{p_0}^{p}\frac{v}{\dot{p}(q)}\,\mathrm{d}q, \tag{3.9}$$

where we introduced $\bar{\mu}$ as the cosine of the particle pitch angle averaged over the range $\mu > 0$ which gives $\bar{\mu} \simeq 1/2$ in the case of an almost isotropic distribution of particles. Note that, even though deviation from isotropy are expected at low energies (for $E \ll E_*$ one does not expect to have a significant flux of particles out of the cloud), the error introduced by the assumption of CR isotropy is at most a factor of 2 (and most likely significantly less than that, as argued by Ivlev et al. 2018). At this point, it is worth mentioning that the symmetry of p_{01} and p_{02} would lead to the following identification:

$$\int_0^{L_c/2}\frac{\partial}{\partial p}\left[\dot{p}(p_{02})p_{02}^2 f(p_{02})\right]\mathrm{d}x' = \int_{L_c/2}^{L_c}\frac{\partial}{\partial p}\left[\dot{p}(p_{01})p_{01}^2 f(p_{01})\right]\mathrm{d}x', \tag{3.10}$$

which could allow the combination of Eq. 3.4 with Eq. 3.8 to simplify into the following form:

$$f_b(p) = f_0(p) - \frac{1}{2v_A p^2}\int_0^{L_c}\frac{\partial}{\partial p}\left[\dot{p}(p_0(x',p))p_0^2(x',p)f_b(p_0(x',p))\right]\mathrm{d}x'. \tag{3.11}$$

Some more simplifications could be made by transforming the integration variable x' in Eq. 3.11 into p_0 which shall be done by noticing that:

$$\begin{cases} \dfrac{\partial}{\partial p}\left[\dot{p}(p_0)p_0^2 f_b(p_0)\right] = \dfrac{\partial}{\partial p_0}\left[\dot{p}(p_0)p_0^2 f_b(p_0)\right]\dfrac{\partial p_0(x',p)}{\partial p} \\ \mathrm{d}x' = \dfrac{\partial x'(p_0,p)}{\partial p_0}\,\mathrm{d}p_0 \\ \dfrac{\partial x'(p_0,p)}{\partial p_0}\dfrac{\partial p_0(x',p)}{\partial p} = -\dfrac{\partial x'(p_0,p)}{\partial p} = -\dfrac{v}{\dot{p}(p)} \end{cases} \tag{3.12}$$

With all the above identities at hand, Eq. 3.11 could now be re-written as a solvable integral equation for $f_b(p)$:

$$f_b(p) = f_0(p) + \frac{v}{4v_A\dot{p}(p)p^2}\int_p^{p_0^{\max}}\frac{\partial}{\partial p_0}\left[\dot{p}(p_0)p_0^2 f_b(p_0)\right]\mathrm{d}p_0, \tag{3.13}$$

where $p_0^{\max} = p_0(L_c, p)$. This can be solved to give:

$$f_b(p) = \frac{f_0(p) + \frac{v}{4v_A \dot{p}(p) p^2} \left[\dot{p}(p_0^{\max}) \left(p_0^{\max}\right)^2 f_b(p_0^{\max})\right]}{1 + \frac{v}{4v_A}}, \tag{3.14}$$

where $p_0^{\max}(p)$ is defined by Eq. (3.9) with $x = L_c$ and represents the momentum of particles at the border of the cloud that turn into particles with momentum p on the other side of the cloud. Indeed, the expression above still does not give the form of $f_b(p)$ as it requires $f_b(p_0^{\max})$ which, in principle, is unknown. However, the asymptotic behavior would be $f_b(p_0^{max}) \simeq f_c(p)$ for sufficiently large particle energies, with $f_c(p)$ given by Eq. 3.5.

It is should be noticed that Eq. 3.14 is not a formal solution of Eq. 3.4 because, in general, one would expect $\langle \cos\vartheta \rangle \neq 1/2$. However, we have checked the result obtained from Eq. 3.8 with the approximate solution obtained by the method of flux balancing (see Section 2 in Morlino & Gabici 2015) and the two results match for particles with $v \gg v_A$.

3.2 Cosmic-Ray Spectra in Diffuse Clouds

In this Section, we will make use of Eq. 3.6 and Eq. 3.14 to determine the spectrum of CR protons and electrons inside a given MC. In order to do so, we will need to specify:

1. the spectrum of CR protons $f_0^p(p)$ and electrons $f_0^e(p)$ far away from the cloud (Zone 1 in Fig. 3.1);
2. the column density N_{H_2} and the size L_c of the cloud;
3. the Alfvén speed v_A in the medium outside of the cloud (Zones 1 and 2).

As pointed out in Morlino & Gabici (2015), it is a remarkable fact that the spectrum of CRs inside the cloud does not depend on the CR diffusion coefficient (this quantity does not appear in neither Eq. 3.6 nor 3.14).

As a reference case, we will assume that the spectra of CR protons and electrons away from the cloud are identical to those measured by the Voyager 1 probe (Stone et al., 2013; Cummings et al., 2016). This is equivalent to assuming that the spectra measured by Voyager 1 are representative of the entire Galaxy, and not only of the local ISM. We will discuss in Sec. 3.4 the implications of such an assumption. To describe Voyager 1 data, we fit the intensity of CRs together with the available high energy data from AMS (Aguilar et al., 2014; Aguilar et al., 2015) with a broken power law:

$$j_0(E) = C \left(\frac{E}{1\ \mathrm{MeV}}\right)^{\alpha} \left(1 + \frac{E}{E_{\mathrm{br}}}\right)^{-\beta} \ \mathrm{eV}^{-1}\mathrm{cm}^{-2}\mathrm{s}^{-1}\mathrm{sr}^{-1}, \tag{3.15}$$

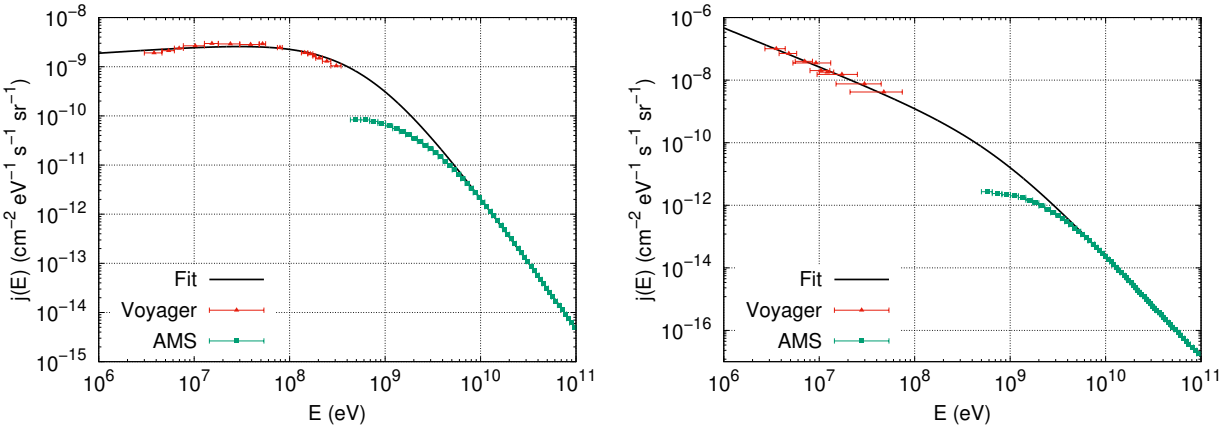

FIGURE 3.3: Data of the CR intensity for protons (left) and electrons (right) taken from Voyager 1 (Cummings et al., 2016) and AMS-02 (Aguilar et al., 2014; Aguilar et al., 2015) compared with the fitted curve used in this work.

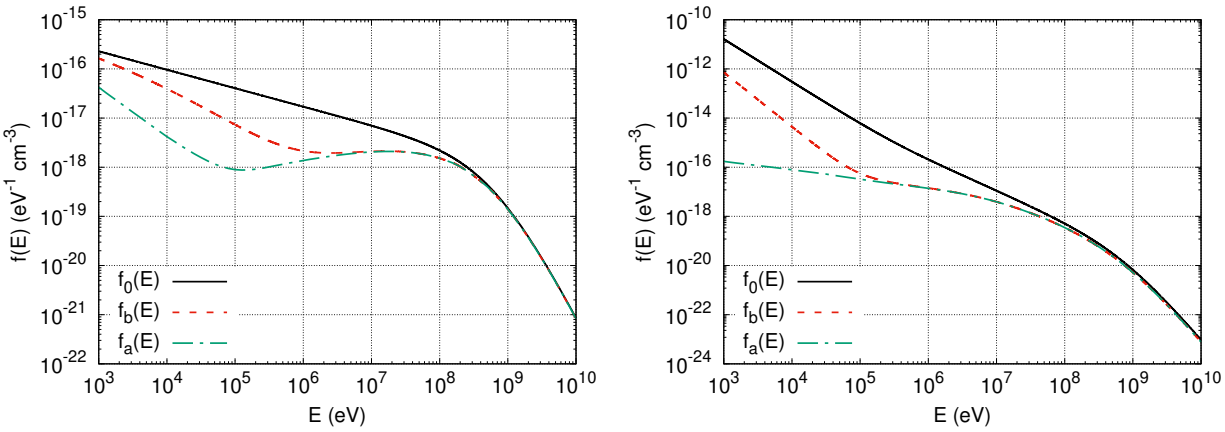

FIGURE 3.4: CR spectra for a cloud of column density $N(\mathrm{H_2}) \simeq 3.1 \times 10^{21}$ cm^{-2} (corresponding to typical values of $n(\mathrm{H_2}) = 100$ cm^{-3} and $L_c = 10$ pc). The left and the right figures are respectively spectra of protons and electrons. Also shown with black solid curves are the ISM spectra given by Eq. (3.15).

where E is the particle kinetic energy and $E_{\rm br}$ is the break energy where the slope changes from $\propto E^{\alpha}$ to $\propto E^{\alpha-\beta}$. The fit parameters are presented in Table 3.1 and the corresponding intensities are plotted in Fig. 3.3.

Even though CR protons and electron spectra have been measured by Voyager only for particle energies larger than few MeV, we extrapolate the fits to lower energies also. As it will be shown in the following, such an extrapolation does not affect at all our results, because particles with energy below few MeV provide a negligible contribution to the ionization rate of clouds.

Results are shown in Fig. 3.4 for both CR protons and electrons, for a cloud of column density $N(\mathrm{H_2}) = 3.1 \times 10^{21}$ cm^{-2} and for a value of the Alfvén speed of $v_A \simeq 200$ km/s. We assume a quite large value for the Alfvén speed to maximize the penetration of CRs into clouds. The reason for this assumption will become clear in the following. The three curves represent the spectrum of CRs far away from

TABLE 3.1: Parameters of the fits to the CR proton and electron intensity measured by Voyager 1 and AMS-02.

Species	C ($\mathrm{eV^{-1}cm^{-2}s^{-1}sr^{-1}}$)	α	β	$E_{\rm br}$ (MeV)
Proton	1.882×10^{-9}	0.129	2.829	624.5
Electron	4.658×10^{-7}	-1.236	2.033	736.2

the cloud $f_0(E) = 4\pi j_0(E)/v$, the spectrum $f_b(E)$ at the cloud border ($x = 0$ and $x = L_c$), and the spectrum averaged over the cloud volume $f_a(E)$. At large enough energies CRs freely penetrate clouds, and the three spectra coincide. As noticed by Morlino & Gabici (2015), this is the case for particles which are not affected by energy losses during their propagation in zones 2 and 3 (see Fig. 3.1) and the characteristic energy E_{loss} (or equivalently momentum p_{loss}) for such a behaviour of the spectrum could be obtained following the simple flux balancing equation which should result in $v_A \tau_l(p_{loss}) = L_c/2$. For the cloud considered in Fig. 3.4 ($N(\mathrm{H_2}) \simeq 3.1 \times 10^{21}$ cm^{-3}) and for a value of the magnetic field of 10 μG this happens at $E_{loss,p} \simeq 39$ MeV for CR protons and $E_{loss,e} \sim 32$ MeV for electrons (see also Eq. 7 and the related discussion in Morlino & Gabici 2015). Below these energies, the proton and electron spectra inside the cloud are suppressed with respect to f_0, but in the energy range $E_{*,p}(E_{*,e}) < E < E_{loss,p}(E_{loss,e})$ we still find that $f_b = f_a$ ($E_{*,p}$ and $E_{*,e}$ have been defined at the end of Sec. 3.1.1). This fact can be easily understood in the following way:

1. for proton (electron) energies larger than $E_{loss,p}$ ($E_{loss,e}$) CRs freely penetrate the cloud, so that $f_0 = f_b = f_a$;

2. for proton (electron) energies in the range $E_{*,p} < E < E_{loss,p}$ ($E_{*,e} < E < E_{loss,e}$) particles suffer ionization energy losses, but this happens after they repeatedly cross the cloud. This implies that the CR spatial distribution inside the cloud is uniform, and thus $f_0 \neq f_b = f_a$;

3. for proton (electron) energies $E < E_{*,p}$ ($E < E_{*,e}$) particles lose energy before completing a single crossing of the cloud, which implies that the spatial distribution of CRs inside the cloud is non-uniform, i.e. $f_0 \neq f_b \neq f_a$.

In Fig. 3.5, we provide also a few spectra to show how our results depend on the exact value of the column density of the cloud. It is clear from this figure that the suppression of the CR spectra inside MCs is more pronounced for larger column densities. For very large column densities, approaching $\sim 10^{23}$ cm^{-2}, the CR proton and electron spectrum is suppressed with respect to f_0 up to quite large energies reaching the GeV domain.

3.3 From the Model to the Observed Ionization Rate

The CR spectra obtained in the previous section can now be used to compute the ionization rates $\zeta(\mathrm{H_2})$ in diffuse clouds. In the absence of a detailed knowledge of the

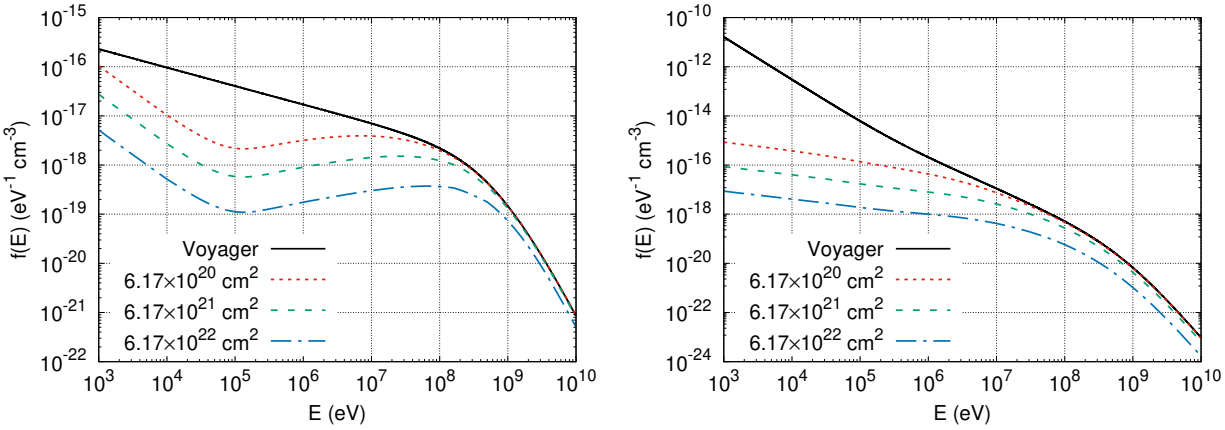

FIGURE 3.5: Average spectra of CR protons (left panel) and electrons (right panel) inside clouds of different column densities as listed in the labels. The average ISM spectra of Eq. (3.15) are also shown with black solid lines.

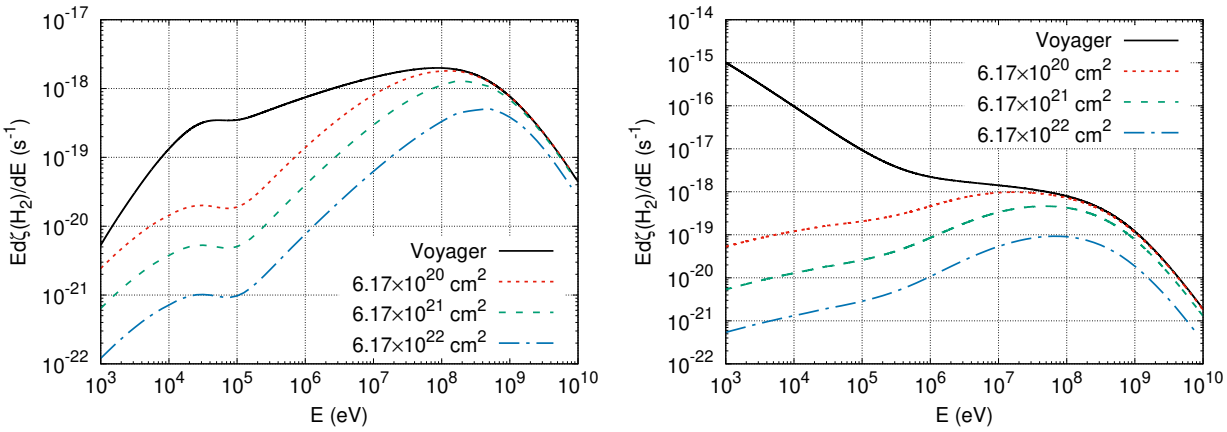

FIGURE 3.6: Differential ionization rate of both proton and electron CRs (left and right panel, respectively) at different column densities with the ISM spectra f_0 assumed to be that from Voyager and AMS-02 fits. The black curves are the differential ionization rates obtained neglecting propagation and ionization losses into the cloud.

distribution of the gas of the cloud along the line of sight, we use in the following the spatially averaged spectrum of CRs f_a to compute the ionization rates using Eq. 2.24 and 2.25 for CR protons and electrons respectively.

Fig. 3.6 shows the differential contribution to the ionization rate of both CR protons and electrons (defined as $E\,\mathrm{d}\zeta(\mathrm{H}_2)/\,\mathrm{d}E$) for a few test clouds with column density 6.2×10^{20}, 6.2×10^{21}, and 6.2×10^{22} cm^{-2}. This corresponds to a MC of size ~ 10 pc with gas density of ~ 20, 200 and 2000 cm^{-3}, respectively. The differential ionization rates computed by using the non-propagated Voyager spectra are also shown as black lines. These results provide an indication for the range of particle energies that contribute to ionization the most. For the particular case considered here (CRs outside of the cloud have a spectrum equal to that observed by Voyager) it is clear that the differential ionization rate peaks at about ≈ 100 MeV for both protons and electrons, with a quite weak dependency on the cloud column density.

The dependence of the ionization rate with respect to the cloud column density predicted from our method are shown in Fig. 3.7, together with the observational data taken from Caselli et al. (1998), Williams et al. (1998), Maret & Bergin (2007), and Indriolo & McCall (2012). The ionization rates for protons and electrons ($\zeta_p(H_2)$ and $\zeta_e(H_2)$, respectively) are plotted together with the total ionization rate, defined in Chapter 2 as $\zeta(H_2) = \eta\zeta_p(H_2) + \zeta_e(H_2)$ where the factor $\eta \simeq 1.5$ accounts for the contribution to the ionization rate from CR heavy nuclei (Padovani et al., 2009).

It should be noticed that the results in Fig. 3.7 have been obtained under the assumption of a quite large value of the Alfven speed (approximately 200 km/s). As said before, that was done to maximize the effect of the penetration of CRs into MCs. In fact, a more appropriate value would be about 60 km/s, corresponding to a magnetic field strength of 3 μG and a density of $n_i \simeq 10^{-2}$ cm^{-3}. If the calculation was done for such a value of the Alfven speed, the result of the ionization rate would be smaller by roughly a factor of two.

Thus, it is evident from Fig. 3.7 that the predicted ionization rate fails to fit data, being too small by a factor of several tens at the characteristic column density of diffuse clouds ($N(H_2) \simeq 10^{21}$ cm^{-2}). It seems, then, that the intensity of CRs measured in the local ISM is by far too weak to explain the ionization rates observed in MCs. A discussion of this issue and possible solutions to such a large discrepancy will be provided in the final section of this chapter. It has to be noticed, however, that the predictions presented in Fig. 3.7 are consistent with the upper limits on the ionization rate measured for a number of clouds (data points represented with filled inverted triangles).

The range of column densities considered in Fig. 3.7 encompasses the typical values of both diffuse and dense clouds (a transition between the two regimes can be somewhat arbitrarily set at $N_H \approx$ few 10^{21} cm^{-2} Snow & McCall 2006), while the model presented in this chapter applies to diffuse clouds only. The propagation of CRs through large column densities of molecular gas may differ from the description provided here mainly because large column densities are encountered in the presence of dense clumps, where the assumption of a spatially homogeneous distribution of gas density and magnetic field are no longer valid. The presence of clumps may affect CR propagation mainly in two ways:

1. *Magnetic mirroring and focusing*: the value of the magnetic field cannot be assumed to be spatially homogeneous in dense MCs, where it is known to correlate with gas density (Crutcher et al., 2010). The presence of a stronger magnetic field in clumps may induce magnetic mirroring and also focusing of CRs and it is suggested by Silsbee et al. (2018) that these two effects cancel out exactly, unless a magnetic pocket forms. An example of the formation of the magnetic pocket is the case investigated by Padovani & Galli (2011) where the CR intensity is suppressed and thus also of the ionization rate. This would further increase the discrepancy between model predictions and data;

2. *Particle losses*: very dense clumps may act as sinks for CR particles. This happens when the energy losses are so effective to prevent CR particles to cross the clump over a time-scale shorter than the energy loss time. Such a

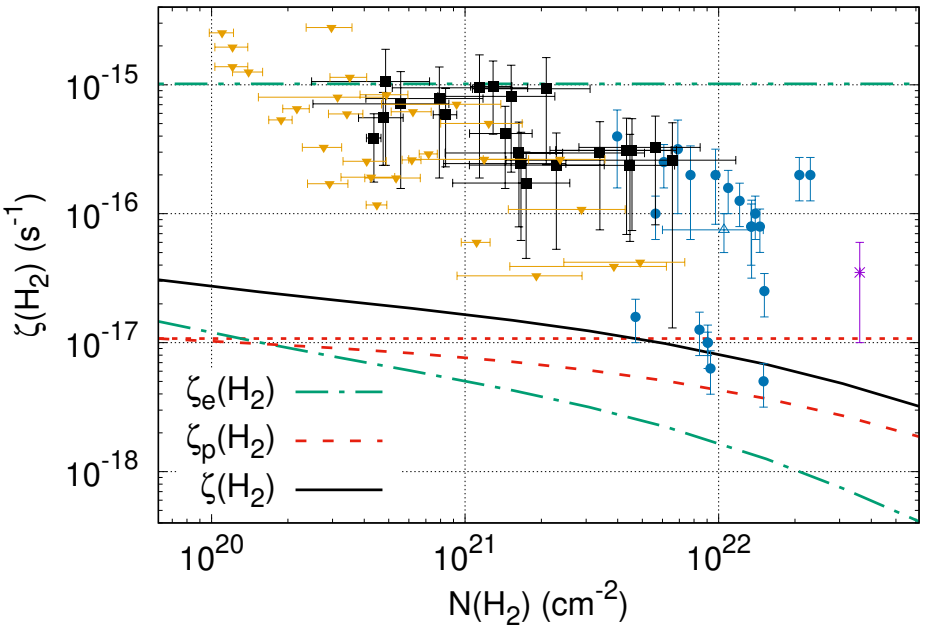

FIGURE 3.7: Ionization rate derived from Voyager spectra compared to observational data as a function of the column density. The two-dot-dashed line and the dotted line correspond to the ionization rates of electrons and protons, respectively, neglecting the effects of propagation and ionization losses. Data points are from Caselli et al. (1998) (filled circles), Williams et al. (1998) (empty triangle), Maret & Bergin (2007) (asterisk), and Indriolo & McCall (2012) (filled squares are data points while filled inverted triangles are upper limits).

scenario was investigated by Ivlev et al. (2018). Under these circumstances, a larger suppression of the CR intensity inside MCs is expected (energy losses are on average more intense), and this would also increase the discrepancy between data and predictions.

3.4 Discrepancy between the Observed and Predicted Ionization Rate?

The main result of this chapter can be summarized as follows: if the CR spectra measured in the local ISM by the Voyager 1 probe are characteristic of the entire ISM, then the ionization rates measured inside MCs are not due to the penetration of such background CRs into these objects, and another source of ionization has to be found. This is a quite puzzling result, which necessarily calls for further studies. Several possibilities can be envisaged in order to explain the discrepancy between model predictions and observations. A non-exhaustive list includes:

1. *Better description of the transition between diffuse and dense media:* at present, all the available models aimed at describing the penetration of CRs into MCs rely on the assumption of a quite sharp transition between a diluted and ionized medium, and a dense and neutral one. A more accurate description should consider a more gradual transition between these two different phases of the ISM. However, we recall that the simple flux-balance argument mentioned in Sec. 3.1 and discussed in great detail in Morlino & Gabici (2015) would most likely hold also in this scenario. It seems thus unlikely that a more accurate modeling could result in a prediction of ionization rates more than one order of magnitude larger than that presented here (as required to fit data);

2. *Inhomogeneous distribution of ionizing CRs in the ISM*: the assumption of a uniform distribution of CRs permeating the entire ISM could be incorrect. Fluctuations in the CR intensity are indeed expected to exist, due for example to the discrete nature of CR sources (see for example Gabici & Montmerle, 2015, and references therein). However, gamma-ray observations of MCs suggests that such fluctuations are not that pronounced for CR protons in the GeV energy domain (Yang et al., 2014). Thus, fluctuations of different amplitude should be invoked for MeV and GeV particles;

3. *Cosmic-ray sources inside clouds*: the ionizing particles could be accelerated locally by CR accelerators residing inside MCs. Obvious candidate could be protostars, which might accelerate MeV CRs, as proposed by Padovani et al. (2015) and Padovani et al. (2016);

4. *The return of the CR carrot?* The existence of an unseen component of low-energy CRs, called *carrot*, was proposed a long time ago by Meneguzzi et al. (1971) in order to enhance the spallative generation of ^{7}Li, which at that time was problematic. Voyager data strongly constrain such a component, that should become dominant below particle energies of few MeV (the energy of

the lowest data points from Voyager). Such a low energy component could also enhance the ionization rate, as recently proposed by Cummings et al. (2016).

Further investigations are needed in order to test these hypotheses and reach a better understanding of both the distribution of low-energy CRs and the dynamics MCs. Some of them will be further investigated in the next chapter.

Chapter 4

How to Explain the Ionization Rate in Diffuse Molecular Clouds?

As shown in the previous chapter, if one assumes that the average low energy proton and electron spectra in the Galaxy are the same as measured by Voyager 1, the inferred ionization rate inside diffuse MCs is $\sim 1-2$ orders of magnitude smaller than the observed one. Since potential improvements of these models which, for instance, include also a description of dense and clumpy media and a more realistic modeling of the transition between different phases of the ISM, are unlikely to enhance the predicted ionization rate by such large factor (see also Morlino & Gabici, 2015; Phan et al., 2018), one should either invoke a new class of sources for ionization inside MCs, or question the validity of assuming the Voyager 1 spectrum to be representative of the whole CR spectrum in Galaxy. In order to reconcile predicted and measured ionization rates, several solutions have been put forward: i) the possible presence of MeV CR accelerators inside MCs (see e.g. Padovani et al. 2015; Padovani et al. 2016); ii) the inhomogeneity in the distribution of low-energy CRs in the Galaxy (see e.g. Cesarsky 1975; Gabici & Montmerle 2015; Nobukawa et al. 2015; Nobukawa et al. 2018); iii) the existence of a still unknown CR component called the *carrot* which emerges at energies below the smallest energy detected by Voyager 1 (Cummings et al., 2016).

In fact, there might exist, within dense MCs, protostars whose jet shocks could possibly accelerate low-energy CRs (see e.g. Padovani et al., 2015; Padovani et al., 2016, for some of the piorneering works on this subject). Since this thesis, however, concentrates more on diffuse MCs, we shall not explore this scenario but rather focus on more simple solutions namely the carrot and the inhomogeneity of Galactic CRs at low energy. Section 4.1 will be dedicated to a critical examination on the existence of the CR carrot which casts serious doubt on the feasibility of this scenario. This should, in turn, provide more support for both the local origin of the CRs observed by Voyager 1 and the possible spatial variations of the CR intensities over the entire Galaxy which shall be investigated in more details in Section 4.2.

4.1 The Cosmic-Ray Carrot

The carrot scenario was first proposed by Meneguzzi et al. (1971) to explain the abundances of light elements, and has recently been reconsidered by Cummings et

TABLE 4.1: Parameters for the different phases of the ISM inside the Galactic disk taken from Osterbrock & Bochkarev (1989)

Phases	$n_{\rm H}$ ($\rm cm^{-3}$)	n_e ($\rm cm^{-3}$)	T (K)	f_V
WNM	0.5	0	8000	25%
WIM	0.5	0.5	8000	25%
HIM	0.006	0.006	10^6	50%

al. (2016) (who called it *suprathermal tail*) to resolve the problem of the ionization rate in MCs. We shall now analyze in detail the implications of the possible presence of a CR population at energies below few MeV following the discussion presented by Recchia et al. (2019)[1]. More specifically, we estimate the power that has to be injected in low-energy CRs in order to keep in the whole Galactic disk a population able to account for the observed ionization rate in MCs. We do so by assuming that the carrot component is uniformly distributed both inside clouds and in the rest of the ISM. The power estimated in that way represents a very conservative lower limit, since in a more realistic scenario low-energy CRs present in the ISM penetrate the cloud and their transport and energy losses in MCs have to be taken into account. As shown by Phan et al. (2018), the ionization rate predicted in this case would be smaller than in the simple scenario presented here. Here, we show that, due to the relatively short ($\lesssim 10^5$ yr, see Fig. 4.1) lifetime of sub MeV CRs in the ISM, in order to maintain a very low energy and hidden CR component able to explain the observed ionization rates, it would be necessary for the potential sources to inject in the ISM a power comparable to or larger than that needed to explain the whole observed CR spectrum. This result poses a serious concern on the viability of a carrot scenario.

We also explore the implications of assuming that such component be accelerated by the turbulent magnetic field in the ISM, through second-order Fermi acceleration (see e.g. Osborne & Ptuskin 1988; Jokipii 2001; Thornbury & Drury 2014; Drury & Strong 2017). However, we show that in this case the level of turbulence required at the scale resonant with CRs at the relevant energies is much larger than the one usually accepted. This brings additional support to the idea that a CR *carrot* at energies below the smallest one detected by Voyager 1 fails to provide a solution to the problem of the ionization rate in MCs.

4.1.1 Power Requirement

Let us assume the presence of a CR (electron and/or proton) component at a given energy $\tilde{\rm E} \lesssim 3$ MeV (energies smaller than those detected by Voyager 1), uniformly distributed in the whole Galactic disk, including the interior of MCs.

[1]We do not consider here the effect of the CR carrot on the production of light elements. For a recent review of this topic see Tatischeff & Gabici 2018

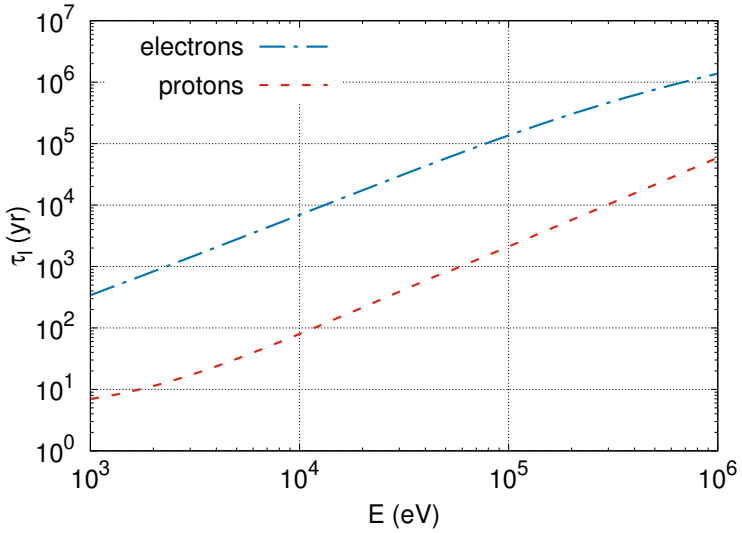

FIGURE 4.1: The energy loss time of CR protons and electrons of energy from 1 keV to 1 MeV inside the Galactic disk.

For simplicity, we assume that the distribution function of such component is:

$$f(E) = A\delta(E - \tilde{E}), \tag{4.1}$$

where A is a normalization constant that has to be determined. This could be done by imposing that the H_2 ionization rate produced by CRs (electrons or protons) with the distribution function given by Eq. 4.1, equals the average value, $\bar{\zeta}(H_2) \approx 4{\times}10^{-16}$ s^{-1}, detected in diffuse clouds (see e.g. Indriolo et al. 2009). Using Eq. 2.24 and Eq. 2.25, the normalization of the carrot at energy $\tilde{E}$ for CR protons and electrons could be determined as:

$$A_p(\tilde{E}) = \frac{\bar{\zeta}(H_2)}{v\left\{\left[1 + \phi_p(\tilde{E})\right]\sigma^p_{ion}(\tilde{E}) + \sigma_{ec}(\tilde{E})\right\}}, \tag{4.2}$$

$$A_e(\tilde{E}) = \frac{\bar{\zeta}(H_2)}{v\left[1 + \phi_e(\tilde{E})\right]\sigma^e_{ion}(\tilde{E})}, \tag{4.3}$$

where $v = v(\tilde{E})$ is the speed of the particle with the corresponding kinetic energy $\tilde{E}$, $\sigma^{p(e)}_{ion}$ is the ionization cross section, σ_{ec} is the electron capture cross section, $\phi_{p(e)}$ are the average secondary ionizations per primary ionization (see Chapter 2 and also Krause et al., 2015).

Once determined the overall normalization of the *carrot* distribution function, the power needed in order to sustain such component in the whole Galactic disk can be estimated as

$$P(\tilde{E}) = \frac{A(\tilde{E})\tilde{E}V_{disk}}{\tau_l(\tilde{E})}. \tag{4.4}$$

Here, V_{disk} is the volume of the Galactic disk (commonly modelled as a cylinder of

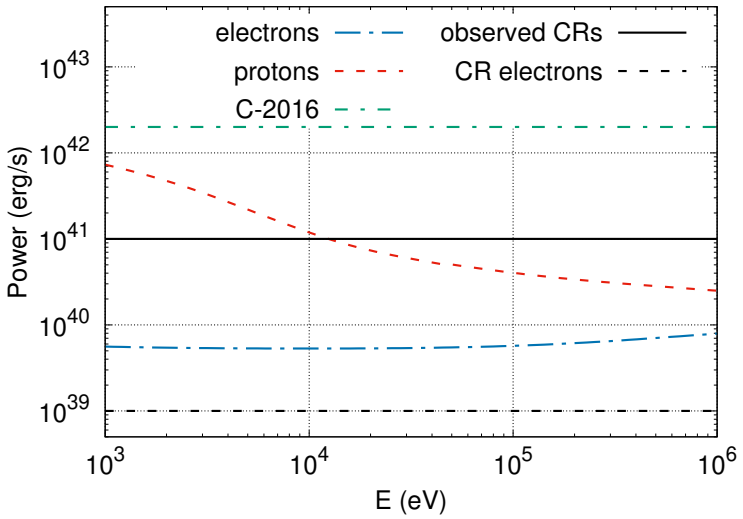

FIGURE 4.2: Power needed in CR protons and electrons in order to keep a *carrot* at a given energy in the whole Galactic disk, able to predict (without taking into account the CR penetration in MCs) an ionization rate of 4×10^{-16} s^{-1}, as compared to the power needed to sustain the observed CR Galactic population (black, solid line) and the observed CR electron spectrum (black, dashed line), respectively. The line marked as C-2016 is the power required in CR protons in order to keep the suprathermal tail invoked in Cummings et al., 2016 in the whole Galactic disk.

radius $R_d \sim 15$ kpc and of height $h_d \sim 300$ pc) and $\tau_l(\tilde{E})$ is the energy loss time inside the Galactic disk for the CR protons or electrons at energy $\tilde{E}$. Such energy losses are mainly due to ionization losses in the neutral phases of the ISM and Coulomb losses in the ionized phases of the ISM (see Chapter 1). In this work, we shall follow Osterbrock & Bochkarev (1989) and describe the ISM inside the Galactic disk with three different phases which are: (1) warm neutral medium (WNM), mostly made of neutral atomic hydrogen; (2) warm ionized medium (WIM), mostly made of ionized atomic hydrogen; (3) hot ionized medium (HIM), mostly made of ionized atomic hydrogen. Each of these phases are typically characterized using the hydrogen atom density n_H, the temperature T, and the volume filling factor f_V whose values are summarized in Table 4.1. The energy loss time could then be computed as:

$$\tau_l(E) = -\frac{p}{\dot{p}} = -\frac{p}{\sum_i \dot{p}_i f_V^{(i)}}, \tag{4.5}$$

where the summation over i has been performed to take into account the contribution of all the different phases of the ISM, p is the momentum of particle with energy E, and $\dot{p}_i$ is the momentum loss rate in the ith phase. The energy loss time in the Galactic disk for CRs of energy from 1 keV to 1 MeV are shown in Fig. 4.1.

In Fig. 4.2, we present the power estimated in Eq. 4.4 for CR electron and proton energies in the range from 1 keV to 1 MeV. We compare it with the total power (see e.g. Strong et al. 2010) injected by sources in the observed CR spectrum ($\sim 10^{41}$ erg/s) and electron spectrum ($\sim 10^{39}$ erg/s). We also show an estimate of the total

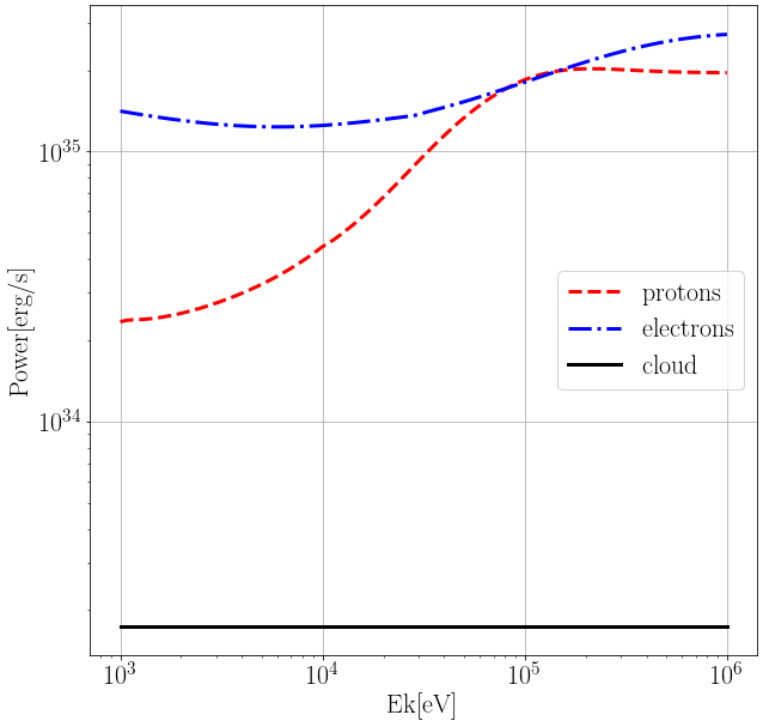

FIGURE 4.3: Power in CR electrons and protons in order to keep a *carrot* at a given energy within a cloud ($n(H_2) = 100$ cm^{-3}, radius $R_c \sim 10$ pc), able to predict an ionization rate of 4×10^{-16} s^{-1}. This is compared with the maximum power that a cloud can provide (black, solid line), given by $P_c = E_{grav}/\tau_{life}$ ($\tau_{life} \sim 10^7$ yr, $E_{grav} = \frac{3}{5}\frac{GM_c^2}{R_c}$).

power in CR protons needed to keep in the whole Galactic disk the suprathermal tail invoked in Cummings et al., 2016 which could be evaluated as:

$$P_{C-2016} = \int_{1\text{ keV}}^{1\text{ MeV}} \frac{4\pi j(E) E}{v_p(E)} \frac{V_{disk}}{\tau_{l,p}(E)} \mathrm{d}E \approx 2 \times 10^{42}\ \text{erg/s}, \tag{4.6}$$

where

$$j(E) = 4.4 \times 10^{-9} \left(\frac{E}{1\text{ MeV}}\right)^{-3/2} \exp\left(-\frac{E}{0.2\text{ MeV}}\right)\ \text{eV}^{-1}\text{cm}^{-2}\text{s}^{-1}\text{sr}^{-1} \tag{4.7}$$

is the CR proton intensity of the suprathermal tail (see Fig. 16 of Cummings et al. 2016).

Remarkably, the plot in Fig. 4.2 illustrates that, due to the short lifetime of low-energy CRs in the ISM (see Fig. 4.1), a CR *carrot* (or the suprathermal tail of Cummings et al. 2016) would require a power injection comparable or even larger than that already needed in order to account for the whole observed CR spectrum ($\sim 10^{41}$ erg/s). The situation is especially dramatic for electrons, given that the observed CR power for them is $\sim 10^{39}$ erg/s.

Note that 10^{41} erg/s roughly corresponds to 10% of the total power of galactic supernova explosions. Since supernova remnants are considered the major source of

Galactic CRs (see e.g. Blasi 2013), our result implies that the existence of a CR *carrot* would require either an unreasonably large (in some cases even larger than 100 %) CR acceleration efficiency for known CR sources, either the existence of another, much more powerful (and thus implausible), class of sources.

We should notice also that this result is not expected to change with different assumptions on the spectral shape of the low energy component. In fact, the required power injection is minimum for a proton (electron) carrot at 1 MeV (1 keV), as shown in Fig. 4.2. Any choice of a broader spectrum in the range from 1 keV to 1 MeV, able to predict the same ionization level in MCs, will inevitably imply a larger power injection.

Moreover, this estimated power is a very conservative lower limit. In fact here we assumed that the unknown CR component is uniformly distributed in the whole Galactic disk and inside clouds. However, CRs have to penetrate the cloud. As illustrated by Phan et al. (2018), taking into account this effect leads to a lower predicted level of ionization. This can be easily seen if, for instance, we consider the average distance travelled by CR electrons and protons inside a cloud before losing all their energy due to ionization losses, that we estimate as:

$$L_{loss}(E) = v(E)\tau_{loss}(E, n(\mathrm{H_2})), \tag{4.8}$$

where

$$\tau_{l,p}(E, n_c) \approx \begin{cases} 500 \left[\dfrac{n(\mathrm{H_2})}{1\ \mathrm{cm^{-3}}}\right]^{-1}\ \mathrm{yr} & (1\ \mathrm{keV} \leq E \leq 0.1\ \mathrm{MeV}) \\ 1.1 \times 10^4 \left(\dfrac{E}{1\ \mathrm{MeV}}\right)^{4/3} \left[\dfrac{n(\mathrm{H_2})}{1\ \mathrm{cm^{-3}}}\right]^{-1}\ \mathrm{yr} & (0.1\ \mathrm{MeV} \leq E \leq 1\ \mathrm{MeV}) \end{cases} \tag{4.9}$$

$$\tau_{l,e}(E, n_c) \approx 10^5 \left(\frac{E}{1\ \mathrm{MeV}}\right) \left[\frac{n(\mathrm{H_2})}{1\ \mathrm{cm^{-3}}}\right]^{-1}\ \mathrm{yr} \qquad (1\ \mathrm{keV} \leq E \leq 1\ \mathrm{MeV}) \tag{4.10}$$

are approximate expressions for the CR ionization loss time (Padovani et al. 2009; Phan et al. 2018) for CR electrons and protons in a cloud of H_2 density given by $n(H_2)$.

In Fig. 4.4 we compare this typical distance for CR electrons and protons of energy in the range from 1 keV to 1 MeV inside a cloud of $n(H_2) = 100\ \mathrm{cm^{-3}}$, with a typical cloud size $L_c = 10$ pc. The result is that protons of these energies and electrons of $E \lesssim 0.1$ MeV would not even be able to cross a typical cloud. We should notice also that keeping a CR *carrot* inside clouds instead that in the whole Galactic disk would lead an unsustainable power requirement. In this case, the rate at which CRs should be provided to the cloud can be derived by using Eq. 4.4 together with Eq. 4.9 or Eq. 4.10 (for protons or electrons), provided that V_{disk} is substituted with V_{cloud}. The CR power obtained in this way is compared in Fig. 4.3 to a characteristic maximal cloud power P_c obtained by dividing the cloud gravitational energy $E_g = \frac{3}{5}\frac{GM_c^2}{R_c}$ by its typical lifetime τ_{life}.

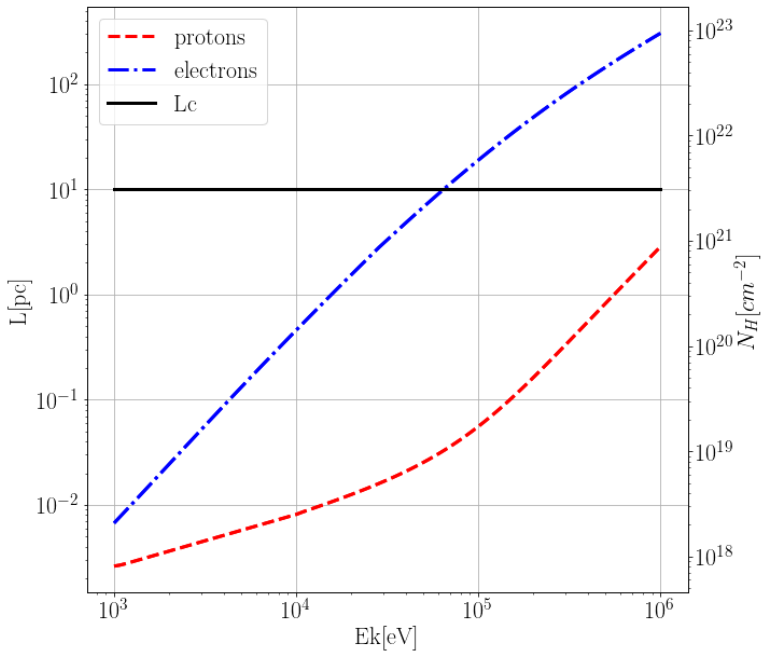

FIGURE 4.4: Average distance travelled by CR electrons (blue, dot-dashed line) and protons (red, dashed line) within a cloud ($n(H_2) = 100$ cm^{-3}) in a loss time. The typical cloud size is assumed to be $L_c = 10$ pc (black, solid line).

We adopt typical cloud parameters $R_c = 10$ pc, $n(H_2) = 100$ cm^{-3} and $\tau_{\rm life} \sim 10^7$ yr (see e.g. Heyer & Dame 2015). The CR power largely exceeds P_c, making the carrot scenario nonviable.

4.1.2 Acceleration in the Turbulent Magnetic Field

The results of the previous subsection already poses serious doubts on the carrot scenario for the explanation of the observed ionization rate in MCs.

In order to bring additional support to this result, we also explore a possible major source of low-energy CRs, namely the second order Fermi acceleration in the turbulent interstellar magnetic field (see e.g. Osborne & Ptuskin 1988; Jokipii 2001; Thornbury & Drury 2014; Drury & Strong 2017). The acceleration time-scale due to this process is given by (see Eq. 20 of Thornbury & Drury 2014)

$$\tau_{acc}(E) = \frac{9D(E)}{4v_A^2}, \tag{4.11}$$

where $D(E) = \frac{v(E) r_L(E)}{3I(k_{res})}$ is the spatial diffusion coefficient for particles of energy E and $v_A = B_0/\sqrt{4\pi\rho_i}$ is the Alfvén speed. Here, v and r_L are the particle velocity and Larmor radius, $I(k_{res}) = W(k_{res})k_{res}$ is the level of turbulence, $(\delta B/B_0)^2$, at the resonant scale $k_{res}(E) = 1/r_L(E)$, B_0 is the background magnetic field and ρ_i the average mass density of the background medium.

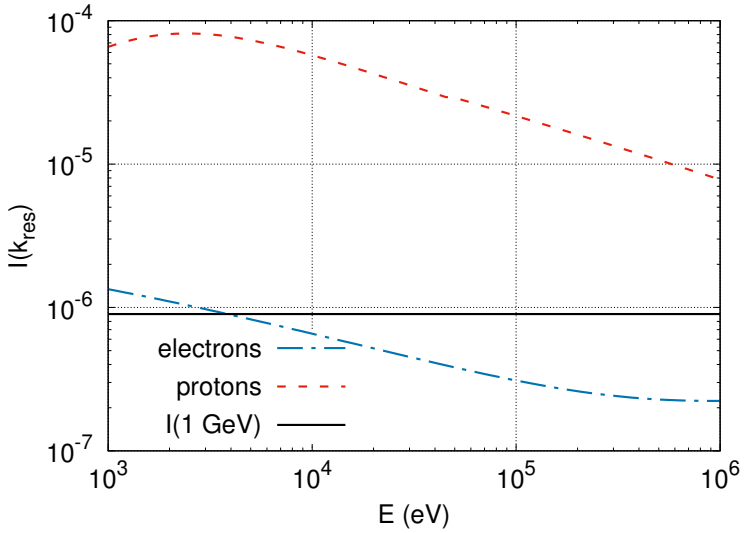

FIGURE 4.5: Level of magnetic turbulence needed to steadily maintain, through second order Fermi acceleration, sub MeV CR electrons and protons in the ISM ($B_0 = 3\mu$G). We show for comparison the turbulence expected at the scale resonant with ~ 1 GeV in order to account for accepted values of the spatial diffusion coefficient (D(1 GeV) $\sim 10^{28}$cm^2/s) at that energy.

Since low-energy CRs lose energy in the ISM on a relatively short time scale (see Fig. 4.1), in order to keep a CR carrot at energy E the level of magnetic turbulence at the resonant scale $k_{res} = 1/r_L(E)$ have to be such that

$$\tau_l(E) = \tau_{acc}(E), \tag{4.12}$$

namely

$$I(k_{res}) = \frac{3vr_L}{4v_A^2\tau_l}. \tag{4.13}$$

A plot of the needed level of turbulence is shown in Fig. 4.5 for $B_0 = 3\mu$G, in the case of CR electrons and protons of energy in the range from 1 keV to 1 MeV.

Remarkably, the inferred $I(k_{res})$ at the energies relevant for this discussion are larger than or comparable to, for instance, that expected at the scale resonant with ~ 1 GeV (see e.g. Trotta et al. 2011) in order to account for accepted values of the spatial diffusion coefficient (D(1 GeV) $\sim 10^{28}$cm^2/s, I(1 GeV) $\sim 9 \times 10^{-7}$). This is quite unlikely to happen, since in any physical model of interstellar magnetic turbulence $I(k)$ is a decreasing function of k (see e.g. Sridhar & Goldreich 1994; Goldreich & Sridhar 1995). The present result, together with the results of the previous subsection, makes it very difficult for a CR carrot (or suprathermal tail) to represent a feasible model able to reconcile the predicted and observed ionization rates in MCs.

4.1.3 End of the Carrot?

Having investigated the carrot component of CRs to account for the average ionization rate detected in diffuse MCs, with a particular focus on the energetics, we found that, due to the energy losses suffered by low-energy CRs in the ISM, the power needed to be injected by the potential sources in such component is comparable or larger than that required for the observed CR spectrum. We note that the effect of penetration of these low-energy CRs inside clouds has not been taking into account which would make this energy requirement even more severe. Moreover, if we consider the interstellar turbulent magnetic field as a possible source of this carrot, through second-order Fermi acceleration, the required turbulence level would be definitely too large compared to the one expected at the scale resonant with such low energy particles.

Our study basically rules out, on an energy basis, any possible source of a CR carrot, thus making such hidden component unlikely to be an appealing and viable source of ionization in MCs. This conclusion encourages further studies of the possible solutions to the discrepancy between predicted and observed ionization rates in MCs. Among them, some promising ones remain the one already mentioned in the introduction and in Phan et al., 2018: i) the possible presence of sub-GeV CR accelerators inside MCs; ii) the prominent inhomogeneity in the distribution of low-energy CRs in the Galaxy. With this respect, we note that, given our peculiar location inside an ISM cavity known as the Local Bubble (LB) (Cox, 1998), the CR spectrum measured by Voyager 1 might simply reflect local properties, rather than representing the typical spectrum of CRs in the Galaxy.

4.2 Stochastic Fluctuations of Cosmic Rays from Supernovae Remnants

It is clear from the discussion in Chapter 3 and in the previous section that the low-energy CR spectra observed by Voyager 1 could not explain the ionization rate in both diffuse and dense isolated MCs in the Galaxy. It might be possible to resolve this problem by arguing that the spectra from the Voyager probes are actually local and, thus, there might exist regions of the ISM where we have more of these low energy particles to induce the ionization rate typically observed. In other words, the assumption of a uniform distribution of CRs permeating the entire ISM as supported by gamma-ray observations of MCs (Yang et al., 2014; Aharonian et al., 2018) should be relaxed in the energy range below a few GeVs. Such an inhomogeneity for low-energy CRs is expected since the relatively short energy loss time of these particles would not allow them to travel far a way from their sources. A better understanding of this problem might require the modelling of CR transport over the entire Galaxy.

As previously mentioned in Chapter 1, the transport of CRs within the Galactic disk is diffusive as could be inferred from the secondary-to-primary ratio of CR intensities. There exists, however, another essential observational constraint which comes from the analyses of unstable secondaries such as the radioactive isotopes ^{10}Be whose life time is roughly of the same order as the residence time of CRs inside

the Galactic disk $\tau(^{10}\mathrm{Be}) \simeq 1.4$ Myr. The decay of this isotope would suppress the ratio between ^{10}Be and stable Be isotopes by a factor of approximately $\tau(^{10}\mathrm{Be})/\tau_{esc}$ from which we could obtain $\tau_{esc} \simeq 10 - 20$ Myr (see e.g. Gabici et al., 2019, and references therein). Since this timescale is much larger than the residence time within the Galactic disk (see Chapter 1), it is believed that CRs are also diffusively confined within a low-density magnetized halo surrounding the Galactic disk. Although the size of this halo is quite poorly constrained, observations of the diffuse sychrotron emission above and below the Galactic plane in the radio domain seem to indicate the thickness of the halo to be much larger than that of the Galactic disk (Beuermann et al., 1985).

In the framework of the Galactic halo model, the standard approach to estimate the intensities of CRs, especially in the hadronic sector at high energy, is to model all the sources together as a jelly-like disk with a continuous CR injection such that the problem could be treated as steady-state (Strong & Moskalenko, 1998; Recchia et al., 2016; Evoli et al., 2019). However, the short energy loss time of low-energy CRs as discussed above could result in a more patchy distribution for these particles such that the contribution from recent or nearby sources could become crucial and, thus, the use of a continuous disk of sources might be no longer valid. In other words, the values for the intensities of low-energy CRs at different positions in the Galaxy could only be predicted if the exact locations and times of explosion for all the CR sources are known. This is indeed not the case even for the most well-studied class of Galactic sources like SNRs since young and distant or very old SNRs are quite hard to observe even though these sources might contribute significantly to the CR intensities in their proximity. Nevertheless, if the temporal and spatial distributions of SNRs are assumed to be predetermined from the extrapolation of current surveys, the CR intensities could be evaluated for different realizations of possible locations and ages of the sources. The variations of these intensities from one realization to another is commonly referred to as the stochastic fluctuations and, in this sense, the intensity of a particular CR species should be treated as a random variable whose expectation value could be estimated from the ensemble average over all the realizations. More importantly, the analysis of the stochastic fluctuations would allow us to identify the uncertainty range within which the values of the CR intensities are most probable. As a remark, we note also that if the energy loss time of CRs is sufficiently large, the stochastic fluctuations will vanish and the intensities will tend to the expectation values which should give the same results as the steady-state continuous model.

In the following, we shall examine the stochastic fluctuations of the CR intensities within the energy range from 1 MeV to about 10 GeV assuming that the principal sources for these particles are SNRs and also their transport is diffusive down to the lowest particle energy considered. The analysis will begin with a thorough discussion on the solution for the transport equation in the case of a single bursting source. Having established the point-source solution, we will proceed to evaluate the total intensities at an arbitrary position in the Galactic disk by summing the contribution from all the sources for different realizations of ages and distances. The corresponding stochastic fluctuations of the CR induced ionization rate will also be

investigated.

4.2.1 Point-Source Solution

For the propagation of CRs on the Galactic scale, we shall apply a more general form of the transport equation as presented in Chapter 1 which takes into account both advection and diffusion in three dimensions:

$$\frac{\partial f}{\partial t} + \mathbf{u}\cdot\nabla f - \nabla\left(D\nabla f\right) - \frac{p}{3}\nabla\cdot\mathbf{u}\frac{\partial f}{\partial p} - \frac{1}{p^2}\frac{\partial}{\partial p}\left(p^2 D_{pp}\frac{\partial f}{\partial p}\right) + \frac{1}{p^2}\frac{\partial}{\partial p}\left(\dot{p}p^2 f\right) = S, \tag{4.14}$$

where $f = f(\mathbf{x}, p, t)$ is the distribution function of CRs. It would be more convenient to rewrite the equation in terms of the spectrum $f(\mathbf{x}, E, t)$. We might sometimes omit the arguments for the spectrum, but please notice that, in the following discussion, $f = f(\mathbf{x}, E, t)$ is always used to refer to the spectrum. We shall adopt the advection velocity profile with only the component perpendicular to the Galactic disk, $\mathbf{u} = \mathbf{e}_z u(z)$, which is quite commonly used for the modelling of Galactic CRs (see e.g. Recchia et al., 2016). For simplicity, the contribution of stochastic reacceleration will not be considered and the effect of this process might be examined in some future works. The transport equation for a bursting point source taking into account advection perpendicular to the Galactic disk, three-dimensional isotropic and homogeneous diffusion, and energy losses during the propagation of CRs reads:

$$\frac{\partial f}{\partial t} + \frac{\partial}{\partial z}\left(uf\right) - D\nabla^2 f + \frac{\partial}{\partial E}\left[\left(\dot{E} + \frac{1}{3}pv\frac{\partial u}{\partial z}\right)f\right] = Q(E)\frac{\delta(r)}{2\pi r}\delta(z)\delta(t - t_0) \tag{4.15}$$

where $D = D(E)$ is the isotropic and homogeneous diffusion coefficient, $\dot{E}$ describes the energy loss rate for CRs both inside the Galactic disk and in the magnetized halo, $Q(E)$ is the injection CR spectrum, and t_0 is the time of injection of CRs in the interstellar medium. We shall now discuss the specific form of all the physical quantities presented in the above equation.

The advection profile is commonly modelled as $u(z) = u_0\left[2H(z) - 1\right]$. Such an advection velocity might be due to the presence of a large-scale Galactic wind or, in the case where the magnetic turbulence is self-generated via streaming instability, CRs would advect away from the Galactic disk with the Alfvén speed (Recchia et al., 2016). For this work, we shall take $u_0 \simeq 7$ km/s which has been found to provide a good fit for Galactic CR data (see recent analyses by Evoli et al., 2019). Since the advection velocity changes its direction only around the Galactic disk, the term for the adiabatic energy loss would contain the factor $\partial u/\partial z = 2u_0\delta(z)$ and, for the numerical solver adopted for the point-source solution, we shall approximate this

term as follows:

$$\frac{\partial}{\partial E}\left(\frac{1}{3}pv\frac{\partial u}{\partial z}f\right) \simeq \frac{\partial}{\partial E}\left[\frac{1}{3}pv\frac{u_0}{h}H\left(|z|-h\right)f\right], \tag{4.16}$$

where h is the half-thickness of the Galactic disk. Notice that, in this approximation, the adiabatic energy loss term acts everywhere within the disk. Such an approximation is quite standard in numerical treatments of Galactic CRs (see e.g. Jaupart et al., 2018; Evoli et al., 2019).

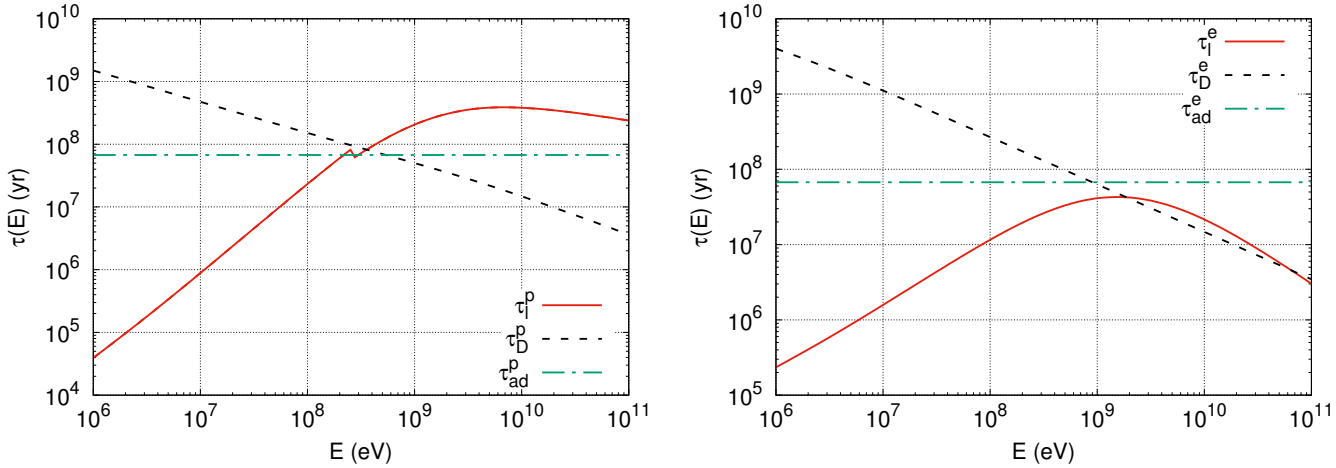

FIGURE 4.6: The energy loss time of CR protons (left panel) and electrons (right panel) inside the Galactic disk in comparison with their respective diffusive escape time from the Galaxy and the adiabatic energy loss time. Notice that the loss rate due to synchrotron radiation and inverse Compton scattering are already included for CR electrons.

Regarding the diffusion coefficient, it is quite puzzling what should be the energy dependence of $D(E)$ at low energy. However, it was suggested from theoretical modeling and Helios observations (Bieber et al., 1994; Schlickeiser et al., 2010) that $D(E) \sim v_p \sim E^{0.5}$ in the non-relativistic energy range since the particle mean free path becomes constant in that energy domain. Also, at high energy, the diffusion coefficient is expected to behave as $D(E) \sim E^{\delta}$ where $\delta \simeq 0.3 - 0.6$ (see Strong et al., 2007; Trotta et al., 2011, for more discussions). Combining the two asymptotic behaviors at high and low energy, we shall assume the following form for the diffusion coefficient:

$$D(E) = D_0\beta\left(1+\frac{E}{mc^2}\right)^{\delta}, \tag{4.17}$$

where $m = m_p$ or $m = m_e$ depending on the species of interest and, for both CR protons and electrons, the index δ has been chosen to be $\delta \simeq 0.63$ similar to the results for high energy CRs from Evoli et al. (2019) (and also that of Mertsch, 2011, used for studying the effects of stochastic sources on the CR electron spectrum at

high energy). We also follow Evoli et al. (2019) to adopt $D_{0,p} \simeq 1.1 \times 10^{28}$ cm^2/s for CR protons. The one for electrons has been normalized such that the diffusion coefficients for both species take the same value at $E = 10$ GeV and, thus, we have $D_{0,e} \simeq 10^{26}$ cm^2/s.

The next element to be considered for the transport of CRs is the energy loss rate. Cosmic-ray protons lose energy mostly inside the Galactic disk via ionization and Coulomb collisions at low energy and proton-proton interaction at high energy. While low-energy CR electrons also suffer from energy loss mostly due to ionization and Coulomb collisions, the high energy population of these particles lose energy via bremsstrahlung radiation, synchrotron radiation, and inverse Compton scattering at high energy electrons (see Chapter 1 for more details). As mentioned in the previous section, the ISM inside the Galactic disk is typically described with three different phases which are: (1) warm neutral medium (WNM), mostly made of neutral atomic hydrogen; (2) warm ionized medium (WIM), mostly made of ionized atomic hydrogen; (3) hot ionized medium (HIM), mostly made of ionized atomic hydrogen. The defining parameters for each of these phases are given in Table 4.1. For CR protons, the loss rate would be:

$$\dot{E}_p = \sum_i f_V^{(i)} \dot{E}_p^{(i)} H(|z| - h), \tag{4.18}$$

where the summation over the index i represents the average over the three phases and $\dot{E}^{(i)}$ is the energy loss rate in the corresponding phase. Also, the Heaviside step function is introduced to mimic the fact that the processes of energy loss happen mostly within the Galactic disk (with thickness $2h \simeq 300$ pc) for CR protons. Concerning CR electrons, it should be noted that these particles at high energy (roughly above 10 GeV) lose energy more efficiently via synchrotron radiation and inverse Compton scattering which occur not only in the disk but also in the magnetized halo and, thus, we shall have:

$$\dot{E}_e = \sum_i f_V^{(i)} \dot{E}_e^{(i)} H(|z| - h) + \dot{E}_{syn+IC}. \tag{4.19}$$

The estimated diffusive escape time $\tau_D(E) = L^2/6D(E)$ ($L \simeq 4$ kpc is the size of the halo) and the adiabatic energy loss time $\tau_{ad} = 3h/u_0$ are shown in Fig. 4.6 together with the energy loss time inside the disk $\tau_l(E) = -pv/\dot{E}$ for both CR species. As we can see, the diffusive escape time becomes sufficiently smaller than the other timescales for CR protons of energy above a few GeVs which means that, in this high energy limit, the transport of these particles could be modelled in a purely diffusive scenario. On the other hand, the effect of energy loss (mostly due to synchroton and inverse Compton scattering) on the transport of CR electrons should always be taken into account even for the ones with energy above a few GeVs. These speculations will allow us to make some approximations to obtain the analytic forms of the point-source solutions for high energy CRs which could be used as boundary conditions in energy for the numerical scheme applied for low-energy CRs.

For this work, we are interested in investigating the capability of SNRs as sources

of low-energy CRs in the hope to better understand the high level of ionization rate observed in diffuse MCs. Thus, the source function shall be modelled to describe the injection of SNRs:

$$Q(E) = \frac{\xi_{CR} E_{SNR}}{(mc^2)^2 \Lambda \beta} \left(\frac{p}{mc}\right)^{2-\alpha}, \tag{4.20}$$

where ξ_{CR} is the efficiency of the source, $E_{SNR} \simeq 10^{51}$ erg is the total kinetic energy of the supernova explosion, and Λ is the following integral:

$$\Lambda = \int_{p_{min}}^{p_{max}} \left(\frac{p}{mc}\right)^{2-\alpha} \left[\sqrt{\left(\frac{p}{mc}\right)^2 + 1} - 1\right] \frac{\mathrm{d}p}{mc}. \tag{4.21}$$

The index of the source spectra is taken to be $\alpha = 4.2$ which could be achieved from nonlinear diffusive shock acceleration mechanism and this value is also compatible with the fit of observational data for high energy CR protons (see e.g. Evoli et al., 2019, for more details). Also, the efficiency of acceleration for CR protons and electrons are chosen to be $\xi^p_{CR} \simeq 10\%$ and $\xi^e_{CR} \simeq 0.5\%$ respectively in order to match the observed data at high energy.

Solution at High Energy

Let's now discuss the point-source solutions in the high energy limit. As briefly mentioned above, the standard framework to describe the transport of Galactic CRs commonly involves the existence of a magnetized halo whose size is supposed to be $L \simeq 4$ kpc for this work. The sources are concentrated within the Galactic disk where the effect of energy loss due to the interactions with matter of the ISM is most severe.

In the following, we will present the analytic solution for a point source at high energy in the approximation of an infinite Galactic disk and, thus, the problem could be modelled with cylindrical symmetry meaning the CR spectra is a function of the form $f(\mathbf{x}, E, t) = f(r, z, E, t)$. More importantly, the spatial boundary conditions are set to be zero at $z = \pm L$ which are commonly referred to as the free-escape boundary conditions.

As said above, for CR protons in the high energy limit, all the mechanisms for energy loss can be neglected. This means that the CR transport equation simplifies into:

$$\frac{\partial f_p}{\partial t} - D\nabla^2 f_p = Q_p(E) \frac{\delta(r)}{2\pi r} \delta(z) \delta(t - t_0), \tag{4.22}$$

where we have neglected also the term for advection since the timescale for advective escape is roughly L/u_0 which is also much larger than the one for diffusion. The above equation could be solved to give (see e.g. Blasi & Amato, 2012, for more

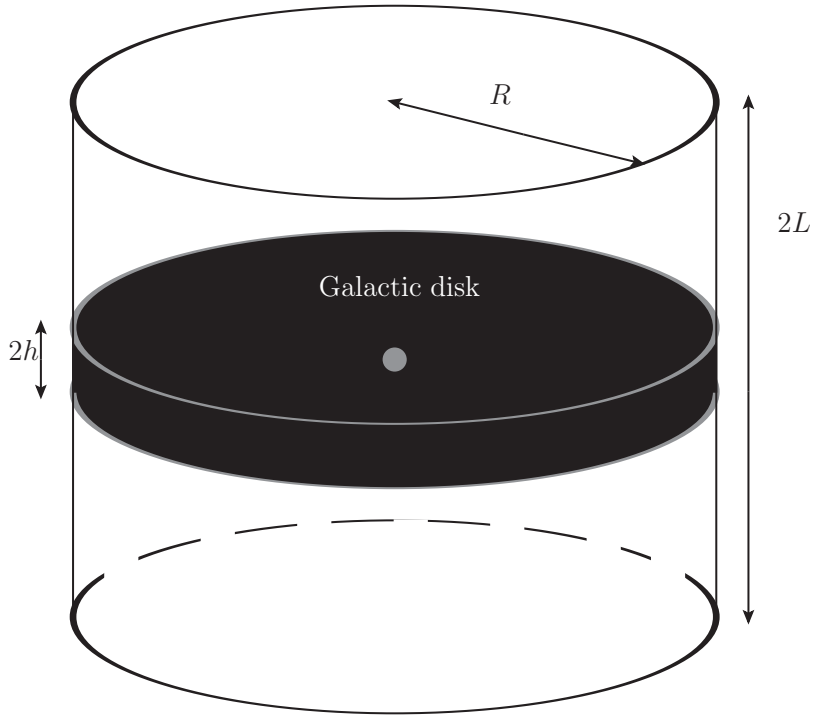

FIGURE 4.7: Geometry of the propagation region for the point-source solution. The source is placed in the center and R is taken to be large enough such that the cylindrical geometry is applicable (see text).

details):

$$f_p(r,z,E,t) = \frac{Q_p(E)}{\left[4\pi D_p(E)\,(t-t_0)\right]^{3/2}} \sum_{n=-\infty}^{\infty} (-1)^n \exp\left[-\frac{(z-2nL)^2+r^2}{4D_p(E)(t-t_0)}\right]. \quad (4.23)$$

Notice that the sum over n has been performed to ensure the free escape boundary conditions.

For CR electrons, the point-source solution in the high energy limit requires the inclusion energy loss due to synchrotron radiation and inverse Compton scattering. The corresponding CR transport equation is:

$$\frac{\partial f_e}{\partial t} - D\nabla^2 f_e - \frac{\partial}{\partial E}\left(\dot{E}_{syn+IC} f_e\right) = Q_e(E)\frac{\delta(r)}{2\pi r}\delta(z)\delta(t-t_0), \quad (4.24)$$

The energy loss rate from Eq. 1.76 for typical values of the Galactic magnetic field and the interstellar radiation field could be parametrized as (Mertsch, 2011):

$$\dot{E}_{syn+IC} = -b_0\left(\frac{E}{E_*}\right)^2, \quad (4.25)$$

where $b_0 \simeq 10^{-7}$ eV^{-1}/s for $E_* = 1$ GeV. In this high energy limit, the point-source solution is (see e.g. Mertsch, 2011, for more details):

$$f_e(r,z,E,t) = \frac{b(E_0)}{b(E)} \frac{Q_e(E_0)}{[4\lambda^2(E_0,E)]^{3/2}} \sum_{n=-\infty}^{\infty} (-1)^n \exp\left[-\frac{(z-2nL)^2+r^2}{4\lambda^2(E_0,E)}\right], \quad (4.26)$$

where $b(E) = -\dot{E}_{syn+IC}$, E_0 and $\lambda(E_0,E)$ could be estimated as follows:

$$E_0 = \frac{E^2}{E - b(E)(t-t_0)}, \quad (4.27)$$

$$\lambda^2 = \int_E^{E_0} \frac{D_e(E')}{b(E')}\,\mathrm{d}E' \simeq \frac{1}{1-\delta}\left[D_e(E)\frac{E}{b(E)} - D_e(E_0)\frac{E_0}{b(E_0)}\right]. \quad (4.28)$$

Here, E_0 could be interpreted as the initial energy of a particle with energy E which has been propagating for a period of time $t - t_0$ and $\lambda(E_0,E)$ is approximately the distance particles have traveled before suffering significant energy loss. It should be noticed that the formula for $\lambda(E_0,E)$ has been estimated in the high energy limit where $D(E) \sim E^\delta$. More importantly, for particles of energy E such that $E > E_*^2/b_0(t-t_0)$, the spectrum should vanish, i.e. $f(r,z,E,t) = 0$, since E_0 becomes negative in this limit[2].

Solution at Low Energy

In the low energy limit, we could solve Eq. 4.15 numerically within the finite region of propagation which is a cylinder of height $2L$ and radius R (see Fig. 4.7). The point source is also placed in the center and the radius R is chosen sufficiently large such that the cylindrical symmetry could also be adopted for the explicit finite difference scheme used to solve the transport equation. The details of the scheme is presented in Appendix A together with the appropriate spatial boundary conditions. Also, we would like to stress again that the derivative in energy requires a boundary condition in energy for which we shall apply the analytic solutions presented above. The numerical solutions shall be applied for CR protons of energy $E \lesssim 3$ GeV and for CR electrons of energy $E \lesssim 10$ GeV.

In Fig. 4.8, we show the profile along the r-coordinate for the numerical solutions inside the Galactic disk ($z = 0$) with the propagation set-up presented above in comparison to the one for the analytic solutions extrapolated down to lower energy. Both CR protons and electrons are considered in this figure. For illustration, the r-profiles are depicted only for CRs of energy $E = 100$ MeV and $E = 1$ GeV for the propagation time of 10^6, 10^7, and 10^8 years after the injection of CRs. As we can see, the numerical and analytic solutions in this energy range are compatible for short propagation timescales for CRs of both species. This is because, at early

[2]The physical interpretation of this limit is that there is no particle with large enough energy E_0 to decay into particles with energy $E > E_*^2/b_0(t-t_0)$ within the propagation time $t - t_0$.

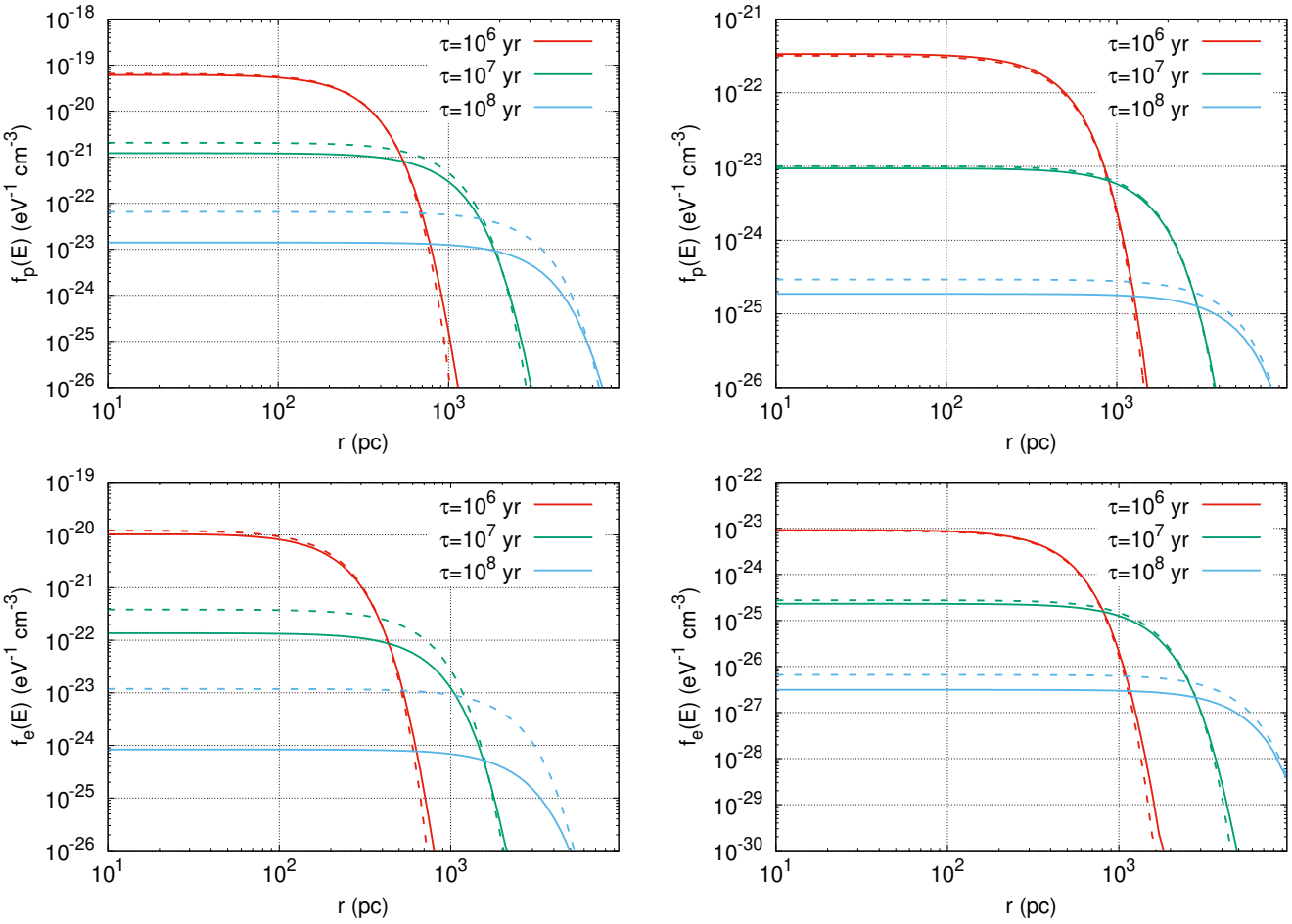

FIGURE 4.8: Comparison of the profile along the r-coordinate at $z = 0$ (inside the Galactic disk) for the numerical (dashed curves) and analytic (solid curves) point-source solutions. Both CR protons (upper panels) and electrons (lower panels) are considered. For each species, the solutions plotted for CRs of energy $E = 100$ MeV (left) and $E = 1$ GeV (right). The red, green, and blue curves correspond to the solution of CR transport from a point source after the time of propagation of $\tau = t - t_0 = 10^6, 10^7$, and 10^8 years.

time, the transport is dominated only by diffusion which has always been taken into account in the analytic solutions. Also, the numerical solutions for particles of energy $E = 1$ GeV remains quite consistent with the analytic ones indicating that the approximations made for the high energy limit might be valid down to energy of around 1 GeV. For lower energy, the energy loss inside the disk (including the adiabatic energy loss) becomes more important at later time which makes the discrepancy between the analytic and numerical become more pronounced.

4.2.2 Stochastic Fluctuations of Cosmic-Ray Intensities

Having discussed the point-source solutions, we could now proceed to investigate the stochastic fluctuations of the CR spectra. In order to estimate the stochastic uncertainty, we shall generate many different realizations of the positions and the

times of explosion for the sources. In the following, we shall use the index r to refer to a particular realization and each source within each realization will be associated with an index i. The CR intensities at an arbitrary position for each realization are evaluated by summing the contribution from all the point sources within a distance of about $s_{max} = 10$ kpc since sources further away could also be considered but they would not contribute significantly if the standard explosion energy is assumed. Let's suppose that all the sources are within the Galactic plane and we shall have for a particular realization:

$$j_{p,e}^{(r)}(E,t) = \sum_{i=1}^{N_s} \frac{v}{4\pi} f_{p,e}(s_i^{(r)}, z=0, E, t - t_i^{(r)}) \tag{4.29}$$

where $f_{p,e}$ is the point-source solutions presented in the previous section, $s_i^{(r)}$ is the distance between the ith source and the point of interest in the rth realization, $t_i^{(r)}$ is the moment of CR release for the ith source in the rth realization, and N_s is the total number of sources within one realization. The oldest sources that we shall consider are the ones releasing CRs around 100 millions years ago. This means that the time of propagation since the injection for CRs is $\tau = t - t_i^{(r)} \leq \tau_{max} = 10^8$ yr which is a few times more than the diffusive escape time of high energy CRs and the energy loss time of low-energy CRs and, thus, the obtained stochastic fluctuations are expected to reach a steady state. Also, the total number of sources in each realization should be estimated roughly as:

$$N_s = \mathcal{R}_{SNR} \tau_{max} \frac{s_{max}^2}{R_d^2} \simeq 1.3 \times 10^6 \tag{4.30}$$

where $\mathcal{R}_{SNR} \simeq 0.03$ yr^{-1} is the rate of supernovae explosions in our Galaxy and $R_d \simeq 15$ kpc is the radius of the Galactic disk. For simplicity, a homogeneous distribution of sources in both space and time has been chosen. An example of the distributions for an arbitrary realization is shown in Fig. 5.3. For this work, the stochasticity effect is investigated with an ensemble of $N_r = 2000$ realizations.

Having calculated the intensities for each realization, the expectation value for the intensity could be evaluated as:

$$\langle j_{p,e}(E,t) \rangle = \frac{1}{N_r} \sum_{r=1}^{N_r} j_{p,e}^{(r)}(E,t) \tag{4.31}$$

It is then straightforward to derive the probability density function for the value of the intensity and interpret the range of its most probable value. In Fig. 4.10, we show the probability density function for CRs of energy 1, 10, and 100 MeV. It should be noticed that not only these distribution functions are not symmetric but also they do not have a well-defined second moment as has been shown for several analyses of the same type at high energy (see e.g. Mertsch, 2011; Bernard et al.,

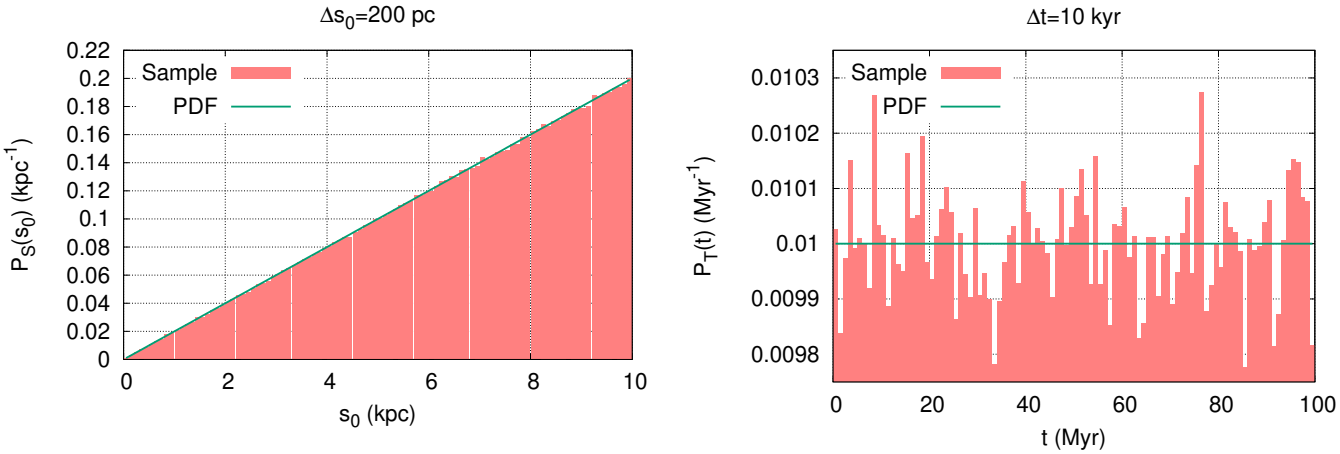

FIGURE 4.9: The probability density functions for SNR distances (left panel) and ages (right panel) assuming they are homogeneously distributed within the Galaxy. An example of the distributions for an arbitrary realization has been shown in comparison with the binning as indicated in each figure. Notice that the distance s_0 presented here is with respect to the position of interest.

2012; Génolini et al., 2017). We shall, therefore, define the uncertainty intervals of the intensity using the percentiles (similar to that of Mertsch, 2011). Let's denote by $\psi_{p,e}(x)$ the probability density function of the random variable $x = j_{p,e}/\langle j_{p,e}\rangle$ and the uncertainty range of x would be within $x_{5\%}$ and and $x_{95\%}$ where:

$$\int_{x_{min}}^{x_{5\%}} \psi_{p,e}(x)\,\mathrm{d}x = 5\%, \tag{4.32}$$

$$\int_{x_{min}}^{x_{95\%}} \psi_{p,e}(x)\,\mathrm{d}x = 95\%. \tag{4.33}$$

The 90% uncertainty range of the total intensity is then $\mathcal{I}_{90\%} = [\langle j_{p,e}\rangle x_{5\%}, \langle j_{p,e}\rangle x_{95\%}]$. In Fig. 4.11, the uncertainty ranges for the intensities of CR protons and electrons with energy from 1 MeV to about 10 GeV are presented as the shaded red region. It is important to stress again that these stochastic fluctuations has been obtained by assuming that SNRs could accelerate particles down to energy of about 1 MeV with the injection spectrum of the form presented in Eq. 4.20.

Although the role of SNRs as low-energy CR sources might be quite questionable, there are observational evidences of enhanced ionization rates in the vincinity of SNRs indicating the presence of a population of low-energy CRs accelerated from these objects (Vaupré et al., 2014; Gabici & Montmerle, 2015). Interestingly, the CR intensities of CRs have been constrained down to energy in the range from about 20 MeV to 300 MeV in an MC interacting with the SNR W28 (see Chapter 6 and also Phan et al., 2020, for more details). More importantly, even if SNRs could accelerate these particles with the mechanisms such as diffusive shock acceleration, the energy

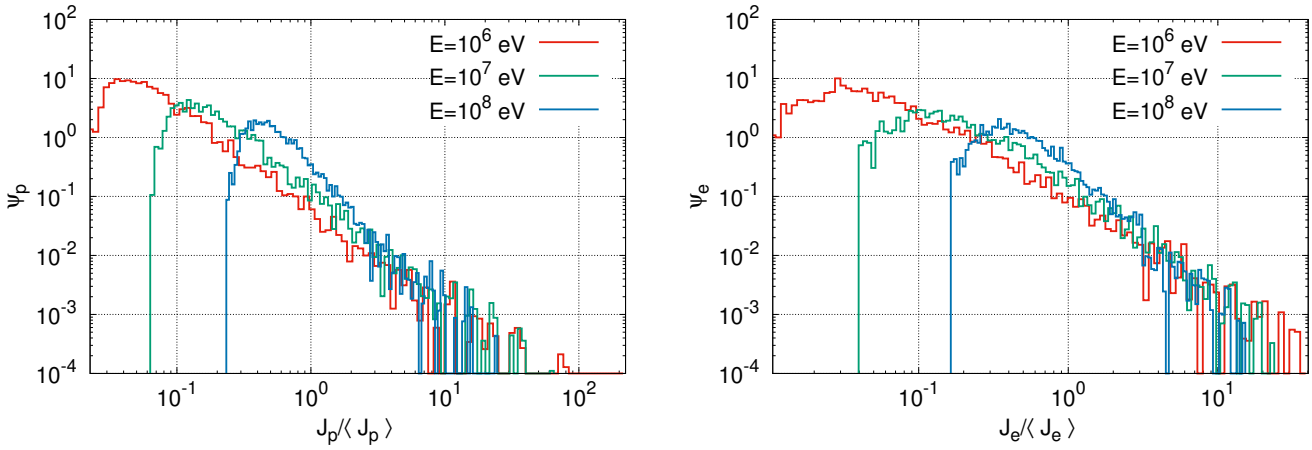

FIGURE 4.10: Probability density functions of the total CR intensities for both protons (upper panels) and electrons (lower panels).

loss due to Coulomb collisions inside the shocked region might create features like spectral breaks in the injection CR spectra which makes the assumption of the simple power law in momentum as indicated in Eq. 4.20 questionable. This problem will be further discussed in the next section. At this point, it is sufficient to note that the injection spectra could still be approximated as a power-law in momentum down to energy of about 1 MeV if CRs are released at the end of the Sedov-Taylor phase (see Section 5.1 for the more details on the phases during the evolution of SNRs).

Also, it is interesting to notice that, for the propagation setup adopted in this study, the most probable values of the total intensity are always above the data from direct observations by Voyager 1 for both CR protons and electrons at low energy. Together with the fact that the Voyager spectrum could not explain the high level of ionization rate seen in many MCs in our Galaxy (Phan et al., 2018), this might be an indication for the fact that the Voyager intensities are, in fact, the CR intensities of only the local ISM. Since we are inside the LB and the suppression with respect to the uncertainty range is particularly more pronounced for CR protons than for electrons, it is likely that this bubble has shielded away the low-energy CRs from the ISM and resulted in a significantly reduced intensity of CRs at the position of the solar system.

4.2.3 Stochastic Fluctuations of the Ionization Rate

We could now translate the stochastic fluctuations of the intensities into the corresponding fluctuations of the ionization rate $\zeta(H_2)$ in diffuse MCs. In principal, it should be done by first evaluating the intensities of CRs inside an arbitrary MC from the transport model presented in Chapter 3 using Eq. 3.8, Eq. 3.14, and Eq. 3.6 with the intensity $j_{p,e}^{(r)}$ of each realization as the boundary condition instead of the intensities set by Voyager 1 and AMS data. It is then quite straightforward to

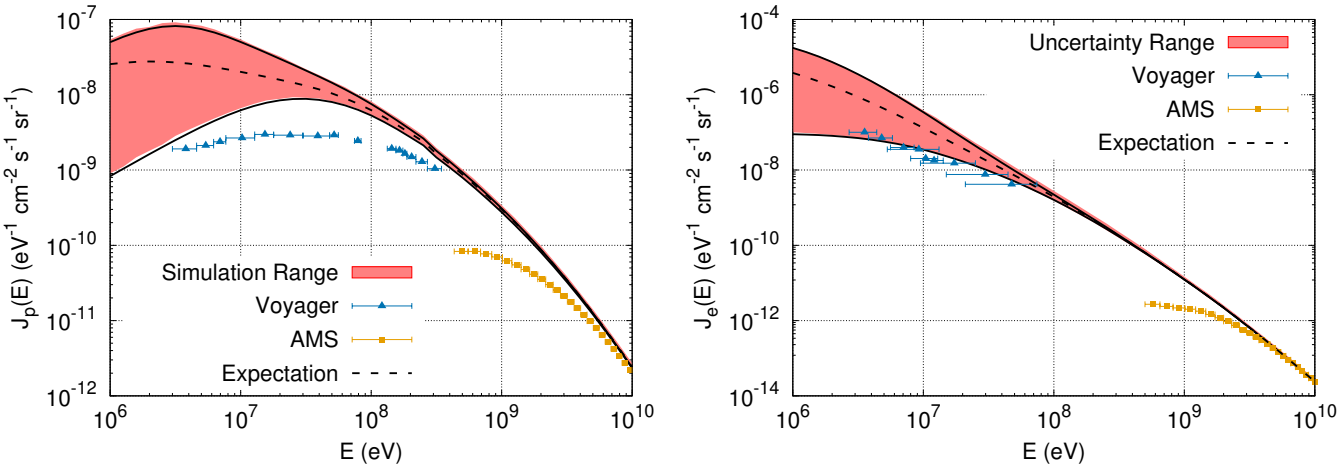

FIGURE 4.11: Stochastic fluctuations of CR intensities for both protons (left panel) and electrons (right panel).

apply Eq. 2.24, Eq. 2.25, and Eq. 2.26 as introduced in Chapter 2 to estimate the respective ionization rate induced by both CR protons and electrons for each realization to derive the most probable range for the values of $\zeta(H_2)$. This method would, however, require quite heavy computational effort. Therefore, we shall simply adopt this procedure for the intensities that are roughly the upper and lower limits of the uncertainty range shown in Fig. 4.11. This should provide us with the approximate ranges of potential values for the ionization rate induced by CR protons and electrons.

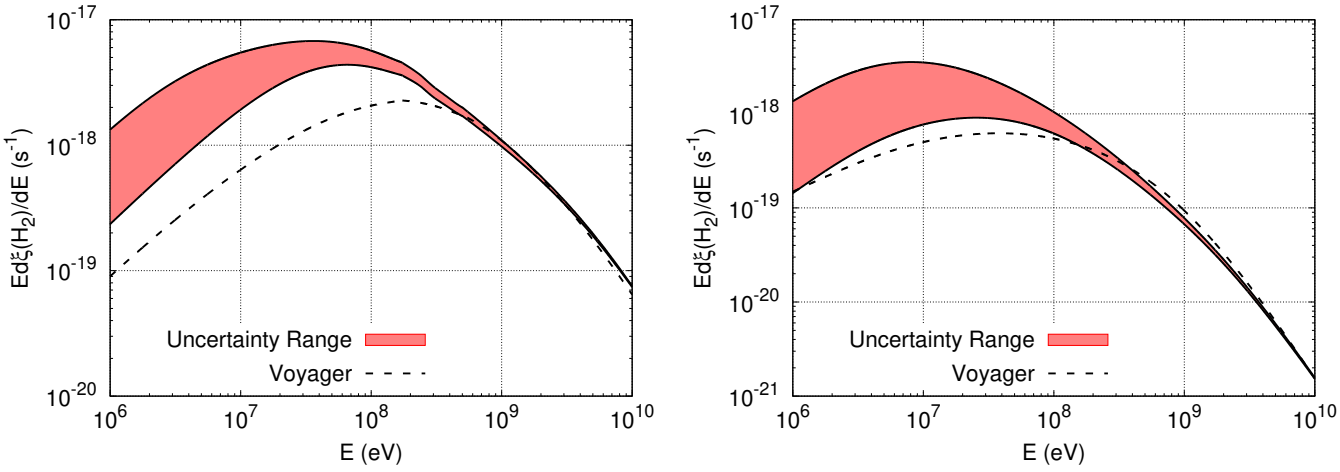

FIGURE 4.12: Differential ionization rates from the stochastic fluctuations for both CR nuclei (left panel) and electrons (right panel) for an MC of density $n(H_2) = 100$ cm^{-3} and of size $L_c = 10$ pc.

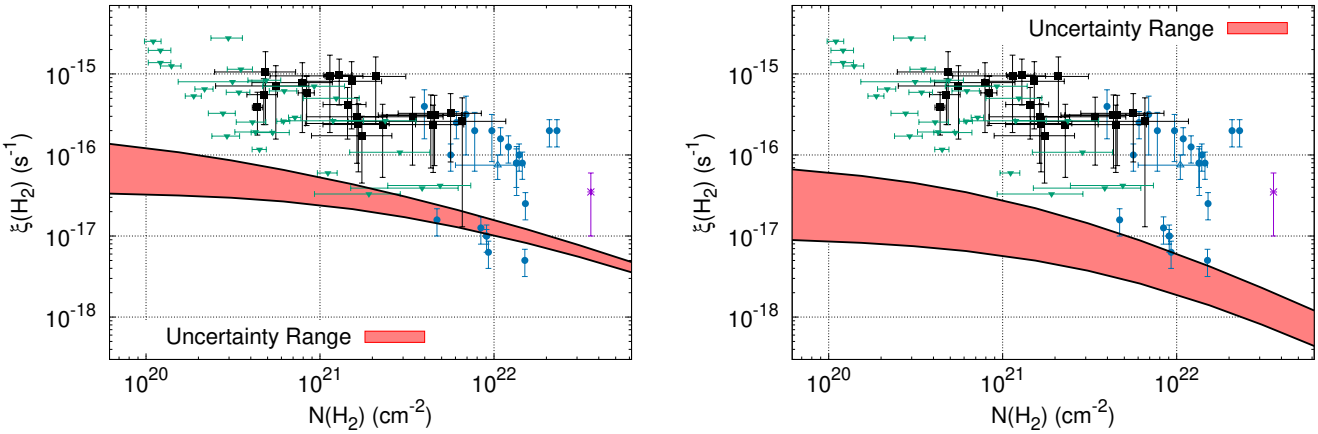

FIGURE 4.13: Cosmic-ray induced ionization rates from the stochastic fluctuations for both CR nuclei (left panel) and electrons (right panel).

The uncertainty ranges of the differential contributions to the ionization rate $E\,\mathrm{d}\zeta(\mathrm{H}_2)/\,\mathrm{d}E$ for a typical MC of density $n(\mathrm{H}_2) = 100$ cm^{-3} and of size $L_c = 10$ pc are shown in Fig. 4.12 together with the ones computed with the CR intensities from Voyager 1 and AMS data. As mentioned in Chapter 3, if the intensities from Voyager are representative of the entire Galaxy, the peaks of the differential ionization rates suggest that the energy ranges most relevant for ionization of CR protons and electrons are roughly within a few tens to a few hundreds MeV for both species. Since the density of low-energy CRs might become much higher when the effects of stochastic fluctuations are taken into account, the bulk of the ionization might also be due to particles of the lower energy components of the upper and lower limit intensities. It is interesting to note also that the propagation effect of diffuse MCs on the upper and lower limit intensities is more pronounced CR protons than CR electrons at low energy such that the energy range of CR electrons responsible for the majority of the induced ionization could span a wide range from a few MeVs to roughly 100 MeV depending on the specific realization of sources while the corresponding energy range for CR protons mostly center around a few tens MeV. This is essentially the reason why, as we shall see below, the ionization rate induced by CR protons does not fluctuate considerably in comparison to the one for CR electrons.

The stochastic fluctuations of the ionization rate are shown in Fig. 4.13 together with the measurements and upper limits of the ionization rate taken from Caselli et al. (1998), Williams et al. (1998), Maret & Bergin (2007), and Indriolo & McCall (2012). It should be noticed that the ionization rate for nuclei CRs has been computed by multiplying the one for protons with the nuclear enhancement factor $\eta \simeq 1.5$ (see Chapter 2). It should be noticed that the uncertainty range which takes into account the contribution of both protons and electrons is not simply the sum of the two since the ionization rate might be enhanced (or reduced) for one CR species but not for the other in a particular realization of sources. However, the bulk of ionization of hadronic origin in diffuse MCs ($N(\mathrm{H}_2) \simeq 10^{21} - 10^{22}$ cm^{-2}) is caused

by CR protons of energy around 100 MeV for and the corresponding stochastic fluctuation of the intensity do not vary more than an order of magnitude within this energy range. Thus, it might be justified to combine uncertainty range for the ionization rate induced by both species (see Fig. 4.14) and, in this case, the stochastic fluctuation is mostly due to CR electrons.

It is important to note also that the stochastic fluctuations of the ionization rate has been derived with the model for CR transport into clouds as introduced in Chapter 3 which includes the effect of exclusion due to the diffusive motion of particles outside the clouds. There exist also models treating the transport of low-energy CRs as purely ballistic (see e.g. Padovani et al., 2009). In that case, we expect the spectra of CRs at the border of the cloud, $f_b(p)$, to be equal to the one in the ISM, $f_0(p)$, even for CRs of energy below the characteristic energy E_{loss} defined above and, thus, the resulting ionization rate could be further boosted to better fit the data. It is, however, not yet clear whether the transport of CRs at low energy should be treated as ballistic or diffusive (Silsbee & Ivlev, 2019). In fact, it could be proven that the diffusive transport model might reduces to the ballistic one if the coherence length of the magnetic field l_c is much shorter than the characteristic length $x_c = D/v_A$ (where D is the diffusion coefficient of CRs and v_A is the Alfén speed, see Chapter 3 for more details). Morlino & Gabici 2015 refer to this situation as the limit where the one-dimensional approximation breaks down since the boundary conditions $\lim_{x\to\pm\infty} f(x,p) = f_0(p)$ are no longer valid. The appropriate boundary conditions, in this case, should be to put the ISM spectra at the end of the flux tube of the field lines threading the clouds and the one-dimensional model should be applicable only within the range of the flux tube. If we restrict ourselves to the energy range where CRs could ballistically cross the cloud, Eq. 3.5 for the high-energy part of the CR spectra inside the cloud in the case of a finite-size flux tube becomes:

$$f_c(p) = f_0(p) + \frac{L_c}{2v_A p^2}\left[1 - \exp\left(-\frac{l_c - L_c}{2x_c}\right)\right]\frac{\partial}{\partial p}\left[\dot{p}(p)p^2 f_c(p)\right] \tag{4.34}$$

where $f_c(p)$ is the spectrum of CRs inside the cloud under consideration, l_c is the coherence length of the field, and L_c is the size of the cloud. It is straightforward from the above equation that $f_c(p) = f_0(p)$ for $l_c \ll D/v_A$ and, in the opposite limit, we shall recover the diffusive model as presented in Chapter 3. The extrapolation of the typical diffusion coefficient with a Kolmogorov turbulence spectrum suggests that $x_c \geq l_c \simeq 100$ pc for CRs of energy $E \geq E_c = 100$ MeV (Morlino & Gabici, 2015). If the effect of self-generated turbulence like streaming instability is taken into account, the value of E_c could be a few hundred times higher which means that the diffusive model of CR transport into clouds is still reasonable at least from a theoretical point of view. Nevertheless, better understanding of both the coherence length of the field and the diffusion coefficient below a few GeVs are required in order to clarify the nature of transport for low-energy CRs.

Although the stochastic effect could manage to boost the ionization rate a few times higher and, in certain cases, even close to 10^{-16} for diffuse MCs, it seems that the extrapolation from high energy CRs using the power-law in momentum injection

spectrum and the diffusion coefficient as mentioned above could not provide to the mean value of roughly 3×10^{-16} s^{-1}. There are at least two possible implications for such a result that we could envisage: i) a different form of the diffusion coefficient with a smaller value at low energy is required which should provide better confinement of low-energy CRs in the Galactic disk and, as a consequence, a higher ionization rate, or ii) an indication for the existence of other classes of sources for low-energy CRs which could be, for instance, OB/Wolf-Rayet stars (Casse & Paul, 1982; Voelk & Forman, 1982; Binns et al., 2005) or even solar-type stars (Scherer et al., 2008).

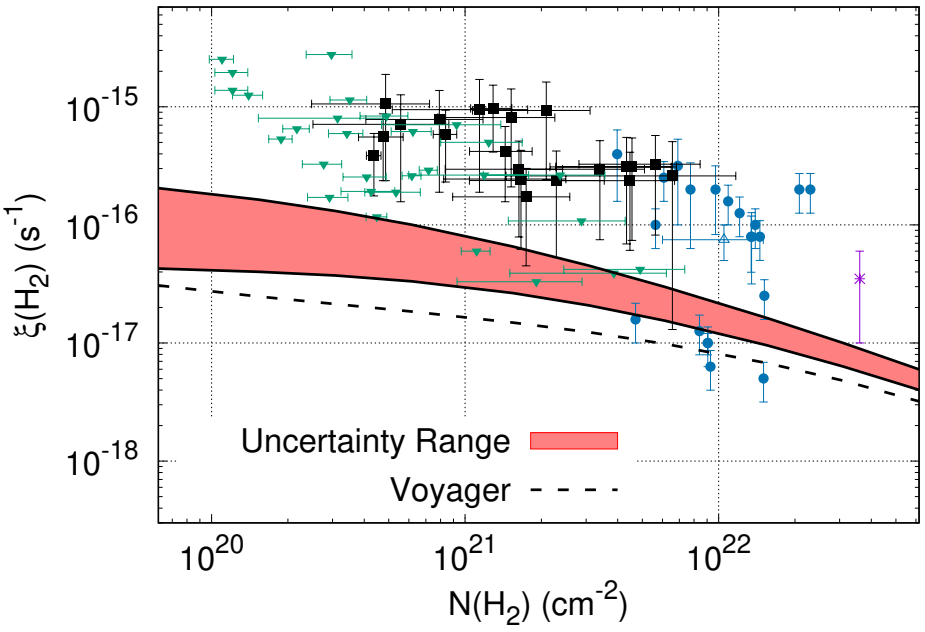

FIGURE 4.14: Combined stochastic fluctuation of the ionization rate induced by both CR species.

It should be noticed that, in fact, the second possibility has been investigated by Scherer et al. (2008) who find that CRs accelerated in the termination shocks of G, K, and F stars might contribute significantly to the Galactic CR proton spectrum in the energy range from 5 MeV to about 300 MeV. In particular, the acceleration mechanism employed for these stars is quite similar to that of anomalous CRs which involve ions originating from neutral atoms of the ISM drifting into the astrosphere of the stars, picked up by the stellar winds, and finally accelerated at the termination shock. The estimated energy density for CRs with energy below 300 MeV accelerated in this way is approximately $\varepsilon_{star} = 0.076$ eV/cm^3 which is 35% and 50% the corresponding energy density calculated from the upper and lower limit intensities. More importantly, we note that the value of ε_{star} from Scherer et al. (2008) has been evaluated for a cylindrical region of radius 15 kpc and thickness

2 kpc which might be much larger than the real confinement volume of low-energy CRs since these particles might lose their energy before they even manage to escape the Galactic disk. In other words, this value should be treated as a lower limit and the contribution from CR-accelerating stars might be much higher.

Chapter 5

Low Energy Cosmic Rays from Supernova Remnants

One of the main assumption for the previous chapter is the fact that the injection spectra of both CR protons and electrons from SNRs are power laws in momentum down to kinetic energy of about 1 MeV. Indeed, there exist observational evidences which suggest the presence of enhanced low-energy CR intensities in the vincinity of SNRs (Ceccarelli et al., 2011; Dumas et al., 2014; Vaupré et al., 2014; Phan et al., 2020). It should be noted, however, that even if these particles could be accelerated at SNR shocks via mechanisms such as diffusive shock acceleration, the injection spectra might emerge with spectral breaks since low-energy CRs suffer also from energy loss due to Coulomb collisions, ionization interactions, and adiabatic energy loss inside the acceleration region which means that the assumption of the simple power laws in momentum as indicated above might be questionable. Section 5.1 of this chapter is particularly to address this problem. We shall see later in this chapter that spectral breaks might appear in the case where CRs are released from the acceleration region in the radiative phase of the SNR evolution. If the time of release for CRs is around the end of the Sedov-Taylor phase, it is reasonable to approximately model the injection spectra as power laws in momentum down to energy of about 1 MeV.

Another problem that we shall discuss here concerns the intensities of low-energy CRs measured by Voyager 1 which, as suggested in Chapter 3, might be of a local origin since they fail to fit the observed ionization rate in MCs. Also, the analysis of the previous chapter seems to indicate that we could not simultaneously fit both the observed ionization rate and the Voyager spectra with a homogeneous distribution of sources. This might come without a surprise given the relatively special position of the solar system inside the LB. More importantly, there are observational evidences coming from the analyses of the ^{60}Fe isotopes in a deep-ocean ferro–manganese (Fe-Mn) crust which suggest that a supernova explosion occurred inside the LB around 2 million years ago (Knie et al., 1999). This has, indeed, motivated us to propose the so-called single-source scenario according to which the low energy population of Galactic CRs are suppressed due to the presence of the LB shell and the CRs of energy from MeV to sub-GeV observed by Voyager originate mostly from the supernova explosion taking place inside the LB (see Section 5.2).

5.1 Spectral Features of Low Energy Cosmic Rays from Supernova Remnants

5.1.1 Dynamics of Supernova Remnant

We present here a simple formalism for the dynamics of SNR using the combination of the analytic solutions by Finke & Dermer (2012) and Cioffi et al. (1988). The evolution of the remnant goes through three phases: i) free expansion phase, ii) Sedov-Taylor phase, and iii) radiative pressure-driven snowplow (PDS) phase.

During the first phase of the SNR, the circumstellar medium has no effect on the expansion of the shock wave. The shock speed is roughly constant and could be calculated simply as $u_0 = \sqrt{2E_{SNR}/M_0}$ where E_{SNR} and M_0 are respectively the total kinetic energy and the initial mass of the remnant (i.e. the mass of the ejecta). This phase ends when the mass of the swept-up material is approximately the same as the ejected mass or equivalently when the shock radius reaches:

$$R_{ST} = \left(\frac{3M_0}{4\pi m_{avg} n_0}\right)^{1/3}, \tag{5.1}$$

where n_0 is the density of hydrogen atoms in the surrounding ISM and m_{avg} is the average atomic mass of the ISM (with solar abundances $m_{avg} \simeq 1.4 m_p$). The transition to Sedov-Taylor phase, in turn, happens at around $t_{ST} = R_{ST}/u_0$. For the dynamics of the SNR from the free expansion to the Sedov-Taylor phase, we shall adopt the approximate solution presented in Finke & Dermer (2012).

According to Cioffi et al., 1988, the transition to the PDS phase is expected at:

$$t_{PDS} \simeq 1.33 \times 10^4 n_0^{-4/7} \zeta_m^{-5/14} E_{SNR,51}^{3/14} \text{ yr}, \tag{5.2}$$

where n_0 is the density of the surrounding ISM in unit of cm^{-3}, ζ_m is the metallicity factor which should take the value $\zeta_m = 1$ for solar abundances, and $E_{SNR,51} = E_{SNR}/\left(10^{51} \text{ erg}\right)$. During this phase, we shall adopt the analytic solution presented by Cioffi et al. (1988) which, in the limit when $t \gg t_{PDS}$, should provide the following scalings for the shock radius $R_s \sim t^{3/10}$ and the shock speed $u_s \sim t^{-7/10}$. The maximum amount of time within which the SNR could evolve and remain in the radiative phase has also been estimated by Cioffi et al. (1988) to be:

$$t_{max} = \min\left[\frac{61 u_{s,8}}{\zeta_m^{9/14} n_0^{3/7} E_{SNR,51}}, \frac{476}{\left(\zeta_m \phi_c\right)^{9/14}}, 153\left(\frac{E_{SNR,51}^{1/14} n_0^{1/7} \zeta_m^{3/14}}{\beta_s c_{s,6}}\right)\right], \tag{5.3}$$

where $u_{s,8}$ is the shock speed normalized at 10^8 cm/s, $\phi_c < 1$ is the ratio between the actual thermal condictivity of the gas in the interior of the remnant and the value estimated by Spitzer (1962), β_s is a dimensionless factor commonly chosen to be $\beta_s \simeq 2$ (see Cioffi et al., 1988, for more details), and $c_{s,6}$ is the sound speed

normalized at 10^6 cm/s. Notice that the sound speed could be estimated as:

$$c_s \simeq 10^6 \left(\frac{T_{ISM}}{10^4 \text{ K}}\right)^{1/2} \text{ cm/s} \tag{5.4}$$

where T_{ISM} is the temperature of the surrounding ISM. Having established all the relevant timescales, we could present the approximate solutions for the radius and the shock speed of the remnant throughout the three phases:

$$R_s(t) = \begin{cases} u_0 t & t < 0.4 t_{ST} \\ u_0 t_{ST} \left(\dfrac{5t}{2t_{ST}}\right)^{2/5} & t_{PDS} > t \geq 0.4 t_{ST} \\ u_0 t_{ST} \left(\dfrac{5t_c}{2t_{ST}}\right)^{2/5} \left(\dfrac{4t}{3t_{PDS}} - \dfrac{1}{3}\right)^{3/10} & t \geq t_{PDS} \end{cases} \tag{5.5}$$

$$u_s(t) = \begin{cases} u_0 & t < 1.84 t_{ST} \\ u_0 \left(\dfrac{5t}{2t_{ST}}\right)^{-3/5} & t_{PDS} > t \geq 1.84 t_{ST} \\ u_0 \left(\dfrac{5t_{PDS}}{2t_{ST}}\right)^{-3/5} \left(\dfrac{4t}{3t_{PDS}} - \dfrac{1}{3}\right)^{-7/10} & t \geq t_{PDS} \end{cases} \tag{5.6}$$

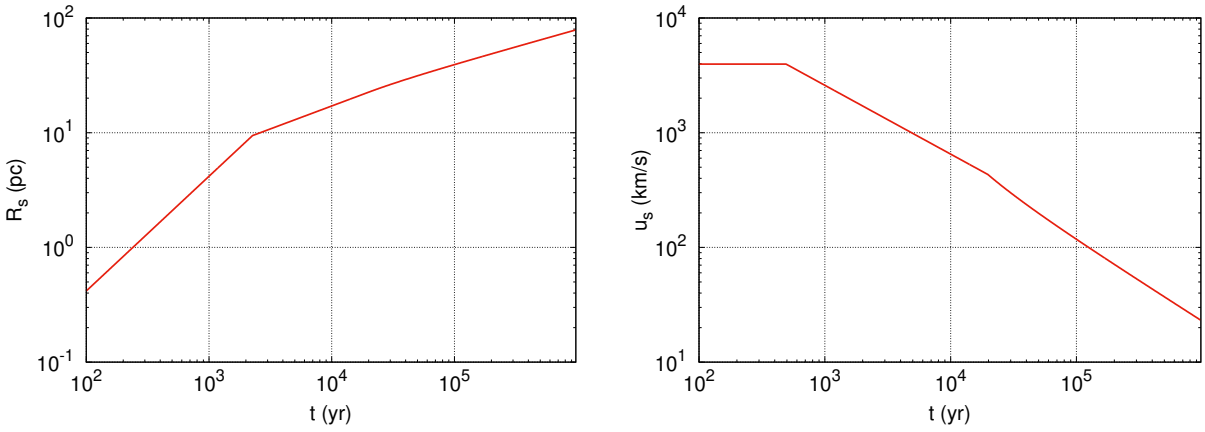

FIGURE 5.1: The radius (left panel) and the shock speed (right panel) of an SNR with the initial mass $M_0 = 6.4 M_\odot$ in the ISM characterized by $n_0 = 0.5$ cm^{-3}, $T_{ISM} = 10^4$ K, and $B = 3$ μG (see text for more details).

Since we would like to investigate the effect of Coulomb and ionization losses on the evolution of the particle distribution accelerated in the shocked region, let's discuss

also the number density of hydrogen atoms in the post-shock medium. During the first two phases, we simply have $n_{ps} \simeq n_e = 4n_0$ as the shock is strong ($u_s \gg c_s$) and adiabatic. For the PDS phase, we shall follow Uchiyama et al., 2010 and estimate $n_{\rm H}$ by balancing the shock ram pressure $n_0 m_p u_s^2$ and the magnetic pressure in the post-shock region $B_{ps}^2/8\pi$:

$$n_0 m_p u_s^2 = \frac{B_{ps}^2}{8\pi} \Rightarrow n_{ps} \simeq 2.65\mathcal{M} \left(\frac{n_0}{1\ \mathrm{cm}^{-3}}\right)^{3/2} \left(\frac{B_0}{3\ \mu\mathrm{G}}\right)^{-1} \left(\frac{c_s}{10\ \mathrm{km/s}}\right)\ \mathrm{cm}^{-3}, \quad (5.7)$$

where $\mathcal{M}$ is the Mach number of the shock front and B_{ps} is the post-shock magnetic field strength calculated from the magnetic field strength in the circumstellar medium B_0 as $B_{ps} = \sqrt{2/3}(n_{ps}/n_0)B_0$ (Uchiyama et al., 2010). The evolution of the post-shock density could then be written as:

$$n_{ps} = \begin{cases} 4n_0 & t < t_{PDS} \\ n_{ps}^c \left(\dfrac{4t}{3t_{PDS}} - \dfrac{1}{3}\right)^{-7/10} & t \geq t_{PDS} \end{cases} \quad (5.8)$$

where n_{ps}^c is calculated using Eq. 5.7 for $u_s = u_s(t = t_{PDS})$. In the following analyses, we shall adopt the model for SNR dynamics presented above to study the spectral features of low-energy CRs for a typical SNR with the initial mass $M_0 = 6.4M_\odot$ in the ISM characterized by $n_0 = 0.5\ \mathrm{cm}^{-3}$, $T_{ISM} = 10^4$ K, and $B = 3\ \mu$G. The radius and the shock speed of a typical SNR with the above parameters are presented in Fig. 5.1 and the corresponding post-shock density is also illustrated in Fig. 5.2.

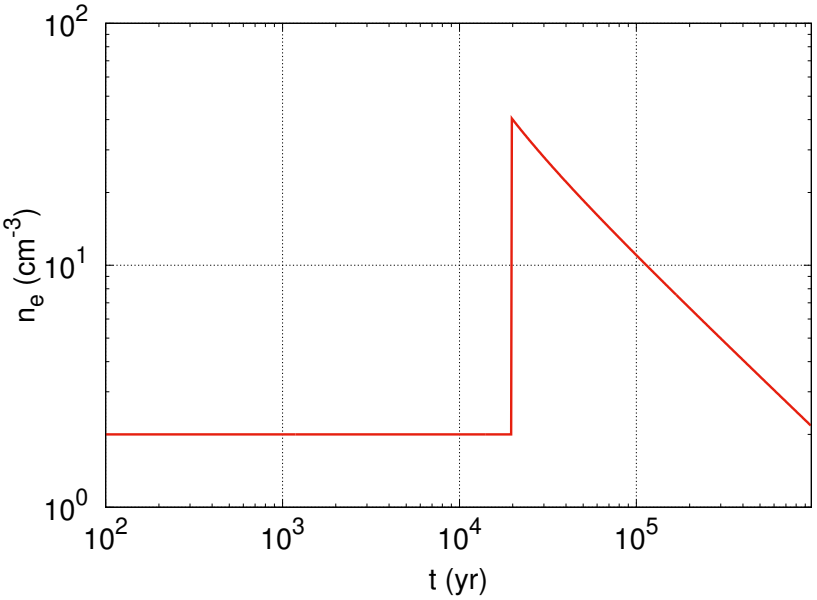

FIGURE 5.2: The post-shock density of an SNR with the initial mass $M_0 = 6.4M_\odot$ in the ISM characterized by $n_0 = 0.5\ \mathrm{cm}^{-3}$, $T_{ISM} = 10^4$ K, and $B = 3\ \mu$G (see text for more details).

5.1.2 Evolution of Accelerated Cosmic Rays

For simplicity, we shall focus on the large-scale behaviour of the injected CRs and study the volume-integrated intensity which shall be defined as:

$$N(p,t) \simeq \int_{V_{SNR}} 4\pi p^2 f(\mathbf{x},p,t) d^3\mathbf{x}, \tag{5.9}$$

where $f(\mathbf{x},p,t)$ is the distribution function and the spatial region over which the integration is carried shall be the volume of the acceleration region $V_{SNR} = 4\pi R_s^3/(3r_c)$ with r_c is the compression factor of the shock. Notice also that we could perform the following approximation for the velocity profile of the expanding SNR shell :

$$\nabla \cdot \mathbf{u} \simeq \frac{1}{V_{SNR}} \frac{\mathrm{d}V_{SNR}}{\mathrm{d}t} \equiv \frac{3k_{ad}}{t}, \tag{5.10}$$

where:

$$k_{ad} = \left(\frac{\dot{R}_s}{R_s} - \frac{\dot{r}_c}{3r_c} \right) t, \tag{5.11}$$

which should give $k_{ad} = 1$, 2/5, and 11/21 during the free expansion, Sedov-Taylor, and radiative phase respectively. For simplicity, we shall adopt the approximation by Finke & Dermer (2012) and take $k_{ad} = 1$ throughout the three phases.

The evolution of the volume-integrated intensity in the shocked region could now be obtained from Eq. 4.14 as follows:

$$\frac{\partial N(p,t)}{\partial t} + \frac{\partial}{\partial p} \left\{ \left[b(p,t) - \frac{k_{ad} p}{t} \right] N(p,t) \right\} = Q(p,t) \tag{5.12}$$

where $b(p,t)$ is the rate of momentum loss dominated by Coulomb and ionization loss for low-energy CRs and $Q(p,t)$ is the source term that describe the CRs accelerated in the shocked region.

Particle Acceleration

Let's assume that the volume-integrated injection intensity is a power law in momentum (Finke & Dermer, 2012) such that $Q(p,t) = Q_0(t)\,(p/mc)^{2-\delta}$ ($m = m_p$ or $m = m_e$ depending on the species of interest) and also the kinetic energy of CRs makes up a fraction ξ_{CR} of the kinetic energy of the shocked fluid which means:

$$Q_0(t) \int_{p_{min}}^{p_{max}} \left(\sqrt{p^2c^2 + m_p^2c^4} - m_pc^2 \right) \left(\frac{p}{m_pc} \right)^{2-\delta} \mathrm{d}p = \xi_{CR} 2\pi R_s^2 n_0 m_p u_s^3, \tag{5.13}$$

and, thus, we shall have:

$$Q_0(t) = \frac{\xi_{CR} 2\pi m_p n_0}{m^2 c^3 \Lambda} R_s^2 u_s^3 \tag{5.14}$$

where Λ is the same integral as introduced in Eq. 4.21 in the previous section for the source term of SNR.

Momentum Loss Rate

Apart from the adiabatic expansion that induces energy loss for CRs throughout the evolution of the shocked region, the rate of energy loss within the energy range of interest is mostly due to Coulomb collisions (in the free expansion and Sedov-Taylor phase) and ionization interactions (in the radiative phase) which has been discussed in Chapter 1 (see also Schlickeiser, 2002). It should be noted that the corresponding $b(p)$ for both of these mechanisms depend on momentum in the same way within the energy range of interest and they are both proportional to the number of hydrogen atoms in the post-shock region. We could, thus, describe the momentum loss rate as:

$$b_p(p,t) \simeq -\frac{\nu_p(t) n_{ps}(t)}{p^2}, \tag{5.15}$$

$$b_e(p,t) \simeq -\nu_e(t) n_{ps}(t), \tag{5.16}$$

where

$$\nu_p(t) = \begin{cases} 2.73 \times 10^{11}\ (\mathrm{eV/c})^3\ \mathrm{s}^{-1}\ \mathrm{cm}^{-3} & t < t_{PDS} \\ 3.20 \times 10^{11}\ (\mathrm{eV/c})^3\ \mathrm{s}^{-1}\ \mathrm{cm}^{-3} & t \geq t_{PDS}, \end{cases} \tag{5.17}$$

$$\nu_e(t) = \begin{cases} 5.68 \times 10^{-7}\ (\mathrm{eV/c})\ \mathrm{s}^{-1}\ \mathrm{cm}^{-3} & t < t_{PDS} \\ 1.88 \times 10^{-7}\ (\mathrm{eV/c})\ \mathrm{s}^{-1}\ \mathrm{cm}^{-3} & t \geq t_{PDS}. \end{cases} \tag{5.18}$$

The changes in the value of ν_p and ν_e at $t = t_{PDS}$ is due to the fact that, $b(p)$ is mostly contributed by ionization interactions in the radiative phase while, for earlier phases, it is dominated by Coulomb loss. Also, it should be noticed that we have considered the non-relativistic limit for protons and relativistic limit for electrons since the relevant range of kinetic energy in our case is between $E = 1$ MeV to 1 GeV and the errors induced for protons of energy above a few GeVs or electrons of energy around a few MeVs are negligible.

Volume-Integrated Cosmic Ray Spectra

With the expression for the momentum loss rate and the source term, we are at the position to solve Eq. 5.12 and investigate the evolution of the injected CR intensities. The solutions could be found in a semi-analytic form using the method of characteristics.

For CR protons, we have:

$$N_p(p,t) = \int_{t_{min}}^{t} \mathrm{d}t' Q_p(q_p,t') \left(\frac{t}{t'}\right)^{k_{ad}} \exp\left[-\int_{t'}^{t} \mathrm{d}t'' \frac{2\nu_p(t'')n_{\mathrm{H}}(t'')}{k_p^3}\right], \tag{5.19}$$

where we have denoted $q_p = p_{i,p}(t';p,t)$ and $k_p = p_{i,p}(t'';p,t)$, $t_{min,p}$ is the solution of the equation $p_{max,p} = p_{i,p}(t_{min};p,t)$, and $p_{i,p}(t_i;p,t)$ is the following function:

$$p_{i,p}(t_i;p,t) = \left[p^3 \left(\frac{t}{t_i}\right)^{3k_{ad}} + 3\int_{t_i}^{t} \nu_p(t_0) n_{\mathrm{H}}(t_0) t_0^{3k_{ad}}\, \mathrm{d}t_0\right]^{1/3}. \tag{5.20}$$

Similarly, the solution for CR electrons is:

$$N_e(p,t) = \int_{t_{min}}^{t} \mathrm{d}t' Q_e(q_e,t') \left(\frac{t}{t'}\right)^{k_{ad}}, \tag{5.21}$$

where we have denoted $q_e = p_{i,e}(t';p,t)$, $t_{min,e}$ is the solution of the equation $p_{max,e} = p_{i,e}(t_{min};p,t)$, and $p_{i,e}(t_i;p,t)$ is the following function:

$$p_{i,e}(t_i;p,t) = p\left(\frac{t}{t_i}\right)^{k_{ad}} + \int_{t_i}^{t} \nu_e(t_0) n_{\mathrm{H}}(t_0) t_0^{k_{ad}}\, \mathrm{d}t_0. \tag{5.22}$$

Results of the injection spectrum $Q(E,t) = N(p,t)/v_p$ are shown together with the ones used in the study of stochasticity effect (see Eq. 4.20) in Fig. 5.3 for both CR protons and electrons at three different moments of CR release $t = t_{ST}$, $t = t_{PDS}$, and $t = t_{max}$. It is straightforward to see that the injection spectra follow quite closely the power-law feature of the accelerated CRs if the confinement of these particles within the acceleration region ends before the end of the Sedov-Taylor phase. This should justify our choice for the power-law in momentum down to around 1 MeV for the analysis of the stochasticity effect in the previous section. Interestingly, there exists a break in the injection spectra of both species at around 30 MeV for the case where particles are released at the end of the PDS phase. Such a spectral feature has been briefly mentioned in the recent review by Tatischeff & Gabici (2018) who proposes that a break in the spectra of the sources at around 200 MeV might help to explain the intensities of low-energy CRs observed by Voyager 1. However, it is clear from the discussion in Chapter 3 and in the previous section that the CR intensities at low energy observed at the position of the solar system could not be taken as the reference value for the entire Galaxy.

In the following, we shall propose another scenario to possibly fit the entire CR intensities from a few MeVs to about 10 GeV which relies on the fact that the solar system is actually located within the LB.

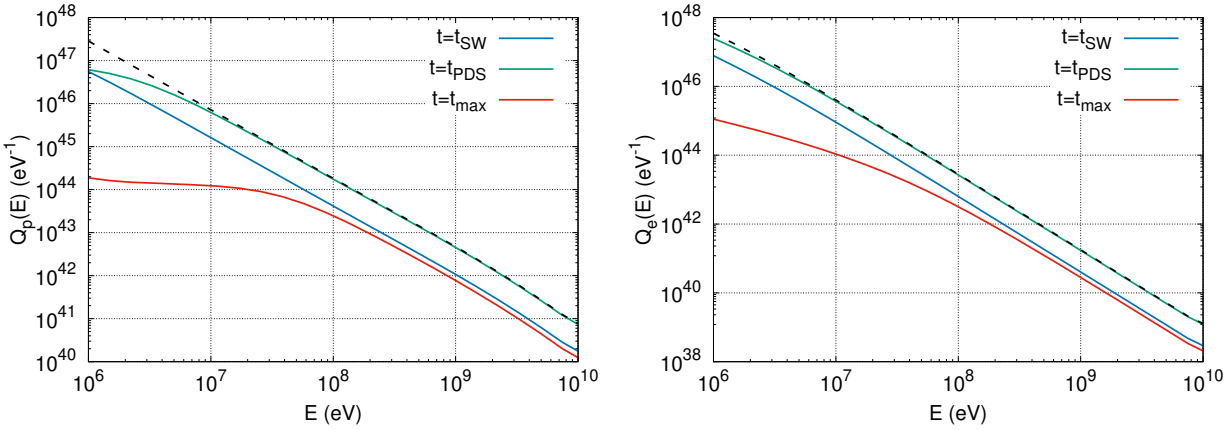

FIGURE 5.3: Volume-integrated CR spectra for an SNR of initial mass $M_0 = 6.4 M_\odot$ for different times of escape. The left and right panels are respectively the results for CR protons and electrons. The blue, green, and red curves represent to the volume-integrated injection spectrum for the times of CR release $t = t_{ST}$ (the end of the free expansion phase), $t = t_{PDS}$ (the end of the Sedov-Taylor phase), $t = t_{max}$ (the end of the radiative phase). The dashed lines are the volume-integrated injection spectra adopted for the study of stochasticity in Chapter 4.

5.2 Cosmic-Ray Intensities from the Voyager Probes and the Local Bubble?

As mentioned above, the analyses of both the ionization rate and the stochasticity effect of sources strongly indicate the Voyager spectra have been shaped by sources within the local ISM. In this section, we shall investigate the scenario where low energy Galactic CRs are shielded by the LB's shell and the local CR intensities below a few hundreds MeV comes mostly from the accelerated CRs of the supernova explosion which occurred around 2 million years ago.

5.2.1 Transport on the Bubble's Shell

Since simulations suggests that outflows perpendicular to the Galactic disk might open up the bubble into the halo (Breitschwerdt et al., 2000; Schulreich et al., 2017), we shall adopt the simplified geometry similar to that presented in Andersen et al. (2018) for the LB which is to assume its cylindrical form with the magnetic field wrapped around its shell made up of mostly by neutral matters. We shall set the radius of the LB to be $R_{LB} \simeq 150$ pc, the thickness of the shell is $L_{sh} = 5$ pc, and the density of hydrogen atoms outside is roughly $n_0 = 0.5$ cm^{-3}. This means that the column density of the LB's shell should be roughly $N_{\rm H} = n_0 R_{LB} \simeq 2 \times 10^{20}$ cm^{-2} which is comparable to the value $N_{\rm H} \simeq 1.5 \times 10^{20}$ cm^{-2} suggested from the observational evidence (see e.g. Andersson & Potter, 2006) and the density inside the shell is roughly $n_{sh} = n_0 R_{LB}/L_{sh}$ (assuming the swept-up materials are all condensed into the shell).

In this case, the transport of particles into the LB's interior proceeds via the perpendicular diffusion which is commonly suppressed in comparison to the typical parallel diffusion along the field line. As we shall see later, most of the CRs from outside which manage to penetrate the LB's shell and contribute to the local CR intensities at low energy are actually within the energy range where the stochastic fluctuations are negligible. For this reason, we will restrict ourselves to the steady-state solution of the transport equation which, in cylindrical coordinates, reads:

$$\frac{D_\perp}{r}\frac{\partial}{\partial r}\left(r\frac{\partial f}{\partial r}\right) - \frac{\partial}{\partial E}\left(\dot{E}f\right) = 0 \tag{5.23}$$

where $D_\perp$ is the perpendicular diffusion, r is the distance from the point of interest to the symmetric axis of the LB, and $f(r, E)$ is the spectrum of CRs. Notice that inside the LB energy loss should be negligible (again in the energy range relevant for penetrating CRs) and the system is under cylindrical symmetry such that $(\partial f/\partial r)_{r=0} = 0$. This means that the derivative $\partial f/\partial r$ should vanish everywhere inside the LB and the spectrum does not depend on r for $r \leq R_{LB}$. We shall, therefore, focus on finding the CR intensities at the inner boundary of the shell meaning at $r = R_{LB}$ which could be done by solving numerically the transport equation with diffusion and energy loss across the shell. The boundary condition at $r = R_{LB}$ is set to be the vanishing derivative of $f(r, E)$ with respect to r and also, at $r = R_{LB}+L_{sh}$, the CR intensities are set to be equal to the upper and lower limit intensities obtained in the analyses for stochasticity of sources (see the black curves in Fig. 4.11). The analogy of this problem to the case of CR transport into MCs suggests that the presence of the shell itself might affect the intensities of CRs immediately outside of the LB, we note, however, that the boundary condition at $r = R_{LB} + L_{sh}$ is justified at least under the assumption that the diffusion coefficient inside the shell is much smaller than the one in the ISM outside the bubble.

We shall investigate the transport for the perpendicular diffusion coefficient of the following form:

$$D_\perp(E) = D(E)/\eta \tag{5.24}$$

where $\eta = 20 - 200$ and D is the diffusion coefficient in the ISM as presented in Eq. 4.17. This scaling has been motivated from several theoretical investigations of CR mean free path inside the heliosphere (see e.g. Bieber et al., 2004, and references therein).Indeed, this provides only a weak justification for the adopted values of $D_\perp$ since the parallel diffusion coefficient inside the LB's shell is actually unknown. Thus, the range chosen here is simply for reference and, in the following, we should keep in mind that $D_\perp$ should be regarded as a fit parameter.

Results are shown in Fig. 5.4 for the perpendicular diffusion coefficient with $\eta = 20$ (yellow shaded region) and $\eta = 200$ (green shaded region). It is straightforward to see that there exists a characteristic energy scale E^* below which the slopes of the penetrating CR intensities are actually fixed by the process of energy loss inside

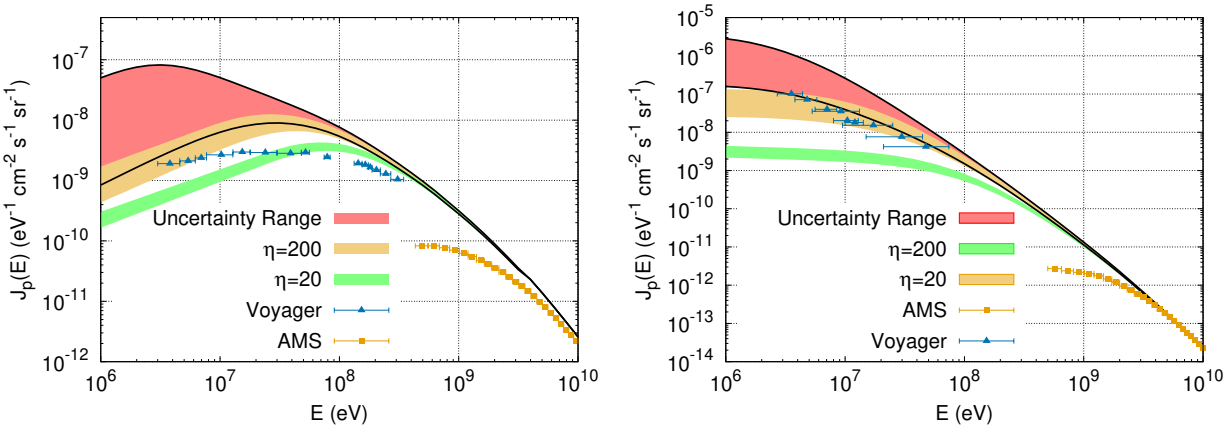

FIGURE 5.4: Predicted intensities of CRs in the LB interior. The left and right panels are respectively the results for CR protons and electrons. The shaded red regions contoured by the black curves represent the stochastic fluctuations presented in the previous chapter. The yellow ($\eta = 20$) and green ($\eta = 200$) shaded regions are the corresponding fluctuations in the intensities after diffusing through the shell.

the LB's shell. In particular, the value of E^* set the lowest possible energy for CRs from outside to transport into the LB and it could be roughly estimated by equating the column density covered by CRs to the column density of the bubble's shell $n_{sh}\sqrt{2D_\perp(E^*)\tau_l(E^*)} = N_{\rm H}$.

There exists also the possibility to have particles transported into the LB by diffusing along the field lines. Such a scenario has been recently investigated by Silsbee & Ivlev (2019) who have presented one of the very first attempt to fit both the ionization rate in diffuse clouds and the intensity of CR protons from Voyager 1. These authors have proposed a spectrum of Galactic CRs with more low energy particles to fit the ionization rate in clouds and, then, find the corresponding column density traversed by these CRs in order to suppress the spectrum such that it fits the data from Voyager 1. This results in a quite large column density which could mean that the density inside the LB's shell is large or the magnetic field lines wrap around this shell a few times before going inside the bubble. We notice, however, that the slope of the CR intensity fitted in this way is also determined by the process of energy loss inside the shell. In other words, different values of the diffusion coefficient could only change the point of the break E^* mentioned above and the slope of the intensity at low energy is always different from the one observed by Voyager regardless of the scenario for CR transport. Thus, it seems quite challenging to fit the low-energy CR intensities simply with Galactic CRs from the exterior of the LB.

5.2.2 The Single-Source Scenario for Low Energy Cosmic Rays

The discussion of the transport on the LB's shell seems to make it even more clear that the intensities of CRs observed by Voyager 1 should have contribution from local sources. One of the potential source for such a scenario could be a supernova

explosion that took place within the LB. It is believed that such an explosion occurred around 2 million years ago as supported by observational evidences from the ^{60}Fe isotopes in a deep-ocean ferro–manganese (Fe-Mn) crust (Knie et al., 1999).

For simplicity, we will study this scenario in a zero-dimension model which employ the volume integrated equation for the CR intensities as introduced in the previous section. Notice that in this case the use of the volume integrated equation is justified since the radius of the remnant by the time it releases CRs presumably at the end of the Sedov-Taylor phase should be comparable to the radius of the LB. In this case, the equation for the volume integrated intensities reads:

$$\frac{\partial N}{\partial t} + \frac{\partial}{\partial p}\left[b(p,t)N\right] + \frac{N}{\tau_D(p)} = 0, \tag{5.25}$$

where $N(p,t)$ as introduced previously is the volume-integrated intensity of CRs, $b(p)$ is the momentum loss rate of CRs, and $\tau_D \simeq r_0^2/6D$ (with $D = D(p)$ is the diffusion coefficient inside the LB and $r_0 \simeq$ is the radius of the remnant at the end of the Sedov-Taylor phase) is the diffusive escape time. We shall follow Joubaud et al. (2020) to describe the diffusion coefficient as:

$$D(E) = D_B \left(\frac{r_L}{\lambda_{inj}}\right)^{1-b_T}, \tag{5.26}$$

where $D_B = r_L v/3$ is the Bohm diffusion coefficient, r_L is the Larmor radius at energy E, λ_{inj} is the turbulence injection scale, and $b_T = 5/3$ in the case of a Kolmogorov turbulence spectrum. Equation 5.25 describes the evolution of the volume-integrated intensities of CRs inside the acceleration region[1] after the release of CRs at the end of the Sedov-Taylor phase of the SNR at $t_{age} - t_{PDS}$ years ago. We shall first solve Eq. 5.12 for the volume-integrated intensities in the acceleration region at $t = t_{PDS}$ and, then, apply these solutions as the initial conditions to seek the volume-integrated intensities at $t = t_{age}$ using Eq. 5.25. Notice also that, at the time of CR release $t = t_{PDS}$, the Mach number of the shock at this time should be relatively low (due to the low density and high temperature of the medium inside the LB) and, thus, we have neglected the adiabatic energy loss due to the expansion of the shocked region for $t \geq t_{PDS}$. We shall denote n_{LB} to be the plasma density inside the LB and the solution for the volume integrated intensities for CR protons could be written as:

$$N_p(p,t) = N_{0,p}(p_0)\exp\left\{-\int_{t_{PDS}}^{t_{age}} \mathrm{d}t' \left[\frac{2\nu_p n_{LB}}{p'^3} + \frac{1}{\tau_D(p')}\right]\right\}, \tag{5.27}$$

[1]It might not be appropriate to call this the acceleration region since we are interested in the evolution of the CR intensities inside this region at $t = t_{age}$ long after CRs are released. Please keep in mind that, for $t \geq t_{PDS}$, the *acceleration region* refers to the shell of plasma around the shock front at $t = t_{PDS}$ when the process of acceleration ends.

where $p_0 = q_p(t_{PDS}; p, t)$, $p' = q_p(t'; p, t)$, and the function of the initial momentum $q_p(t_0; p, t)$ is:

$$q_p(t_0; p, t) = \left[p^3 + \nu_p n_{LB}(t - t')\right]^{1/3}. \tag{5.28}$$

Similarly, we have for CR electrons:

$$N_e(p, t) = N_{0,e}(p_0) \exp\left[-\int_{t_{PDS}}^{t_{age}} \mathrm{d}t' \frac{1}{\tau_D(p')}\right], \tag{5.29}$$

where $p_0 = q_e(t_{PDS}; p, t)$, $p' = q_e(t'; p, t)$, and the function of the initial momentum $q_e(t_0; p, t)$ is:

$$q_p(t_0; p, t) = p + \nu_e n_{LB}(t - t'). \tag{5.30}$$

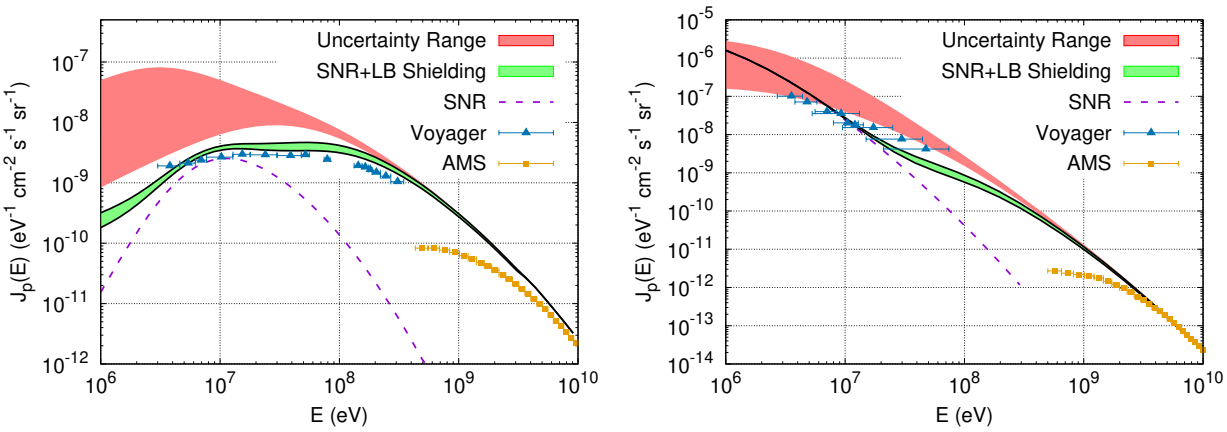

FIGURE 5.5: Intensities of CRs after transported through the shell of the LB into its interior together with the one from the local SNR fitted with the data from Voyager 1 (Cummings et al., 2016) and AMS 02 (Aguilar et al., 2014; Aguilar et al., 2015). The left and right panels are respectively the results for CR protons and electrons. The shaded red regions correspond to the stochastic fluctuations presented in the previous chapter, the purple dashed lines are the intensities from the local SNR, and the combined intensities are presented as the green shaded regions.

It should be noticed that the momentum loss rate in this case is simply due to Coulomb interactions since we are modeling CRs within the LB. This means that:

$$\nu_p = 2.73 \times 10^{11}\ (\mathrm{eV/c})^3\ \mathrm{s}^{-1}\ \mathrm{cm}^{-3}, \tag{5.31}$$
$$\nu_e = 5.68 \times 10^{-7}\ (\mathrm{eV/c})\ \mathrm{s}^{-1}\ \mathrm{cm}^{-3}. \tag{5.32}$$

We note also that the function $N_{0,p}(p_0)$ and $N_{0,e}(p_0)$ are the volume integrated intensities calculated at the end of the Sedov-Taylor phase when CRs are released from Eq. 5.19 and Eq. 5.21 respectively for $t = t_{PDS} \simeq 2.4 \times 10^5$ yr. Here, the

end of the Sedov-Taylor phase for the SNR has to be evaluated using the density of hydrogen atoms and the temperature of the plasma characterizing the ISM inside the LB. The widely accepted values for these parameters are $n_{LB} \simeq 0.005$ cm^{-3} and $T_{ISM} \simeq 10^6$ K (see e.g. Welsh & Shelton, 2009). For the fit of the Voyager spectra, we keep $T_{ISM} = 10^6$ K and set $n_{LB} = 0.02$ cm^{-3}. It should be noticed, however, that the spectra of CRs from the local SNR are very sensitive to the particular value of n_{LB} and the transition between two components of the fit becomes smoother for higher density. Another essential point to be discussed is the density of the acceleration region which, at the end of the Sedov-Taylor phase, should become a shell of plasma with density $n = 4n_{LB}$ and it is not very clear to us how long would it take for this structure to dissipate and merge with the plasma of the ISM inside the LB. We have, therefore, decided to set the density of this region to $n = n_{LB}$ right after the release of CRs. Also, the suppression for the diffusion coefficient in the LB's shell has been chosen to be $\eta = 200$, the acceleration efficiency has been set to be respectively $\xi_{CR} = 5\%$ and 0.5% for CR protons and electrons, the injection scale for turbulence inside the LB adopted for the fit is $\lambda_{inj} \simeq 20$ pc (this value is a bit higher than the one suggested from MHD simulations which is about 10 pc, see e.g. Ntormousi et al., 2017). The results for both CR protons and electrons are shown in Fig. 5.5.

The shaded green regions are the combined intensities of both Galactic CRs and the ones of the local SNR which, for both CR protons and electrons (left and right panels respectively) could provide acceptable fits with the data from Voyager 1 (Cummings et al., 2016) and AMS 02 (Aguilar et al., 2014; Aguilar et al., 2015). We note, however, that the quality of the fits is very sensitive to the plasma density inside the LB and it requires this parameter to be about 4 times higher than the commonly quoted value. This could be due to the compression of the medium by the shock inside the bubble, but more comprehensive studies of the merging phase of the SNR in such an environment are needed for better insight into this problem.

Chapter 6

Cosmic Rays in the Vicinity of the Supernova Remnant W28

Supernova remnants interacting with MCs are ideal laboratories to study the acceleration of particles at astrophysical shocks (Gabici & Montmerle, 2015). The study of such systems is of particular importance in connection with the problem of the origin of Galactic Cosmic Rays (CRs). This is because CRs are believed to be accelerated at SNR shocks, and injected into the ISM with an energy spectrum which is a power law in momentum over a very broad range of particle energies (see e.g. Drury & Strong, 2017; Gabici et al., 2019).

The SNR W28 is a middle-aged remnant (estimated age equal to few times 10^4 years) located at a distance of about 2 kpc (Velázquez et al., 2002). It is classified as a mixed-morphology SNR with center-filled thermal X-ray emission and shell-like radio morphology (Rho & Borkowski, 2002; Dubner et al., 2000). Also, observations in CO(1-0) have revealed molecular gas within the field of W28 (Dame et al., 2001), concentrated in a number of massive MCs (Aharonian et al., 2008). Most importantly the detection of 1750 OH maser from the MC located on the northeastern side of the SNR suggests that this cloud is interacting with the blast wave of the remnant (Claussen et al., 1997). The W28 SNR/MC system has been observed at all wavelengths, including radio (see Dubner et al., 2000, and references therein), millimeter (Vaupré et al., 2014), X-rays (see Zhou et al., 2014, and references therein),and high-energy and very-high-energy gamma rays (Aharonian et al., 2008; Abdo et al., 2010a). This makes it an ideal target for studies of CR acceleration and escape from SNRs (e.g., Nava & Gabici, 2013, and references therein).

The MCs in the vicinity of W28 are prominent gamma-ray sources (Aharonian et al., 2008; Abdo et al., 2010a). The origin of this emission is due to interactions of GeV and TeV CR protons that were accelerated in the past at the SNR shock and that now fill a vast region surrounding the remnant (e.g., Gabici et al., 2010). Remarkably, measurements performed in the millimeter domain revealed an enhanced ionization rate from the northeastern MC (Vaupré et al., 2014). The ionization of the MC could be due either to the interactions of CRs (either protons or electrons) with the molecular gas, or to the presence of X-rays coming from the SNR shock-heated gas. X-rays have been proposed as a possible source of ionization in the vicinity of a number of SNRs (Schuppan et al., 2014).

As we will see in the following, X-rays are, in this case, not a viable explanation for the enhanced ionization, and therefore CRs are left as the only possible ionizing agents present inside the cloud. This fact opens up the possibility to combine high- and low-energy observations of the SNR/MC system (gamma rays and millimeter waves, respectively), and constrain the spectrum of CRs present in the region over an interval of particle energies of unprecedented breadth: from the MeV to the TeV domain. We show that data are best explained if an enhanced flux of CR protons is present, and if such protons are characterized by energies spanning from $\lesssim 100$ MeV up to tens of TeV.

This chapter is organized as follows: in Section 6.1 we summarize the multi-wavelength observations of the W28 SNR/MC system, in Section 6.2 we compute the photoionization rate induced in the MC by X-ray photons. The role of CRs in ionizing the gas is investigated in Section 6.3, where constraints on the CR proton and electron spectra are also obtained. We discuss and summarize our results in Section 6.4.

6.1 Multi-Wavelength Observations of the W28 Region

In this section we review the status of the multi-wavelength observations of the W28 and its surroundings. The purple (dot-dot-dashed) circle in Fig. 6.1 indicates the approximate contours of the SNR shell as traced by its radio emission (Dubner et al., 2000; Brogan et al., 2006). Observations in the CO molecular line revealed the presence of a number of dense ($\approx 10^3$ cm^{-3}) and massive ($\approx 10^5 M_\odot$) MCs in the region (Matsunaga et al., 2001; Aharonian et al., 2008). Remarkably, the H.E.S.S. collaboration reported the detection of very-high-energy gamma-ray emission from the vicinity of W28, which correlates spatially very well with the position of the MCs (Aharonian et al., 2008). The blue contours in Fig. 6.1 show the 4σ significance excess in TeV gamma rays. The spatial correlation points towards a hadronic origin of the gamma-ray emission, which results from the interactions of CR nuclei with the dense gas that forms the MCs. Gamma-ray data are best explained by assuming that CR protons were accelerated in the past at the SNR when the shock speed was larger than the present one. Such particles then escaped the system, and now fill a large volume which encompasses all the gamma-ray-bright MCs (Fujita et al., 2009; Gabici et al., 2010; Li & Chen, 2010; Ohira et al., 2011; Nava & Gabici, 2013).

The detection of OH maser emission from the northeastern MC indicates that the SNR shock is currently interacting with that cloud (Claussen et al., 1997; Hewitt et al., 2008). The other TeV-bright MCs are located in the south, outside of the SNR radio boundary and therefore have not yet been reached by the shock. In the following, we focus mainly on the interaction region, and for this reason we also show, as a dashed red circle, the position and extension of the *Fermi*-LAT source associated to the northeastern cloud (Abdo et al., 2010a; Cui et al., 2018).

The presence of the gamma-ray emission from the MCs reveals an overdensity of CRs with respect to the Galactic background, both in the GeV and TeV energy

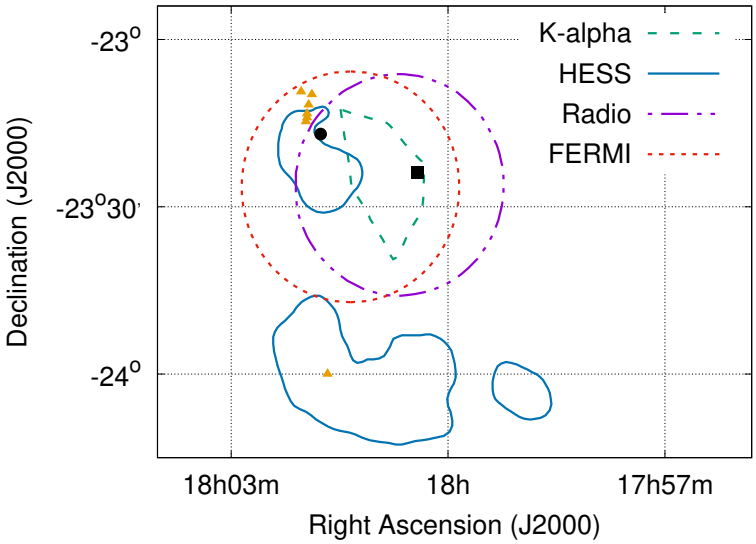

FIGURE 6.1: Contour map for the W28 region. The approximate radio boundary of the SNR shell is shown as a purple dot-dot-dashed circle. The solid blue contours represent the 4σ significance excess TeV emission observed by H.E.S.S. (Aharonian et al., 2008). The short-dashed red circle is the best-fit disk size for the *Fermi*-LAT GeV source associated to the northeastern MC (Cui et al., 2018). The enhanced region of Fe slowromancapi@ Kα line emission is the area enclosed by the dashed green line (Nobukawa et al., 2018). The CR ionization rate has been measured from IRAM observations in the directions indicated by the yellow triangles (Vaupré et al., 2014). The filled black circle and square indicate the centroids of the X-ray emission for the northeast and central X-ray sources, respectively (Rho & Borkowski, 2002).

domain. In addition to that, observations of millimeter lines performed with the IRAM 30m telescope (orange triangles in the figure) allow us to infer that an excess in the gas ionization rate is also present at the position of the SNR/MC interaction, but not at the position of the southern MC complex (Vaupré et al. (2014), see also Chapter 2 for more details on how the ionization rate is derived). Such enhanced ionization rate could be interpreted as an excess of CRs (either protons or electrons) of low energy ($\approx$ MeV energy domain). However, the SNR is a powerful thermal X-ray source (Rho & Borkowski, 2002; Zhou et al., 2014), and the X-ray photons might also penetrate the cloud and be responsible for the enhanced ionization rate, as was proposed for other SNR/MC systems (Schuppan et al., 2014). The spatial morphology of the X-ray emission is quite extended, and can be roughly described as the sum of two extended sources, whose centroids are shown in Fig. 6.1 as a filled black square (central source, C) and circle (northeastern source, NE). Determining whether the enhanced ionization rate is due to CR protons, electrons, or X-ray photons is one of the goals of this chapter (see Sect. 6.2).

Finally, additional constraints on the origin of the enhanced ionization rate can be obtained from hard X-ray observations of W28 performed by *Suzaku* (Nobukawa et al., 2018). These observations revealed the presence of the Fe I Kα line in the X-ray spectrum. This line could be produced by interactions between low-energy

TABLE 6.1: Fit parameters of the *vnei* model for the X-ray sources adopted from Zhou et al., 2014

Objects	NE	C
kT_c (keV)	0.33	0.60
τ_c (10^{11} cm^{-3}s)	6.00	2.35
[1,2]Abun	0.26	0.12
Si	0.40	0.16
S	0.88	0.39
Fe	0.22	0.10
[3]ϕ_s (10^{-11} erg cm^{-2} s^{-1})	6.61	10.43

1. All the abundances are relative to solar ones (see Sec. 6.2 for more explanations).

2. Abundances of C, N, O, Ne, Mg, Ar, Ca, and Ni.

3. Unabsorbed fluxes in the 0.3–5.0 keV band.

(MeV domain) CRs and cold gas, and it is therefore tempting to propose a common origin for the line emission and the excess in the ionization rate measured in the northeastern MC. Puzzlingly, Fe I Kα line emission has been detected from a region (green dashed contour in Fig. 6.1) close to but not coincident with the position of the gamma-ray bright northeastern MC.

6.2 Photoionization

Based on XMM-Newton observations, Zhou et al. (2014) claimed that the X-ray emission from the SNR W28 is predominantly thermal, with a possible subdominant nonthermal contribution from source NE, and an indication for the presence of a multi-temperature gas for source C (see also Rho & Borkowski 2002).

In order to estimate the level of photoionization induced by the SNR X-ray emission in the northeastern MC, we make use of the spectral fits to XMM data obtained by Zhou et al. (2014). For simplicity, we consider single-temperature nonequilibrium ionization models where the abundances, ionization timescale, and plasma temperature are allowed to vary to fit the X-ray emission of both the NE and C source (*vnei* models in XSPEC[1]). We refer the interested reader to Vink, 2012 for a more detailed discussion of these plasma models. The best-fit parameters are provided in Table 6.1, where the abundances are defined as the ratio between the abundances of the sources and the abundances in the Solar System. Even though more sophisticated models obtained by adding a power law or a hot component with higher temperature to the spectrum of the NE and C sources could improve the spectral fits (see some of the proposed models by Zhou et al., 2014), this has very little effect in our estimate of the photoionization rate.

The intensity of the X-ray radiation inside the northeastern MC has been computed by assuming that the X-ray sources NE and C are point-like and located at

[1] `https://heasarc.gsfc.nasa.gov/xanadu/xspec/`

the position of the two centroids of the X-ray emission (filled black circle and square in Fig. 6.1). The contribution to the density of X-ray photons at a given location **r** away from the source can be computed as:

$$n_{ph}(E,\mathbf{r}) = \frac{F(E)D_s^2}{cr^2}\exp\left[-\frac{n(\mathrm{H_2})\sigma_{abs}(E)}{f_{\mathrm{H_2}}}d(r)\right], \tag{6.1}$$

where $F(E)$ is the X-ray source's unabsorbed differential photon flux, $D_s \sim 2$ kpc is the distance from the source to Earth, c is the speed of light, $n(\mathrm{H_2})$ is the density of $\mathrm{H_2}$ molecules in the absorbing medium (which in this case is the MC), $f_{\mathrm{H_2}} = n(\mathrm{H_2})/(2n(\mathrm{H_2}) + n(\mathrm{H}))$ is the fractional density of $\mathrm{H_2}$ molecules relative to the total number of H atom, $\sigma_{abs}(E)$ is the photoelectric absorption cross-section per H atom, and $d(r)$ is the distance travelled inside of the cloud by the X-ray photons that reached a distance r from the source (see Fig. 6.2). For MCs, it is appropriate to set $f_{\mathrm{H_2}} \sim 0.5$ (see e.g. Vaupré et al., 2014), and we further assume solar abundances to describe the gas in the MC. This latter assumption allows us to use the absorption cross-section $\sigma_{abs}(E)$ taken from Morrison & McCammon (1983). In fact, the exact value adopted for the element abundances in the MC might have some impact: changing from the solar abundances to the ones of the NE source as reported in Table 6.1 (~ 0.3 times the solar abundances for most elements) would increase the estimate of the photoionization rate by a factor of approximately three (see Fig. 6.3).

With Eq. 6.1 at hand, the photoionization rate ξ_{ph} induced by X-ray photons inside the cloud can be obtained following the approach presented in Maloney et al. (1996). Due to the relatively low temperatures of the emitting plasmas (< 1 keV), the contribution from Compton scattering to the photoionization rate can be safely neglected. Moreover, most of the ionization in the MC will be induced by secondary electrons generated as a result of the X-ray photoionization, meaning that we can write:

$$\xi_{ph}(\mathbf{r}) = 2f_{\mathrm{H_2}}\sum_s \int_I^{E_{max}} \sigma_{abs}(E)cn_{ph}^s(E,\mathbf{r})M_{sec}(E)\,\mathrm{d}E, \tag{6.2}$$

where the sum indicates that both X-ray sources (s = NE and C) are considered. Here, $I \approx 15.4$ eV is the ionization potential of $\mathrm{H_2}$, and $M_{sec}(E) = (E-I)/W$ is the mean multiplicity for ionization by a secondary electron in a H_2 gas, with $W \sim 40$ eV (see Dalgarno et al., 1999; Dogiel et al., 2013).

Before proceeding, a discussion of the geometry of the problem is in order (see Fig. 6.2). We model the X-ray emission from the SNR as two point sources located at the position of the centroids of the emission (Rho & Borkowski, 2002). The ionization rate in the northeastern MC has been measured along several lines of sight (yellow triangles in Fig. 6.1, Vaupré et al. 2014). To maximise the effect of photoionization, we have chosen to study the line of sight which is the closest to the centroids of the X-ray emission, which has been labeled by Vaupré et al., 2014 as J1801-N1. This line of sight is also the one characterized by the smaller measured value of the density of $\mathrm{H_2}$, which is equal to $n(\mathrm{H_2}) \simeq 600$ cm^{-3} (Vaupré et al., 2014). In the following, we assume that this density characterizes the entire cloud. This

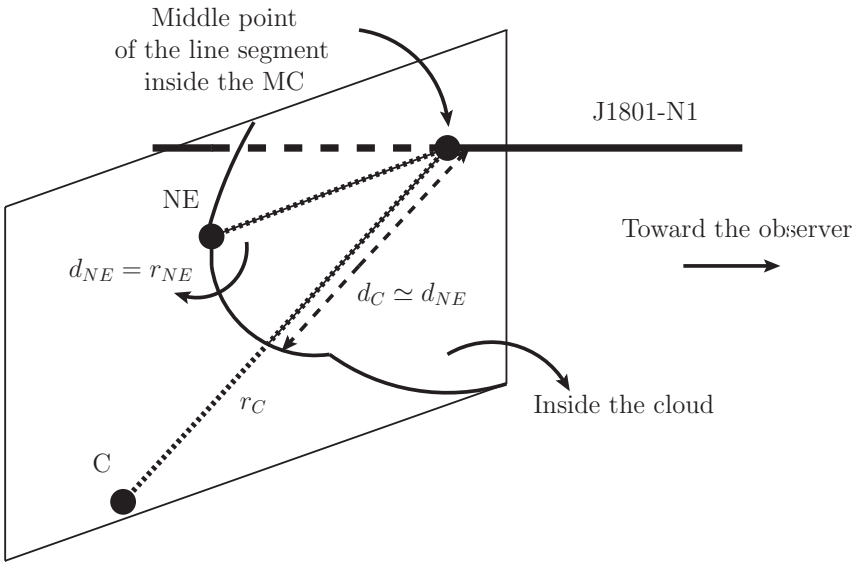

FIGURE 6.2: Adopted geometry for the calculation of photoionization. The centroids of the X-ray emission are indicated by the points labeled NE and C, and the line of sight labeled J1801-N1 is the IRAM pointing closest to the X-ray sources.

TABLE 6.2: Coordinates and relative distances of the two X-ray sources and of the line of sight J1801-N1.

Objects	α (hms)	δ ($'''$)	d_{NE} (pc)	d_C (pc)
NE source	18 01 45.7	-23 16 58.3	–	–
C source	18 00 25.5	-23 23 47.2	–	–
J1801-N1	18 01 58.0	-23 14 44.0	2.10	13.43

is of course not true, given that larger values of this quantity have been estimated by Vaupré et al. (2014) for all the lines of sight other than J1801-N1, but such an assumption will provide us with the most optimistic (larger) estimate of the photoionization rate in the cloud. We further assume that the two X-ray sources lay on a plane orthogonal to the line of sight J1801-N1, and that the northeastern MC is spatially symmetric with respect to that plane. The coordinates of the two X-ray sources and of the line of sight J1801-N1 are listed in Table 6.2 together with their relative distances.

Adopting the geometry presented in Fig. 6.2, we can now estimate the X-ray photo-ionization rate as a function of the gas column density along the line of sight $N(\mathrm{H_2})$. Figure 6.3 shows the differential photo-ionization rate averaged along the line of sight for different values of the column densities along the line of sight: $N(\mathrm{H_2}) = 10^{21}$, 10^{22}, 10^{23} cm^{-2}, respectively. For typical values in the range $N(\mathrm{H_2}) \approx 10^{21}$ - 10^{23} cm^{-2}, the left panel of Fig. 6.3 shows that the contribution to ionization comes mainly from X-ray photons with energy in the range from $\lesssim 1$ keV to a few keV.

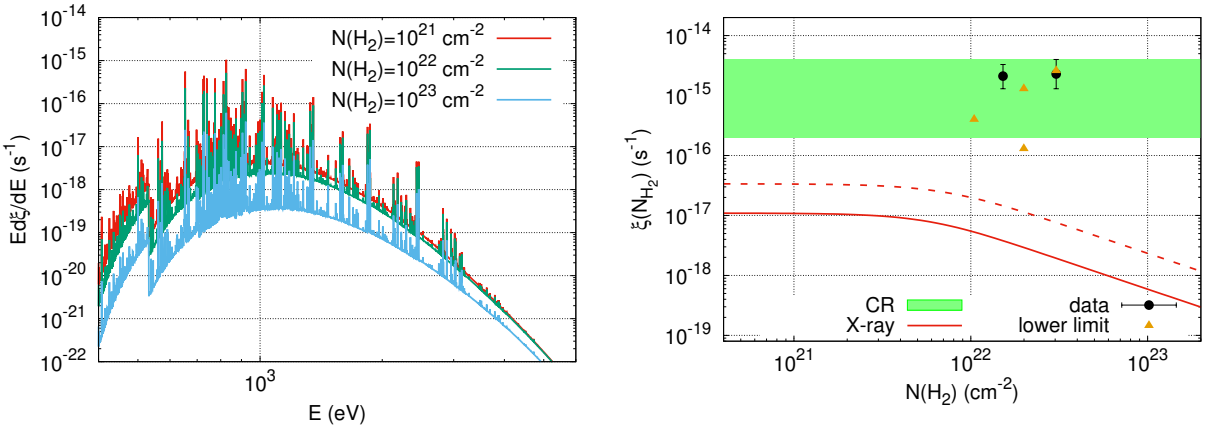

FIGURE 6.3: *Left*: Average differential ionization rate for different assumed gas column densities along the line of sight N1 and solar abundance. *Right*: Predictions for the photoionization rate are shown by the solid and dashed red lines (for the cloud with solar abundances and the abundances of the NE source, respectively). Observational data taken from Vaupré et al., 2014 are presented as filled circles (measurements) and filled triangles (lower limits). The shaded region indicates a reference range of values of the ionization rate which has been used to constrain the CR spectrum (see text).

The right panel of Fig. 6.3 shows the expected photo-ionization rates as a function of the gas column density for a cloud of solar (solid red curve) and 0.3 times solar metallicity (dashed red curve). These predictions can be compared with the measurements of the ionization rate in the northeastern cloud (data points and lower limits in the figure). One can clearly see that the contribution from X-rays to the observed ionization rate is negligible even in the most optimistic scenario considered here. Therefore, the ionization rate must be due to CRs, either protons (or nuclei) or electrons. We consider this scenario in the following Section.

6.3 Cosmic-Ray Induced Ionization

The gamma-ray emission detected from the MCs in the vicinity of the SNR W28 is interpreted as the result of hadronic interactions between CR nuclei (mostly protons) accelerated in the past at the SNR shock. These particles escaped the remnant and now fill a vast region that encompasses the clouds. The gamma-ray emission results from the decay of neutral pions produced in inelastic proton–proton interactions. The energy threshold to produce pions at rest is $T_p^{th} \sim 280$ MeV. Therefore, gamma-ray observations can be used, generally, to determine the shape of the spectrum of CR protons of kinetic energy exceeding T_p^{th} contained in the MCs.

It is definitely less straightforward to infer the energy spectrum of the CR electrons contained within the cloud. The SNR W28 is a bright synchrotron radio source (Dubner et al., 2000), and this indicates the presence of relativistic electrons and magnetic field in the region. Even though the morphology of the radio emission does not correlate with that of molecular clouds, the brightest region in radio roughly coincides with the position of the northeastern cloud.

In the following, we investigate the possibility that either CR protons or electrons are the responsible for the enhanced ionization rate measured from the northeastern cloud. The H_2 ionization rate induced by proton and electron CRs could be obtained using Eq. 2.24 and Eq. 2.25 as introduced in Chapter 2 (see also Padovani et al., 2009; Phan et al., 2018; Recchia et al., 2019).

6.3.1 Cosmic-Ray Protons and Nuclei

Let us assume that the spectrum of CR protons in the cloud can be described as a power law in momentum $\propto p^{-(\delta_p+2)}$ as expected if protons are accelerated at the SNR shock via a first-order Fermi mechanism. In terms of the particle kinetic energy T_p, this writes:

$$n_p(T_p) = A_p \left(T_p + m_p c^2\right) \left[T_p^2 + 2T_p m_p c^2\right]^{-\frac{\delta_p+1}{2}} , \tag{6.3}$$

where all energies are in GeV and A_p is a normalization factor. Both A_p and the spectral index δ_p can be obtained by fitting the gamma-ray data.

Assuming that the observed gamma rays are produced by proton–proton interactions, the expected gamma-ray flux measured at Earth would be:

$$\phi(E_\gamma) \;=\; \frac{M_{cl}}{4\pi D_s^2 m_{avg}} \int_{T_p^{min}}^{T_p^{\max}} 4\pi j_p(T_p) \varepsilon(T_p) \frac{\mathrm{d}\sigma_{pp}(T_p, E_\gamma)}{\mathrm{d}E_\gamma} \,\mathrm{d}T_p, \tag{6.4}$$

where $j_p(T_p) = (v/4\pi) n_p(T_p)$ is the CR proton intensity as a function of the particle kinetic energy T_p (v is the particle velocity). Moreover, M_{cl} is the mass of the whole cloud ($\sim 5 \times 10^4 M_\odot$, see Aharonian et al. 2008), m_{avg} is the average atomic mass of the gas from the MC (with solar abundance $m_{avg} \simeq 1.4 m_p$), $T_p^{\max}$ is the maximum kinetic energy of the accelerated particle (its exact value is irrelevant, as long as $\gg 100$ TeV), and T_p^{min} is the threshold energy for π^0 production in proton–proton interactions. Also, $\mathrm{d}\sigma_{pp}(T_p, E_\gamma)/\,\mathrm{d}E_\gamma$ is the differential cross-section for gamma-ray production and $\varepsilon(T_p)$ is the nuclear enhancement factor to take into account gamma-ray production from nucleus–nucleus interaction (both taken from Kafexhiu et al., 2014). A fit to the gamma-ray data is shown in Fig. 6.4 (left panel), where data points are from Aharonian et al. (2008) and Abdo et al. (2010a). The values obtained for A_p and δ_p are reported in the first row of Table 6.3. Of course, the CRs responsible for the gamma ray emission are characterized by particle energies in the GeV and TeV domains, and therefore their contribution to the ionization rate is negligible (e.g., Padovani et al., 2009; Phan et al., 2018).

In order to estimate the possible contribution from CR protons to the measured ionization rate in the cloud, we extrapolate the power law spectrum obtained after fitting the gamma-ray data down to the MeV energy domain. In other words, we assume a spectrum as in Eq. 6.3 down to an arbitrary particle kinetic energy T_c. We then compute the ionization rate due to CR protons using Eq. 2.24 and multiply by a factor $\eta = 1.5$ to take into account the contribution from CR nuclei (Padovani et al., 2009). This allows us to constrain the value of T_c so that the ionization rate

falls in the range indicated by the green shaded region in Fig. 6.3. The range of values $T_c^{min} < T_c < T_c^{max}$ obtained in this way are reported in Table 6.3.

There are several reasons to envisage a change in the CR proton spectrum at certain particle energies T_c. Let us first consider the scenario where the region of enhanced ionization is upstream of the shock and the ionizing CRs have already escaped the remnant. In this case, the range of possible numerical values of T_c can be estimated as follows.

1. Cosmic-ray protons have been produced at the SNR shock τ_{inj} years ago, and since then they have suffered energy losses (mainly ionization losses) in the dense gas, over a characteristic time $\tau_{ion}(T_p)$, which is proportional to the gas density and an increasing function of particle energy (see Fig. 2 in Phan et al. 2018). In fact, energy losses can be effective only for particles characterized by an energy smaller than T_c, defined as $\tau_{ion}(T_c) = \tau_{inj}$, because particles of higher energy simply do not have time to cool. The maximum possible value for τ_{inj} is of course the age of the SNR $\tau_{age} \approx 4 \times 10^4$ yr (Gabici et al., 2010), which provides an upper limit for T_c. For a typical gas density of $n_{\rm H_2} \sim 10^3$ cm^{-3} this gives $T_c \lesssim 4 \times 10^2$MeV, which is quite close to the value of T_c^{max} in Table 6.3.

2. Cosmic-ray protons have to penetrate deep into the cloud in order to ionize the gas there. If we define τ_p as the time it takes them to reach the center of the cloud moving a distance L away from the position of the shock, we can estimate T_c by imposing $\tau_{ion} = \tau_p$. The shortest possible penetration time τ_p is obtained after assuming that CR protons move along straight lines at a velocity $v \sim \sqrt{2T_c/m_p}$. If we assume that CR protons have to cross a gas column density of $\sim 3 \times 10^{22} (n_{\rm H_2}/10^3 \text{ cm}^{-3})(L/10 \text{ pc})$ cm^{-2} we get $T_c \gtrsim 7$ MeV, which is a factor of a few smaller than T_c^{min} in Table 6.3.

It should be noted that, in this scenario, the range of possible values for T_c obtained by means of the phenomenological consideration made above overlaps very well with the range of values obtained observationally (Table 6.3), that is, by fitting the millimeter and gamma-ray data simultaneously.

Another possible scenario is that the SNR shock has overrun the region of enhanced ionization, engulfing it with low-energy CRs which are still inside the shell in the downstream region. This is similar to the case of the region of enhanced ionization W51C-E which has been shown to be in the downstream region of the SNR W51C (see Dumas et al. 2014 for more detailed discussion). If this is true then we may expect a hardening in the low-energy part of the spectrum below T_c due to the difference in spectral features of the escaped CRs at high energy and the still confined CRs at low energy. However, our understanding of the escape of CRs from SNR shocks is still quite poor, making an accurate estimate of the numerical value of T_c problematic.

There exists also the possibility to have spectral breaks due to nonlinear effects of CR transport. This situation is similar to the case of isolated clouds investigated in Dogiel et al. (2018) (see also Ivlev et al., 2018) where low-energy CRs are depleted

TABLE 6.3: Fit parameters for the CR proton spectrum and upper limit for the CR electron spectrum.

Species	$A_{p,e}$ (eV^{-1} cm^{-3})	$\delta_{p,e}$	$T_c^{\mathrm{min}} - T_c^{\mathrm{max}}$ (MeV)
Proton	3.15×10^{-17}	2.76	$26 - 320$
Electron	$\ll 6.4 \times 10^{-19}$	2.7	$\ll 20 - 130$

from the interior of clouds by self-excited MHD turbulence generated by streaming instability.

Independently of the scenario, the important point that needs to be stressed is that gamma-ray observations allow us to constrain the spectrum of CR protons for particle energies above ≈ 1 GeV. Therefore, the explanation of the enhanced ionization rate requires extrapolation of the proton spectrum only by a factor of $\approx 3 - 30$ down to lower particle energies.

It follows that the presence of an excess of CR protons characterized by a relatively steep power-law spectrum ($\delta_p \approx 2.8$) extending from the MeV to multi-TeV domain can explain very naturally both the bright gamma-ray emission from the northeastern cloud and the observed enhancement in the ionization rate.

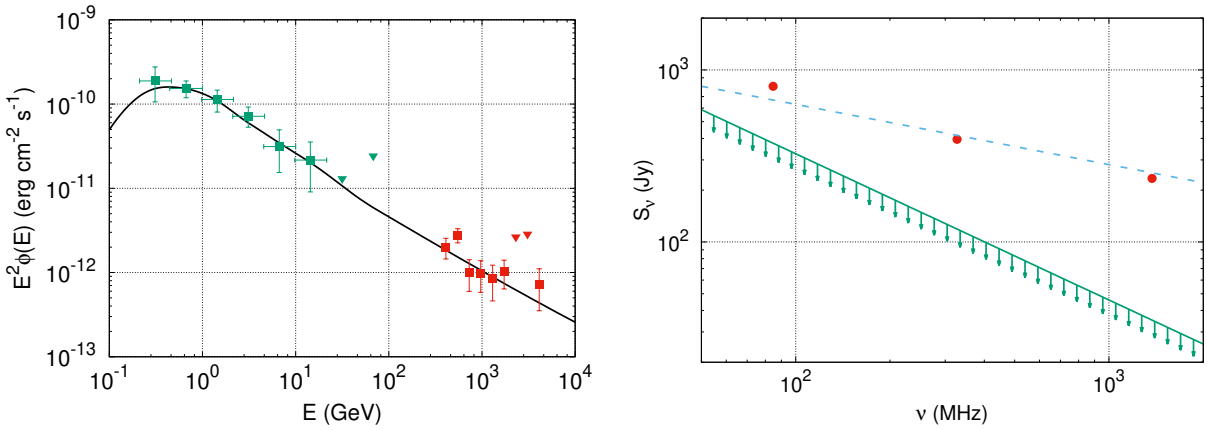

FIGURE 6.4: *Left*: Gamma-ray differential energy spectrum of the northeastern MC (J1801-233). *Fermi*-LAT and HESS data have been fitted with a hadronic model see Aharonian et al., 2008; Abdo et al., 2010a, for references. *Right*: Synchrotron emission spectrum observed from the entire SNR (Kovalenko et al., 1994; Dubner et al., 2000). A fit to data is shown as a dashed line. The maximum contribution from the northeastern cloud is also shown (see text for details).

6.3.2 Cosmic-Ray Electrons

As stated above, the decay of neutral pions produced in inelastic interactions between CR protons (and nuclei) and the dense gas in the cloud provides the most natural explanation for the gamma-ray emission observed in the GeV and TeV energy domain (see e.g. Aharonian et al., 2008; Nava & Gabici, 2013). Leptonic models

where the emission is due to nonthermal Bremsstrahlung have been shown to be problematic, as they require the SNR to accelerate the same number of nuclei and electrons, and only provide a good fit to gamma-ray data if unrealistic values of the local magnetic field strength and gas density are assumed (Abdo et al., 2010a).

This implies that the nonthermal Bremsstrahlung emission from CR electrons must provide a subdominant contribution to the observed gamma-ray emission. If $n_e(E_e) = A_e(E_e/\mathrm{GeV})^{-\delta_e}$ is the density of relativistic electrons of energy E_e inside the cloud, the expected Bremsstrahlung emission can be roughly estimated as:

$$E_\gamma^2 L_B(E_\gamma \sim E_e) \sim \frac{E_e^2 n_e(E_e) V_{cl}}{\tau_B}, \tag{6.5}$$

where

$$\tau_B \sim 4 \times 10^7 \left(\frac{n_H}{\mathrm{cm}^{-3}}\right)^{-1} \ \mathrm{yr} \tag{6.6}$$

is the energy loss time due to Bremsstrahlung in a gas characterized by an atomic hydrogen density n_H (Aharonian, 2004) and V_{cl} is the volume of the cloud.

By imposing that the Bremsstrahlung flux $E_\gamma^2 L_B/(4\pi D_s^2)$ should be significantly smaller than the observed one $E_\gamma^2 \phi(E_\gamma)$ we get:

$$E_e^2 n_e(E_e) \ll 4\pi D_s^2 \left(\frac{\tau_B}{n_H}\right) E_\gamma^2 \phi(E_\gamma) m_p M_{cl}^{-1}, \tag{6.7}$$

where we introduced the source distance D_s and the cloud mass $M_{cl} = m_p n_H V_{cl}$. At a photon energy equal to $E_\gamma = 1$ GeV the observed gamma-ray flux is roughly $E_\gamma^2 \phi(E_\gamma) \approx 10^{-10}$ erg/cm^2/s, and above such energy the spectrum can be described by a power law $E_\gamma^{-\alpha}$ with $\alpha \sim 2.7$ (Abdo et al., 2010a; Aharonian et al., 2008). This gives:

$$E_e^2 n_e(E_e) \ll 10^{-12} \left(\frac{E_e}{\mathrm{GeV}}\right)^{-0.7} \ \mathrm{erg/cm}^3, \tag{6.8}$$

which corresponds to $A_e \ll 6.4 \times 10^{-19}$ eV^{-1} cm^{-3}.

We note that the ratio between the intensity of CR protons and electrons inside the cloud is $A_p/A_e \gg 50$ for particle energies of the order of 1 GeV, and varies very little for larger particle energies (because $\delta_p \sim \delta_e$).

The constraints obtained above on the electron spectrum in the cloud can be used to estimate the contribution given by such electrons to the observed radio emission from the SNR. Radio observations of W28 have been performed in a frequency range spanning from $\lesssim 100$ MHz to several gigahertz. The radio spectrum is shown in the right panel of Fig. 6.4: the flux at 1.4 GHz is $S_{1.4} \sim 246$ Jy, and the radio spectrum can be described by a power law $S_\nu \propto \nu^{-\alpha}$ with $\alpha \sim 0.35$ (Dubner et al., 2000). Even though the radio emission is observed from a region which is spatially more extended than the northern cloud, the radio brightness roughly peaks at that position. Therefore, it is natural to ask whether a contribution to the radio emission might come from relativistic electrons located inside the cloud.

Electrons of energy E emit synchrotron photons of frequency (Aharonian, 2004):

$$\nu_s \sim \nu_c/3 = \frac{\Omega_L}{2}\left(\frac{E_e}{m_e c^2}\right)^2 \sim 0.2\left(\frac{B}{40\ \mu\mathrm{G}}\right)\left(\frac{E_e}{\mathrm{GeV}}\right)^2 \mathrm{GHz}, \tag{6.9}$$

where ν_c is the critical synchrotron frequency, Ω_L the nonrelativistic Larmor frequency, and $m_e c^2$ the electron rest mass energy. This implies that the observed radio emission is produced by electrons of energies $0.1 \lesssim (E_e/\mathrm{GeV})(B/40\ \mu\mathrm{G})^{1/2} \lesssim 10$. Electrons of such energies emit Bremsstrahlung in the energy domain of the Fermi Gamma-Ray Telescope.

The value of the magnetic field in cloud B has been normalized to what is expected from the observational relationship $B \approx 10(n/100\ \mathrm{cm}^{-3})^{0.5}\mu\mathrm{G}$ between the cloud magnetic field and the density of the gas (Crutcher et al., 2010). For the northeastern cloud, Aharonian et al. (2008) estimated a gas density equal to $n \sim 1.4 \times 10^3\ \mathrm{cm}^{-3}$, which would give $B \sim 37\mu\mathrm{G}$.

The upper limit on the CR electron spectrum obtained above (Eq. 6.8) can now be used to estimate the maximum contribution to the observed synchrotron emission coming from the northeastern cloud. This is shown in the right panel of Fig. 6.4. The contribution is subdominant at all frequencies. This implies that the radio emission is largely produced by electrons located outside the cloud.

Therefore, it is not at all straightforward to estimate the possible contribution of CR electrons to the ionization rate in the cloud. Even though we do not know the spectral slope δ_e and normalization A_e of the CR electrons inside the MC, we have obtained an upper limit for the latter value from gamma-ray observations (see Table 6.3) which applies to electrons of particle energy above $E_e^{min} \approx E_\gamma^{min} \approx 0.2$ GeV. Electrons of energy larger than E_e^{min} and characterized by an intensity well below the upper limit reported in Eq. 6.8 would produce an ionization rate of the order of $\ll 1.4 \times 10^{-16}\ \mathrm{s}^{-1}$ (the upper limit for the electron-induced ionization rate is calculated using Eq. 2.25). Therefore, as one can easily see from Fig. 6.3, electrons of energy exceeding E_e^{min} cannot explain the observed ionization rate in the cloud.

An extrapolation of the upper limit electron spectrum to much lower particle energies might possibly result in a value of the ionization rate comparable with observations. Using again the upper limit for A_e, together with a spectral index of $\delta_e \simeq 2.7$, which is quite steep and therefore maximizes the impact of electrons, we find that values of T_c well below 20–130 MeV are needed in order to match the observed ionization rate (see Table 6.3). However, the validity of such an extrapolation is questionable since the spectral index for electrons is not as well constrained as that of protons.

Even though we cannot reach a firm conclusion, explaining the excess in the ionization rate with CR protons is very natural (Sect. 6.3.1) and therefore the hadronic scenario remains, in our view, the preferred one.

6.3.3 Constraints from the 6.4 keV Line Emission

Interestingly, the SNR W28 is also observed by *Suzaku* in the Fe slowromancapi@ Kα line emission and quite recently Nobukawa et al., 2018 found that there is an

excess of this emission from the central region of the remnant with intensity $I^{en}_{6.4\mathrm{keV}} = (3.14 \pm 0.43) \times 10^{-8}$ cm^{-2}s^{-1}arcmin^{-2} compared to the background of the Galactic ridge X-ray emission $I^{bg}_{6.4\mathrm{keV}} = (2.33 \pm 0.29) \times 10^{-8}$ cm^{-2}s^{-1}arcmin^{-2}. These latter authors concluded that this excess emission is produced by the interaction of MeV CR prorons from the SNR with the ambient cold gas. However, this explanation seems quite puzzling since it would require a relatively high column density of gas comparable to that of the molecular cloud in the northeastern part of the remnant ($N(\mathrm{H_2}) \simeq 10^{22}$ cm^{-2}). However, the region of enhanced emission as defined in Nobukawa et al., 2018 and the TeV gamma-ray contour by HESS (respectively the area enclosed with the dashed blue line and the green contour in Fig. 6.1) do not overlap. It should also be noted that an earlier analysis of *Suzaku* data performed by Okon et al. (2018) found a region of enhanced Fe slowromancapi@ Kα line emission at a different position (centered around the NE source). Since the position of the enhanced emission varies for different analyses, it is difficult to investigate its origin.

Nevertheless, the Fe slowromancapi@ Kα line emission is quite an informative channel for the study of low-energy CRs and could also be used to put some constraints on the CR spectra. In particular, the total flux coming from the excess measured by Nobukawa et al. (2018) can be computed as $F_{ex} = \Delta\vartheta(I^{en}_{6.4\mathrm{keV}} - I^{bg}_{6.4\mathrm{keV}})$ where $\Delta\vartheta \approx 15^2$ arcmin^2 is the extension of the excess region. Such a flux, if produced by CR protons in the northeastern cloud, would have been detected.

The nondetection of the iron line from the northeastern cloud can be used to impose an additional constraint on the parameter T_c introduced in Sect. 6.3.1. The intensity of the Fe slowromancapi@ Kα line emission from the region of the molecular cloud can be calculated as:

$$F_{6.4\mathrm{keV}} = \frac{M_{cl}}{4\pi D_s^2 m_{avg}} \int_{T_c}^{\infty} \mathrm{d}T_i \sigma_{\mathrm{K}\alpha}(T_i) 4\pi J_i(T_i), \tag{6.10}$$

where $\sigma_{\mathrm{K}\alpha}(T_i)$ is the cross section of the Kα line emission (Tatischeff et al., 2012). A lower limit for T_c can be obtained by imposing $F_{6.4\mathrm{keV}} < F_{ex}$. This gives $T_c > 30$ MeV, which is consistent with the range of possible values of T_c reported in Table 6.3.

6.4 Summary for the Case of the Supernova Remnant W28

In this chapter, we derive constraints on the CR proton and electron spectra in the region of the SNR W28. The gamma-ray emission from the MCs in the region demonstrates that an excess of CR protons is present there. The present study focuses on the northeastern cloud, which is interacting with the SNR shock.

Vaupré et al. (2014) tentatively proposed that the excess of CR protons in the region might also explain the enhanced ionization rate observed from the northeastern cloud. However, CR electrons and/or X-ray photons coming from the SNR shock can also contribute to the ionization.

We develop a model for the transport of X-ray photons into the cloud and demonstrate that their contribution to the observed ionization rate is negligible. Moreover, even though we cannot completely rule out CR electrons as the main ionizing agents, we show that the most natural explanation for the enhanced ionization rate is explained in terms of interactions of CR protons.

To explain both the gamma-ray emission from the cloud and the enhanced ionization rate, the spectrum of protons in the cloud must extend to particle energies smaller than those constrained by gamma-ray observations ($\gtrsim$ 1 GeV). However, an extrapolation of the spectrum by an order of magnitude only in particle energy would suffice to explain both high- and low-energy observations. This makes protons the most plausible dominant ionizing agents inside the cloud.

The minimal scenario that would simultaneously explain high- and low-energy data would require the presence of CR protons characterized by a single power-law spectrum of slope $\delta_p \sim 2.8$ extending over a very broad energy range, spanning from $T_c \lesssim 100$ MeV up to several tens of TeV: almost six orders of magnitude in energy. In fact, the presence of a spectral break cannot be ruled out below a particle energy of $\approx$ 1 GeV because the ionization rate depends only on the integral of the CR spectrum over particle energy. The presence of a break would require modification of the value of T_c accordingly in order to correctly reproduce the observed ionization rate, but this would not affect the main conclusion of our study in any significant way.

The work presented in this chapter shows how the combination of high- and low-energy observations of SNR/MC systems can be used as a very powerful tool to gather information on the CR spectrum at specific locations in the Galaxy over an energy range of unprecedented breadth. More studies in this direction are desirable, as they will shed light on the process of CR acceleration and escape from SNR shocks (Gabici & Montmerle, 2015).

Conclusion and Outlook

Summary of Main Results

Cosmic rays are generally believed to be of fundamental importance in driving both the physics and the chemistry of MCs (see e.g., Dalgarno 2006 and Wurster et al. 2018) since they are the most capable agent to ionize the interior of these star-forming regions. Observations in the last twenty years (Caselli et al., 1998; Indriolo & McCall, 2012, see also Padovani et al., 2009; Padovani et al., 2020 for reviews) have suggested that the ionization rate decreases with increasing column density of MCs and it varies from around 10^{-16} s^{-1} for diffuse MCs to 10^{-17} s^{-1} for dense ones. These measurements tentatively suggest that the ionization of MCs is caused as a result of the penetration of ambient CRs into clouds (see Padovani et al., 2009 for discussion). In fact, testing such a hypothesis was quite a daunting task as it requires the knowledge of not only the typical spectrum of low-energy CRs in the Galaxy but also the details of the transport process of CRs into MCs. Remarkably, recent updates on Voyager 1 data at large distances from the Sun (see (Stone et al., 2013; Cummings et al., 2016)) have given us a better insight into the spectra of both proton and electron CRs in the local interstellar medium (ISM) at least down to particle energy of a few MeVs. It seems, however, unclear whether or not such spectra could be regarded as the representative of the Galactic CR spectra (this is an old standing issue, see e.g., Cesarsky, 1975) especially for MeV CRs.

Over the years, several theoretical estimates of the CR-induced ionization rate in MCs have been performed. A well-known result was that presented in Spitzer & Tomasko, 1968, which were done by simply extrapolating to low energies the spectra of CRs observed at high energies, without taking into account the effect of CR propagation into clouds. The predicted value of the CR ionization rate was approximately 10^{-17} s^{-1}, which is now known as the *Spitzer value*. In fact, it is an order of magnitude below the observed data for diffuse clouds, and roughly similar to the value found in dense ones. Later works included also the role of energy losses (mainly ionization) suffered by CRs in dense and neutral environments. This was done, most notably, in Padovani et al. (2009), where CRs were assumed to penetrate MCs by moving along straight lines. For a more realistic description, we have to take into account also the effect of streaming instability which results in particle exclusion due to self-generated turbulence. The study of this effect was first conducted in the pioneering works of Skilling & Strong (1976), Cesarsky & Volk (1978), and Morfill (1982), while recent studies in this direction include Morlino & Gabici (2015), Schlickeiser et al. (2016), Ivlev et al. (2018), Phan et al. (2018), and Silsbee & Ivlev (2019). We have presented in Chapter 3 one of the first comparisons between the theoretical predictions from detailed models of CR transport and the measured

values of the CR ionization rate in MCs, with a focus onto diffuse ones. The main result of this chapter can be summarized as follows: there exists a difference of about 1 to 2 orders of magnitude between the ionization rate in diffuse MCs estimated from the Voyager spectra and the observed data.

Indeed, such a puzzling result calls for further investigations. We have, therefore, dedicated Chapter 4 to two of the suggested solutions mentioned in Chapter 3 which are the carrot and the inhomogeneity of the low energy CR distribution in our Galaxy. Concerning the CR carrot, the main finding is that if such a component of the CR spectrum exists, the power needed to sustain these very low energy particles is comparable or even larger than that required for the observed CR spectrum. It should be noticed that the calculation performed in Chapter 4 has not included the effect of CR penetration into clouds which might boost this power requirement even higher. In other words, it seems that, on an energy basis, the CR carrot is not viable solution to the discrepancy between the predicted and observed ionization rates in MCs. This conclusion encourages further studies of the remaining solutions already mentioned above which includes either the presence of sub-GeV accelerators inside MCs or the prominent inhomogeneity in the distribution of low energy CRs in the Galaxy. The former has been employed to explain the high levels of ionization and the presence of synchrotron emission in protostellar systems in dense MCs where the ambient CRs could not to reach. In fact, it has been suggested by the pioneering works by Padovani et al. (2015) and Padovani et al. (2016) that low energy CRs could be efficiently accelerated at prostellar surfaces and jet shocks. The other solution concerning the inhomogeneous distribution of CRs in our Galaxy has been investigated in Chapter 4. In particular, we have studied the stochastic fluctuations for the intensities of CRs using a homogeneous distribution of SNRs both in space and time and it seems that the corresponding range of the ionization rate could even reach the value of about 10^{-16} s^{-1} which is quite close to the mean value of 3×10^{-16} s^{-1} observed in diffuse MCs. We note, however, that the observed values of the ionization rate could only be fitted with the upper limit of the CR intensities. This might imply that either we must have a much smaller value of the diffusion coefficient at low energy to provide better confinement of low energy CRs around SNRs (for example due to streaming instability) or a different class of sources should be involved, for instance, OB/Wolf-Rayet stars (Casse & Paul, 1982; Voelk & Forman, 1982; Binns et al., 2005) or even solar-type stars (Scherer et al., 2008). In fact, this has been suggested by Scherer et al. (2008) who find that the termination shocks of G, K, and F stars could provide a significant fraction of low energy CRs proton in the energy range from 5 MeV to about 300 MeV.

Chapter 5 has been devoted to explain the origin of the CR intensities measured by Voyager 1. The so-called single-source scenario which suggests that low energy CRs observed in the local ISM comes mostly from the supernova explosion taking place around 2 million years ago has been investigated. We study, in the first part of Chapter 5, the evolution of the CR intensities at low energy in the acceleration region around the SNR shocks to better understand the spectral features for different times of release. The solution of the volume-integrated transport equation of CRs

seems to indicate that, if the acceleration process ends before the end of the Sedov-Taylor phase, the injection spectra could be approximated with simple power laws in momentum. On the other hand, spectral breaks in the low energy part of the spectra might appear for the case where the release of CRs occurs during the radiative phase. We then apply this model to predict the intensities of low energy CRs from the SNR inside the LB at about 2 million years after their release under the assumption that the accelerator stopped being active at around 2 million years ago and CRs started to diffusively escape the acceleration region. The observed data from both Voyager 1 and AMS are then fitted by combining the intensities of Galactic CRs transported into the LB and the ones from the local SNR. This scenario seems to provide acceptable fits for the data at low energy under some assumptions on the diffusion coefficient both inside the LB's shell and its interior, but it requires the plasma density inside the bubble to be 4 times higher than the commonly accepted value of about 0.005 cm^{-3}.

Having discussed mostly the effect of low energy CRs on clouds, we provide in Chapter 6 an example where the argument could be reversed meaning some constraints on the CR proton and electron spectra at low energy could be obtained using the measured values of the ionization rates in MCs. We have, in particular, studied the cloud in the north east region of the SNR W28 where there exists an excess of CR protons at high energy as inferred from the gamma-ray emission in this region. Interestingly, it has been proposed in the analyses by Vaupré et al. (2014) that the surprisingly high value of ionization rate observed from this cloud could also be explained with a population of low energy CRs accelerated from the SNR shock. However, the ionization rate in this cloud could also be induced by CR electrons and/or X-ray photons coming from the SNR shock. Thus, the transport of X-ray photons into the cloud has also been investigated and it has been found that their contribution to the observed ionization rate is negligible. Although it is not clear yet the relative importance of the CR protons and electrons to the ionization of this MC, the hadronic scenario seems to provide the most natural explanation for the enhanced ionization rate. By using a single power-law spectrum of slope $\delta_p \sim 2.8$ to characterize CR protons, an extrapolation of the CR proton spectrum constrained by gamma-ray data of only an order of magnitude in particle energy would suffice provide the justification both the gamma-ray emission from the cloud and the enhanced ionization rate. The minimal scenario that would require the presence of CR protons with a very broad energy range, spanning from $T_c \lesssim 100$ MeV up to several tens of TeV: almost six orders of magnitude in energy. In fact, we could not exclude the possible presence of a spectral break below a particle energy of ≈ 1 GeV because the ionization rate depends only on the integral of the CR spectrum over particle energy. Such a break might modify the value of T_c accordingly in order to correctly reproduce the observed ionization rate, but this would not affect the main conclusion of our study in any significant way. The combined data of high- and low-energy observations of SNR/MC systems has, therefore, allowed us gain more insight into the CR spectrum at specific locations in the Galaxy over an energy range of unprecedented breadth and this should encourage the analyses of few more systems of this type to better understand the capability of SNRs as sources of low

energy CRs (Gabici & Montmerle, 2015).

Future Perspectives

Indeed, there are still several open issues that seem to be essential for a better understanding of both low energy CRs and their impact on the ISM. We shall now present some future perspectives of research in this direction that could help to resolve the discrepancy between the predicted and observed ionization rate:

- *Supernova remnants as sources of low energy CRs:* Within the standard paradigm of Cosmic Ray Physics, Galactic CRs are generally thought to be accelerated at the shocks of SNRs with spectra which are power laws in momentum over a very broad range of particle energies. Observations of enhanced gamma-rays in MCs interacting with SNRs have indicated that this is, indeed, a realistic scenario for CRs of energy above a few GeVs. Recent improvements in the instruments in the submm-mm band have allowed us to detect also enhanced ionization rates in a few MCs interacting with SNR shocks. The combined modelling of these radiative signatures at both high and low energy could clearly be used as a very powerful tool to gather information on the CR spectrum over a broad energy range as illustrated for the cloud in the north-eastern part of the SNR W28 (see Chapter 6.4). This particular case seems to hint the presence of low energy CRs accelerated at SNR shocks. There exists also two more systems of this type namely the SNR/MC associations W51 and IC 443 (Gabici & Montmerle, 2015) where the same analyses could be carried on thanks the availability of multi-wavelength data and this could certainly help us to better understand the capability of SNRs as sources of low energy CRs.

- *Cosmic-ray transport in the vicinity of sources:* Beyond the modelling of the multi-wavelength signals, it should be noticed that the transport of CRs into an MC in the vicinity of a source is still not yet fully understood since most of the theoretical works have focused essentially on isolated MCs where observational data are more abundant. One could expect qualitatively that, during the process of penetration, CRs lose energy mostly due to ionization of hydrogen molecules and also effective proton-proton interaction inside the clouds. Consequently, a gradient in the spatial distribution of CRs is formed and would drive the excitation of Alfvén waves by a mechanism called streaming instability which, in turn, controls the transport of CRs themselves. It is, therefore, straightforward to see the complexity of this highly non-linear phenomenon and determining the penetration efficiency of CRs is quite a daunting task. However, finding the solution to this problem is crucial for a more complete and insightful understanding of systems like MCs in interaction with SNR shocks. Another issue also related to the transport of CRs around their sources is the confinement of these particles due to self-generated turbulence via streaming instability. This has been thoroughly investigated for high energy CRs for both warm ionized and warm neutral media and the results indicate that,

around SNRs, the CR diffusion coefficient could be significantly suppressed in comparison to the typical values inferred from B/C data (Nava et al., 2016; Nava et al., 2019) which seems to be consistent with the interpretation of the diffusion properties constrained from the gamma-ray observations of molecular clouds located in the vicinity of these objects (see e.g. Gabici et al., 2010). It would be interesting to understand whether or not the diffusion coefficient of low-energy CRs could be suppressed in the same way since better confinement of these particles around their sources might result in much higher stochastic fluctuations which may explain the high level of ionization observed in clouds.

- *Contribution of low-energy CRs from stars:* Another essential point to be mentioned is the possibility to study stars as the source of low-energy CRs. Observations of Voyager 1 at the solar wind termination shock have revealed an unexpectedly high flux of anomalous CRs at energy below a few ten MeVs. However, theoretical and simulational works to predict whether or not solar-type stars could provide a significant or even dominant contribution to Galactic CRs at low energy are still not yet fully explored. As mentioned above, the modeling of CR acceleration around stellar termination shocks from Scherer et al. (2008) suggest that, in terms of the energetic, it might be possible to have a significant fraction of low-energy CRs coming from stars. A more qualitative approach to this problem would be to analyze the stochastic fluctuations induced by the temporal and spatial distributions of stars in our Galaxy.

Appendix A

Numerical Scheme for the Point Source Solution

Let's first denote i, j, k, and l as the respective indices for the coordinates t, z, r, and E. For simplicity, we shall perform the code in uniform step for the coordinates t and z and in logarithmic step for r and E. This means that the discretized coordinates could be written as:

$$t_i = i\Delta t \quad z_j = j\Delta z \quad r_k = r_{min}10^{k\Delta \log r} \quad E_l = E_{min}10^{l\Delta \log E} \tag{A.1}$$

Where all the steps are chosen such that they satisfy the general Courant condition. The finite difference scheme for the transport equation 4.15 used for this work is as followed:

$$f^{i+1}_{0,k,l} = f^{i+1}_{1,k,l} \tag{A.2}$$

$$\begin{aligned} f^{i+1}_{j,k,l} = f^{i}_{jkl} &- \frac{u_0\Delta t}{\Delta z}(f^i_{j,k,l} - f^i_{j-1,k,l}\delta_{j1}) + \frac{D(E_l)\Delta t}{\Delta z^2}(f^i_{j+1,k,l} - 2f^i_{j,k,l} + f^i_{j-1,k,l}) \\ &+ \left(1 - 10^{-2\Delta \log r}\delta_{k0}\right)\frac{D(E_l)\Delta t}{(r_k \ln 10 \Delta \log r)^2}\left[f^i_{j,k+1,l} - (2-\delta_{k0})\, f^i_{j,k,l} + \delta_{k0} f^i_{j,k-1,l}\right] \\ &+ \frac{\Delta t}{E_l \log 10 \Delta \log E}\left[b(E_{l+1}) f^i_{j,k,l+1} - b(E_l) f^i_{j,k,l}\right] H(|z_j| < h) \\ &\qquad (\text{for } j = \overline{1, j_{max}}) \end{aligned} \tag{A.3}$$

$$f^{i+1}_{j_{max},k,l} = f^{i}_{j_{max},k,l} = 0 \tag{A.4}$$

$$f^{i+1}_{j,k_{max},l} = f^{i}_{j,k_{max},l} = 0 \tag{A.5}$$

It should be noticed that there is a pre-factor in front of the diffusion term in r-coordinate (the third term on the RHS in Eq. A.3) to ensure the particle conservation. This is because we have chosen to use the logarithmic binning in the r-coordinate. Also, the last two equations are in fact the free escape boundary conditions in both r- and z- coordinates. More importantly, since the source is bursting,

we have treated the source function as an initial condition meaning:

$$f^0_{0,k,l} = f^0_{1,k,l} \tag{A.6}$$

$$f^0_{j,k,l} = \frac{Q(E_l)}{2\pi r^2_{min}\Delta z}\delta_{j1}\delta_{k0} \text{ (for } j = \overline{1, j_{max}}) \tag{A.7}$$

In this sense, r_{min} should be chosen to be approximately the radius of the source in consideration ($r_{min} \simeq 30$ pc for SNRs) and Δz should be roughly of the same value.

Bibliography

Abdo, A. A. et al. (2010a). "Fermi Large Area Telescope Observations of the Supernova Remnant W28 (G6.4-0.1)". In: *ApJ* 718.1, pp. 348–356. DOI: 10.1088/0004-637X/718/1/348. arXiv: 1005.4474 [astro-ph.HE].

Abdo, A. A. et al. (Feb. 2010b). "Fermi Observations of Cassiopeia and Cepheus: Diffuse Gamma-ray Emission in the Outer Galaxy". In: *ApJ* 710.1, pp. 133–149. DOI: 10.1088/0004-637X/710/1/133. arXiv: 0912.3618 [astro-ph.HE].

Abdo, A. A. et al. (June 2011). "Observations of the Young Supernova Remnant RX J1713.7-3946 with the Fermi Large Area Telescope". In: *ApJ* 734.1, 28, p. 28. DOI: 10.1088/0004-637X/734/1/28. arXiv: 1103.5727 [astro-ph.HE].

Ackermann, M. et al. (Jan. 2011). "Constraints on the Cosmic-ray Density Gradient Beyond the Solar Circle from Fermi γ-ray Observations of the Third Galactic Quadrant". In: *ApJ* 726.2, 81, p. 81. DOI: 10.1088/0004-637X/726/2/81. arXiv: 1011.0816 [astro-ph.HE].

Aguilar, M. et al. (2014). "Precision Measurement of the (e^++e^-) Flux in Primary Cosmic Rays from 0.5 GeV to 1 TeV with the Alpha Magnetic Spectrometer on the International Space Station". In: *Phys. Rev. Lett.* 113.22, 221102, p. 221102. DOI: 10.1103/PhysRevLett.113.221102.

Aguilar, M. et al. (2015). "Precision Measurement of the Proton Flux in Primary Cosmic Rays from Rigidity 1 GV to 1.8 TV with the Alpha Magnetic Spectrometer on the International Space Station". In: *Phys. Rev. Lett.* 114.17, 171103, p. 171103. DOI: 10.1103/PhysRevLett.114.171103.

Aharonian, F. et al. (Feb. 2006). "Discovery of very-high-energy γ-rays from the Galactic Centre ridge". In: *Nature* 439.7077, pp. 695–698. DOI: 10.1038/nature04467. arXiv: astro-ph/0603021 [astro-ph].

Aharonian, F. et al. (2008). "Discovery of very high energy gamma-ray emission coincident with molecular clouds in the W 28 (G6.4-0.1) field". In: *A&A* 481.2, pp. 401–410. DOI: 10.1051/0004-6361:20077765. arXiv: 0801.3555 [astro-ph].

Aharonian, Felix et al. (Nov. 2018). "Probing the "Sea" of Galactic Cosmic Rays with Fermi-LAT". In: *arXiv e-prints*, arXiv:1811.12118, arXiv:1811.12118. arXiv: 1811.12118 [astro-ph.HE].

Aharonian, Felix A. (2004). *Very high energy cosmic gamma radiation : a crucial window on the extreme Universe*. DOI: 10.1142/4657.

Amenomori, M. et al. (May 2008). "The All-Particle Spectrum of Primary Cosmic Rays in the Wide Energy Range from 10^{14} to 10^{17} eV Observed with the Tibet-III Air-Shower Array". In: *ApJ* 678.2, pp. 1165–1179. DOI: 10.1086/529514. arXiv: 0801.1803 [hep-ex].

Andersen, K. J., M. Kachelriess, & D. V. Semikoz (July 2018). "High-energy Neutrinos from Galactic Superbubbles". In: *ApJ* 861.2, L19, p. L19. DOI: 10.3847/2041-8213/aacefd. arXiv: 1712.03153 [astro-ph.HE].

Andersson, B. G. & S. B. Potter (Mar. 2006). "The Magnetic Field Strength in the Wall of the Local Bubble toward l, b ~300, 0". In: *ApJ* 640.1, pp. L51–L54. DOI: 10.1086/503199.

Apel, W. D. et al. (July 2013). "KASCADE-Grande measurements of energy spectra for elemental groups of cosmic rays". In: *Astroparticle Physics* 47, pp. 54–66. DOI: 10.1016/j.astropartphys.2013.06.004.

Atoyan, Armen & Charles D. Dermer (Apr. 2012). "Gamma Rays from the Tycho Supernova Remnant: Multi-zone versus Single-zone Modeling". In: *ApJ* 749.2, L26, p. L26. DOI: 10.1088/2041-8205/749/2/L26. arXiv: 1111.4175 [astro-ph.HE].

Axford, W. I., E. Leer, & G. Skadron (Jan. 1977). "The Acceleration of Cosmic Rays by Shock Waves". In: *International Cosmic Ray Conference*. Vol. 11. International Cosmic Ray Conference, p. 132.

Baade, W. & F. Zwicky (May 1934). "Cosmic Rays from Super-novae". In: *Proceedings of the National Academy of Science* 20.5, pp. 259–263. DOI: 10.1073/pnas.20.5.259.

Bamba, Aya et al. (June 2003). "Small-Scale Structure of the SN 1006 Shock with Chandra Observations". In: *ApJ* 589.2, pp. 827–837. DOI: 10.1086/374687. arXiv: astro-ph/0302174 [astro-ph].

Becker, Julia K. et al. (Oct. 2011). "Tracing the Sources of Cosmic Rays with Molecular Ions". In: *ApJ* 739.2, L43, p. L43. DOI: 10.1088/2041-8205/739/2/L43. arXiv: 1106.4740 [astro-ph.GA].

Bell, A. R. (Jan. 1978). "The acceleration of cosmic rays in shock fronts - I." In: *MNRAS* 182, pp. 147–156. DOI: 10.1093/mnras/182.2.147.

Berezinskii, V. S. et al. (1990). *Astrophysics of cosmic rays*.

Bernard, G. et al. (Aug. 2012). "Variance of the Galactic nuclei cosmic ray flux". In: *A&A* 544, A92, A92. DOI: 10.1051/0004-6361/201219502. arXiv: 1204.6289 [astro-ph.HE].

Beuermann, K., G. Kanbach, & E. M. Berkhuijsen (Dec. 1985). "Radio structure of the Galaxy: thick disk and thin disk at 408 MHz." In: *A&A* 153, pp. 17–34.

Bieber, John W. et al. (Jan. 1994). "Proton and Electron Mean Free Paths: The Palmer Consensus Revisited". In: *ApJ* 420, p. 294. DOI: 10.1086/173559.

Bieber, John W. et al. (May 2004). "Nonlinear guiding center theory of perpendicular diffusion: General properties and comparison with observation". In: *Geophys. Res. Lett.* 31.10, L10805, p. L10805. DOI: 10.1029/2004GL020007.

Binns, W. R. et al. (Nov. 2005). "Cosmic-Ray Neon, Wolf-Rayet Stars, and the Superbubble Origin of Galactic Cosmic Rays". In: *ApJ* 634.1, pp. 351–364. DOI: 10.1086/496959. arXiv: astro-ph/0508398 [astro-ph].

Blandford, R. D. & J. P. Ostriker (Apr. 1978). "Particle acceleration by astrophysical shocks." In: *ApJ* 221, pp. L29–L32. DOI: 10.1086/182658.

Blasi, Pasquale (Nov. 2013). "The origin of galactic cosmic rays". In: *A&ARv* 21, 70, p. 70. DOI: 10.1007/s00159-013-0070-7. arXiv: 1311.7346 [astro-ph.HE].

Blasi, Pasquale & Elena Amato (Jan. 2012). "Diffusive propagation of cosmic rays from supernova remnants in the Galaxy. I: spectrum and chemical composition". In: *J. Cosmology Astropart. Phys.* 2012.1, 010, p. 010. DOI: 10.1088/1475-7516/2012/01/010. arXiv: 1105.4521 [astro-ph.HE].

Blasi, Pasquale, Elena Amato, & Pasquale D. Serpico (Aug. 2012). "Spectral Breaks as a Signature of Cosmic Ray Induced Turbulence in the Galaxy". In: *Phys. Rev. Lett.* 109.6, 061101, p. 061101. DOI: 10.1103/PhysRevLett.109.061101. arXiv: 1207.3706 [astro-ph.HE].

Breitschwerdt, D., M. J. Freyberg, & R. Egger (Sept. 2000). "Origin of H I clouds in the Local Bubble. I. A hydromagnetic Rayleigh-Taylor instability caused by the interaction between the Loop I and the Local Bubble". In: *A&A* 361, pp. 303–320.

Brogan, C. L. et al. (2006). "Discovery of 35 New Supernova Remnants in the Inner Galaxy". In: *ApJ* 639.1, pp. L25–L29. DOI: 10.1086/501500. arXiv: astro-ph/0601451 [astro-ph].

Casanova, Sabrina et al. (June 2010). "Molecular Clouds as Cosmic-Ray Barometers". In: *PASJ* 62, p. 769. DOI: 10.1093/pasj/62.3.769. arXiv: 0904.2887 [astro-ph.HE].

Caselli, P. (Oct. 2002). "Deuterated molecules as a probe of ionization fraction in dense interstellar clouds". In: *Planet. Space Sci.* 50.12-13, pp. 1133–1144. DOI: 10.1016/S0032-0633(02)00074-0. arXiv: astro-ph/0204127 [astro-ph].

Caselli, P. et al. (1998). "The Ionization Fraction in Dense Cloud Cores". In: *ApJ* 499.1, pp. 234–249. DOI: 10.1086/305624.

Casse, M. & J. A. Paul (July 1982). "On the stellar origin of the Ne-22 excess in cosmic rays". In: *ApJ* 258, pp. 860–863. DOI: 10.1086/160132.

Ceccarelli, C. & C. Dominik (Sept. 2005). "Deuterated H_3^+ in proto-planetary disks". In: *A&A* 440.2, pp. 583–593. DOI: 10.1051/0004-6361:20052991. arXiv: astro-ph/0506254 [astro-ph].

Ceccarelli, C. et al. (Oct. 2011). "Supernova-enhanced Cosmic-Ray Ionization and Induced Chemistry in a Molecular Cloud of W51C". In: *ApJ* 740.1, L4, p. L4. DOI: 10.1088/2041-8205/740/1/L4. arXiv: 1108.3600 [astro-ph.GA].

Cesarsky, C. J. (1975). "Interstellar Propagation of Low Energy Cosmic Rays". In: *International Cosmic Ray Conference*. Vol. 2. International Cosmic Ray Conference, p. 634.

— (Jan. 1980). "Cosmic-ray confinement in the galaxy". In: *ARA&A* 18, pp. 289–319. DOI: 10.1146/annurev.aa.18.090180.001445.

Cesarsky, C. J. & H. J. Volk (1978). "Cosmic Ray Penetration into Molecular Clouds". In: *A&A* 70, p. 367.

Cioffi, Denis F., Christopher F. McKee, & Edmund Bertschinger (Nov. 1988). "Dynamics of Radiative Supernova Remnants". In: *ApJ* 334, p. 252. DOI: 10.1086/166834.

Claussen, M. J. et al. (1997). "Polarization Observations of 1720 MHz OH Masers toward the Three Supernova Remnants W28, W44, and IC 443". In: *ApJ* 489.1, pp. 143–159. DOI: 10.1086/304784. arXiv: astro-ph/9706067 [astro-ph].

Cox, D. P. (1998). "Modeling the Local Bubble". In: *IAU Colloq. 166: The Local Bubble and Beyond*. Ed. by Dieter Breitschwerdt, Michael J. Freyberg, & Joachim Truemper. Vol. 506, pp. 121–131. DOI: 10.1007/BFb0104706.

Crutcher, Richard M. et al. (2010). "Magnetic Fields in Interstellar Clouds from Zeeman Observations: Inference of Total Field Strengths by Bayesian Analysis". In: *ApJ* 725.1, pp. 466–479. DOI: 10.1088/0004-637X/725/1/466.

Cui, Yudong et al. (2018). "Leaked GeV CRs from a Broken Shell: Explaining 9 Years of Fermi-LAT Data of SNR W28". In: *ApJ* 860.1, 69, p. 69. DOI: 10.3847/1538-4357/aac37b. arXiv: 1805.03372 [astro-ph.HE].

Cummings, A. C. et al. (2016). "Galactic Cosmic Rays in the Local Interstellar Medium: Voyager 1 Observations and Model Results". In: *ApJ* 831.1, 18, p. 18. DOI: 10.3847/0004-637X/831/1/18.

Dalgarno, A. (2006). "Interstellar Chemistry Special Feature: The galactic cosmic ray ionization rate". In: *Proceedings of the National Academy of Science* 103.33, pp. 12269–12273. DOI: 10.1073/pnas.0602117103.

Dalgarno, A., Min Yan, & Weihong Liu (1999). "Electron Energy Deposition in a Gas Mixture of Atomic and Molecular Hydrogen and Helium". In: *ApJS* 125.1, pp. 237–256. DOI: 10.1086/313267.

Dame, T. M., Dap Hartmann, & P. Thaddeus (2001). "The Milky Way in Molecular Clouds: A New Complete CO Survey". In: *ApJ* 547.2, pp. 792–813. DOI: 10.1086/318388. arXiv: astro-ph/0009217 [astro-ph].

Dermer, Charles D. & Govind Menon (2009). *High Energy Radiation from Black Holes: Gamma Rays, Cosmic Rays, and Neutrinos*.

Dogiel, V. A. et al. (2013). "The Origin of the 6.4 keV Line Emission and H_2 Ionization in the Diffuse Molecular Gas of the Galactic Center Region". In: *ApJ* 771.2, L43, p. L43. DOI: 10.1088/2041-8205/771/2/L43. arXiv: 1306.1654 [astro-ph.HE].

Dogiel, V. A. et al. (Dec. 2018). "Gamma-Ray Emission from Molecular Clouds Generated by Penetrating Cosmic Rays". In: *ApJ* 868.2, 114, p. 114. DOI: 10.3847/1538-4357/aae827. arXiv: 1810.05821 [astro-ph.HE].

Drury, L. O'C., F. A. Aharonian, & H. J. Voelk (July 1994). "The gamma-ray visibility of supernova remnants. A test of cosmic ray origin". In: *A&A* 287, pp. 959–971. arXiv: astro-ph/9305037 [astro-ph].

Drury, Luke O. 'C. & Andrew W. Strong (2017). "Power requirements for cosmic ray propagation models involving diffusive reacceleration; estimates and implications for the damping of interstellar turbulence". In: *A&A* 597, A117, A117. DOI: 10.1051/0004-6361/201629526. arXiv: 1608.04227 [astro-ph.HE].

Dubner, G. M. et al. (2000). "High-Resolution VLA Imaging of the Supernova Remnant W28 at 328 and 1415 MHZ". In: *AJ* 120.4, pp. 1933–1945. DOI: 10.1086/301583.

Dumas, G. et al. (2014). "Localized SiO Emission Triggered by the Passage of the W51C Supernova Remnant Shock". In: *ApJ* 786.2, L24, p. L24. DOI: 10.1088/2041-8205/786/2/L24. arXiv: 1404.1447 [astro-ph.GA].

Everett, John E. & Ellen G. Zweibel (2011). "The Interaction of Cosmic Rays with Diffuse Clouds". In: *ApJ* 739.2, 60, p. 60. DOI: 10.1088/0004-637X/739/2/60. arXiv: 1107.1243 [astro-ph.GA].

Evoli, Carmelo, Roberto Aloisio, & Pasquale Blasi (May 2019). "Galactic cosmic rays after the AMS-02 observations". In: *Phys. Rev. D* 99.10, 103023, p. 103023. DOI: 10.1103/PhysRevD.99.103023. arXiv: 1904.10220 [astro-ph.HE].

Fenu, F. & Pierre Auger Collaboration (Jan. 2017). "The cosmic ray energy spectrum measured using the Pierre Auger Observatory". In: *35th International Cosmic Ray Conference (ICRC2017)*. Vol. 301. International Cosmic Ray Conference, p. 486.

Fermi, Enrico (Apr. 1949). "On the Origin of the Cosmic Radiation". In: *Physical Review* 75.8, pp. 1169–1174. DOI: 10.1103/PhysRev.75.1169.

Finke, Justin D. & Charles D. Dermer (May 2012). "Cosmic-Ray Electron Evolution in the Supernova Remnant RX J1713.7-3946". In: *ApJ* 751.1, 65, p. 65. DOI: 10.1088/0004-637X/751/1/65. arXiv: 1203.4242 [astro-ph.HE].

Fujita, Yutaka et al. (2009). "Molecular Clouds as a Probe of Cosmic-Ray Acceleration in a Supernova Remnant". In: *ApJ* 707.2, pp. L179–L183. DOI: 10.1088/0004-637X/707/2/L179. arXiv: 0911.4482 [astro-ph.HE].

Fukui, Y. et al. (Feb. 2012). "A Detailed Study of the Molecular and Atomic Gas toward the γ-Ray Supernova Remnant RX J1713.7-3946: Spatial TeV γ-Ray and Interstellar Medium Gas Correspondence". In: *ApJ* 746.1, 82, p. 82. DOI: 10.1088/0004-637X/746/1/82. arXiv: 1107.0508 [astro-ph.GA].

Gabici, S. & F. A. Aharonian (Nov. 2014). "Hadronic gamma-rays from RX J1713.7-3946?" In: *MNRAS* 445, pp. L70–L73. DOI: 10.1093/mnrasl/slu132. arXiv: 1406.2322 [astro-ph.HE].

Gabici, S. & T. Montmerle (2015). "On the connection of gamma rays from supernova remnants interacting with molecular clouds and cosmic ray ionization measured". In: *34th International Cosmic Ray Conference (ICRC2015)*. Vol. 34. International Cosmic Ray Conference, p. 29.

Gabici, S. et al. (2010). "Constraints on the cosmic ray diffusion coefficient in the W28 region from gamma-ray observations". In: *SF2A-2010: Proceedings of the Annual meeting of the French Society of Astronomy and Astrophysics*. Ed. by S. Boissier et al., p. 313. arXiv: 1009.5291 [astro-ph.HE].

Gabici, Stefano (Jan. 2013). "Cosmic Rays and Molecular Clouds". In: *Cosmic Rays in Star-Forming Environments*. Ed. by Diego F. Torres & Olaf Reimer. Vol. 34, p. 221. DOI: 10.1007/978-3-642-35410-6_16. arXiv: 1208.4979 [astro-ph.HE].

Gabici, Stefano et al. (2019). "The origin of Galactic cosmic rays: Challenges to the standard paradigm". In: *International Journal of Modern Physics D* 28.15, 1930022-339, pp. 1930022–339. DOI: 10.1142/S0218271819300222. arXiv: 1903.11584 [astro-ph.HE].

Gaisser, Thomas K. (1990). *Cosmic rays and particle physics.*

Geballe, T. R. & T. Oka (Nov. 1996). "Detection of H_3^+ in interstellar space". In: *Nature* 384.6607, pp. 334–335. DOI: 10.1038/384334a0.

Génolini, Yoann et al. (Dec. 2017). "Indications for a High-Rigidity Break in the Cosmic-Ray Diffusion Coefficient". In: *Phys. Rev. Lett.* 119.24, 241101, p. 241101. DOI: 10.1103/PhysRevLett.119.241101.

Ginzburg, V. L. & S. I. Syrovatskii (1964). *The Origin of Cosmic Rays*.

Giordano, F. et al. (Jan. 2012). "Fermi Large Area Telescope Detection of the Young Supernova Remnant Tycho". In: *ApJ* 744.1, L2, p. L2. DOI: 10.1088/2041-8205/744/1/L2. arXiv: 1108.0265 [astro-ph.HE].

Goldreich, P. & S. Sridhar (1995). "Toward a Theory of Interstellar Turbulence. II. Strong Alfvenic Turbulence". In: *ApJ* 438, p. 763. DOI: 10.1086/175121.

Hayakawa, S., S. Nishimura, & T. Takayanagi (1961). "Radiation from the Interstellar Hydrogen Atoms". In: *PASJ* 13, p. 184.

HESS Collaboration et al. (Mar. 2016). "Acceleration of petaelectronvolt protons in the Galactic Centre". In: *Nature* 531.7595, pp. 476–479. DOI: 10.1038/nature17147. arXiv: 1603.07730 [astro-ph.HE].

Hewitt, J. W., F. Yusef-Zadeh, & M. Wardle (2008). "A Survey of Hydroxyl toward Supernova Remnants: Evidence for Extended 1720 MHz Maser Emission". In: *ApJ* 683.1, pp. 189–206. DOI: 10.1086/588652. arXiv: 0802.3878 [astro-ph].

Heyer, Mark & T. M. Dame (2015). "Molecular Clouds in the Milky Way". In: *ARA&A* 53, pp. 583–629. DOI: 10.1146/annurev-astro-082214-122324.

Hinton, J. A. & W. Hofmann (Sept. 2009). "Teraelectronvolt Astronomy". In: *ARA&A* 47.1, pp. 523–565. DOI: 10.1146/annurev-astro-082708-101816. arXiv: 1006.5210 [astro-ph.HE].

Hörandel, Jörg R. (Jan. 2008). "Cosmic-ray composition and its relation to shock acceleration by supernova remnants". In: *Advances in Space Research* 41.3, pp. 442–463. DOI: 10.1016/j.asr.2007.06.008. arXiv: astro-ph/0702370 [astro-ph].

Indriolo, Nick & Benjamin J. McCall (2012). "Investigating the Cosmic-Ray Ionization Rate in the Galactic Diffuse Interstellar Medium through Observations of H^+_3". In: *ApJ* 745.1, 91, p. 91. DOI: 10.1088/0004-637X/745/1/91. arXiv: 1111.6936 [astro-ph.GA].

Indriolo, Nick, Brian D. Fields, & Benjamin J. McCall (2009). "The Implications of a High Cosmic-Ray Ionization Rate in Diffuse Interstellar Clouds". In: *ApJ* 694.1, pp. 257–267. DOI: 10.1088/0004-637X/694/1/257. arXiv: 0901.1143 [astro-ph.HE].

Indriolo, Nick et al. (Feb. 2015). "Herschel Survey of Galactic OH^+, H_2O^+, and H_3O^+: Probing the Molecular Hydrogen Fraction and Cosmic-Ray Ionization Rate". In: *ApJ* 800.1, 40, p. 40. DOI: 10.1088/0004-637X/800/1/40. arXiv: 1412.1106 [astro-ph.GA].

Inoue, Tsuyoshi et al. (Jan. 2012). "Toward Understanding the Cosmic-Ray Acceleration at Young Supernova Remnants Interacting with Interstellar Clouds: Possible Applications to RX J1713.7-3946". In: *ApJ* 744.1, 71, p. 71. DOI: 10.1088/0004-637X/744/1/71. arXiv: 1106.3080 [astro-ph.HE].

Ivlev, A. V. et al. (2018). "Penetration of Cosmic Rays into Dense Molecular Clouds: Role of Diffuse Envelopes". In: *ApJ* 855.1, 23, p. 23. DOI: 10.3847/1538-4357/aaadb9. arXiv: 1802.02612 [astro-ph.HE].

Jaupart, Étienne, Étienne Parizot, & Denis Allard (Nov. 2018). "Contribution of the Galactic centre to the local cosmic-ray flux". In: *A&A* 619, A12, A12. DOI: 10.1051/0004-6361/201833683. arXiv: 1808.02322 [astro-ph.HE].

Jokipii, J. R. (Nov. 1966). "Cosmic-Ray Propagation. I. Charged Particles in a Random Magnetic Field". In: *ApJ* 146, p. 480. DOI: 10.1086/148912.

Jokipii, Randy (2001). "Transport and Acceleration of Cosmic Rays in a Turbulent Astrophysical Plasma". In: *The 7th Taipei Astrophysics Workshop on Cosmic Rays in the Universe*. Ed. by Chung-Ming Ko. Vol. 241. Astronomical Society of the Pacific Conference Series, p. 223.

Joubaud, T. et al. (Mar. 2020). "The cosmic-ray content of the Orion-Eridanus superbubble". In: *A&A* 635, A96, A96. DOI: 10.1051/0004-6361/201937205. arXiv: 2001.10139 [astro-ph.HE].

Kafexhiu, Ervin et al. (2014). "Parametrization of gamma-ray production cross sections for p p interactions in a broad proton energy range from the kinematic threshold to PeV energies". In: *Phys. Rev. D* 90.12, 123014, p. 123014. DOI: 10.1103/PhysRevD.90.123014. arXiv: 1406.7369 [astro-ph.HE].

Kennel, C. F. & F. Engelmann (Dec. 1966). "Velocity Space Diffusion from Weak Plasma Turbulence in a Magnetic Field". In: *Physics of Fluids* 9.12, pp. 2377–2388. DOI: 10.1063/1.1761629.

Kim, Yong-Ki, José Paulo Santos, & Fernando Parente (Nov. 2000). "Extension of the binary-encounter-dipole model to relativistic incident electrons". In: *Phys. Rev. A* 62.5, 052710, p. 052710. DOI: 10.1103/PhysRevA.62.052710.

Knie, K. et al. (July 1999). "Indication for Supernova Produced ^{60}Fe Activity on Earth". In: *Phys. Rev. Lett.* 83.1, pp. 18–21. DOI: 10.1103/PhysRevLett.83.18.

Kovalenko, A. V., A. V. Pynzar', & V. A. Udal'Tsov (Jan. 1994). "Observations of supernova remnants at Pushchino: Catalog of flux densities at meter wavelengths". In: *Astronomy Reports* 38.1, pp. 95–104.

Krause, J., G. Morlino, & S. Gabici (2015). "CRIME - cosmic ray interactions in molecular environments". In: *34th International Cosmic Ray Conference (ICRC2015)*. Vol. 34. International Cosmic Ray Conference, p. 518.

Krolik, J. H. & T. R. Kallman (1983). "X-ray ionization and the Orion Molecular Cloud." In: *ApJ* 267, pp. 610–624. DOI: 10.1086/160897.

Krumholz, Mark R. (June 2014). "The big problems in star formation: The star formation rate, stellar clustering, and the initial mass function". In: *Phys. Rep.* 539, pp. 49–134. DOI: 10.1016/j.physrep.2014.02.001. arXiv: 1402.0867 [astro-ph.GA].

Krymskii, G. F. (June 1977). "A regular mechanism for the acceleration of charged particles on the front of a shock wave". In: *Akademiia Nauk SSSR Doklady* 234, pp. 1306–1308.

Kulsrud, Russell & William P. Pearce (May 1969). "The Effect of Wave-Particle Interactions on the Propagation of Cosmic Rays". In: *ApJ* 156, p. 445. DOI: 10.1086/149981.

Lee, H. H., R. P. A. Bettens, & E. Herbst (Oct. 1996). "Fractional abundances of molecules in dense interstellar clouds: A compendium of recent model results." In: *A&AS* 119, pp. 111–114.

Lerche, I. (Aug. 1968). "Quasilinear Theory of Resonant Diffusion in a Magneto-Active, Relativistic Plasma". In: *Physics of Fluids* 11.8, pp. 1720–1727. DOI: 10.1063/1.1692186.

Li, Hui & Yang Chen (2010). "γ-rays from molecular clouds illuminated by accumulated diffusive protons from supernova remnant W28". In: *MNRAS* 409.1, pp. L35–L38. DOI: 10.1111/j.1745-3933.2010.00944.x. arXiv: 1009.0894 [astro-ph.HE].

Longair, Malcolm S. (2011). *High Energy Astrophysics*.

Maloney, Philip R., David J. Hollenbach, & A. G. G. M. Tielens (1996). "X-Ray–irradiated Molecular Gas. I. Physical Processes and General Results". In: *ApJ* 466, p. 561. DOI: 10.1086/177532.

Maret, Sébastien & Edwin A. Bergin (2007). "The Ionization Fraction of Barnard 68: Implications for Star and Planet Formation". In: *ApJ* 664.2, pp. 956–963. DOI: 10.1086/519152. arXiv: 0704.3188 [astro-ph].

Matsunaga, Ken'ichi et al. (2001). "Detection of Eight Molecular Supershells in the Southern Milky Way with NANTEN". In: *PASJ* 53.6, pp. 1003–1016. DOI: 10.1093/pasj/53.6.1003.

McCall, B. J. et al. (Sept. 1999). "Observations of H_3^+ in Dense Molecular Clouds". In: *ApJ* 522.1, pp. 338–348. DOI: 10.1086/307637.

McCall, B. J. et al. (Apr. 2003). "An enhanced cosmic-ray flux towards ζ Persei inferred from a laboratory study of the H_3^+-e^- recombination rate". In: *Nature* 422.6931, pp. 500–502. DOI: 10.1038/nature01498. arXiv: astro-ph/0302106 [astro-ph].

McKee, Christopher F. (1989). "Photoionization-regulated Star Formation and the Structure of Molecular Clouds". In: *ApJ* 345, p. 782. DOI: 10.1086/167950.

Meneguzzi, M., J. Audouze, & H. Reeves (1971). "The production of the elements Li, Be, B by galactic cosmic rays in space and its relation with stellar observations." In: *A&A* 15, p. 337.

Mertsch, P. (Feb. 2011). "Cosmic ray electrons and positrons from discrete stochastic sources". In: *J. Cosmology Astropart. Phys.* 2011.2, 031, p. 031. DOI: 10.1088/1475-7516/2011/02/031. arXiv: 1012.0805 [astro-ph.HE].

Mestel, L. & Jr. Spitzer L. (Jan. 1956). "Star formation in magnetic dust clouds". In: *MNRAS* 116, p. 503. DOI: 10.1093/mnras/116.5.503.

Morfill, G. E. (1982). "Secondary electron spectra in interstellar clouds, and the bremsstrahlung gamma-ray luminosity". In: *ApJ* 262, pp. 749–759. DOI: 10.1086/160470.

Morlino, G. & D. Caprioli (Feb. 2012). "Strong evidence for hadron acceleration in Tycho's supernova remnant". In: *A&A* 538, A81, A81. DOI: 10.1051/0004-6361/201117855. arXiv: 1105.6342 [astro-ph.HE].

Morlino, G. & S. Gabici (2015). "Cosmic ray penetration in diffuse clouds." In: *MNRAS* 451, pp. L100–L104. DOI: 10.1093/mnrasl/slv074. arXiv: 1503.02435 [astro-ph.HE].

Morrison, R. & D. McCammon (1983). "Interstellar photoelectric absorption cross sections, 0.03-10 keV." In: *ApJ* 270, pp. 119–122. DOI: 10.1086/161102.

Naito, Tsuguya & Fumio Takahara (Mar. 1994). "High energy gamma-ray emission from supernova remnants". In: *Journal of Physics G Nuclear Physics* 20.3, pp. 477–486. DOI: 10.1088/0954-3899/20/3/009.

Nath, Biman B. & Peter L. Biermann (1994). "Cosmic ray ionization of the interstellar medium". In: *MNRAS* 267.2, pp. 447–451. DOI: 10.1093/mnras/267.2.447. arXiv: astro-ph/9311048 [astro-ph].

Nava, L. & S. Gabici (2013). "Anisotropic cosmic ray diffusion and gamma-ray production close to supernova remnants, with an application to W28". In: *MNRAS* 429.2, pp. 1643–1651. DOI: 10.1093/mnras/sts450. arXiv: 1211.1668 [astro-ph.HE].

Nava, L. et al. (Oct. 2016). "Non-linear diffusion of cosmic rays escaping from supernova remnants - I. The effect of neutrals". In: *MNRAS* 461.4, pp. 3552–3562. DOI: 10.1093/mnras/stw1592. arXiv: 1606.06902 [astro-ph.HE].

Nava, L. et al. (Apr. 2019). "Non-linear diffusion of cosmic rays escaping from supernova remnants - II. Hot ionized media". In: *MNRAS* 484.2, pp. 2684–2691. DOI: 10.1093/mnras/stz137. arXiv: 1903.03193 [astro-ph.HE].

Nobukawa, K. K. et al. (July 2015). "Enhancement of the 6.4 keV Line in the Inner Galactic Ridge: Proton-induced Fluorescence?" In: *ApJ* 807.1, L10, p. L10. DOI: 10.1088/2041-8205/807/1/L10. arXiv: 1506.00759 [astro-ph.HE].

Nobukawa, Kumiko K. et al. (2018). "Evidence for a Neutral Iron Line Generated by MeV Protons from Supernova Remnants Interacting with Molecular Clouds". In: *ApJ* 854.2, 87, p. 87. DOI: 10.3847/1538-4357/aaa8dc. arXiv: 1801.07881 [astro-ph.HE].

Ntormousi, Evangelia et al. (Mar. 2017). "The role of magnetic fields in the structure and interaction of supershells". In: *A&A* 599, A94, A94. DOI: 10.1051/0004-6361/201629268. arXiv: 1701.03696 [astro-ph.GA].

Ohira, Yutaka, Kohta Murase, & Ryo Yamazaki (2011). "Gamma-rays from molecular clouds illuminated by cosmic rays escaping from interacting supernova remnants". In: *MNRAS* 410.3, pp. 1577–1582. DOI: 10.1111/j.1365-2966.2010.17539.x. arXiv: 1007.4869 [astro-ph.HE].

Oka, Takeshi (Aug. 2006). "Interstellar Chemistry Special Feature: Interstellar H3+". In: *Proceedings of the National Academy of Science* 103.33, pp. 12235–12242. DOI: 10.1073/pnas.0601242103.

Okon, Hiromichi et al. (2018). "The origin of recombining plasma and the detection of the Fe-K line in the supernova remnant W 28". In: *PASJ* 70.3, 35, p. 35. DOI: 10.1093/pasj/psy022. arXiv: 1802.02814 [astro-ph.HE].

Osborne, J. L. & V. S. Ptuskin (1988). "Cosmic-Ray Reacceleration in the Interstellar Medium". In: *Soviet Astronomy Letters* 14, p. 132.

Osterbrock, D. E. & N. G. Bochkarev (1989). "Book-Review - Astrophysics of Gaseous Nebulae and Active Galactic Nuclei". In: *Soviet Ast.* 33, p. 694.

Padovani, M. & D. Galli (2011). "Effects of magnetic fields on the cosmic-ray ionization of molecular cloud cores". In: *A&A* 530, A109, A109. DOI: 10.1051/0004-6361/201116853. arXiv: 1104.5445 [astro-ph.SR].

Padovani, M., D. Galli, & A. E. Glassgold (2009). "Cosmic-ray ionization of molecular clouds". In: *A&A* 501.2, pp. 619–631. DOI: 10.1051/0004-6361/200911794. arXiv: 0904.4149 [astro-ph.SR].

Padovani, M. et al. (2015). "Cosmic-ray acceleration in young protostars". In: *A&A* 582, L13, p. L13. DOI: 10.1051/0004-6361/201526874. arXiv: 1509.06416 [astro-ph.SR].

Padovani, M. et al. (2016). "Protostars: Forges of cosmic rays?" In: *A&A* 590, A8, A8. DOI: 10.1051/0004-6361/201628221. arXiv: 1602.08495 [astro-ph.HE].

Padovani, Marco & Daniele Galli (Jan. 2013). "Cosmic-Ray Propagation in Molecular Clouds". In: *Cosmic Rays in Star-Forming Environments*. Ed. by Diego F. Torres & Olaf Reimer. Vol. 34, p. 61. DOI: 10.1007/978-3-642-35410-6_6. arXiv: 1305.5393 [astro-ph.GA].

Padovani, Marco et al. (Mar. 2020). "Impact of Low-Energy Cosmic Rays on Star Formation". In: *Space Sci. Rev.* 216.2, 29, p. 29. DOI: 10.1007/s11214-020-00654-1. arXiv: 2002.10282 [astro-ph.GA].

Parker, E. N. (Aug. 1969). "Galactic Effects of the Cosmic-Ray Gas". In: *Space Sci. Rev.* 9.5, pp. 651–712. DOI: 10.1007/BF00174032.

Phan, V. H. M., G. Morlino, & S. Gabici (2018). "What causes the ionization rates observed in diffuse molecular clouds? The role of cosmic ray protons and electrons". In: *MNRAS* 480.4, pp. 5167–5174. DOI: 10.1093/mnras/sty2235. arXiv: 1804.10106 [astro-ph.HE].

Phan, V. H. M. et al. (Mar. 2020). "Constraining the cosmic ray spectrum in the vicinity of the supernova remnant W28: from sub-GeV to multi-TeV energies". In: *A&A* 635, A40, A40. DOI: 10.1051/0004-6361/201936927. arXiv: 1910.09987 [astro-ph.HE].

Potgieter, Marius S. (June 2013). "Solar Modulation of Cosmic Rays". In: *Living Reviews in Solar Physics* 10.1, 3, p. 3. DOI: 10.12942/lrsp-2013-3. arXiv: 1306.4421 [physics.space-ph].

Recchia, S., P. Blasi, & G. Morlino (Oct. 2016). "On the radial distribution of Galactic cosmic rays". In: *MNRAS* 462.1, pp. L88–L92. DOI: 10.1093/mnrasl/slw136. arXiv: 1604.07682 [astro-ph.HE].

Recchia, S. et al. (2019). "Can a cosmic ray carrot explain the ionization level in diffuse molecular clouds?" In: *MNRAS* 485.2, pp. 2276–2280. DOI: 10.1093/mnras/stz555. arXiv: 1901.04912 [astro-ph.HE].

Rho, Jeonghee & Kazimierz J. Borkowski (2002). "ROSAT/ASCA Observations of the Mixed-Morphology Supernova Remnant W28". In: *ApJ* 575.1, pp. 201–216. DOI: 10.1086/341192. arXiv: nlin/0204007 [nlin.AO].

Rudd, M. E. (Dec. 1988). "Differential cross sections for secondary electron production by proton impact". In: *Phys. Rev. A* 38.12, pp. 6129–6137. DOI: 10.1103/PhysRevA.38.6129.

Scherer, K. et al. (June 2008). "Are Anomalous Cosmic Rays the Main Contribution to the Low-Energy Galactic Cosmic Ray Spectrum?" In: *ApJ* 680.2, p. L105. DOI: 10.1086/589969.

Schlickeiser, R., M. Lazar, & M. Vukcevic (Aug. 2010). "The Influence of Dissipation Range Power Spectra and Plasma-wave Polarization on Cosmic-ray Scattering

Mean Free Path". In: *ApJ* 719.2, pp. 1497–1502. DOI: 10.1088/0004-637X/719/2/1497.

Schlickeiser, R., M. Caglar, & A. Lazarian (2016). "Cosmic Rays and MHD Turbulence Generation in Interstellar Giant Molecular Clouds". In: *ApJ* 824.2, 89, p. 89. DOI: 10.3847/0004-637X/824/2/89.

Schlickeiser, Reinhard (Jan. 1989). "Cosmic-Ray Transport and Acceleration. I. Derivation of the Kinetic Equation and Application to Cosmic Rays in Static Cold Media". In: *ApJ* 336, p. 243. DOI: 10.1086/167009.

Schlickeiser, Reinhard (2002). *Cosmic Ray Astrophysics*. Springer. ISBN: 978-3-662-04814-6.

Schulreich, M. M. et al. (Aug. 2017). "Numerical studies on the link between radioisotopic signatures on Earth and the formation of the Local Bubble. I. ^{60}Fe transport to the solar system by turbulent mixing of ejecta from nearby supernovae into a locally homogeneous interstellar medium". In: *A&A* 604, A81, A81. DOI: 10.1051/0004-6361/201629837. arXiv: 1704.08221 [astro-ph.HE].

Schuppan, Florian, Christian Röken, & Julia Becker Tjus (2014). "Theoretical study of ionization profiles of molecular clouds near supernova remnants. Tracing the hadronic origin of GeV gamma radiation". In: *A&A* 567, A50, A50. DOI: 10.1051/0004-6361/201423614. arXiv: 1402.2521 [astro-ph.HE].

Shalchi, Andreas (2009). *Nonlinear Cosmic Ray Diffusion Theories*. Vol. 362. DOI: 10.1007/978-3-642-00309-7.

Silk, J. & C. Norman (1983). "X-ray emission from pre-main-sequence stars, molecular clouds and star formation." In: *ApJ* 272, pp. L49–L53. DOI: 10.1086/184115.

Silsbee, Kedron & Alexei V. Ivlev (July 2019). "Diffusive versus Free-streaming Cosmic-Ray Transport in Molecular Clouds". In: *ApJ* 879.1, 14, p. 14. DOI: 10.3847/1538-4357/ab22b4. arXiv: 1904.01588 [astro-ph.HE].

Silsbee, Kedron et al. (Aug. 2018). "Magnetic Mirroring and Focusing of Cosmic Rays". In: *ApJ* 863.2, 188, p. 188. DOI: 10.3847/1538-4357/aad3cf. arXiv: 1807.05025 [astro-ph.HE].

Skilling, J. (Sept. 1975). "Cosmic ray streaming - I. Effect of Alfvén waves on particles." In: *MNRAS* 172, pp. 557–566. DOI: 10.1093/mnras/172.3.557.

Skilling, J. & A. W. Strong (1976). "Cosmic ray exclusion from dense molecular clouds." In: *A&A* 53.2, pp. 253–258.

Snow, Theodore P. & Benjamin J. McCall (2006). "Diffuse Atomic and Molecular Clouds". In: *ARA&A* 44.1, pp. 367–414. DOI: 10.1146/annurev.astro.43.072103.150624.

Spitzer Lyman, Jr. & Martin G. Tomasko (June 1968). "Heating of H i Regions by Energetic Particles". In: *ApJ* 152, p. 971. DOI: 10.1086/149610.

Spitzer, L. (1962). *Physics of Fully Ionized Gases*.

Sridhar, S. & P. Goldreich (1994). "Toward a Theory of Interstellar Turbulence. I. Weak Alfvenic Turbulence". In: *ApJ* 432, p. 612. DOI: 10.1086/174600.

Stone, E. C. et al. (2013). "Voyager 1 Observes Low-Energy Galactic Cosmic Rays in a Region Depleted of Heliospheric Ions". In: *Science* 341.6142, pp. 150–153. DOI: 10.1126/science.1236408.

Stone, Edward C. et al. (Nov. 2019). "Cosmic ray measurements from Voyager 2 as it crossed into interstellar space". In: *Nature Astronomy* 3, pp. 1013–1018. DOI: 10.1038/s41550-019-0928-3.

Strong, A. W. et al. (2010). "Global Cosmic-ray-related Luminosity and Energy Budget of the Milky Way". In: *ApJ* 722.1, pp. L58–L63. DOI: 10.1088/2041-8205/722/1/L58. arXiv: 1008.4330 [astro-ph.HE].

Strong, Andrew W. & Igor V. Moskalenko (Dec. 1998). "Propagation of Cosmic-Ray Nucleons in the Galaxy". In: *ApJ* 509.1, pp. 212–228. DOI: 10.1086/306470. arXiv: astro-ph/9807150 [astro-ph].

Strong, Andrew W., Igor V. Moskalenko, & Vladimir S. Ptuskin (Nov. 2007). "Cosmic-Ray Propagation and Interactions in the Galaxy". In: *Annual Review of Nuclear and Particle Science* 57.1, pp. 285–327. DOI: 10.1146/annurev.nucl.57.090506.123011. arXiv: astro-ph/0701517 [astro-ph].

Tatischeff, V., A. Decourchelle, & G. Maurin (2012). "Nonthermal X-rays from low-energy cosmic rays: application to the 6.4 keV line emission from the Arches cluster region". In: *A&A* 546, A88, A88. DOI: 10.1051/0004-6361/201219016. arXiv: 1210.2108 [astro-ph.HE].

Tatischeff, Vincent & Stefano Gabici (Oct. 2018). "Particle Acceleration by Supernova Shocks and Spallogenic Nucleosynthesis of Light Elements". In: *Annual Review of Nuclear and Particle Science* 68.1, pp. 377–404. DOI: 10.1146/annurev-nucl-101917-021151. arXiv: 1803.01794 [astro-ph.HE].

Thornbury, Andrew & Luke O'C. Drury (2014). "Power requirements for cosmic ray propagation models involving re-acceleration and a comment on second-order Fermi acceleration theory". In: *MNRAS* 442.4, pp. 3010–3012. DOI: 10.1093/mnras/stu1080. arXiv: 1404.2104 [astro-ph.HE].

Trotta, R. et al. (2011). "Constraints on Cosmic-ray Propagation Models from A Global Bayesian Analysis". In: *ApJ* 729.2, 106, p. 106. DOI: 10.1088/0004-637X/729/2/106. arXiv: 1011.0037 [astro-ph.HE].

Uchiyama, Yasunobu & Felix A. Aharonian (Apr. 2008). "Fast Variability of Non-thermal X-Ray Emission in Cassiopeia A: Probing Electron Acceleration in Reverse-Shocked Ejecta". In: *ApJ* 677.2, p. L105. DOI: 10.1086/588190. arXiv: 0803.3410 [astro-ph].

Uchiyama, Yasunobu et al. (Oct. 2007). "Extremely fast acceleration of cosmic rays in a supernova remnant". In: *Nature* 449.7162, pp. 576–578. DOI: 10.1038/nature06210.

Uchiyama, Yasunobu et al. (Nov. 2010). "Gamma-ray Emission from Crushed Clouds in Supernova Remnants". In: *ApJ* 723.1, pp. L122–L126. DOI: 10.1088/2041-8205/723/1/L122. arXiv: 1008.1840 [astro-ph.HE].

Vaupré, S. et al. (2014). "Cosmic ray induced ionisation of a molecular cloud shocked by the W28 supernova remnant". In: *A&A* 568, A50, A50. DOI: 10.1051/0004-6361/201424036. arXiv: 1407.0205 [astro-ph.GA].

Velázquez, P. F. et al. (2002). "Investigation of the Large-scale Neutral Hydrogen near the Supernova Remnant W28". In: *AJ* 124.4, pp. 2145–2151. DOI: 10.1086/342936. arXiv: astro-ph/0207530 [astro-ph].

Vink, Jacco (2012). "Supernova remnants: the X-ray perspective". In: *A&ARv* 20, 49, p. 49. DOI: 10.1007/s00159-011-0049-1. arXiv: 1112.0576 [astro-ph.HE].

Vink, Jacco & J. Martin Laming (Feb. 2003). "On the Magnetic Fields and Particle Acceleration in Cassiopeia A". In: *ApJ* 584.2, pp. 758–769. DOI: 10.1086/345832. arXiv: astro-ph/0210669 [astro-ph].

Voelk, H. J. & M. Forman (Feb. 1982). "Cosmic rays and gamma-rays from OB stars". In: *ApJ* 253, pp. 188–198. DOI: 10.1086/159623.

Völk, H. J., E. G. Berezhko, & L. T. Ksenofontov (Apr. 2005). "Magnetic field amplification in Tycho and other shell-type supernova remnants". In: *A&A* 433.1, pp. 229–240. DOI: 10.1051/0004-6361:20042015. arXiv: astro-ph/0409453 [astro-ph].

Webber, W. R. (1998). "A New Estimate of the Local Interstellar Energy Density and Ionization Rate of Galactic Cosmic Cosmic Rays". In: *ApJ* 506.1, pp. 329–334. DOI: 10.1086/306222.

Welsh, Barry Y. & Robin L. Shelton (Sept. 2009). "The trouble with the Local Bubble". In: *Ap&SS* 323.1, pp. 1–16. DOI: 10.1007/s10509-009-0053-3. arXiv: 0906.2827 [astro-ph.GA].

Wentzel, D. G. (1974). "Cosmic-ray propagation in the Galaxy: collective effects." In: *ARA&A* 12, pp. 71–96. DOI: 10.1146/annurev.aa.12.090174.000443.

Williams, Jonathan P. et al. (1998). "The Ionization Fraction in Dense Molecular Gas. I. Low-Mass Cores". In: *ApJ* 503.2, pp. 689–699. DOI: 10.1086/306034.

Wurster, James, Matthew R. Bate, & Daniel J. Price (2018). "The effect of extreme ionization rates during the initial collapse of a molecular cloud core". In: *MNRAS* 476.2, pp. 2063–2074. DOI: 10.1093/mnras/sty392. arXiv: 1802.04872 [astro-ph.SR].

Yang, Rui-zhi, Emma de Oña Wilhelmi, & Felix Aharonian (2014). "Probing cosmic rays in nearby giant molecular clouds with the Fermi Large Area Telescope". In: *A&A* 566, A142, A142. DOI: 10.1051/0004-6361/201321044. arXiv: 1303.7323 [astro-ph.HE].

Yusef-Zadeh, F. et al. (Sept. 2000). "Radio Continuum Emission from the Central Stars of M20, and the Detection of a New Supernova Remnant near M20". In: *ApJ* 540.2, pp. 842–850. DOI: 10.1086/309352. arXiv: astro-ph/0003295 [astro-ph].

Zhou, Ping et al. (2014). "An XMM-Newton Study of the Mixed-morphology Supernova Remnant W28 (G6.4-0.1)". In: *ApJ* 791.2, 87, p. 87. DOI: 10.1088/0004-637X/791/2/87. arXiv: 1407.6717 [astro-ph.HE].

Zweibel, E. G. & J. M. Shull (1982). "Confinement of cosmic rays in molecular clouds". In: *ApJ* 259, pp. 859–868. DOI: 10.1086/160220.